Causes and consequences of behavioral variation in large mammals

A Dissertation
Presented in Partial Fulfillment of the Requirements for the
Degree of Doctor of Philosophy
with a
Major in Natural Resources
in the
College of Graduate Studies
University of Idaho
by
Reena H. Walker

Approved by:
Major Professor: Ryan Long, Ph.D.
Committee Members: Simon Chamaillé-Jammes, Ph.D.; John Fryxell, Ph.D.; Janet Rachlow, Ph.D.
Department Administrator: Janet Rachlow, Ph.D.

May 2023

Abstract

Behavioral plasticity is a key mechanism by which animals buffer themselves against environmental change. The degree to which behavioral plasticity is constrained by morphological and physiological traits, and the factors that drive such relationships, have strong implications for animal fitness yet remain poorly understood. In an effort to derive overarching mechanisms that underpin behavioral trade-offs in complex natural environments, I examined how morphological and physiological traits shape the behavior and performance of large mammals across three ecologically important contexts: foraging, reproduction, and post-disturbance. First, I evaluated physiological traits mediating individual dietary specialization in an African antelope (bushbuck, *Tragelaphus sylvaticus*). I found that animals in better nutritional condition have narrower diets because they invest more time in searching for nutritious foods. These findings are consistent with predictions from optimal foraging theory about the energetic underpinnings of individual specialization, suggesting a potentially generalizable framework for understanding how individual's diets are constrained by behavior and physiology. Next, I evaluated whether individual behaviors buffer climatic constraints on reproductive success in an endangered carnivore (African wild dog, *Lycaon pictus*). We find that (1) packs that use favorable thermal environments, which reduce energetic constraints of heat dissipation on the pregnant female, produced larger litters, and (2) fecundity is constrained by competition among packs wherein larger packs exclude smaller ones from thermally favorable. Our study is among the first to elucidate the mechanistic underpinnings of thermal constraints on reproductive success in a wild population of large mammals and suggests that thermal refugia are a key component of habitat quality that will likely increase in importance as the climate warms. Finally, I quantified the responses of a large-mammal community to an extreme tropical cyclone to identify mechanisms underlying animal robustness to disturbance. In March 2019, the worst tropical cyclone on record in the southern hemisphere, Cyclone Idai, passed directly over Gorongosa National Park. Utilizing multiple data streams for 13 ungulate species and 2 carnivores, I found that small species are most vulnerable to cyclones due to limited mobility, which increased likelihood of death during the flood and constrained animals' capacity to withstand food shortage afterwards. This study is the first to identify individual-level mechanisms that underpin community-level responses to severe disturbance and suggests a general trait-based theory for predicting the impacts of extreme climatic events.

Acknowledgments

The mentorship and support of Dr. Ryan A. Long made this work possible. His penchant for transformative ideas, enthusiasm for teaching, and commitment to his work have inspired and instructed me over the last five years. I will always be grateful for his model of a superb mentor and ecologist and hope to live up to his example. I am additionally thankful for the members of the Long Lab, who have been my closest community and strongest support throughout my years in Moscow, and of the Pringle Lab at Princeton, who taught me the ropes of life in Chitengo and DNA metabarcoding. Drs. Neil R. Jordan, K. Golabeck, and J.W. McNutt gave me my first glimpse of life in the field and lit the path that led to this dissertation. Drs. Janet Rachlow, Simon Chamaillé-Jammes, and John Fryxell have shaped my career by sharing their expertise and advice at critical stages of my development as student and scientist. I am grateful to M. Stalmans, R. Branco, J. Denlinger, and M. Marchington for providing logistical support and thank A. Paulo, M. Angela, L. van Wyk and M. Pingo for assistance in the field. I thank Gorongosa National Park and the Republic of Mozambique as well as the Office of the President of Botswana and the Department of Wildlife and National Parks for permission to this conduct research. In particular, I thank the Sankuyo, Khwai, Mababe and Shorobe communities for allowing this research on their land in Botswana. This work and its participants were supported by the U.S. National Science Foundation (GRFP to RHW; IOS-1656642 to RAL.; IOS-1656527 to RMP), the Greg Carr Foundation, the Cameron Schrier Foundation, the High Meadows Institute at Princeton University, and the Botswana Predator Conservation Trust.

Dedication

To Cameron, who took the leap with me to Idaho, to Mozambique, and beyond.

Table of Contents

List of Tables

List of Figures

Statement of Contribution

The three subsequent chapters represent collaborative research efforts. In the first chapter: RHW, RAL, and RMP conceptualized and designed the study; RHW, JAB, and ABP collected data; MCP and ABP conducted laboratory work; RHW conducted data analyses, compiled figures and tables, and prepared the original manuscript draft; RAL and RMP supervised and funded the study; all authors reviewed and edited the manuscript. In the second chapter: RHW, JAB, MCH, JHD, MES, RMP and RAL conceived and designed the study; RHW, JAB, MCH, JHD, KMG and MSP performed statistical analyses; JHD and JD provided flood depth data; RHW, JAB, RMP and RAL provided antelope movement data; DDG and RAL provided elephant movement data; NA, FP, and JM provided sable movement data; ABP, MCH and RMP provided diet data; KMG and MSP provided camera trap data; MA, AP, and PB provided predator data; MES provided aerial survey data; RHW compiled figures and drafted the original manuscript draft; RMP and RAL supervised the research; all authors reviewed and edited the manuscript. In the third chapter: RHW, KAG, NRJ, and RAL conceptualized and designed the study; PDM and WPP developed software; RHW, KAG, NRJ, and JWM collected data; RHW conduced data analyses, compiled figures, and tables, and prepared the original manuscript draft; RAL, NJR, and JWM supervised and funded the study; all authors reviewed and edited the manuscript.

Chapter 1: Mechanisms of individual variation in large herbivore diets: roles of spatial heterogeneity and state-dependent foraging

Walker, R. H., M. C. Hutchinson, A. B. Potter, J. A. Becker, R. A. Long, and R. M. Pringle. 2022. Mechanisms of individual variation in large herbivore diets: roles of spatial heterogeneity and state-dependent foraging. *Ecology* e3921. https://doi.org/10.1002/ecy.3921.

Abstract

Many populations of consumers consist of relatively specialized individuals that eat only a subset of the foods consumed by the population at large. Although the ecological significance of individual-level diet variation is recognized, such variation is difficult to document and its underlying mechanisms are poorly understood. Optimal foraging theory provides a useful framework for predicting how individuals might select different diets, positing that animals balance the 'opportunity cost' of stopping to eat an available food item against the cost of searching for something more nutritious; diet composition should be contingent on the distribution of food, and individual foragers should be more selective when they have greater energy reserves to invest in searching for high-quality foods. We tested these predicted mechanisms of individual niche differentiation by quantifying environmental (resource heterogeneity) and organismal (nutritional condition) determinants of diet in a widespread browsing antelope (bushbuck, *Tragelaphus sylvaticus*) in an African floodplain-savanna ecosystem. We quantified individuals' realized dietary niches (taxonomic richness and composition) using DNA metabarcoding of fecal samples collected repeatedly from 15 GPS-collared animals (range 6–14 samples per individual, median 12). Bushbuck diets were structured by spatial heterogeneity and constrained by individual condition. We observed significant individual-level partitioning of food plants by bushbuck both within and between two adjacent habitat types (floodplain and woodland). Individuals with home ranges that were closer together and/or had similar vegetation structure (measured using LiDAR) ate more similar diets, supporting the prediction that heterogenous resource distribution promotes individual differentiation. Individuals in good nutritional condition had significantly narrower diets (fewer plant taxa), searched their home ranges more intensively (intensity-of-use index), and had higher-quality diets (percent digestible protein) than those in poor condition, supporting the prediction that animals with greater endogenous reserves have narrower realized niches because they can invest more time in searching for nutritious foods. Our results support predictions from optimal foraging theory about the energetic basis of individual-level dietary variation and provide a potentially generalizable framework for understanding

how individuals' realized niche width is governed by animal behavior and physiology in heterogenous landscapes.

Introduction

Classic niche theory and most models of trophic interactions assume that individuals in a population are ecologically equivalent (Voltera 1926, Hutchinson 1957, Macarthur and Levins 1967). Yet, many populations consist of relatively specialized individuals that use only a subset of the resources exploited by the population at large (Van Valen 1965, Bolnick et al. 2003, Araújo et al. 2011). Consistent differences among conspecific individuals can increase a population's resilience to disturbance (Reusch et al. 2005), influence competition and coexistence (Hart et al. 2016), and increase the probability of speciation events (Fryxell and Lundberg 1994). In strongly interacting species such as large mammalian herbivores, which shape community structure and ecosystem functions (Pringle et al. 2007, Ripple et al. 2015, Guy et al. 2021), individual-level diet variation may also have system-wide consequences. To date, however, few studies have investigated the occurrence and/or degree of individual diet variation in ungulates, let alone the mechanisms that produce it (but see, e.g., Bison et al. 2015, Pansu et al. 2019b, Jesmer et al. 2020).

Optimal foraging theory (OFT) provides one framework for predicting how individual herbivores should choose foods (MacArthur and Pianka 1966, Belovsky 1978, Owen-Smith and Novellie 1982, Stephans and Krebs 1986). OFT posits that animals should seek to maximize the average rate of energy intake, both in the choice of where to feed (i.e., the marginal value theorem; Charnov 1976) and in the diet chosen there (i.e., the basic prey model; Emlen 1966, Stephens and Krebs 1986) by balancing the 'opportunity cost' of stopping to consume an available food item against the cost of moving on to search for something more nutritious. Accordingly, individual diets are predicted to be contingent on encounter rate and the relative availability of profitable food items, which together should determine the amount of time a forager spends searching for preferred foods and whether a food item is accepted or rejected when it is encountered (MacArthur and Pianka 1966, Westoby 1974, Charnov 1976). Thus, in systems where high-quality foods are heterogeneously distributed, individual diets may be both differentiated and 'optimal' depending on the distribution of resources in each individual's home range (Stephens and Krebs 1986). Despite the prominent role of food distribution in OFT models, few studies have evaluated how landscape heterogeneity influences individual diet variation in wild populations (Araújo et al. 2011).

Experimental studies have shown that conspecifics select different diets even when exposed to identical resources (Parent et al. 2014), indicating that factors other than spatial heterogeneity shape patterns of

individual diet variation. State-dependent behavior—patterns of activity modulated by an individual's underlying physiological state (McNamara and Houston 1996)—might interact with resource distribution to drive dietary variation. Nutritional condition (i.e., energy reserves available for maintenance, growth, and reproduction; Parker et al. 2009) is a state variable with especially high potential for influencing the behavior of foraging animals (Cook et al 2013, Long et al. 2014). Animals in poor condition are weakly buffered against starvation, which decreases the opportunity cost of handling low-quality resources relative to searching for higher-quality food items (Mathot and Dall 2013). OFT predicts that foraging animals in poor condition should be less selective and more willing to accept lower-quality foods in order to maximized caloric yield per time by reducing energy invested in searching (Emlen 1966, Stephens and Krebs 1986, Owen-Smith et al. 2010). Simulations have supported this prediction by showing that optimal model foragers with greater energy reserves invest more time searching for high-quality food items than those with low energy reserves (Nonacs 2001). In addition, controlled experiments have shown that satiated individuals choose different prey than those that are less well-buffered against starvation (Perry 1987, Gill 2003). Despite this theoretical foundation, however, we know of no previous study that has explored state-dependent foraging behavior as a mechanism for generating individual dietary variation among free-ranging large herbivores.

We studied the interaction between environmental (resource heterogeneity) and organismal (nutritional condition) determinants of diet composition in bushbuck (*Tragelaphus sylvaticus*), a ~45-kg African bovid. We longitudinally sampled bushbuck diets in Mozambique's Gorongosa National Park by collecting multiple fecal samples from 15 GPS-collared individuals (6–14 samples per animal collected over 42–56 days). We analyzed these samples using DNA metabarcoding, enabling taxonomically precise measurement of diet composition and richness at the individual level (Kartzinel et al. 2015, Pansu et al. 2019b, Pringle and Hutchinson 2020). Bushbuck in Gorongosa show high fidelity to small (generally < 3-km^2) home ranges distributed across two broad habitat types (Atkins et al. 2019), which allowed us to evaluate the role of spatial resource heterogeneity at different scales (population level and partitioned by habitat affiliation) in generating individual diet differentiation. Further, bushbuck are non-seasonal breeders, leading to wide variation among individuals in reproductive status and associated nutritional condition (owing to the high costs of gestation and lactation; Cook et al. 2013). This life-history trait allowed us to evaluate the role of state-dependent foraging behavior in shaping individual diets.

We hypothesized that diet selection is constrained by spatial variation in the distribution of food plants because foragers with small home ranges, high site fidelity, and limited mobility have only a subset of the population-level resource base available to them. Based on this hypothesis, we predicted that (a) individuals consistently eat distinct diets (i.e., each individual uses a small fraction of the food plants used

by the population at large) and (b) dietary dissimilarity between individuals increases as a function of the distance and vegetation dissimilarity between home ranges. We further hypothesized that state-dependent foraging behavior is a key mechanism generating variation in diet selection among conspecific individuals because trade-offs faced by consumers (e.g., forage intake vs. search time) are modulated by nutritional condition. Accordingly, we predicted that bushbuck in better condition have less variable diets because they invest more time searching for the best food items and thus (a) accept fewer food types (leading to lower dietary richness), (b) search their home ranges more exhaustively (higher intensity-of-use index), and (c) have diets that are higher quality on average (higher percent digestible protein) than individuals in poor condition.

Methods

Study site and species

Gorongosa is situated at the southern end of the Great Rift Valley (-18.97, 34.35; Figure 1.1ab). Our study site at the southern end of the park comprises two main habitat types: savanna woodland and floodplain grassland (Figure 1.1c; Stalmans et al. 2019, Atkins et al. 2019, Becker et al. 2021). These habitats have very different plant communities (Figure 1.1de; Figure A.1). The woodland is a mix of *Acacia*, *Combretum*, and palm savanna dotted with termitaria thickets; the floodplain is an open and comparatively homogeneous landscape of grasses, forbs, and subshrubs (Stalmans and Beifuss 2008). The majority of annual rainfall (700-900 mm; Stalmans et al. 2019) occurs during the wet season (November–April), and primary productivity peaks during this period. Food and water become increasingly limited as the dry season advances. We quantified bushbuck diets during the mid-dry seasons (June–August) of 2018 and 2019.

Bushbuck are spiral-horned antelopes (Bovidae: Bovinae: Tragelaphini) that occur widely across sub-Saharan Africa. They are solitary but not aggressively antisocial, such that home ranges overlap and individuals often forage in close proximity (Estes 1991). As strict browsers, bushbuck feed almost exclusively on trees, shrubs, and forbs to the exclusion of grasses (Pansu et al. 2019b, Kartzinel and Pringle 2020, Potter et al. 2022). Bushbuck also use woody plants for concealment and are considered "dependent on thick cover" for predator avoidance (Kingdon 1997: 352). In Gorongosa, however, bushbuck have increasingly occupied the Lake Urema floodplain over the last 20 years; in that period, large-mammal populations were recovering from >90% declines during the Mozambican Civil War (1977-1992) and predation risk was low, enabling bushbuck to expand into the treeless floodplain (Atkins et al. 2019). By 2018, ungulate biomass in Gorongosa had recovered to nearly pre-war levels, with large

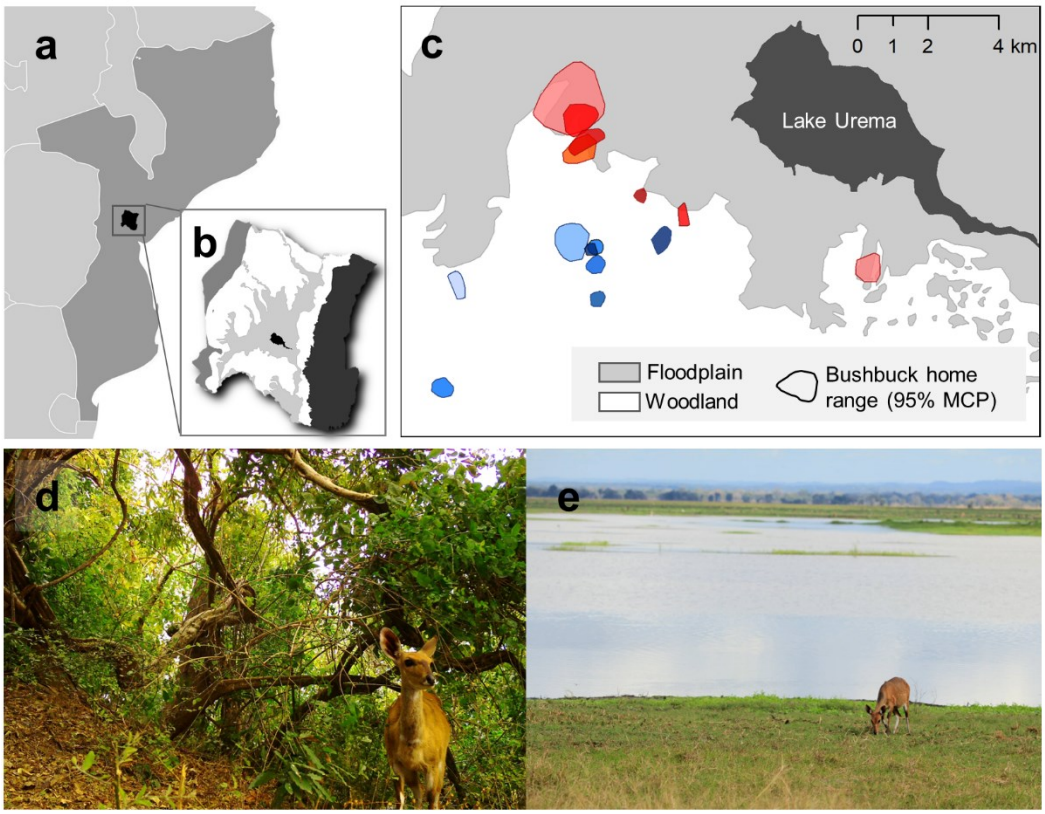

Figure 1.1. Bushbuck habitat affiliations in Gorongosa National Park, Mozambique. Gorongosa is located in central Mozambique (**A**) and consists of four major habitat zones (**B**, from left, western escarpment (medium grey), woodland (white), floodplain (light grey), eastern escarpment (dark grey) and Lake Urema (black)). Bushbuck home ranges (95% minimum convex polygons) are drawn within our study area in (**C**); blue polygons (different shades indicate different individuals) represent individual home ranges that lie only within woodland habitat, whereas red polygons represent individual home ranges that overlap with floodplain habitat. A female bushbuck foraging in typical woodland habitat (i.e., mix of Acacia-Combretum and Hyphaene palm savanna) is illustrated in (**D**); photo credit: R.H.W. A female bushbuck foraging in typical floodplain habitat (i.e., open landscape of grasses, forbs, and subshrubs) is illustrated in E; photo credit: M.C.H.

populations of mid-sized browsing antelopes, including 1,700 bushbuck, 1,900 nyala (*T. angasii*), 1,900 kudu (*T. strepsiceros*), and 6,000 impala (*Aepyceros melampus*) (Stalmans et al. 2019). Lions (*Panthera leo*) were the dominant top carnivore (≥100 individuals), but bushbuck were not among their recorded prey (Bouley et al. 2018). African wild dogs (*Lycaon pictus*) and leopards (*P. pardus*) were extirpated during the war, but a pack of 14 wild dogs was reintroduced in June 2018 (the start of our study) and have fed heavily on bushbuck (Bouley et al. 2021); at least one leopard was also present in the area by 2018. Thus, Gorongosa's large-mammal fauna was abundant and nearly intact at the time of our study, but species' relative abundances remained skewed and predation pressure low (but increasing) relative to the pre-war baseline.

Animal handling and condition measurements

In June of 2018 and 2019 we captured adult female (n = 20) and male (n = 10) bushbuck as part of the long-term ASHAMED study (Allometry of Spiral-Horned Antelopes: Movement Ecology & Diet). We chemically immobilized bushbuck via remote injection (1.5–2.5 mg Thiafentanil, 50–60 mg Ketamine, 10–15 mg Azaperone) from a vehicle. Darts were equipped with radio-transmitters to facilitate recovery of darted individuals. We fit each individual with an iridium satellite GPS collar (VERTEX Lite, Vectronic Aerospace) programmed to record hourly locations and equipped with a VHF transmitter that we used to relocate collared individuals for diet sampling via radio telemetry. GPS collars were remotely triggered to drop off one year after deployment.

We collected a fecal sample (>5 pellets) from the rectum of each immobilized bushbuck for molecular analysis (see *Diet analysis*). For female bushbuck, we used an ultrasound (Ibex Pro, EI Medical Imaging) to confirm presence of a fetus and palpated the udder to determine lactation status (lactating or not lactating). For each individual, we collected body measurements (weight, body and hind-foot length, chest girth), ultrasonography data (maximum rump-fat depth, thickness of biceps femoris and longissimus dorsi muscles), and palpation scores at the sacrosciatic ligament, lumbar vertebrae, sacrum, base of the tail, and caudal vertebrae (based on protocols developed for North American ungulates; Cook et al. 2010, Stephenson et al. 2020). Because equations for converting these measurements to an estimate of ingesta-free body fat have not been validated for African ungulates, we followed Atkins et al. (2019) and Becker et al. (2021) in using principal component analysis to develop an index of relative nutritional condition (Tables A.1-2, Figure A.2). All animal-handling procedures were approved by the Animal Care and Use Committees of the University of Idaho (#IACUC-2019-32) and Princeton University (#2075F-16) and followed guidelines established by the American Society of Mammologists (Sikes et al. 2016).

Habitat and space-use analyses

We used 95% minimum convex polygons (MCP) derived from a subset of the hourly GPS-location data to estimate individual bushbuck home ranges during the diet-sampling period in each year (June – August; Table A.3). We used two complementary approaches to assess the role of spatial heterogeneity in structuring diet composition. First, following Tobler's (1970) first law of geography ("everything is related to everything else, but near things are more related than distant things"), we calculated the distance between each pair of bushbuck home-range centroids (the arithmetic mean position of GPS fixes from each individual) as a proxy for similarity of the vegetation communities available to bushbuck. We lacked home-range-specific measurements of plant community composition, but we verified that plant community dissimilarity increased with geographic distance, both between and within habitats (see *Supplemental Text*; Figure A.3). Second, we quantified dissimilarity of vertical vegetation structure

between each pair of bushbuck home ranges using airborne light detection and ranging (LiDAR) data collected in August 2019 (Wooding Geospatial Solutions Ltd.). LiDAR flights were conducted at 880 m above ground level at 110 knots; the resulting terrain and vegetation elevation measurements had a horizonal spatial resolution of 0.5 m and a vertical resolution of 0.1 m. For each home range, we calculated the proportion of LiDAR points classified as ground (0 m), low vegetation (<0.3 m), medium vegetation (0.3–1.6 m), and high vegetation (>1.6 m), following guidelines of the American Society for Photogrammetry and Remote Sensing (ASPRS 2008). We then calculated the Bray-Curtis index of compositional dissimilarity in vegetation structure (proportion of LiDAR points classified as ground, low, medium, and high) between each pair of bushbuck home ranges.

We quantified differences in searching behavior by bushbuck within their home ranges using the intensity-of-use index (Hailey and Coulson 1996, Loretto and Vieira 2005, Almeida et al. 2019). We calculated intensity of use as the ratio of total movement distance to the square of the area of movement (100% MCP) during the diet sampling period for each bushbuck (Table A.3) using the *intensity_use* function in the *amt* package (Singer et al. 2019) in R (version 3.5.3, R Core Team 2018). Bushbuck sampled in 2019 had hourly GPS data only during the first 21 days after capture, owing to a change in sampling rate required for a separate research project; thus, we restricted all GPS data to 21 days after capture to avoid bias due to unequal sample sizes. Results using restricted vs. full data sets were qualitatively equivalent (Figure A.4). Although this index does not distinguish among active behaviors (e.g., cannot distinguish movements related to searching for food versus seeking shade), intensity of use is proportional to the time spent active per unit of area and increases when animals (*i*) follow highly tortuous paths, (*ii*) move slowly, or (*iii*) perform search loops (Almeida et al. 2019). Thus, the index quantifies how active bushbuck are within their home ranges, enabling us to test the prediction that bushbuck in good condition spend more time searching than do individuals in poor condition (see *Statistical analyses).*

DNA metabarcoding

We quantified bushbuck diet composition using fecal DNA metabarcoding following protocols that we have previously used to study herbivore diets in Gorongosa (Atkins et al. 2019, Branco et al. 2019, Pansu et al. 2019b, Guyton et al. 2020. Becker et al. 2021, Potter et al. 2022). After collecting an initial fecal sample at the time of capture, we used radio telemetry to relocate each collared bushbuck every 1–2 days. Upon relocation we confirmed individual identity via an ID number written on the collar belting and then observed individuals for up to 2 hours from distances of 5–100 m (depending on the density of vegetation and wariness of the animal). Bushbuck typically returned to a non-vigilant state (eyes not fixated on the observer and ears relaxed while resting or foraging) after <10 minutes of observation. We observed

individuals until they defecated, whereupon we recorded their distance from the observer and the nearest landmarks to the defecation site. We then searched that area for the fresh fecal sample, selected >5 debris-free fecal pellets using nitrile gloves and deposited them in an unused plastic zip bag. We stored samples on ice for <6 hours before pre-processing them in Gorongosa's laboratory as follows. We homogenized each fecal sample and transferred a pea-sized subsample into a labeled tube containing silica beads and buffer (Xpedition Stabilization/Lysis Solution, Zymo Research Corporation). We vortexed samples to lyse cells and froze them at -20°C pending transport to Princeton University, where we stored them at -80°C. Prior to transport, we subjected each sample to an antiviral heat treatment (72°C for 30 minutes) as mandated by the US Department of Agriculture (permit #130123 to RMP).

DNA extraction and PCR were conducted in a Biosafety Level 2 facility dedicated to fecal DNA analysis, with physically separated pre- and post-PCR rooms and laminar flow hoods for PCR preparation. We extracted DNA from each sample in a biosafety cabinet using Zymo Xpedition Soil/Fecal MiniPrep kits (as per manufacturer protocols) in batches of 29 samples and 1 negative extraction control. In triplicate PCR replicates of each sample, we amplified the P6 loop of the chloroplast *trn*L(UAA) intron, a standard region for metabarcoding degraded plant DNA, using primers with a unique 8-nt tag at the 5' end that enabled pooling of uniquely identifiable PCR products for sequencing in a single high-throughput run (Taberlet et al. 2007).

A detailed description of the laboratory and bioinformatic protocols used to analyze our samples is in Guyton et al. (2020). Briefly, sequencing was performed on an Illumina HiSeq 2500 and data were processed using the OBITools pipeline (Boyer et al. 2016). Sequences of low quality (low alignment score, unexpected barcode length, ambiguous nucleotides, singletons) were discarded; the remaining sequences were considered molecular operational taxonomic units (mOTUs, 'taxa') and identified by primary comparison to a local plant DNA reference library collected in Gorongosa (Pansu et al. 2019a) and secondary comparison to a global database compiled from the European Molecular Biology Laboratory (release 134) only if the local library assignment score was <98%. After filtering, we averaged the number of reads across all retained PCR replicates for each sample and removed mOTUs accounting for <1% of reads per sample (Guyton et al. 2020). We rarefied sample read depth to 7,000 to facilitate comparisons among samples. From these data, we determined the presence/absence and relative read abundance (RRA) of each plant taxon in each sample, which we used to quantify individual dietary richness and variation (Walker et al. 2022). Results in the main text are based on RRA (as are Table A.4, Figures A.5-6), which is an informative proxy for the proportional consumption of plant taxa in comparative analyses of large-herbivore diets using the *trn*L-P6 markers (Willerslev et al. 2014, Craine et al. 2015, Kartzinel et al. 2015) and generally provides a more robust portrait of diet composition than

occurrence-based data (Deagle et al. 2019) as the latter inflate the importance of uncommon food items (which in turn account for the majority of foods in vertebrate diets; Hutchinson et al. 2022). While RRA is subject to several sources of error that can influence the proportional representation of particular plant taxa (e.g., amplification bias, differential digestion, variation in chloroplast density) and is thus an imperfect reflection of true biomass consumption, any systematic biases should be consistent across the samples analyzed here, and idiosyncratic biases should be mitigated by our standardized pipeline and quality-control steps (Deagle et al. 2019). As a further sensitivity check, we also present results based on presence/absence data which yielded similar inferences about the generality of individual niche differences and their dependence on spatial heterogeneity (Table A.5, Figures A.7-10).

We were unable to obtain a fecal sample from every individual during every observation period, which resulted in unequal sample sizes across individuals. We limited our analyses to individuals for which we obtained ≥6 samples in the two months after collaring (Table A.3). For analyses of individual variation and dietary richness (which require multiple samples per individual and may be sensitive to which samples are included for each individual; see *Statistical analyses*), we rarified to 6 samples per individual and performed the statistical test in each of 1,000 re-sampling iterations (bootstrapping). For other analyses that require just one measure of diet per individual (see *Statistical analyses*), we calculated 'standardized diets' for each individual as the mean RRA of each mOTU across 1,000 bootstrapping iterations.

Diet quality

Dry-season digestible protein (DP) content of foliage from 204 of Gorongosa's most common plant species was quantified as part of a concurrent study (Potter et al. 2022). We estimated the quality of individual bushbuck diets by calculating weighted average of DP in the standardized diet of each bushbuck using the RRA of each mOTU as the weighting factor (Atkins et al. 2019, Branco et al. 2019, Becker et al. 2021, Walker et al. 2022). While this approach is subject to the caveats above about the quantitative interpretation of RRA (see *DNA metabarcoding*), we verified our RRA-based results with occurrence (presence/absence) data by calculating the weighted average of DP with each plant mOTU in bushbuck diets weighted equally (Figure A.10). Plant taxa for which nutrient data were available accounted for a median of 98% of standardized bushbuck diets (range 83-100%).

Statistical analyses

We tested each of our predictions at two scales: the population level and partitioned by habitat affiliation (floodplain or woodland). Following Atkins et al. (2019), we classified bushbuck as "floodplain-associated" if their home range (95% MCP) overlapped with the treeless floodplain grassland during the sampling period (Figure 1; Table A.3). Floodplain-associated bushbuck (n = 7) spent an average of 40%

(range 6-71%) of their time in this treeless interior of the floodplain, differentiating them from bushbuck that spent 0% of their time in the floodplain grassland ('woodland-associated' bushbuck; n = 8).

We calculated the Bray–Curtis index of compositional dissimilarity between each pair of fecal samples and ordinated the values using non-metric multidimensional scaling (NMDS) to visualize patterns of dietary dissimilarity both within and among individual bushbuck (Kartzinel et al., 2015, Pansu et al., 2019b). To test our prediction that individuals consistently eat distinct diets, we conducted permutational multivariate analysis of variance (perMANOVA) on the Bray-Curtis distance matrix for each pair of fecal samples, running 9,999 permutations with year (2018 or 2019) as a blocking factor to control for any year effects and individual ID as the main predictor (*adonis2* in the *vegan* package in R; Oksanen et al. 2020). To test for pairwise differences among bushbuck diets, we conducted post-hoc tests using a Holm-Bonferroni adjustment to control for the familywise error rate both across and within habitats (*pairwise.adonis* in the *funfuns* package in R; Holm 1979, Trachsel 2021).

To test our prediction that bushbuck occupying home ranges with similar forage availability (proxied by distance between home-range centroids; see *Appendix A: Supplemental Text,* Figure A.3) and vegetation structure would consume similar diets, we used Mantel tests (Pansu et al. 2019b) to evaluate relationships between pairwise inter-individual dissimilarity of standardized diets (Bray-Curtis distance) and (*i*) pairwise geographic distance between home-range centroids, and (*ii*) pairwise dissimilarity of vegetation structure (Bray-Curtis distance).

We used linear regressions to evaluate the relationship between nutritional condition and intensity of use, percent dietary DP, and dietary richness to test our prediction that bushbuck in better nutritional condition invest more time searching for high-quality foods and thus have less variable diets than bushbuck in poorer condition. We calculated population-level dietary richness as the mean number of mOTUs present in all standardized bushbuck diets across bootstrapping iterations. We calculated individual dietary richness as the mean number of mOTUs in each bushbuck's standardized diet across bootstrapping iterations. To evaluate the influence of nutritional condition on dietary richness relative to other factors, we fit competing multiple regression models that included nutritional condition, reproductive state (lactating female, non-lactating female, or male), and habitat affiliation (woodland or floodplain) as candidate predictors. We ranked models using Akiake's information criterion for small sample size (AICc) and evaluated relative model performance by calculating Akaike weights (AIC$\widehat{w}$) (Burnham and Anderson 2002). To assess the importance of longitudinal sampling for accurately characterizing individual diets, we (*i*) re-ran all analyses using one randomly drawn sample from the full suite of samples collected from each individual to estimate dietary richness (averaged over n = 1,000 random trials), (*ii*) compared these estimates with those from standardized longitudinal bootstrapping (n = 6 per

individual) using Welch's two-sample *t*-tests, and (*iii*) plotted species-accumulation curves (*spaccum* function in the *vegan* package in R; Oksanen et al. 2020) to evaluate how the cumulative number of mOTUs present in a bushbuck diet varied as a function of sample size using all samples per individual (Soberon and Llorente 1993, Colwell and Coddington 1994).

Results

Role of spatial heterogeneity in individual diet variation

Population-level dietary richness was 95.6 ± 3.34 taxa (mean ± *SD* across 1,000 resampling iterations), whereas individual-level dietary richness ranged from 12.8 ± 1.44 to 31.1 ± 3.40 taxa (mean ± *SD* among all individuals = 21.2 ± 5.81). Thus, individual diets comprised 13–33% of the total plant taxa used by the population.

After controlling for year effects, we observed marked differences in diet composition among individuals both at the population level (perMANOVA: pseudo-$F_{14,144}$ = 15.21, $P < 0.001$, $R^2 = 0.60$) and within habitat types (woodland: pseudo-$F_{7,80} = 9.97$, $P < 0.001$, $R^2 = 0.47$; floodplain: pseudo-$F_{6,62} = 8.39$, $P < 0.001$, $R^2 = 0.45$); 96% of 105 pairwise contrasts between individuals were statistically significant after controlling for multiple comparisons (Table A.4). These differences are clear in NMDS ordinations of all samples collected per individual (Figure 1.2). Notably, we observed strong shifts in the diets of two females that moved from woodland into the floodplain immediately after capture: the sample collected at capture from each of these individuals reflects a woodland-type diet while the rest are characteristic of floodplain-affiliated animals (Figure 1.2a). The two initial samples from these individuals were excluded from floodplain-specific diet analyses.

The location and vegetation structure of bushbuck home ranges strongly influenced diet composition. Geographic distance between home-range centroids, our validated proxy for plant community dissimilarity (see: *Appendix A: Supplemental Text*; Figure A.3), was positively related to dietary dissimilarity between individuals at the population level (Mantel test, $P < 0.001$; Figure 1.3a) and within woodland habitat (Figure 1.3b) but not within floodplain (Figure 1.3c). Similarly, dissimilarity in vegetation structure between home ranges was positively related to dietary dissimilarity at the population level and in woodland (Mantel test, $P < 0.001$; Figure 1.3de) but not in the floodplain (Figure 1.3f). Analyses based on occurrence-based dietary data in lieu of RRA gave similar results (Figure A.9).

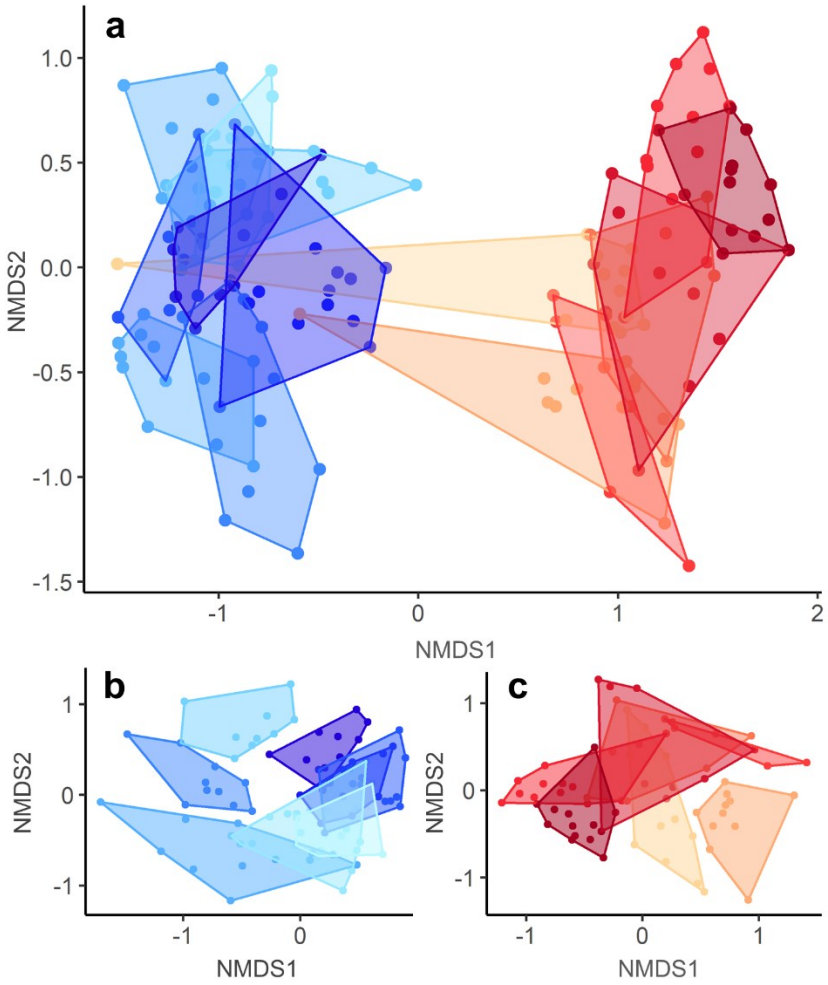

Figure 1.2. Non-metric multidimensional scaling (NMDS) ordinations showing relative dissimilarity in the taxonomic composition of individual fecal samples (points; n = 160) and dry-season diets (polygons; n = 15) of bushbuck in Gorongosa. Results for the full population are shown in (**A**), and results partitioned by habitat association are shown in (**B**) (woodland, blue) and C (floodplain, red). Points in closer proximity to one another indicate more similar diets; polygons are convex hulls around all samples from each individual. Two individuals captured in woodland habitat moved into the floodplain shortly after collaring (outlying red points in A are those collected at capture); we excluded the initial woodland samples from these individuals from our analysis of floodplain diets (**C**). We observed significant differences among individual diets both at the population level (perMANOVA: pseudo-$F_{14,144}$ = 15.21, $P < 0.001$, $R^2 = 0.60$) and within habitat types (woodland: pseudo-$F_{7,80}$ = 9.97, $P < 0.001$, $R^2 = 0.47$; floodplain: pseudo-$F_{6,62} = 8.39$, $P < 0.001$, R^2 = 0.45).

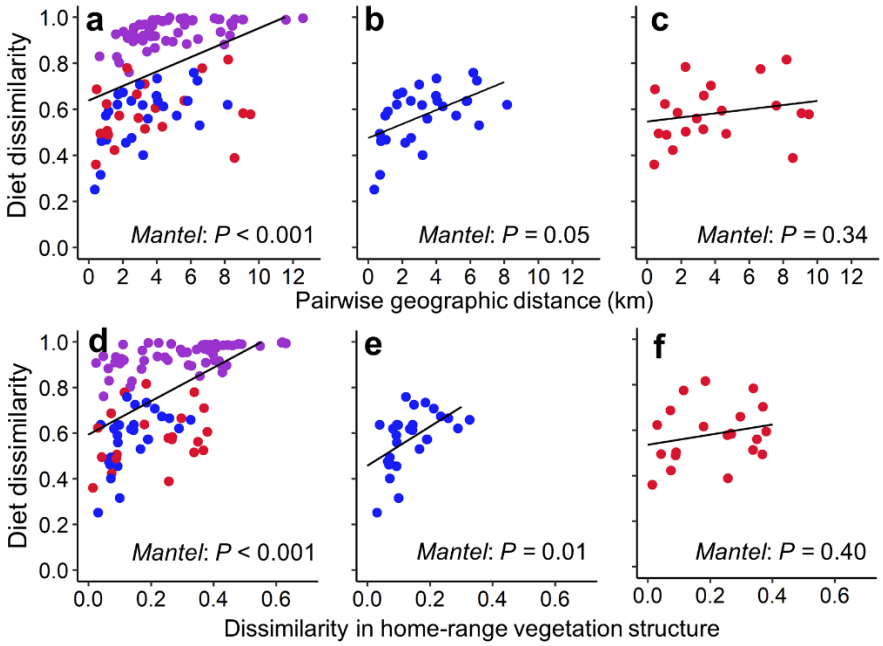

Figure 1.3. Relationships between bushbuck diet composition and spatial variation in the distribution of resources at Gorongosa. We evaluated the relationship between pairwise diet dissimilarity (Bray-Curtis index) and distance between home-range centroids (km) for all pairs of GPS-collared bushbuck (**A**), bushbuck with home ranges affiliated with woodland habitat (**B**), and those affiliated with floodplain habitat (**C**). Additionally, we evaluated the relationship between pairwise diet dissimilarity and dissimilarity in home-range vegetation structure (Bray-Curtis index) between all pairs of GPS-collared bushbuck (**D**), bushbuck with home ranges in woodland habitat (**E**), and bushbuck with home ranges in floodplain habitat (**F**). Blue points illustrate comparisons between pairs of woodland-affiliated individuals, red points between pairs of floodplain-affiliated individuals, and purple points between woodland- and floodplain-affiliated individuals. We quantified vegetation structure by calculating the proportion of LiDAR points classified as ground-level, low, medium, and high vegetation, and by using the Bray-Curtis index to quantify pairwise compositional dissimilarity between home ranges based on those proportions. P-values in each panel are from Mantel's permutation tests for similarity between two matrices.

Role of state-dependent foraging in individual diet variation

Nutritional condition influenced bushbuck searching behavior, diet quality, and dietary richness. Bushbuck in better condition had higher intensity-of-use indices—i.e., spent more time actively searching their home ranges per unit area—than those in poorer condition. This correlation was evident at the population level ($\beta_{condition} = 24.3$, $P < 0.001$, $R^2 = 0.49$; Figure 1.4a) and within each habitat (woodland: $\beta_{condition} = 32.3$, $P = 0.07$, $R^2 = 0.37$; floodplain: $\beta_{condition} = 24.9$, $P = 0.01$, $R^2 = 0.71$; Figure 1.4bc), as well as when we used all hourly GPS locations collected during the diet sampling period instead of limiting them to the first 21 days after capture (Figure A.4).

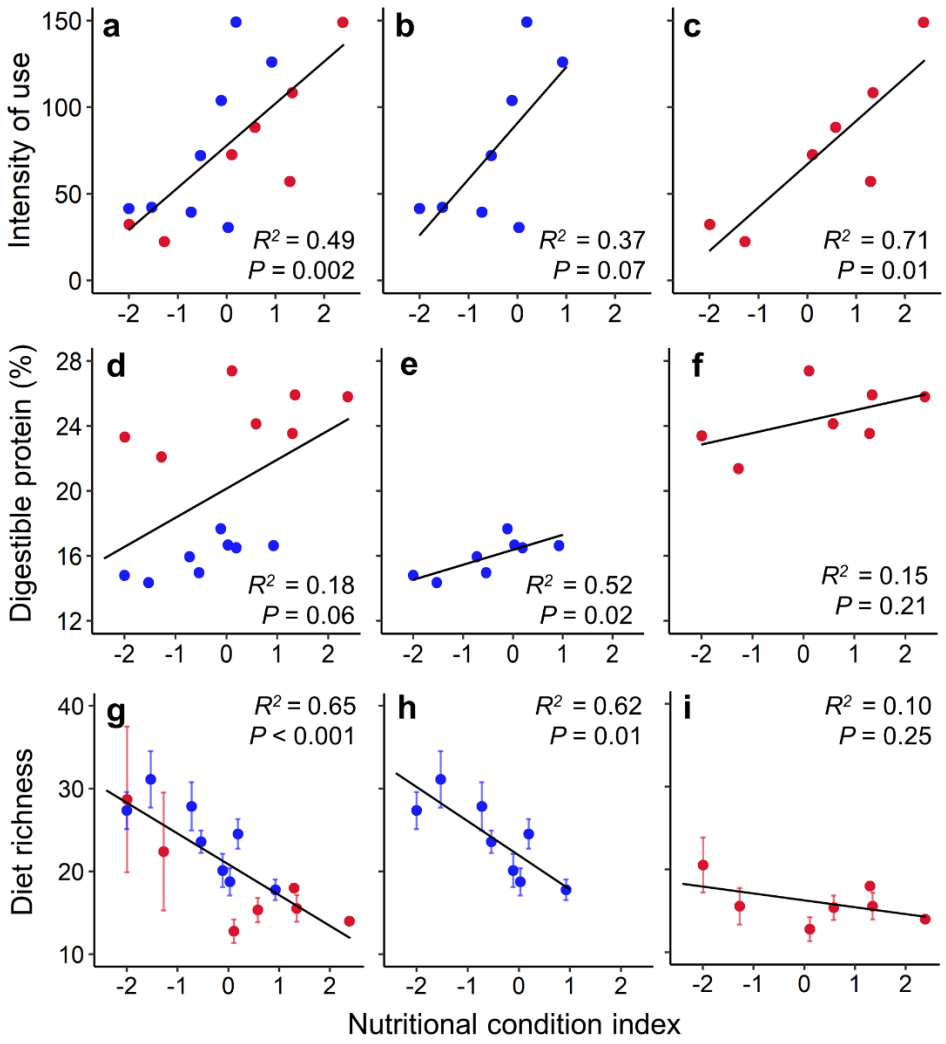

Figure 1.4. Relationships between a multivariate index of nutritional condition (see *Methods*) and bushbuck foraging behaviors in Gorongosa. Blue points represent bushbuck with home ranges affiliated with woodland habitat; red points represent bushbuck with home ranges affiliated with floodplain habitat. Consistent with predictions of optimal foraging theory, individuals in good nutritional condition searched their home ranges more intensively (**A**) and had higher-quality (**D**), narrower diets (**G**; mean ± SD unique mOTUs). These relationships were still evident when we analyzed only bushbuck that lived within woodland habitat (**B,E,H**), but not for bushbuck that lived within floodplain habitat (**C, F, I**). R^2 and P-values are from ordinary least-squares linear regression models.

Bushbuck in better condition tended to eat higher-quality diets (DP: $\beta_{condition} = 1.79$, $P = 0.06$, $R^2 = 0.18$; Fig. 4d). This population-level trend was driven by the higher average values of nutritional condition and dietary DP in the floodplain (Welch's two sample *t*-test: $\overline{DP}_{floodplain} = 24.5$, $\overline{DP}_{woodland} = 15.9$, $P < 0.001$). However, nutritional condition was also positively correlated with dietary DP within woodland ($\beta_{condition} = 0.92$, $P = 0.03$, $R^2 = 0.52$; Figure 4e), whereas we found no correlation within the floodplain ($\beta_{condition} = 0.07$, $P = 0.21$, $R^2 = 0.15$; Figure 4f).

Bushbuck in better condition had lower dietary richness (narrower realized niches) than those in poorer condition (Figure 1.4g). Indeed, nutritional condition was the sole predictor variable in the best regression model of diet richness ($\beta_{condition}$ = -3.71, $P < 0.001$, $R^2 = 0.65$) and was included in all of the top four candidate models (Table 1.1). This relationship held for bushbuck in woodland habitat ($\beta_{condition}$ = -4.12, $P = 0.01$, $R^2 = 0.62$) but was not observed among bushbuck in the floodplain ($\beta_{condition}$ = -0.083, $P = 0.25$, $R^2 = 0.10$) (Figure 4h,i). Analyzing dietary Shannon diversity in lieu of richness gave qualitatively similar results (Figure A.11). The size of bushbuck home ranges was not related to individual dietary richness (Figure A.12).

Table 1.1. Competing multiple regression models for explaining variation in individual dietary richness. 'Habitat' is a categorical indicator of which habitat type (floodplain or woodland) affiliated with each bushbuck home range. 'Lactation' is a categorical indicator of reproductive status (lactating, non-lactating, or male). We included these covariates to control for variation in diet richness unaccounted for by nutritional condition (see *Methods*).

Model	Adj. R^2	ΔAICc	AICŵ
Nutritional Condition	0.65	0	0.541
Nutritional Condition + Habitat	0.70	0.433	0.436
Nutritional Condition + Lactation	0.63	6.843	0.018
Nutritional Condition + Habitat + Lactation	0.65	10.173	0.003
Habitat	0.21	12.244	0.001
Lactation	0.27	14.807	0.000
Habitat + Lactation	0.27	16.940	0.000

Role of longitudinal sampling in inferences about individual diet variation

Analyzing a single diet sample per individual underestimated diet breadth: diets inferred from one sample had <50% of the food-plant richness estimated from standardized longitudinal sampling (Welch's two sample *t*-test: $\bar{X}_{single} = 10$, $\bar{X}_{longitudinal} = 21$, $P < 0.001$). Species-accumulation curves showed that even 6 or 10 samples were not universally sufficient for individual dietary richness to asymptote (Figure A.13), despite being far greater than the (typically single) individual sample size commonly used in studies of individual diet variation in ungulates (Bison et al. 2015, Pansu et al. 2019b, Jesmer et al. 2020) and other taxa (Araujo et al. 2011).

Discussion

Although patterns of diet variation and individual specialization have been documented in diverse taxa (Bolnick et al. 2003, Araújo et al. 2011), empirical investigation of the mechanisms that lead to differentiation among individuals is limited. This is especially true for large herbivores, which are often depicted as highly generalized consumers but may in fact specialize on narrow sets of plant taxa (Hutchinson et al. 2022). By drawing on the ability to repeatedly sample individual diets with high taxonomic resolution, we show that bushbuck eat distinct subsets of the foods used by the population across both large and small spatial scales. We further show that individual differences in diet richness and composition arise from two complementary mechanisms: spatial heterogeneity in resource distribution and variation in nutritional condition among individuals. These findings are consistent with predictions from OFT about the energetic underpinnings of individual specialization, suggesting a potentially generalizable framework for understanding how individual's realized dietary niches are constrained by behavior and physiology.

Spatial heterogeneity structures individual dietary niche

OFT predicts that the opportunity cost of stopping to consume an available food item versus the cost of moving on to search for a more nutritious food item is modulated by the distribution of high-quality food across the landscape (e.g., marginal value theorem and basic prey choice models; Emlen 1966, MacArther and Painka 1966, Charnov 1976). Thus, individual dietary differences should emerge in environments where food types are heterogeneously distributed and each forager's search area is limited. Consistent with these predictions, we observed significant differences among bushbuck diets both at the population level and within habitat types. Much of the individual dietary variation we observed stemmed from differences in the structure and composition of food plants among bushbuck home ranges, as evidenced by both the clear separation of woodland- and floodplain-associated bushbuck diets and the interactive effect of landscape heterogeneity and home-range location on individual dietary niches. In general, bushbuck that lived closer together (and thus had access to more similar food plants; Appendix S4) and had similar vegetation structure within their home ranges consumed more similar diets.

These trends were not significant for floodplain bushbuck, despite generally pronounced individual niche differences in that habitat. This might at first seem intuitive, given that the treeless floodplain interior is structurally homogenous relative to woodland (Figure A.1). Yet floodplain bushbuck varied in their use of the savanna at the floodplain edge (Figure 1.1c), such that the range of structural dissimilarity between floodplain home ranges was as great as that in woodland (Figure 1.3ef); moreover, plant community dissimilarity increased with geographic distance within and across habitats (Figure A.3). We hypothesize that the weak influence of distance and structural dissimilarity on diet differentiation in the floodplain

stems from the more uniformly high-quality forage in that habitat (Atkins et al. 2019, Becker et al. 2021), where flooding annually resets succession and replenishes soil nutrients (Tinley 1977). Floodplain diets were uniformly lower in richness and higher in DP than woodland diets (Figure 1.4), and the top-5 floodplain food taxa (*Mimosa pigra*, *Ludwigia adscendens*, *Ambrosia maritima*, *Faidherbia albida*, *Bergia mossambicensis*) collectively accounted for >50% of each individual's standardized diet and were among the most protein-rich plants in either habitat (Walker et al. 2022). By foraging selectively on a subset of abundant, high-quality plants in their home ranges, floodplain bushbuck might decouple individual dietary variation from the geographic structure in plant community composition. In this respect, our null results in that habitat would be consistent with OFT, because trade-offs between intake and search time are relaxed in environments with a homogenous distribution of high-quality food.

Despite the importance of resource abundance and distribution in theoretical models of prey choice (Stephans and Krebs 1986) and niche differentiation (Van Valen 1965), few studies of diet variation and individual specialization in wild populations explicitly consider the role of resource distribution in driving differences among individuals (Araújo et al. 2011). Consequently, there is little empirical support for the rather intuitive prediction that segregation across habitat types leads to greater diet differentiation among individuals (Araújo et al. 2011; but see: Layman et al. 2007, Darimont et al. 2009). Our results show that the spatial distribution of resources influences diet composition across scales, underscoring the importance of incorporating measures of resource availability into future studies of individual diet differentiation. Further exploration of the role of landscape heterogeneity would benefit from detailed data on food-plant availability and palatability. However, the latter is extremely difficult to quantify for free-ranging animals, and our results show that even selectivity (use relative to availability) is hard to measure at the individual level. For example, we have shown that the subpopulation of bushbuck in Gorongosa's floodplain strongly selects for the shrub *M. pigra* (Pansu et al. 2019b), but accurate individual-level assessment would entail measuring plant availability within each bushbuck's home range.

The effects of landscape heterogeneity on dietary specialization could have important implications for herbivore community dynamics. Population-wide, bushbuck diets include plant taxa from both woodland and floodplain habitats, which should relax intraspecific competition via niche complementarity (Bolnick et al. 2011) but leads to higher dietary overlap with heterospecific competitors (Pansu et al. 2019b). The impacts of such diffuse interspecific niche overlap on species coexistence and population abundance remain unresolved; theoretically, alternative outcomes are possible. On the one hand, individual variation can destabilize coexistence by weakening between-species niche differences and compounding the effects of demographic stochasticity; on the other, it can ease interspecific competition and dampen population fluctuations across heterogeneous landscapes (Bolnick et al. 2011, Hart et al. 2016, Stump et al. 2022).

Evaluating the strength and outcomes of interspecific competition in antelopes remains a formidable challenge (Prins 2016), and our study highlights the need to incorporate intraspecific niche variation in this effort.

State-dependent foraging constrains individual diet variation

OFT models of patch use and prey choice predict that in heterogenous resource landscapes, individuals with high energy reserves should invest more time searching, be more discriminating, and thus have narrower, higher-quality diets than individuals that are less well buffered against starvation (Emlen 1966, Mathot and Dall 2013). We found that bushbuck in better condition generally searched their home ranges more intensively for less diverse but more nutritious diets than bushbuck in poorer condition. This pattern diverged only in the floodplain, where the trade-off between search time and food quality is relaxed and the corresponding relationships between nutritional condition, search intensity, and diet quality are therefore expected to dissipate. These results are consistent with OFT (Emlen, 1966, Svänback and Bolnick 2005) and with simulation models of state-dependent foraging showing that individuals with higher energy reserves search longer for higher quality food (Nonacs 2001). Moreover, experimental work has demonstrated that animals at higher risk of starvation are less 'choosy' when selecting among food types or patches (Barnett et al. 2007), suggesting that our findings may be general across diverse taxa.

State-dependent foraging can result in consistent dietary differences among individuals when positive feedbacks exist between nutritional condition and constraints on forage selection (i.e., individuals in good condition face fewer constraints; Sih et al. 2015). In this 'rich get richer' scenario, differences in diet variation between individuals in good versus poor condition should be sustained through time (Bolnick et al. 2003). Such 'disruptive' intraspecific resource partitioning, in which some individuals are able to be increasingly specialized while others are forced to remain generalized, is reported less frequently than the scenario in which all individuals are similarly specialized on subsets of the population-level diet (Estes et al. 2003, Araujo et al. 2011, Vander Zanden et al. 2013; but see West 1986, Darimont et al. 2007, Jesmer et al. 2020), and may be a potent selective force insofar as differences in condition are correlated with fitness. State-dependent behavior may thus provide a mechanistic explanation for patterns of nested resource partitioning (Araújo et al. 2010, Calson et al. 2021) which, under OFT, emerge when individuals share similar food preferences but differ in the degree to which they accept less-preferred resources (Svänback and Bolnick 2005). We note, however, that nutritional condition is dynamic and varies with factors other than foraging success (e.g., reproductive state), which may disrupt the feedback loop and result in individuals intermittently trading places along a generalist-specialist continuum.

Although we lack the data to explicitly test whether mechanisms other than state-dependent foraging modulate food preference or diet composition (e.g., inherited or learned preferences; Taper and Case 1985, Estes et al. 2003), our results are consistent with simulation analyses in which behavioral adjustments to physiological state enhanced fitness in the absence of individual preferences (Nonacs 2001). Together with evidence that nutritional condition is likely to be 'reset' many times during the average lifespan of a bushbuck due to factors other than foraging strategy (Parker et al. 2009), we suggest these lines of evidence indicate that the observed relationships among nutritional condition and diet breadth/quality are more likely to reflect animals' behavioral adjustment to their state than intrinsic preferences consistently leading to a competitive advantage and good nutritional condition. Parsing the roles of inherited or learned preference versus state-dependent foraging in generating diet variation among free-ranging animals represents a fruitful avenue for future research.

Caveats and considerations

We focused on the roles of spatial heterogeneity and state-dependent behavior in driving individual variation, but predation risk also modulates these relationships. A study conducted in Gorongosa before the return of wild dogs and leopards in 2018 documented a "landscape of fearlessness" in which bushbuck increasingly occupied the floodplain from 2002–2016 (Atkins et al 2019). In this way, risk relaxation enabled bushbuck to capitalize on the ecological opportunity presented by high-quality forage in the floodplain, contributing to the broad-scale pattern of individual variation documented here; the recovery of large carnivores in the park may increasingly limit bushbuck to habitats with more concealment cover and thereby reduce the extent of individual differentiation at the population level. Crucially, however, all of the same patterns observed at the population level also held within the woodland habitat historically preferred by bushbuck (Tinley 1977), and predation on bushbuck was accelerating during our study (Bouley et al. 2021), indicating that our conclusions are not an artifact of predation regime.

Our results are based on just 15 individuals, yet this sample size is commensurate with previous studies investigating mechanisms of diet selection by large mammalian herbivores (e.g., Cerling et al. 2006, Atkins et al. 2019). Moreover, we know of no previous study that has quantified and compared large-herbivore diets with high taxonomic resolution via longitudinal sampling of known individuals. Collecting multiple fecal samples per individual allowed us to characterize individual diets more thoroughly than in previous studies, most of which have used single samples of fecal or gut contents to represent individual niche width (e.g., Costa et al. 2008, Araujo et al. 2009, Redjadj et al. 2014, Pansu et al. 2019b). Although analyzing single samples would not have qualitatively altered the conclusions of this study (to the contrary, it would have tended to exaggerate the degree of individual differentiation; see Figure 1.2), the fact that even ≥6 samples per individual failed to fully capture individual dietary richness

is a caveat to our quantitative metrics. The potential impacts of overestimating individual dietary differentiation by under sampling depends on the question being asked. For example, some studies of individual diet variation specify a simple threshold for determining whether a population is comprises specialist or generalist individuals (e.g., Vander Zanden et al. 2013). However, our results support the contention (e.g., Novak and Tinker 2015) that measures of diet variation are highly sensitive to temporal scale and intensity of sampling and that reliance on threshold values may therefore compromise inference when sampling intensity is insufficient to robustly quantify individual-level diet breadth.

Conclusions

Foraging decisions are conditioned upon a variety of extrinsic and intrinsic constraints. Empirical evidence increasingly shows that broad-scale patterns of habitat selection can constrain fine-scale differences in resource use among individuals (e.g., Zerba and Collins 1992, L'Hérault et al. 2013, Feiner et al. 2019), and theory shows that these differences can scale up to exert strong (albeit variable) effects on interspecific interactions and population dynamics (Bolnick et al. 2011, Hart et al. 2016, Stump et al. 2022). Understanding the mechanistic bases of individual variation is thus crucial to understanding community organization. By drawing on an uncommon wealth of information on landscape structure, animal movement, diet composition, and nutritional condition, we have shown that spatial heterogeneity and state dependence interact with space use to regulate individual variation. Accounting for these factors is now more possible than ever and should lead to rapid progress in understanding both the causes and consequences of individual specialization.

Our study provides empirical support for OFT as a framework for generating and testing hypotheses about the behavioral mechanisms that drive variation in individual realized niche width in the context of energy supply and demand. Given their strong mechanistic underpinnings, we propose that the relationships documented in our study are likely generalizable across an array of taxa and ecosystems. We encourage future tests of this proposition that focus on parsing the relative roles of extrinsic versus intrinsic constraints in determining individual niche width.

Literature Cited

Almeida, P. J., M. V. Viera, M. Kajin, G. Forero-Medina, and R. Cerqueira. 2010. Indices of movement behavior: conceptual background, effects of scale and location errors. *Zoologia* 27:674-680.

ASPRS LAS Specification. 2008. https://www.asprs.org/a/society/committees/standards/asprs_las_format_v12.pdf (accessed on 3 January 2022).

Atkins, J. L., R. A. Long, J. Pansu, J. H. Daskin, A. B. Potter, M. E. Stalmans, C. E. Tarita, and R. M. Pringle. 2019. Cascading impacts of large-carnivore extirpation in an African ecosystem. *Science* 368:173-177.

Araújo, M. S., D. I. Bolnick, and C. A. Layman. 2011. The ecological causes of individual specialization. *Ecology Letters* 14:948-958.

Araújo, M. S., E. G. Martins, L. D. Cruz, F. R. Fernandes, A. X. Linhares, S. F. Dos Reis, and P. R. Gulmarães Jr. 2010. Nested diets: a novel pattern of individual-level resource use. *Oikos* 119:81-88.

Araújo, M. S., D. I. Bolnick, L. A. Martinelli, A. A. Gieretta, and S. F. dos Reis. 2009. Individual-level diet variation in four species of Brazilian frogs. *Journal of Animal Ecology* 78:848-856.

Barnett, C. A., M. Bateson, and C. Rowe. 2007. State-dependent decision making: educated predators strategically trade off the costs and benefits of consuming aposematic prey. *Behavioral Ecology* 18:645-665.

Becker, J. A., M. C. Hutchinson, A. B. Potter, et al. 2021. Ecological and behavioral mechanisms of density-dependent habitat expansion in a recovering African ungulate population. *Ecological Monographs* 91:e01476.

Belovsky, G. E. Diet optimization in a generalist herbivore: the moose. *Theoretical Population Biology* 14:105-134.

Bison, M., S. Ibanez, C. Redjadj, F. Boyer, E. Coisser, C. Miquel, D. Rioux, S. Said, D. Maillard, P. Taberlet, N. G. Yoccoz, and A. Loison. 2015. Upscaling the niche variation hypothesis from the intra- to the inter-specific level. *Oecologia* 179:835-842.

Bolnick, D.I., R. Svänback, J.A, Fordyce, L.H. Yang, J.M. Davis, C.D. Hulsey, and M.L. Forister. 2003. The ecology of individuals: Incidence and implications of individual specialization. *American Naturalist* 161:1-28.

Bolnick, D. I., P. Amaraskare, M. S. Araújo, et al. 2011. Why intraspecific trait variation matters in community ecology. *Trends in Ecology and Evolution* 26:183-192.

Bouley, P., A. Paulo, M. Angela, C. Du Plessis, and D. G. Marneweck. 2021. The successful reintroduction of African wild dogs (*Lycaon pictus*) to Gorongosa National Park, Mozambique. *PloS ONE* 16:e0249860.

Boyer, F., C. Mercier, A. Bonin, Y. Le Bras, P. Taberlet, and E. Coissac. 2016. OBITOOLS: a UNIX-inspired software package for DNA metabarcoding. *Molecular Ecology Resources* 16:176-182.

Branco, P. S., J. A. Merkle, R. M. Pringle, J. Pansu, A. B. Potter, A. Reynolds, M. Stalmans, and R. A. Long. 2019. Determinants of elephant foraging behavior in a coupled human-natural system: is brown the new green? *Journal of Animal Ecology* 88:780-792.

Braun-Blanquet, J. 1932. *Plant sociology: Study of plant communities*. New York, NY: McGraw-Hill.

Burnham, K. P. and D.R. Anderson. 2002. Model selection and mulitmodel inference. 2nd edition. Springer, New York.

Carlson, B.S., S. Rotics, M. Wikelski, and W. Jetz. 2021. Individual environmental niches in mobile organisms. *Nature Communications* 12:4572.

Cerling, T.E., G. Wittemyer, H.B. Rasmussen, F. Vollrath, C.E. Cerline, T.J. Robinson, and I. Douglas-Hamilton. 2006. Stable isotopes in elephant hair document migration patterns and diet changes. *Proceedings of the National Academy of the Sciences of the USA* 103:371-373.

Charnov, E. 1976. Optimal foraging, the marginal value theorem. *Theoretical Population Biology* 9:129-136.

Colwell, R.K., and J.A. Coddington. 1994. Estimating terrestrial biodiversity through extrapolation. *Philosophical Transactions of the Royal Society B* 345:101–118.

Cook, R.C., J.G. Cook, T.R. Stephenson, et al. 2010. Revisions of rump fat and body scoring indices for deer, elk, and moose. *Journal of Wildlife Management* 74:880-896.

Cook, R.C., J.G. Cook, D.J. Vales, et al. 2013. Regional and seasonal patterns of nutritional condition and reproduction in elk. *Wildlife Monographs* 184:1-44.

Costa, G.C., D.O. Mesquita, G.R. Colli, and L.J. Vitt. 2008. Niche expansion and the Niche Variation Hypothesis: Does the degree of individual variation increase in depauperate assemblages? The *American Naturalist* 172:868-877.

Craine, J. M., E.G. Towne, M. Miller, and N. Fierer. 2015. Climatic warming and the future of bison as grazers. *Scientific Reports* 5:16738.

Darimont, C.T., P.C. Paquet, and T.E. Reimchen. 2007. Stable isotope niche predicts fitness of prey in a wolf-deer system. *Biological Journal of the Linnean Society* 90:125-137.

Darimont, C.T., P.C. Paquet, and T.E. Reimchen. 2009. Landscape heterogeneity and marine subsidy generate extensie intrapopulation niche diversity in a large terrestrial vertebrate. *Journal of Animal Ecology* 78: 126-133.

Daskin, J. H., J. A. Becker, T. R. Kartzinel, A. B. Potter, R. H. Walker, F. A. A. Ericksson, C. Buoncore, A. Getraer, R. A. Long, and R. M. Pringle. 2022. Allometry of behavior and niche differentiation among congeneric African antelopes. *Ecological Monographs* (in press).

Davies, A. B., and G. P. Asner. 2014. Advances in animal ecology from 3D-LiDAR ecosystem mapping. *Trends in Ecology and Evolution* 29:681-691.

Davies, A. B., S. R. Levick, G. P. Asner, M. P. Robertson, B. J. van Rensburg, and C. L. Parr. 2014. Spatial variability and determinates of termite mounds throughout a savanna catchment. *Ecography* 37: 1-11.

Davies, A. B., C. A. Baldeck, and G. P. Asner. 2015. Termite mounds alter the spatial distribution of African savanna tree species. *Journal of Biogeography* 43:301-313.

Deagle, B. E., A. C. Thomas, J. C. McInnes, L. J. Clarke, E. J. Verterinen, E. L. Clare, T. R. Kartzinel, J. P. Eveson. 2019. Counting the DNA in metabarcoding studies: How should we convert sequence reads to dietary data? *Molecular Ecology* 28:391-406.

Emlen, J. M. 1966. The role of time and energy in food preference. *American Naturalist* 100:611-617.

Estes, R. D. 1991. The behavior guide to African mammals. University of California Press, Berkeley, CA.

Estes, J. A., M. L. Riedman, M. M. Staedler, M. T. Tinker, and B. E. Lyon. 2003. Individual variation in prey selection by sea otters: Patterns, causes and implications. *Journal of Animal Ecology* 72:144-155.

Feiner, Z. S., C. J. Foley, R. K. Swihart, H. Bootsma, S. Czesny, J. Janssen, J. Rinchard, and T. O. Höök. 2019. Individual and spatial variation as species-level variation to the trophic complexity of a lentic food web. *Ecology of Freshwater Fish* 28:516-532.

Fryxell, J.M., and P. Lundberg. 1994. Diet choice and predator-prey dynamics. *Evolutionary Ecology* 8:407-421.

George-Chacon, S. P., J. M. Dupuy, A. Peduzzi, and J. L. Hernandez-Stefanoni. 2019. Combining high resolution satellite imagery and lidar data to model woody species diversity of tropical dry forests. *Ecological Indicators* 101:975-984.

Gill, A. B. 2003. The dynamics of prey choice in fish: the importance of prey size and satiation. *Journal of Fish Biology* 63: 105-116.

Grant, C. and M. Scholes. 2006. The importance of nutrient hot-spots in the conservation and management of large wild mammalian herbivores in semi-arid savannas. *Biological Conservation* 130:426-437.

Guo, X., N. C. Coops, P. Tompalski, S. E. Nielsen, C. W. Bater, and J. J. Stadt. 2017. Regional mapping of vegetation structure for biodiversity monitoring using airborne lidar data. *Ecological Informatics* 38:50-61.

Guy, T. J., M. C. Hutchinson, K. C. R. Baldock, E. Kayser, B. Baiser, P. P. A. Staniczenko, J. R. Goheen, R. M. Pringle, and T. M. Palmer. Large herbivores transform plant-pollinator networks in an African savanna. *Current Biology* 31:2964-2971.

Guyton, J. A., J. Pansu, M. C. Hutchinson, T. R. Kartzinel, A. B. Potter, T. C. Coverdale, J. H. Daskin, A. G. da Conceição, M. J. Peel, M. E. Stalmans, and R. M. Pringle. 2020. Trophic rewilding revives biotic resistance to shrub invasion. *Nature Ecology & Evolution* 4:712-724.

Hailey, A. and I. A. Coulson. 1996. Differential scaling of home-range area to daily movement distance in two Africa tortoises. *Canadian Journal of Zoology* 74:97-102.

Hart, S. P., S. J. Schreiber, and J. M. Levine. 2016. How variation between individuals affects species coexistence. *Ecology Letters* 19:825-838.

Holm, S. 1979. A simple sequentially rejective multiple test procedure. *Scandinavian Journal of Statistics* 6: 65-70.

Hutchinson, G. E. 1957. Concluding remarks: Cold Spring Harbor symposium. *Quantitative Biology* 22:415-427.

Hutchinson, M. C., A. P. Dobson, and R. M. Pringle. 2022. Dietary abundance distributions: dominance and diversity in vertebrate diets. *Ecology Letters* 25:992-1008.

Jesmer, B. R., M. J. Kauffman, M. A. Murphy, and J. R. Goheen. 2020. A test of the Niche Variation Hypothesis in a ruminant herbivore. *Journal of Animal Ecology* 89:2825-2839.

Johnson, D. H. 1980. The comparison of usage and availability measurements for evaluating resource preference. *Ecology* 61:65-71.

Kartzinel, T. R., P. A. Chen, T. C. Coverdale, D. L. Erickson, W. J. Kress, M. L. Kuzmina, D. I. Rubenstein, W. Wang, and R. M. Pringle. 2015. DNA metabarcoding illuminates dietary niche partitioning by African large herbivores. *Proceedings of the National Academy of Sciences of the USA* 112:8019-8024.

Kartzinel, T. R., J. C. Hsing, P. M. Musili, B. R. P. Brown, and R. M. Pringle. 2019. Covariation of diet and gut microbiome in African megafauna. *Proceedings of the National Academy of Sciences of the USA* 116:23588-23593.

Kartzinel, T. R. and R. M. Pringle. 2020. Multiple dimensions of dietary diversity in large mammalian herbivores. *Journal of Animal Ecology* 89:1482-1496.

Kingdon, J. 1997. The Kingdon field guide to African mammals. A&C Black, London.

Kie, J. G., R. T. Bowyer, M. C. Nicholson, B. B. Boroski, and E. R. Loft. 2002. Landscape hetero-geneity at differing scales: effects on spatial distribution of mule deer. *Ecology* 83:503-544.

Layman, C. A., J. P. Quattrochi, C. M. Peyer, and J. E. Allgeier. 2007. Niche width collapse in a resilience top predator following ecosystem fragmentation. *Ecology Letters* 10:937-944.

Levick, S. R., G. P. Asner, T. Kennedy-Bowdoin, and D. E. Knapp. 2010. The spatial extent of termite influences on herbivore browsing in an African savanna. *Biological Conservation* 143:2462-2467.

L'Hérault, V., A. Franke, N. Lecomte, A. Alogut, and J. Bêty. 2013. Landscape heterogeneity drives intra-population niche variation and reproduction in an arctic top predator. *Ecology and Evolution* 3:2867-2879.

Long, R. A., T. Bower, W. P. Porter, P. Matthewson, K. L. Monteith, and J. G. Kie. 2014. Behavior and nutritional condition buffer a large-bodied endotherm against direct and indirect effects of climate. *Ecological Monographs* 84:513-532.

Loretto, D., and M. V. Vieira. 2005. The effects of reproductive and climatic season on movements in the black-eared opossum (*Didelphis aurita*). *Journal of Mammalogy* 86:287-293.

MacArthur, R. H., and E. R. Pianka. 1966. On optimal use of a patchy environment. *American Naturalist* 100:603-609.

MacArther, R. H., and R. Levins. 1967. The limiting similarity, convergence, and divergence of coexisting species. *American Naturalist* 101:377-385.

McNamara, J. M., and A. I. Houston. 1996. State-dependent life histories. *Nature* 380:215-221.

Mathot, K. J., and S. R. Dall. 2013. Metabolic rates can drive individual differences in information and insurance use under the risk of starvation. *American Naturalist* 182:611-620.

Nonacs, P. 2001. State dependent behavior and the marginal value theorem. *Behavioral Ecology* 12:71-83.

Novak, M., and M. T. Tinker. 2015. Timescales alter the inferred strength and temporal consistency of intraspecific diet specialization. *Oecologia* 178:61-74.

Oksanen, J., F. Guillaume Blanchett, M. Friendly, R. Kindt, P. Legendre, D McGlinn, P.R. Minchin, R.B. O'Hara, G.L. Simpson, P. Soymos, M.H.H. Stevens, E. Szoecas, and H. Wagner. 2020. *Vegan*: Community Ecology Package. R package v.2.5-6.

Owen-Smith, N. and P. Novellie. 1982. What should a clever ungulate eat? *American Naturalist* 119:151-178.

Owen-Smith, N., J. M. Fryxell, and E. H. Merrill. 2010. Foraging theory upscaled: the behavioral ecology of herbivore movement. *Philosophical Transactions of the Royal Society B* 365:2267-2278.

Pansu, J, J. A. Guyton, A. B. Potter, J. L. Atkins, J. H. Daskin, B. Wursten, T. R. Kartzinel, and R. M. Pringle. 2019a. Data from: Trophic ecology of large herbivores in a reassembling African ecosystem, Dryad, Dataset, https://doi.org/10.5061/dryad.63tj806

Pansu, J, J. A. Guyton, A. B. Potter, J. L. Atkins, J. H. Daskin, B. Wursten, T. R. Kartzinel, and R. M. Pringle. 2019b. Trophic ecology of large herbivores in a reassembling African ecosystem. *Journal of Ecology* 107:1355-1376.

Parent, C .E., D. Agashe, and D. I. Bolnick. 2014. Intraspecific competition reduces niche width in experimental populations. *Ecology and Evolution* 4:3978-3990.

Parker, K. L., P. S. Barboza, and M. P. Gillingham. 2009. Nutrition integrates environmental responses of ungulates. *Functional Ecology* 23:57-69.

Perry, D. M. 1987. Optimal diet theory: behavior of a starved predatory snail. *Oecologia* 72: 360-365.

Potter, A. B., M. C. Hutchinson, J. Pansu, B. Wursten, R. A. Long, J. M. Levine, and R. M. Pringle. 2022. Mechanisms of dietary resource partitioning in large-herbivore assemblages: a plant-trait based approach. *Journal of Ecology* 110:817-832.

Pringle, R. M., T. P. Young, D. I. Rubenstein, and D. J. McCauley. 2007. Herbivore-initiated interaction cascades and their modulation by productivity in an African savanna. *Proceedings of the National Academy of Sciences of the USA* 104:193-197.

Pringle, R. M. and M. C. Hutchinson. 2020. Resolving food-web structure. *Annual Review of Ecology, Evolution, and Systematics* 51:55-80.

Prins, H. H. T. 2016. Interspecific resource competition in antelopes: search for evidence. p. 51-77 *in* J. Bro-Jørgensen and D.P. Mallon, Editors. Antelope conservation: from diagnosis to action. John Wiley & Sons, Chichester, UK.

R Core Team. 2018. R: A language and environment for statistical computing. R Foundation for Statistical Computing, Vienna, Austria.

Redjadj, C., G. Darmon, D. Maillard, et al. 2014. Intra- and interspecific differences in diet quality and composition in a large herbivore community. *PLoS ONE* 9:e84756.

Reusch, T. B. H., A. Ehlers, A. Hämmerli, and B. Worm. 2005. Ecosystem recovery after climatic extremes enhanced by genotypic diversity. *Proceedings of the National Academy of Sciences of the USA* 102:2826-2831.

Ripple, W. J., T. M. Newsome, C. Wolf, R. Dirzo, K. T. Everatt, M. Galetti, M. W. Hayward, G. I. Kerley, T. Levi, and P. A. Lindsey. 2015. Collapse of the world's largest herbivores. *Science Advances* 1:e1400103.

Sih, A., K. J. Mathot, M. Moirón, P. O. Montiglio, M. Wolf, and N. J. Dingemanse. 2015. Animal personality and state-behavior feedbacks: a review and guide for empiricists. *Trends in Ecology & Evolution* 30:50-60.

Sikes, R. and the Animal Care and Use Committee of the American Society of Mammologists. 2016. 2016 Guidelines of the American Society of Mammologists for the use of wild mammals in research and education. *Journal of Mammalogy* 97:663-688.

Simonson, W. D., H. D. Allen, and D. A. Coomes. 2012. Use of airborne lidar system to model plant species composition and diversity of Mediterranean oak forests. *Conservation Biology* 26:840-850.

Singer, J., J. Fieberg, and T. Avgar. 2019. Animal movement tools (amt): R package for managing tracking data and conducting habitat selection analyses. Ecology and Evolution **9**:880-890.

Soberon, J. and J. Llorente. 1993. The use of species accumulation functions for the prediction of species richness. *Conservation Biology* 7:480–488.

Stalmans, M., and R. Beilfuss. 2008. *Landscapes of the Gorongosa National Park*. Parque Nacional Da Gorongosa, Mocambique: Gorongosa Research Center.

Stalmans, M.E., T.J. Massad, M.J.S. Peel, C.E. Tarnita, and R.M. Pringle. 2019. War induced collapse and asymmetric recovery of large-mammal populations in Gorongosa National Park, Mozambique. *PLoS ONE* 14:e0212864.

Stephens, D.W., and J.R. Krebs. 1986. Foraging theory. Princeton University Press, Princeton, NJ.

Stephenson, T. R., D. W. German, E. F. Cassirer, D. P. Walsh, M. E. Blum, M. Cox, K. M. Stewart, K. L. Monteith. 2020. Linking population performance to nutritional condition in an alpine ungulate. *Journal of Mammalogy* 101:1244-1256.

Stump, S. M., C. Song, S. Saavedra, J. M. Levine, and D. A. Vasseur. 2022. Synthesizing the effects of individual-level variation on coexistence. *Ecological Monographs* 92:e01493.

Svabäck, R. and D.I. Bolnick. 2005. Intraspecific competition affects the strength of individual specialization: an optimal diet theory method. *Evolutionary Ecology Research* 7:993-1012.

Taper, M. L., and T. J. Case. 1985. Quantitative genetic models for the coevolution of character displacement. *Ecology* 66:355-371.

Taberlet, P., E. Coissac, F. Pompanon, et al. 2007. Power and limitation of the chloroplast *trn*L (UAA) intron for plant DNA barcoding. *Nucleic Acids Research* 35:e14.

Tinley, K. 1977. A framework of the Gorongosa ecosystem. Department of Zoology, University of Pretoria, Pretoria, South Africa.

Tobler, W. 1970. A computer movie simulating urban growth in the Detroit region. *Economic Geography* 46:234-240.

Trachsel, J. 2021. *funfuns*. R package version 0.1.2.

Vander Zanden, H.B., K.A. Bjorndal, and A.B. Bolten. 2013. Temporal consistency and individual specialization in resource use by green turtles in successive life stages. *Oecologia* 173:767-777.

Voltera, V. 1926. Fluctuations in the abundance of a species considered mathematically. *Nature* 118: 558-560.

Walker, R. H., M. C. Hutchinson, A. B. Potter, J. A. Becker, R. A. Long, and R. M. Pringle. 2022. Mechanisms of individual variation in large herbivore diets: roles of spatial heterogeneity and state-dependent foraging, Dryad, Dataset, https://doi.org/10.5061/dryad.crjdfn364.

West, L. 1986. Interindividual variation in prey selection by the snail *Nucella* (= *Thais*) *emarginata*. *Ecology* 67:798-809.

Westoby, M. An analysis of diet selection by large generalist herbivores. *American Naturalist* 108:290-304.

Willersley, E., J. Davison, J. Moora, *et al.* 2014. Fifty thousand years of Arctic vegetation and megafaunal diet. *Nature* 506:47-15.

Zaccarelli, N., D.I. Bolnick, and G. Mancinelli. 2013. RInSp: an R package for the analysis of individual specialization in resource use. *Methods in Ecology and Evolution* 4:1018-1023.

Zerba, K.E., and J.P. Collins. 1992. Spatial heterogeneity and individual variation in diet of an aquatic top predator. *Ecology* 73:268-279.

Chapter 2: Trait-based sensitivity of large mammals to a catastrophic tropical cyclone

Walker, R. H., M. C. Hutchinson, J. A. Becker, J. H. Daskin, K. M. Gaynor, M. S. Palmer, D. D. Gonçalves, M. E. Stalmans, J. Denlinger, P. Bouley, M. Angela, A. Paulo, A. B. Potter, N. Arumoogum, F. Parrini, J. Marshal, R. M. Pringle, and R. A. Long. 2022. Trait-based sensitivity of large mammals to a catastrophic tropical cyclone. In Revision: *Nature*. 31 December 2022.

Abstract

Extreme climatic events are becoming more frequent and intense. Body size and other traits may mediate animals' vulnerability to such events, but it has rarely been possible to test this idea. We show how Mozambican megafauna responded to Cyclone Idai, the deadliest storm on record in Africa, across scales ranging from individual decisions in the hours after landfall to community-level responses 18 months later. Animals occupying low-elevation habitats exhibited strong spatial responses to rising floodwaters. Body size predicted species' numerical responses: small-bodied species exhibited the greatest declines. We trace this sensitivity to limited mobility, which increased likelihood of death during the flood and constrained animals' capacity to withstand food shortage afterwards. Our results identify trait-based mechanisms underlying animal responses to severe weather and can inform impact-mitigation and adaptation strategies.

Main Text

Extreme climatic events—statistically rare, discrete weather events with intensity outside normal variability (Smith 2011)—are becoming more frequent and severe (Ummenhofer & Meehl 2017). This trend includes tropical cyclones (Elsner et al. 2008, Wang & Toumi 2021; but see, Chand et al. 2022), prompting urgent calls for research on cyclones' ecological effects (Smith 2011, Pruitt et al. 2019, Lin et al. 2020). However, the unpredictable nature of severe cyclones makes them difficult to study (Jentsch et al. 2007). While remote sensing and long-term vegetation plots facilitate assessment of cyclone effects on landscapes (Zeng et al. 2009, Tanner et al. 2014), there are comparatively few direct studies of animals, and most of those involve small-bodied species on oceanic islands (Wiley et al. 1993, Spiller & Losos 1998, Schoener et al. 2004, Schoener & Spiller 2006, Grant et al. 2017, Donihue et al. 2008). In the 1990s, a succession of hurricanes struck small experimental islands in the Bahamas, supplying unusually

rich insight into the effects of cyclones on animal communities and suggesting that species' responses were predictably related to their traits: larger species (lizards) were more resistant to cyclone effects, whereas better dispersers (arthropods) recovered faster (Spiller & Losos 1998). These results suggest a general trait-based theory of animal robustness—defined as the maintenance (resistance) and recovery (resilience) of normal abundance and behavior patterns (Levin et al. 2008)—to climatic catastrophes (Schoener & Spiller 2006). Yet, the scalability of these principles to large animals in continental systems, where body size and dispersal ability are generally linked (Noonan et al. 2020), is unknown. Moreover, no study to our knowledge has been able to track the individual-level behavioral mechanisms that underpin community-level responses to cyclones.

We investigated how a diverse assemblage of large mammals in Mozambique's Gorongosa National Park responded to Cyclone Idai, one of the strongest tropical cyclones on record in the Southern Hemisphere (Warren 2019, Charrua et al. 2021). The historically abundant megafauna of Gorongosa's mesic savannas (842 mm rainfall yr-1) and productive floodplain grasslands was reduced by >90% during the Mozambican Civil War (1977–1992) but have since recovered dramatically (Stalmans et al. 2019). Ongoing long-term research on the movements, distribution, diets, and population dynamics of 13 herbivore species—from 17-kg oribi to 4000-kg elephant (Kingdon 1997)—and their predators (lion and African wild dog) provided a unique opportunity to assess the impacts of an extreme climatic event across a community comprising some of the world's largest terrestrial animals (Figure B.1). Using multiple data streams, including GPS telemetry, we compared animal behaviors in the hours, days, and months before Cyclone Idai made landfall to those observed after the cyclone and during the same intervals in normal years (Appendix B). We tested two general trait-based hypotheses. First, species affiliated with woody, higher-elevation habitats are more robust to cyclones than those affiliated with open, lower-elevation habitat, which is more prone to flooding (Figure B.2). Second, species' robustness to cyclones scales positively with body size, because larger mammals have (a) higher mobility and can more easily escape affected habitats and (b) lower mass-specific metabolic rates and therefore greater ability to buffer the impacts of reduced food supply in the months after the storm.

Cyclone Idai made landfall on 15 March 2019 (the end of the wet season in a typical year) and passed directly over Gorongosa (~100 km inland), bringing maximum wind speeds >188 km hr-1, torrential rains of >200 mm in <24 hours, and floodwaters >5 m deep around Lake Urema at the core of the park (Figure 2.1, Figures B.3-4).

Some animals were unable to evade the rising floodwaters: three of eight GPS-collared bushbuck, the smallest individually monitored herbivore species, died within a week of landfall. The bushbuck that perished in the flood were much smaller than the survivors (mean 35.7 vs. 46.0 kg) and included the

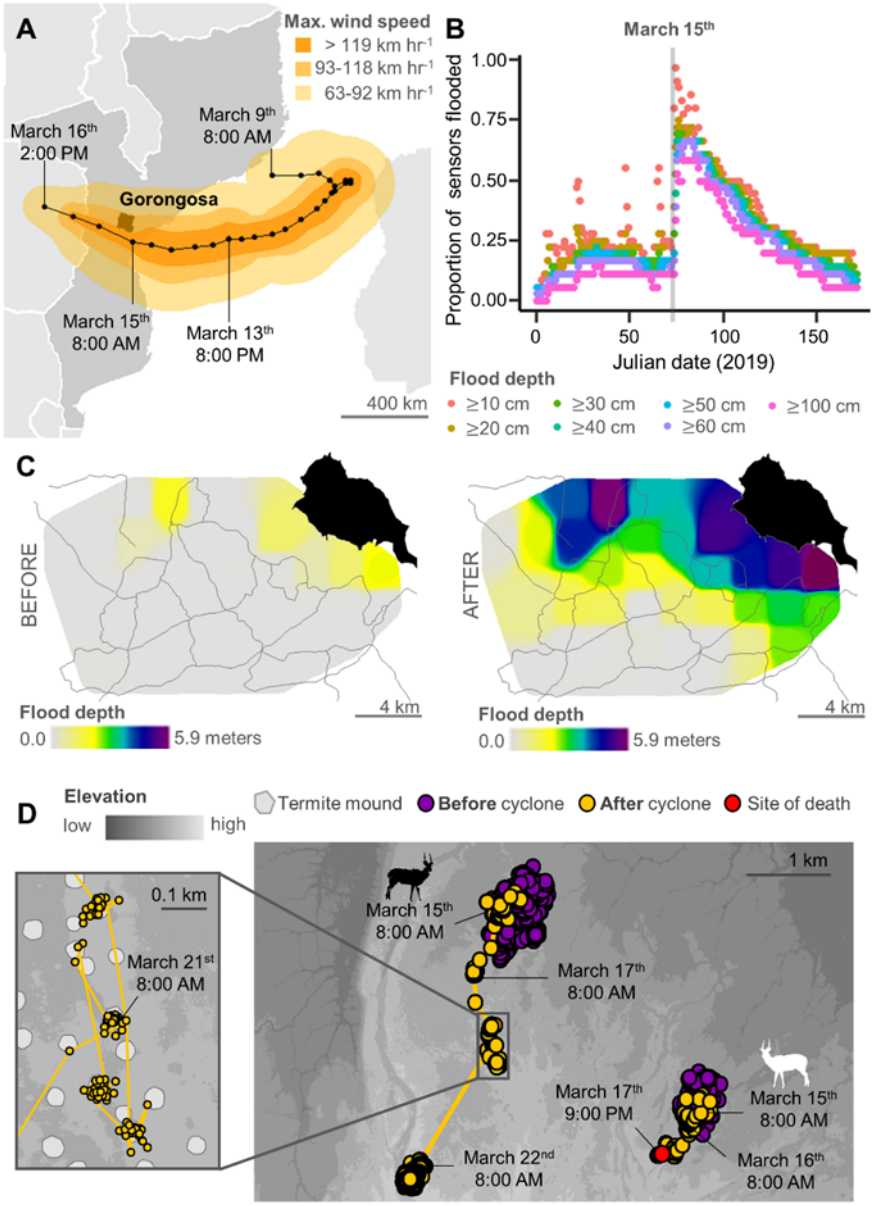

Figure 2.1. Cyclone Idai led to extensive flooding in Gorongosa. (**A**) After making landfall on 15 March 2019, Idai's central path (black line, black dots illustrate position every 6 hours, local time; Global Disaster Alert and Coordinate System, 2019) passed within 50 km of Gorongosa National Park (black polygon). (**B**) Heavy rains from Idai inundated a network of 37 active flood sensors in the park; flood extent did not return to pre-cyclone levels until roughly 1 June (Julian day 152). (**C**) Within one week of landfall, flooding extent (areas inundated >50 cm) expanded by 388% (one week prior = 24.1 km^2; one week after = 117.7 km^2; total sensor area = 165.8 km^2) and maximum flood depth increased by 195% (before = 2.0 m; after = 5.9 m). Lake Urema (black polygon) and roads (black lines) are shown to facilitate comparison. (**D**) Hourly GPS fixes of two representative bushbuck, one that survived (black silhouette) and another that died (white silhouette). Purple points show positions in the month before the cyclone; yellow points show positions in the month afterwards; red point shows the site of death. The surviving individual left its home range and moved up the elevational gradient, away from Lake Urema, using termite mounds as refuges from the flood (inset) before making a beeline up the elevational gradient and establishing a new home range ~3.5 km away. The individual that died began moving upslope but did not outpace the rising floodwaters and died within 500 m of its original home range. This pattern was consistent across the 5 bushbuck that survived and the 3 that died (Figure B.5).

smallest collared male and smallest two collared females (Figure B.5a,b). Although these individuals selected for higher elevation, they did not avoid the flood edge and died in areas inundated with >1.5 m of water (Figure 2.1e, Figure B.5c). Notably, bushbuck selected for high ground at both macro- and microtopographic scales, with individuals moving upslope and selecting for termite mounds (Figure 2.2a), which had become tiny islands; the movement path of one surviving bushbuck shows how the animal 'hopped' from mound to mound, passing quickly through the flooded area in between (Figure 2.1d). We did not detect any mortalities among four larger-bodied herbivore species for which known-fate data were available [nyala (98 kg, n = 4), kudu (210 kg, n = 12), sable (223 kg, n = 3), and elephant (4,000 kg, n = 13)]. Many surviving GPS-collared herbivores moved out of their previously established home ranges, selecting higher-elevation areas away from floodwaters, before eventually settling in areas of relative safety (Figure 2.2, Figure B.6). Affiliation with floodplain habitat strongly predicted the degree of displacement from home ranges, whereas body mass did not have a significant effect after accounting for habitat affiliation (Figure B.7).

Data from an established 300-km^2 camera-trap grid [n = 48-60 cameras in 5-km^2 hexagonal cells; Figure B.8 (Gaynor et al. 2021)] showed that other herbivore species shifted their space use in similar ways. We observed strong interactive effects of time since cyclone landfall and distance to Lake Urema on distribution of the three most common herbivore species [impala (56 kg), warthog (83 kg), and waterbuck (215 kg)] (Table B.1). In general, the cyclone pushed herbivores away from the lake into elevated woodland habitats, increasing herbivore activity in those areas far above levels observed in typical years (Figures B.9-10). Together, GPS-collar and camera-trap data indicate that body size, mobility, and behavioral flexibility were key for surviving the immediate aftermath of the cyclone.

In addition to crowding herbivores into elevated woodlands, Cyclone Idai altered forage availability during the subsequent season. The extreme and unseasonal flooding after Idai reversed the typical phenological progression of understory plants in the sparsely wooded flood zone (Figure 2.3a, Figure B.11a). Vegetation in this area remained significantly less productive than usual for three months after the cyclone (March–May) (Figure 2.3a, Figure B.11a). By contrast, productivity in the flood zone was significantly higher than usual in the late dry season after Idai (October), presumably due to atypically high water availability (Figure 2.3a, Figure B.11a). These effects were far less pronounced in elevated woodland areas that were not flooded after Idai (Figure B.11b).

Cyclone-induced changes in forage availability, coupled with the sustained upland shift in herbivore distribution, led to changes in herbivore diets. Herbivores generally ate a significantly different suite of plant taxa in 2019 than in 2018 (Figure B.12). Although these multidimensional differences varied across species and seasons, several broad trends emerged. After Idai, herbivore diets tended to comprise a

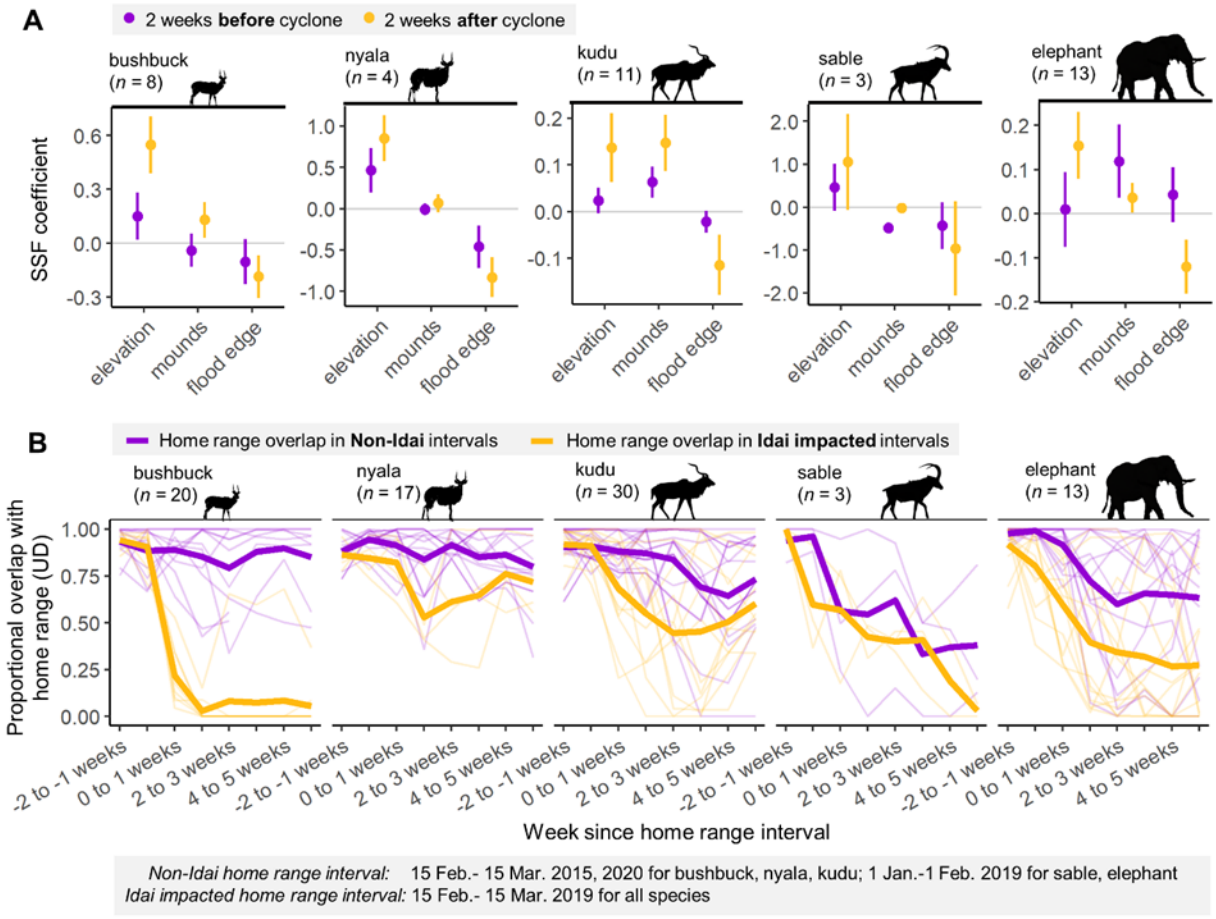

Figure 2.2. Herbivores changed their movement behavior to avoid cyclone-induced flooding. (**A**) Coefficients and 95% confidence intervals (CI) from step-selection functions (SSFs) for 39 GPS-collared herbivores of 5 species, indicating the extent to which animals selected for high elevation and termite mounds and avoided floodwaters, in the two weeks before (purple) and two weeks after (yellow) Cyclone Idai passed over Gorongosa. CIs not overlapping zero indicate a significant influence of the covariate on movement behavior; CIs not overlapping each other indicate significant differences before vs. after landfall. All herbivores increased their selection for higher elevations and their avoidance of floodwaters, significantly so for bushbuck, kudu, and elephant. (**B**) Many herbivores departed their home ranges in the weeks after Idai made landfall (overlap of utilization distributions via 95% kernel density estimation: thin yellow lines, individuals; bold yellow line, mean), a trend not observed in periods unaffected by a cyclone (purple lines). The degree of displacement scaled negatively with species' degree of floodplain association (Figure B.7).

smaller proportion of grasses (Figure B.13), a more diverse array of plant families (Figure B.14), and plant species that were taller (Figure 2.3b) and less nutritious (lower in digestible protein, phosphorus, and sodium, higher in lignin; Figure 2.3c, Figure B.15) than in non-cyclone years, consistent with a shift toward 'woodier' diets (Potter et al. 2022). Dietary niche differences among herbivore species were also stronger in the post-cyclone early dry season (July) than in normal years (Figure 2.3d). The depletion of understory food resources and crowding of survivors into high and dry areas likely intensified

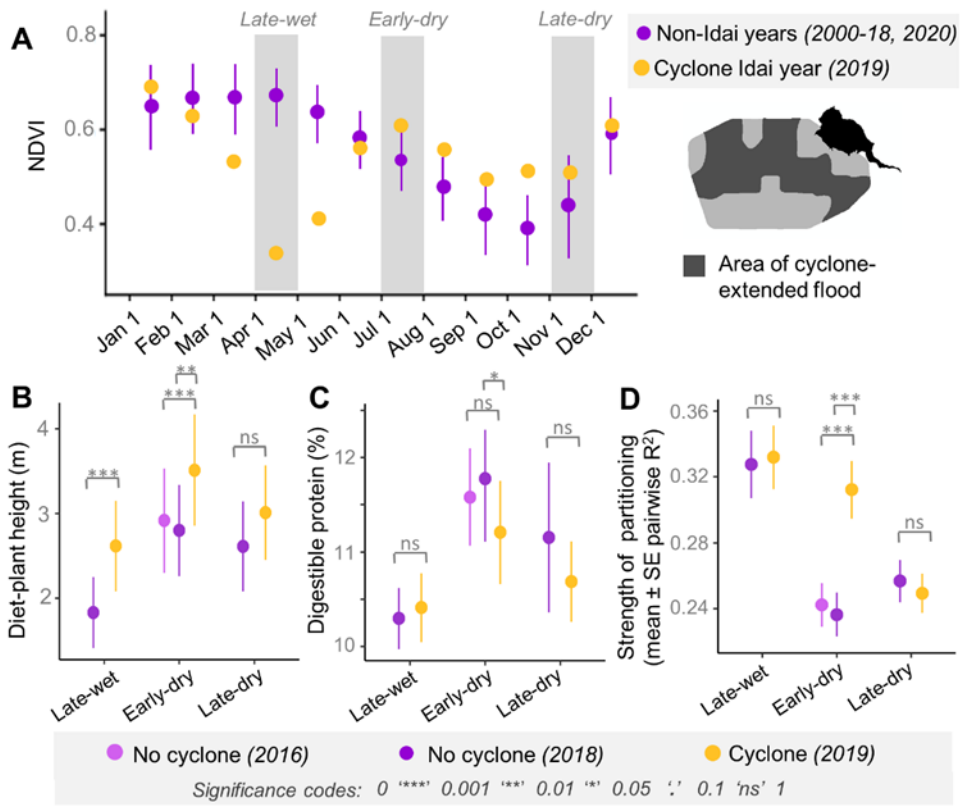

Figure 2.3. Cyclone-induced flooding depleted understory forage and altered herbivore diets. Points and error bars show mean ± SE. (**A**) Mean monthly normalized difference vegetation index (NDVI) values, a proxy for aboveground productivity, in the flood zone (areas that were dry the week before Idai but under >0.5 m of water within two weeks after; see inset) in the year of Idai (2019; yellow) and in 20 other years (2000-2018, 2020; purple). Flooding from Idai significantly decreased productivity for three months after landfall (March–May) but significantly increased it in the late-dry season (October). Gray shading shows periods in which we sampled herbivore diets. (**B-D**) On average relative to non-cyclone years (2016, 2018), herbivore diets after Idai (B) comprised taller plant species (linear mixed-effects models: late-wet, β_{2018} = -0.29, *SE* = 0.07, *P* < 0.001; early-dry, β_{2016} = -0.40, *SE* = 0.09, *P* < 0.001; β_{2018} = -0.25, *SE* = 0.08, *P* = 0.003; late-dry, β_{2018}= -0.10, *SE* = 0.07, *P* = 0.17); (C) contained less protein in the early-dry season (linear mixed-effects models: late-wet, β_{2018} = -0.005, *SE* = 0.02, *P* = 0.82; early-dry, β_{2016} = 0.04, *SE* = 0.02, *P* = 0.11; β_{2018} = 0.05, *SE* = 0.02, *P* = 0.03; late-dry, β_{2018} = 0.02, *SE* = 0.03, *P* = 0.38); and (D) were more strongly differentiated between species, as indexed by the mean R^2 of pairwise perMANOVA between each pair of 13 species in the early dry season (*26*) (mixed-effects models with beta-error distribution and per-species random intercepts: late-wet, β_{2018} = -0.09, *SE* = 0.08, *P* =0.26, early dry, β_{2016} = -0.37, *SE* = 0.04, *P* < 0.001; β_{2018} = -0.40, *SE* = 0.04, *P* < 0.001); late-dry, β_{2018} = -0.06, *SE* = 0.04, *P* = 0.11).

interspecific competition, forcing herbivores to differentiate their diets and accept relatively low-quality forage (Pansu et al. 2022).

The post-cyclone period of limited food availability and quality was associated with reduced nutritional condition (Appendix B) in small- to mid-sized herbivores (Figure 2.4). Bushbuck and nyala, the two smallest GPS-collared herbivores (≤100 kg), were in significantly worse condition after Idai (June-July 2019) than in previous years (June-July 2014–2018). The nutritional condition of kudu, a larger and

wider-ranging congener with comparable dietary habits (Daskin et al. 2022), was unaffected by the cyclone (Figure 2.4a). Coupled with evidence of low diet quality after Idai, both in general (Figure B.15) and for these species in particular (Figure B.16), this result supports our hypothesis that larger animals were better buffered against nutritional limitation (Peters 1983).

The disproportionate individual-level effects of Cyclone Idai on small-bodied, floodplain-associated grazers translated into skewed population-level impacts the following year. From 1994–2018, the 13 herbivore populations in this study had grown almost monotonically (Stalmans et al. 2019). In contrast, the post-cyclone aerial survey in October-November 2020 (18 months after landfall) documented the first substantial population declines for several of these species since the end of the Mozambican civil war (Figure B.17). Oribi, reedbuck, warthog, hartebeest, sable, and waterbuck—small to medium-sized (17–223 kg) grazers with moderate-to-high floodplain affiliation—declined by 12–53% (median 34%). In contrast, larger-bodied species with moderate-to-low floodplain affiliation—wildebeest, buffalo, and elephant (214–4,000 kg)—each increased by ~27%. In a set of 16 candidate linear models including main effects and interactions of herbivore size, trophic guild (% grass consumption), and habitat affiliation (Table B.2), body mass alone best explained proportional change in abundance (R^2 adj. = 0.28, P = 0.04) (Figure 2.4b). Floodplain affiliation alone was the 2nd-best model (ΔAIC_c = 0.96, R^2 adj. = 0.22, P = 0.06) (Figure 2.4c). These relationships were not observed across normal years: neither herbivore body mass nor floodplain association predicted proportional changes in species' abundance from 2014-2016 or 2016-2018 (all $P > 0.3$) (Figure 2.4b,c).

Waterbuck, a 215-kg floodplain-associated grazer, exemplified this trend. From 1994 to 2018, the waterbuck population grew logistically from < 1,000 to >55,000 individuals (Stalmans et al. 2019, Becker et al. 2021). In the 2020 census, observers found an unprecedented number of dead waterbuck, prompting them to record carcass statistics. In total, 3,300 carcasses were estimated from a systematic transect survey, almost exclusively in the floodplain (7.44 km^2 vs. 0.24 km^2 in woodland) (Figure B.18). These mortalities accounted for roughly half of the 6,800-individual difference in abundance between 2018 and 2019 and contributed to the first definite waterbuck population decline (-12%) in >25 years.

The two extant large-carnivore species in Gorongosa were comparatively robust to cyclone disturbance. We did not observe any mortalities among 22 carnivores for which known-fate data were available [14 wild dogs, 30 kg; 8 lions, 190 kg; (Kingdon 1997)]. Like herbivores, GPS-collared wild dogs and lions increased their selection for higher elevations and their avoidance of floodwaters in the weeks after landfall (Figure B.19a) and showed some displacement from their home ranges in the weeks after the cyclone (Figure B.19b). Lion diets were unaffected by the cyclone, while wild dog diets shifted in concert with the altered distribution of prey, with waterbuck temporarily displacing bushbuck as the predominant

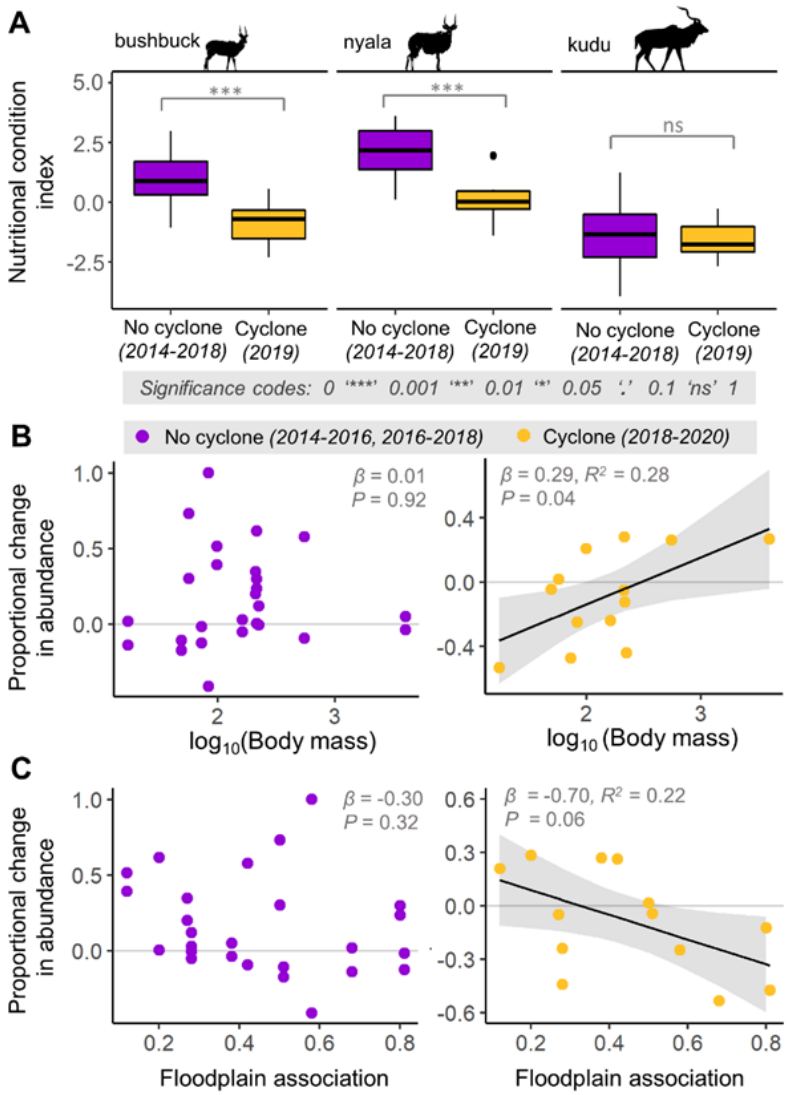

Figure 2.4. Cyclone impacts on herbivore condition and abundance varied with body size. (**A**) Nutritional condition of bushbuck and nyala, the two smallest GPS-collared antelopes, was significantly lower after Idai (2019) than in other years (2014–2018; asterisks show significant differences between groups in Welch's two-sample *t*-tests, bushbuck: $t = 6.74$, $df = 28.5$, $P < 0.001$; nyala: $t = 4.47$, $df = 10.2$, $P = 0.001$; kudu: $t = 0.61$, $df = 36.9$, $P = 0.55$). Boxes show median and interquartile range, whiskers show outer quartiles, points show outliers. (**B-C**) Proportional change in abundance between aerial counts in 2018 and 2020 (yellow points) was best predicted by (B) herbivore body size, with the smallest herbivores experiencing the steepest declines, and (C) species' affiliation with floodplain habitat (Table B.2, Figure B.17). These traits did not predict changes in abundance between normal years (2014–2016, 2016–2018; purple points), either when considered together (as plotted) or separately (2014-2016: $\beta_{\log(Mass)} = 0.01$, adj. $R^2 = -0.09$, $P = 0.93$; $\beta_{floodplain} = -0.29$, adj. $R^2 = -0.04$, $P = 0.46$; 2016–2018: $\beta_{\log(Mass)} = 0.01$, adj. $R^2 = -0.09$, $P = 0.96$; $\beta_{floodplain} = -0.31$, adj. $R^2 = -0.05$, $P = 0.51$). Body size and floodplain affiliation were uncorrelated (Figure B.1).

prey species; this pattern reverted by the late dry season (Figure B.20). Moreover, both lion and wild dog populations increased between 2018 and 2020 (Figure B.17). Several factors likely contributed to the robustness of carnivores relative to herbivores, including their high mobility and large home ranges in

stark contrast to herbivores [mean pre-Idai home ranges for lion (126 km^2) and wild dog (94 km^2) were, respectively, 25- and 200-fold larger than similarly-sized herbivores (kudu, 5 km^2; bushbuck, 0.4 km^2)], and the abundance of unusually vulnerable and densely concentrated food.

Our results provide strong support for trait-based hypotheses about animal robustness to climatic catastrophes and show how responses propagate across multiple spatiotemporal scales and levels of organization, from individuals to populations to the community. Small body size and association with exposed habitat made herbivores less resistant to the effects of a powerful cyclone across timescales ranging from hours and days (differential ability to evade rising floodwaters) to more than a year (differential degree of nutritional shortfall and ability to withstand it). Our findings are broadly consistent with previous work linking body size and mobility to cyclone robustness on small islands (Spiller et al. 1998), supporting the scalability of these relationships and the proposition (Schoener & Spiller 2006) that a general trait-based theory may enable researchers to predict the impacts of extreme events across terrestrial animals at large.

More time will be needed to know whether Cyclone Idai has long-lasting effects on community structure, and how a more frequent and/or intense cyclone regime will affect community dynamics. For example, it is possible that the higher fecundity of small-bodied species will enable faster recovery, offsetting the costs of low resistance on long-term robustness (cf. Spiller et al. 1998). Yet, it is noteworthy that Idai reversed the prevailing trend in community reassembly back toward the historically dominant large-bodied species, possibly signaling a tipping point in Gorongosa's postwar recovery trajectory and highlighting the role of disturbance in rewilding efforts. As the frequency of severe weather events increases in concert with increasing efforts to restore depleted megafaunal assemblages (Perino et al. 2019), predicting how severe perturbations will filter community structure is a pressing goal (Thibault & Brown 2008, Betts et al. 2019). Although traits conferring fast population growth (small body size) and high visibility (open habitat affiliation) may be appealing for restoration and ecotourism initiatives, these same traits increase vulnerability to extreme climatic events.

Literature Cited

Becker, J. A., M. C. Hutchinson, A. B. Potter, *et al*. 2021. Ecological and behavioral mechanisms of density-dependent habitat expansion in a recovering African ungulate population, *Ecological Monographs* 91 e01476.

Betts, M. G., C. Wolf, M. Pfeifer, *et al.* 2019. Extinction filters mediate the global effects of habitat fragmentation on animals. *Science* 366:1236-1239.

Chand, S. S., K. J. E. Walsh, S. J. Camargo, *et al*. 2022. Declining tropical cyclone frequency under global warming, *Nature Climate Change* 12:655-661.

Charrua, A. B., R. Padmanaban, P. Cabral, S. Bandeira, and M. M. Romeiras. 2021. Impacts of the tropical Cyclone Idai in Mozambique: a multi-temporal Landsat satellite imagery analysis. *Remote Sensing* 13:1-17.

Elsner, J., J. Kossin, and T. Jagger. 2008. The increasing intensity of the strongest tropical cyclones. *Nature* 455:2-5.

Daskin, J. H., J. A. Becker, T. R. Kartzinel, A. B. Potter, R. H. Walker, F. A. A. Ericksson, C. Buoncore, A. Getraer, R. A. Long, and R. M. Pringle. 2022. Allometry of behavior and niche differentiation among congeneric African antelopes. *Ecological Monographs* e1549.

Donihue, C. M., A. Herrel, A. C. Fabre, A. Kamath, A. J. Geneva, T. W. Schoener, J. J. Kolbe, and J. B. Losos. 2018. Hurricane-induced selection on the morphology of an island lizard. *Nature* 560:88-91.

Gaynor, K. M., J. H. Daskin, L. N. Rich, and J. S. Brashares. 2021. Post-war wildlife recovery in an African savanna: evaluating patterns and drivers of species occupancy and richness. *Animal Conservation* 24:510-522.

Global Disaster Alert and Coordination System. 2019. Overall Red alert Tropical Cyclone for IDAI-19. Joint Research Center of the European Union.

Grant, P. R., B. R. Grant, R. B. Huey, M. T. J. Johnson, A. H. Knoll, and J. Schmitt. 2017. Evolution caused by extreme events. *Philosophical Transactions of the Royal Society B* 372:20160146.

Jentsch, A., J. Kreyling, and C. Beierkuhnlein. 2007. A new generation of climate-change experiments: events, not trends. *Frontiers in Ecology and the Environment* 5:365-374.

Kingdon, J. 1997. *The Kingdon field guide to African mammals* (Bloomsbury, London, ed. 2).

Levin, S. A., and J. Lubchenco. 2008. Resilience, robustness, and marine ecosystem-based management, *BioScience* 58:27-32.

Lin, T. C., J. A. Hogan, and C. T. Chang. 2020. Tropical cyclone ecology: a scale-link perspective. *Trends in Ecology and Evolution* 35:594-604.

Noonan, M. J., C. H. Fleming, M. A. Tucker, *et. al*. 2020. Effects of body size on estimation of mammalian area requirements. *Conservation Biology* 34:1017-1028.

Pansu, J., M. C. Hutchinson, T. M. Anderson, *et.al.* 2022. Generality of cryptic dietary niche differentiation in diverse large-herbivore assemblages. *Proceedings of the National Academy of the Sciences USA* 119:e2204400119.

Perino, A., H. M. Pereira, L. M. Navarro, N. Fernández, *et al.*. 2019. Rewilding complex ecosystems. *Science* 364:eaav5570.

Peters, R. H. 1983. *The Ecological Implications of Body Size* (Cambridge University Press, New York).

Potter, A. B., M. C. Hutchinson, J. Pansu, B. W. Wursten, R. A. Long, J. M. Levine, and R. M. Pringle. 2022. Mechanisms of dietary resource partitioning in large-herbivore assemblages: a plant-trait-based approach. *Journal of Ecology* 110:817-832.

Pruitt, N.,A. G. Little, S. J. Majumdar, T. W. Schoener, and D. N. Fisher. 2019. Call-to-Action: A global consortium for tropical cyclone ecology. *Trends in Ecology and Evolution* 34:588-590.

Schoener, T. W., D. A. Spiller, and J. B. Losos. 2004. Variable ecological effects of hurricanes: the importance of seasonal timing for survival of lizards on Bahamian islands. *Proceedings of the National Academy of the Sciences USA* 101:177-181.

Schoener, T. W., and D. A. Spiller. 2006. Nonsynchronous recovery of community characteristics in island spiders after a catastrophic hurricane. *Proceedings of the National Academy of the Sciences USA* 103:2220-2225.

Smith, M. 2011. An ecological perspective on extreme climatic events: A synthetic definition and framework to guide future research. *Journal of Ecology* 99:656-663.

Spiller, D. A., J. B. Losos, and T. W. Schoener. 1998. Impact of a catastrophic hurricane on island populations. *Science* 281:695-697.

Stalmans, M. E., T. J. Massad, M. J. S. Peel, C. E. Tarnita, and R. M. Pringle. 2019. War-induced collapse and asymmetric recovery of large-mammal populations in Gorongosa National Park, Mozambique. *PLoS ONE* 14:e0212864.

Tanner, E. V., F. Rodriquez-Sanchez, J. R. Healey, R. J. Holdway, and P. J. Bellingham. 2014. Long-term hurricane damage effects on tropical forest tree growth and mortality. *Ecology* 95:2974-2983.

Thibault, K., and J. Brown. 2008. Impact of an extreme climatic event on community assembly. *Proceedings of the National Academy of the Sciences USA* 105:3410-3415.

Ummenhofer, C. C., and G. A. Meehl. 2017. Extreme weather and climate events with ecological relevance: a review. *Philosophical Transactions of the Royal Society B* 372:20160135.

Wang, S., R. Toumi. 2021. Recent migration of tropical cyclones toward coasts. *Science* 371:514-177.

Wiley, J. W., and J. M. Wunderle Jr. 1993. The effects of hurricanes on birds, with special reference to Caribbean islands. *Bird Conservation International* 3:319-349.

Zeng, H., J. O. Chambers, R. I Negrón-Juárez, and M. D. Powell. 2009. Impacts of tropical cyclones on U. S. forest tree mortality and carbon flux from 1851 to 2000. *Proceedings of the National Academy of the Sciences USA* 106:7888-7892.

Warren, M., Why Cyclone Idai is one of the Southern Hemisphere's most devastating storms. *Nature* (26 March 2019).

Chapter 3: Competition mediates fitness costs of heat sensitivity in a tropical carnivore

Walker, R. H., P. D. Mathewson, W. P. Porter[2], K. A. Golabek, N. R. Jordan, J. W. McNutt, and R. A. Long. 2023. Competition mediates fitness costs of heat sensitivity in a tropical carnivore. In preparation. 22 March 2023.

Abstract

Because climate change is likely to outpace the ability of large, K-selected mammals to respond via genetic adaption, behavioral plasticity will likely be many species' primary buffer against heat stress. However, our understanding of how large mammals prioritize competing ecological pressures in changing environments and the consequences of that prioritization for fitness remain largely unknown. Here, we combine movement and demographic data with spatiotemporally explicit predictions of thermoregulatory costs from a biophysical model to evaluate behaviorally-mediated effects of the thermal environment on survival and reproductive success of endangered African wild dogs (*Lycaon pictus*). We find that fecundity is constrained by competition among packs wherein larger packs exclude smaller ones from thermally favorable habitats that reduce energetic constraints of heat dissipation on the pregnant female, freeing additional energy to devote to production and resulting in larger litters. Conversely, survival of pups to weaning is not mediated by thermoregulatory costs but likely by improved nutritional provisioning stemming from the better hunting success of larger packs. Our results suggest that (1) thermal refugia are a key component of habitat quality for wild dogs that will likely increase in importance as the climate warms, (2) behavioral responses to variation in the thermal landscape have important effects on fitness of this endangered carnivore, and (3) behavioral plasticity at the pack level is constrained by pack size and corresponding competitive ability.

Main Text

Introduction

Behavioral plasticity is the central mechanism by which animals cope with rapid environmental change (Huey et al. 2003, Beever et al. 2017). The ability to shift ranges in response to human development, employ new foraging strategies to exploit increasingly fragmented habitats, or use thermal refugia to buffer the impacts of rising temperatures will shape the trajectories of animal populations in the

Anthropocene (Kearney et al. 2009, Sih et al. 2010, van Buskirk 2012). Behavioral responses to environmental variation, however, are often constrained by other ecological factors. For example, competition and predation risk shape animal movement decisions and can restrict access to favorable habitats (Fretwell and Lucas 1970, Lima and Dill 1990). Understanding the nature and strength of such tradeoffs and identifying thresholds of risk and reward that modulate the prioritization of competing ecological pressures will be critical for predicting population and community dynamics in a rapidly changing world.

Because reproduction (pregnancy and lactation) dramatically increases endogenous heat loads (Speakman and McQueenie 1996, Urison and Buffenstein 1995, Bowers et al. 2009), the ability to dissipate heat can constrain reproductive performance even when energy supplies are effectively unlimited ('heat dissipation limit theory'; Król et al. 2003, Król and Speakman 2003a,b, Speakman and Król 2010a,b). Increasing temperatures over the next century may exacerbate this constraint, especially for large, heat-sensitive mammals faced with tradeoffs between costs of thermoregulation and other factors. Although large mammals possess considerable capacity for adjusting their behavior temporally (e.g., by shifting from diurnal to nocturnal or crepuscular activity; du Toit and Yetman 2005, Owen-Smith and Goodall 2014, Gaynor et al. 2018) and/or spatially (e.g., by selecting thermally favorable habitats; Kinahan et al. 2007; van Beest et al. 2012; Long et al. 2014, 2016) to reduce costs of thermoregulation, such changes often carry costs of a different nature. For example, many apex predators (e.g., African lion, *Panthera leo*) hunt at night, increasing the risk to prey or competitors of shifting away from diurnal activity (Cozzi et al. 2012, Veldhuis et al. 2020). Dominant competitors also exclude others from favorable areas (i.e., 'ideal despotic distribution', Fretwell 1972), limiting access to spatially restricted thermal refugia (Hamilton et al. 2016, Legault et al. 2020, Veldhuis et al. 2020). Long-lived, iteroparous animals are well known for favoring their own survival over reproductive investment (Gaillard et al. 2000, Ellison 2003, Brown and Sibly 2006, Therrien et al. 2008), and thus temperature thresholds at which costs of thermoregulation begin to outweigh direct mortality risks are likely to be relatively high in such species. This life-history strategy, in combination with limits to heat dissipation imposed by large body size, highlight the potential for climate warming to directly impact reproductive success, and thus population performance, of large mammals.

African wild dogs (*Lycaon pictus*; hereafter, 'wild dogs') are large tropical mammals that may be particularly vulnerable to climate warming. As cursorial predators, wild dogs commonly travel at >10-km per day while foraging (Hubel et al. 2016a), expending energy each day at levels approaching physiological limits on sustained metabolic rates (Hammond and Diamond 1997, Gorman et al. 1998). The energetic extremes experienced by wild dogs make them especially vulnerable to constraints and

tradeoffs related to heat dissipation. Previous work has shown that higher ambient temperatures are associated with reduced hunting time (Woodroffe et al. 2017), shifts in reproductive phenology (McNutt et al. 2009, Abrhams et al. 2022), and declines in reproductive success across three sub-Saharan populations (Woodroffe et al. 2017). As obligately social animals, wild dogs rely on helpers to take down larger prey (Creel and Creel 1995), defend kills from kleptoparasitism (Fanshawe and Fitzgibbon 1993), and provision pups (Forssman et al. 2018, Jordan et al. 2022). Pack size is thus a critical component of wild dog's ability to survive and reproduce (Courchamp and Macdonald 2001, Creel and Creel 2015), with larger packs garnering better success in hunting (Creel and Creel 1995) and defense (Carbone et al. 1997, Jackson et al. 2017) than smaller packs. Given these life history traits, wild dogs make an ideal study species to evaluate whether individual behaviors can mitigate climatological constraints and whether competition mediates use of favorable thermal environments.

Here, we combine movement and demographic data with output from a spatiotemporally explicit biophysical model to assess fitness consequences of space-use decisions by wild dogs in northern Botswana. Our objectives were to (1) evaluate whether and to what degree wild dogs buffered themselves against effects of climate on reproductive success by optimizing selection of the thermal landscape, and (2) identify ecological mechanisms underpinning differences in heat stress, and associated fitness consequences, among packs. In accordance with heat dissipation limit theory (Speakman and Król 2010b), we hypothesized (H1) that variation in use of the thermal landscape (i.e., spatiotemporal variation in energy and water costs of thermoregulation) would lead to corresponding variation in reproductive performance among packs. We predicted that (1) packs that use less costly areas when the reproductive female is pregnant will produce larger litters than packs that use costlier areas, and (2) packs that rear their offspring in less costly areas will recruit proportionally more young to weaning than those that use costlier areas while the reproductive female is lactating. We also hypothesized (H2) that free-ranging wild dogs assess costs of thermoregulation as a critical component of habitat quality and that more dominant competitors would exclude subordinates from the least costly habitats as predicted by ideal despotic distribution theory (Fretwell and Lucas 1969, Fretwell 1972). Because wild dogs are territorial and larger packs exclude smaller packs from contested areas (Creel and Creel 2002, Jackson et al. 2017), we used pack size as an index of competitive ability. Accordingly, we predicted that larger packs would consistently show stronger selection for low-cost habitats, and that pack size would be positively correlated with litter size and recruitment rates.

Results and discussion

We first evaluated the relative physiological costs experienced by a breeding female in our study area at each phase of the communal pup rearing cycle (Malcom and Marten 1982; Figure 3.1-2). Wild dog

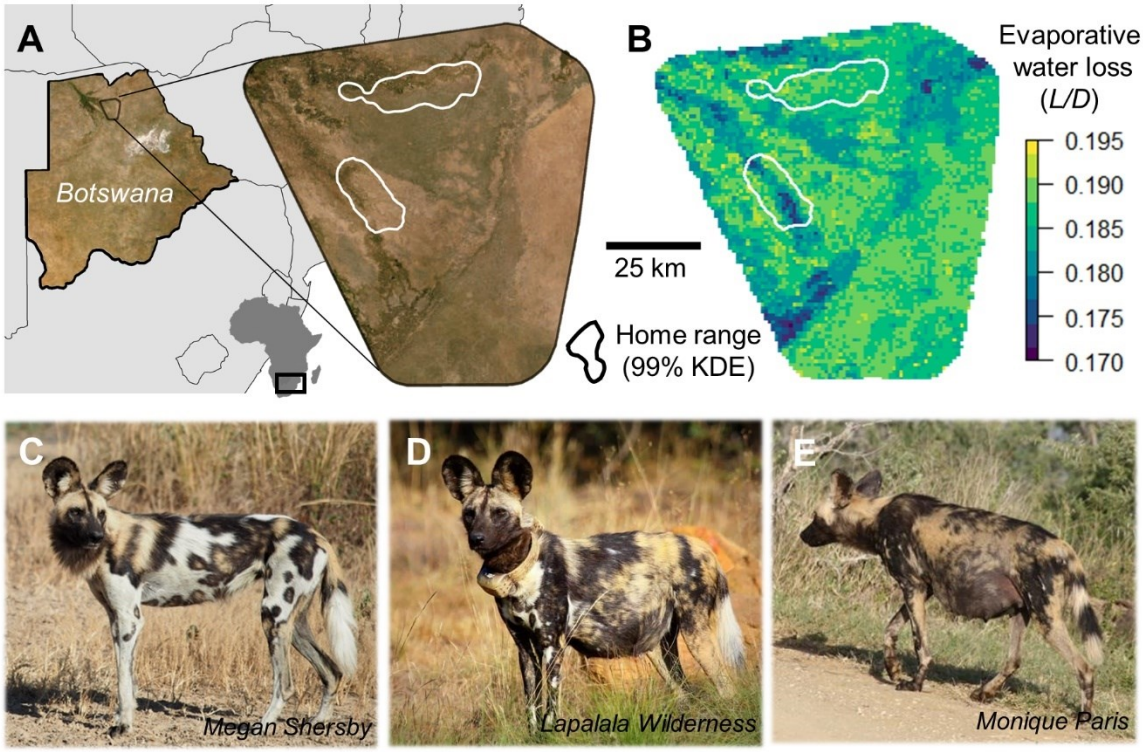

Figure 3.1. Microclimate and physiological data were used to parameterize biophysical models and estimate spatiotemporally explicit costs of thermoregulation (evaporative water loss, L/D) for African wild dogs. (**A**) We used publicly available climatological data to quantify the thermal environment at a 1-km^2 spatial resolution and weekly temporal grain (2012-2016) across our study area in northern Botswana. Two pack home ranges (white polygons; estimated via 99% kernel density estimation) during the pregnancy phase of the pup rearing cycle (see: Figure 2) are drawn for comparison with panel (B). We integrated output from the microclimate model with morphological and physiological data from (**C**) nonreproductive, (**D**) pregnant, and (**E**) lactating wild dogs to solve the heat balance equation and estimate the evaporative water loss required for each demographic to maintain homeothermy in the modeled environment. Panel (**B**) shows spatial variation in predicted evaporative water loss (L/D) for a pregnant female to maintain heat balance in June 2012. Pack home ranges (white polygons; during the pregnancy phase of the pup rearing cycle (see: Figure 2) illustrate differential use of the energetic landscape: the northern pack occupies a more energetically costly habitat than the southern pack.

reproduction is highly seasonal, with one female per pack breeding at the start of winter and moving with the pack throughout gestation. Prior to parturition, the pack selects fixed den sites at which the reproductive female typically remains to rear her pups for 3 months post birth while the pack communally provisions her and supplements her dependent pups (Malcom and Marten 1982; Figure 3.2a). We used the biophysical model, Niche Mapper (Porter and Gates 1969, Porter and Mitchell 2006, Kearney and Porter 2009, Kearney and Porter 2016, Mathewson et al 2020, Rogers et al. 2021, Campbell-Staton et al. 2021, Verzuh et al. 2022), to estimate the (1) hourly rates of evaporative water loss necessary for wild dogs to achieve heat balance for the breeding female during the course of an average day in each phase of the pup rearing cycle (non-reproductive, pregnant, and lactating) at a representative location in our study area

(Figure 3.2b) and (2) mean daily rates of evaporative water loss necessary to maintain homeothermy at a 1-km^2 spatial resolution at weekly intervals in each stage of the pup rearing cycle from 2012–2016 (Figure 3.1b, Figure 3.2c, Tables C.1-3). Costs of thermoregulation were substantially higher for reproductive than non-reproductive individuals at both hourly (22% increase in mean rate of evaporative water loss; reproductive = 0.005 mL/s; nonreproductive = 0.004 mL/s) and daily (110% increase in mean rate of evaporative water loss rates; reproductive = 0.26 L/D; nonreproductive = 0.12 L/D) time scales (Figure 3.2b,c). This result highlights the potential for heat-dissipation capacity to limit reproductive performance of wild dogs and for behavioral strategies that reduce thermoregulatory costs to influence fitness.

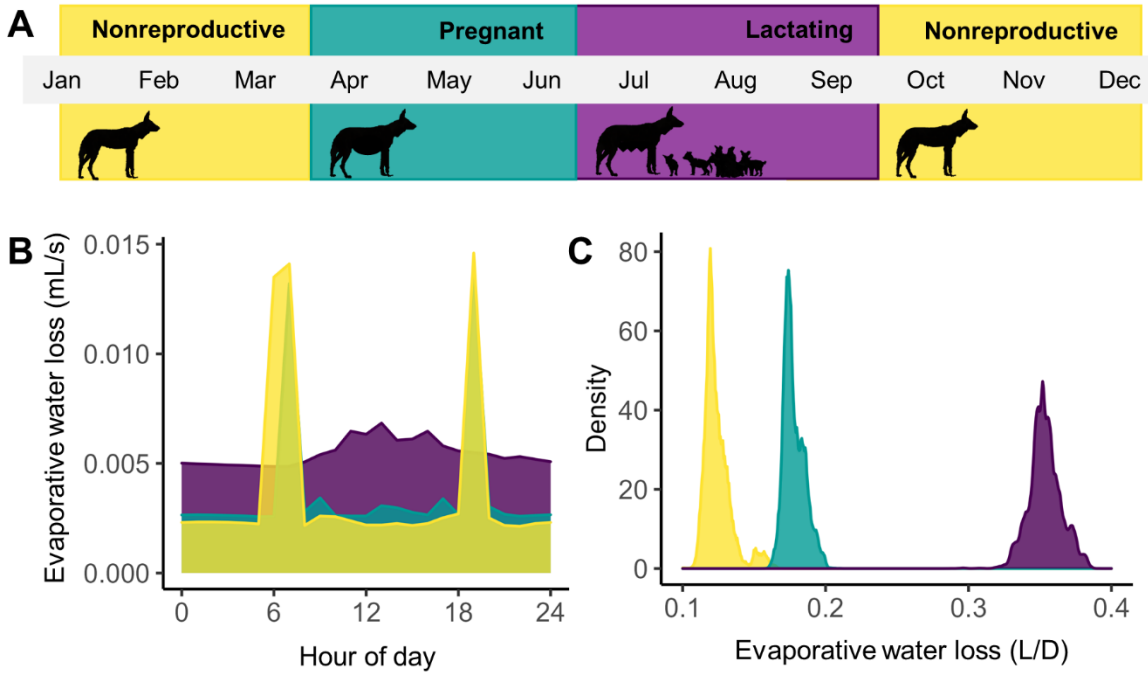

Figure 3.2. Costs of thermoregulation vary over phases of the pup rearing cycle. (**A**) The average yearly pup rearing cycle in northern Botswana consists of a nonreproductive phase (yellow) from August–March, a ~70 day pregnancy phase (light blue) in which pregnant females move with the pack until whelping in early June, and a 3-month lactation phase (dark purple) during which pups are guarded in dens. Peak lactation occurs in the first month after parturition, during which the reproductive female and pups remain in a den and pups are fully dependent on milk for sustenance. During subsequent weeks of the ~3-month denning period, pups begin to wean by venturing above ground to solicit regurgitation of predigested meat from pack mates. (**B**) Hourly evaporative water loss predicted for an average day during each phase of the pup rearing cycle varies substantially, with lactating females incurring the greatest costs despite being sedentary. The two daily peaks in energetic costs show the added heat dissipation load incurred by crepuscular hunting activity during the nonreproductive and pregnant phases of the pup rearing cycle; costs during all other hours assume individuals are at rest in the shade. (**C**) The distribution of predicted costs across the study area for resting African wild dogs during each phase of the pup rearing cycle illustrate significantly higher costs for reproductive than for nonreproductive individuals.

We next evaluated whether pregnant wild dogs could reduce thermal constraints on reproduction by using less costly habitats. To quantify the thermal costs of space use during pregnancy, we (1) partitioned hourly location data from a GPS collared individual in each pack to encompass the 70 days prior to whelping (gestation length for wild dogs; Monfort et al. 1997) for the 12 litters for which we had both movement and demographic data (Table C.4), (2) extracted weekly evaporative water loss estimates for a pregnant wild dog from each raster cell to the GPS locations that intersected that cell during the corresponding week, and (3) found the mean of location-specific values to estimate the typical evaporative water loss (L/D) required for the breeding female in each pack to maintain homeothermy during the pregnancy phase of the pup rearing cycle. We then assessed relationships between litter size and both use (i.e., rate of evaporative water loss across GPS points) and selection (use relative to availability at the landscape and pack-range scales) of the thermal landscape (Figures C.5-6). We quantified availability by extracting evaporative water loss to random points distributed across the landscape or pack-range. Previous work has suggested that pack size has a positive impact on reproductive performance by increasing hunting success, and thus nutrient intake by the breeding female during gestation (Courchamp and Macdonald 2001). We therefore also evaluated the direct influence of pack size on litter size.

Larger packs generally had larger litters, though not significantly so (Figure 3.3a). We find packs' use of the thermal environment during pregnancy underpins this relationship. Breeding females in packs that used costlier areas during the pregnancy phase of the pup rearing cycle produced significantly smaller litters (Figure 3.3b). The direction of this relationship remained consistent when we analyzed selection rather than use of the thermal landscape, although the selection results were not statistically significant at either scale (Figures C.5-6). These results support our prediction that reproductive performance in wild dogs is constrained by the ability of pregnant females to dissipate the additional endogenous heat generated during fetal development. To our knowledge, our study is the first to report of behaviorally-mediated impacts of the thermal environment on fecundity of a wild large mammal. Our results contribute to growing literature on impacts of the thermal environment on activity budgets (Woodroffe et al. 2017, Rogers et al. 2021), accumulation of fat reserves (van Beest et al. 2013, Long et al. 2016), and reproductive phenology (McNutt et al. 2019, Abhrams et al. 2022) of free-ranging large mammals, and align with previous research on the impacts of heat stress on fecundity of mammals in agricultural or lab environments (Hansen 2009, Takahashi 2012).

We next considered the potential role of competition in generating heterogeneity among packs in use of the thermal landscape during pregnancy. We tested the predicted that if African wild dogs assess costs of thermoregulation as a component of habitat quality, packs should compete for access to thermally

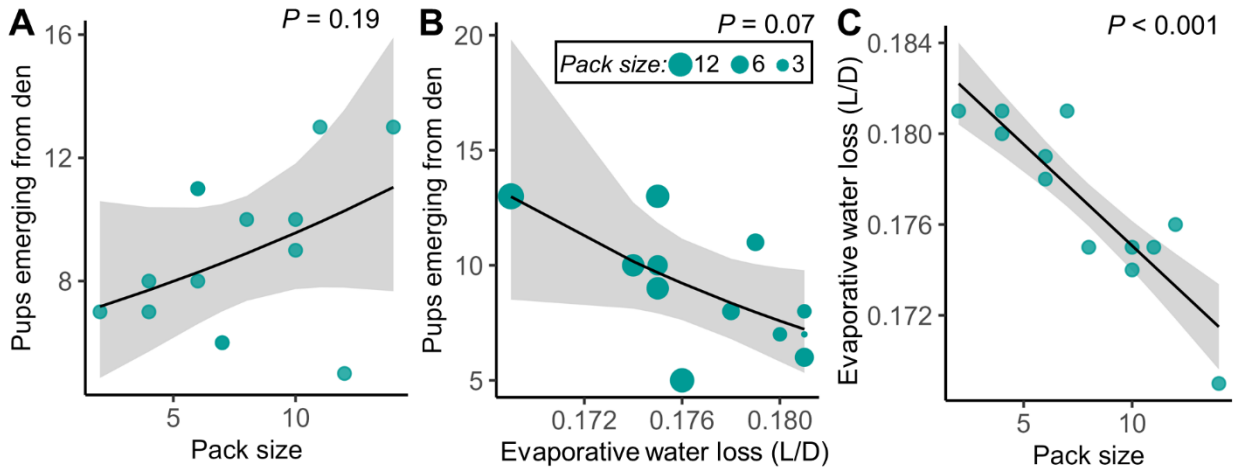

Figure 3.3. Use of the energy landscape constrains litter size. (A) Pack size had a positive, nonsignificant (α = 0.10) effect on litter size (generalized linear model with a Poisson error distribution: $\beta_{Pack\ size}$ = 0.04, SE = 0.03, P = 0.19), which aligns with previous research underscoring the importance of pack size for wild dog reproductive success (Courchamp and Macdonald 2001, Creel and Creel 2015). Unlike previous studies that credit this relationship to increased nutritional provisioning, we find that pack's use of the thermal environment is the mechanism driving this relationship. (**B**) Pregnant females in packs that used habitats with lower costs of thermoregulation (i.e., evaporative water loss, L/D) had significantly larger litters (pups counted when first emerging from the den) than females in packs that used costlier habitats during the pregnancy phase of the pup rearing cycle (generalized linear model with a Poisson error distribution: β_{EWL} = -48.8, SE = 26.2, P = 0.07). (**C**) Use of the energy landscape was strongly associated with pack size: larger packs used less costly habitats than smaller packs (linear model: $\beta_{Pack\ size}$ = -0.001, SE = 0.0001, P < 0.001). Together, these results suggest that larger packs competitively exclude smaller packs from higher-quality, more thermally favorable habitats, with concomitant effects on reproductive performance.

favorable habitats, by fitting a linear model with use of the thermal landscape during pregnancy (quantified as described above) as the response and pack size as the predictor variable. We additionally considered the role of variation in the nutritional landscape in driving pack distribution. In our study area, wild dogs prefer to hunt in grassland or mixed woodland habitats, which are selected by wild dogs' favored prey (impala, *Aepyceros melampus*) (Alting et al. 2021). Accordingly, we also evaluated relationships between (1) litter size and use of high-quality foraging habitats (i.e., grassland or mixed woodland ecotypes) during pregnancy, and (2) pack size and use of high-quality foraging habitats during pregnancy.

Consistent with our prediction, we observed a strong, negative relationship between pack size and costs of thermoregulation incurred during pregnancy (Figure 3.3c), with the largest packs using the most thermally favorable habitats. Moreover, we found no relationship between litter size (mixed effects model with Poisson error distribution and per-pack random intercepts: $\beta_{\text{Prey habitat}}$ = -0.82, SE = 0.68, P = 0.23; Figure C.7a) or pack size (mixed effects model with beta error distribution and per-pack random intercepts: $\beta_{\text{Pack size}}$ = -0.82, SE = 0.68, P = 0.23; Figure C.7b) and use of high-quality foraging habitats. Together, these results suggest that African wild dogs are more sensitive to spatiotemporal variation in

costs of thermoregulation than to variation in prey density during pregnancy, with members of more dominant packs gleaning the fitness benefits of using less costly habitats.

Although not as marked as during pregnancy, endogenous heat production also increases during lactation (Friebe et al. 2014, Græsli et al. 2022). Accordingly, we evaluated whether relationships between reproductive performance and selection of the thermal landscape persisted during the lactation phase of the pup rearing cycle when the reproductive female typically resides at one or more fixed den sites and is provisioned by her packmates. To assess whether thermoregulatory costs led to declines in pup survivorship (ostensibly by constraining milk production) during lactation, we first extracted the mean weekly rate of evaporative water loss required for a lactating female to maintain homeothermy while resting in the shade at each den site used to rear each litter (N = 25 litters; median number of dens per litter = 3; min. = 1, max. = 7; Table C.4) across the 3-month lactation period from Niche Mapper output. We first evaluated the relationship between pack size and pup survivorship. We then evaluated the relationships between mean energetic costs experienced during lactation and (1) proportional pup survivorship to weaning and (2) pack size. To address the potential role of energy supplies in modulating pup recruitment, we evaluated (1) packs' use of prey preferred habitats during the denning and pup survivorship, and (2) pack size and use of the areas associated with high prey density during denning.

Consistent with prior work on wild dog pup recruitment (Courchamp and Macdonald 2001, Creel and Creel 2015), we observe a positive relationship between pack size and pup survival (Figure 3.4a). Contrary to our results during pregnancy, costs of thermoregulation incurred by lactating females at den sites did not predict pup recruitment to weaning (Figure 3.4b) and was unrelated to pack size (Figure 3.4c). These results suggest that milk production was not constrained by thermoregulatory costs and that the thermal landscape was not a primary determinant of den site selection and that factors other than the cost side of the energy balance equation, but that still vary with pack size, constrain reproductive success after pups are born. We found no relationship between pack size and use of high-quality foraging habitats (mixed effects model with beta-error distribution and per-pack random intercepts: $\beta_{Pack\ size}$ = -0.0003, SE = 0.04, P = 0.99; Figure C.8a) or between use of those habitats and pup survival (mixed effects model with beta-error distribution and per-pack random intercepts: $\beta_{Prey\ \text{habitat}}$ = -0.52, SE = 3.9, P = 0.89; Figure C.8a). Nevertheless, larger packs in our study population have better hunting success than smaller packs because of increased opportunistic encounters with prey (Hubel et al. 2016a,b) and can thus better provision the reproductive female and pups during lactation while avoiding potentially risky habitat. Previous work has similarly demonstrated the influence of pack size on pup survivorship through provisioning and protection from competitors (Courchamp and Macdonald 2001, Creel and Creel 2015, Forssman et al. 2018), and that den site selection is primarily driven by efforts to mitigate exposure to risk

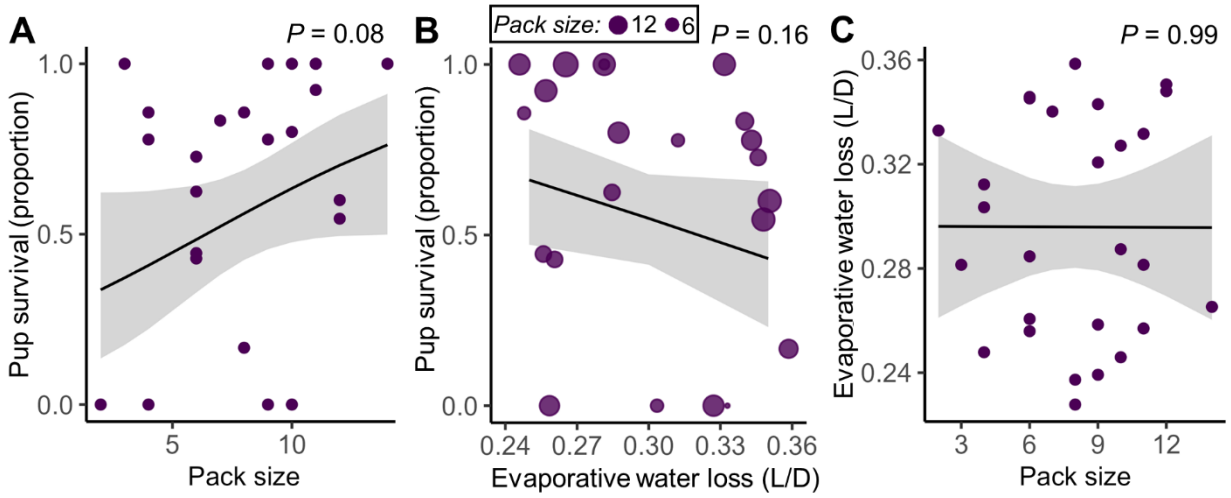

Figure 3.4. Pack size predicts pup survivorship through the denning period. (**A**) Pack size had a positive effect on pup survivorship to 3 months: larger packs had significantly ($\alpha = 0.10$) higher pup survival than smaller packs through the lactation phase of the pup rearing cycle (mixed effects model with a beta error distribution and per-pack random intercepts: $\beta_{Pack\ size} = 0.15$, SE = 0.09, $P = 0.08$). Unlike the pregnancy phase of the pup rearing cycle, this relationship was not explained by packs' use of the thermal environment. (**B**) Thermoregulatory costs incurred during lactation did not significantly influence the proportion of pups surviving to 3 months of age (mixed effects model with a beta error distribution and per-pack random intercepts: $\beta_{EWL} = -9.5$, SE = 6.7, $P = 0.16$). (**C**) Larger packs did not use den sites that were less costly for lactating individuals than smaller packs (mixed effects model with a Gaussian error distribution and per-pack random intercepts: $\beta_{Pack\ size} = -0.00004$, SE = 0.003, $P = 0.99$). Together, these results suggest that energetic costs are no longer a primary determinant of recruitment rates after pups are born. Instead, other mechanisms associated with pack size, such as energy 'gain' through the provisioning of regurgitated food for pups and the lactating female or better protection from adversaries (e.g., competing packs or dominant guild members), likely underpin variation in pup survivorship through the denning period.

of predation from lions (Jackson et al. 2014, Davies et al 2014, Alting et al. 2021). Our mechanistic results illustrate context dependent trade-offs among nutrition, thermoregulatory costs, and risk and highlight the consequences of use of the thermal environment for pup production, the vital rate the most contributes to population growth for this endangered species (Creel et al. 2004).

Our study is among the first to elucidate the mechanistic underpinnings of thermal constraints on reproductive success in a wild population of large mammals and answers recent calls to investigate the degree to which mammals can use behavior to buffer themselves against such constraints (Speakman and Król 2010a, Fuller et al. 2016, Beever et al. 2016). Consistent with heat dissipation limit theory (Speakman and Król 2010b), fecundity of African wild dogs in Botswana was limited by the ability of the breeding female to dissipate heat. Experimental work with smaller mammals has produced similar results. For example, laboratory mice rearing young at room temperature (21°C) ate less food, produced less milk, and weaned smaller offspring than mice exposed to cooler temperatures (8°C) (Johnson and

Speakman 2001). Similarly, shaved mice ate more food, produced more milk, and weaned larger offspring than unshaved mice at the same temperatures (Krol et al. 2007). Lab mice's ability to dissipate heat during lactation, their most energetically demanding life stage, thus constrained reproductive success even when nutritional resources were unlimited. Thermal constraints on production have long been documented in livestock, where high ambient temperatures limit mammalian reproductive rates despite abundant nutritional resources (Krishnan et al. 2017, Sinha et al. 2017). Our finding that wild dogs' ability to dissipate heat during pregnancy, when the breeding female must meet both the metabolic demands of fetal growth and extreme energetic requirements of cursorial hunting (Gorman et al. 1998, Hubel et al. 2016a,b), mediates the number of offspring that are born and survive to emerge from the den contributes evidence to a growing body of literature that free-ranging mammals are sensitive to and limited by energetic costs of thermoregulation (Speakman and Król 2010b, Long et al. 2014,2016, Wells et al. 2016, Rogers et al. 2021, Verzuh et al. 2022).

During pregnancy, variation in the thermal landscape led to an ideal despotic distribution (Fretwell and Lucas 1970) of packs, wherein larger, more dominant (Creel and Creel 2002, Jackson et al. 2017) packs occupied the least costly areas. Competitive use of the thermal environment has never before, to our knowledge, been documented in large mammals despite an abundance of literature predicting the vulnerability of the taxa to high ambient temperatures (Khaliq et al. 2014, Fuller et al. 2016, Veldhuis et al. 2019) and documenting competition for thermal refugia in ectothermic species [e.g., bearded dragons (Khan et al. 2010), salmonids (Hitt et al. 2016), skinks (Michelangeli et al. 2018)]. Ecologists have historically focused energetic "supply" (i.e., nutritional resources) as the central driver of intraspecific competition (e.g., Huxley 1942, Stearns 1976, McNab 2002), but in many situations animals are not externally limited by food resources (Boutin 1990, Speakman and Krol 2010b). Indeed, such is the case for wild dogs for which foraging success and population growth do not vary as a function of prey density (Creel and Creel 1998, Creel et al. 2004). In this context, we find that energetic "costs" drive the distribution of packs across our study area during pregnancy and underpin variation in fecundity within the population. Ultimately, high quality environments are those that increase residents' survival and production (VanHorne 1983, Mosser et al. 2009), underscoring the need to incorporate mechanistically derived estimates of thermoregulatory costs into evaluations of suitable habitat in future, hotter environments.

Materials and Methods

Study system

Our study area lies in the Moremi Game Reserve and surrounding Wildlife Management Areas at the edge of the Okavango Delta (19°31'S, 23°37'E; Figure 3.1a). Annual precipitation (300-600-mm) in this region is highly seasonal and occurs in the hot season (October – April), while the annual flood peaks in the delta terminus during the cool season (May – September) (McNutt and Silk 2008). Long-term monitoring of the African wild dog population in our study area was initiated in 1989 and has run continuously to the present day (McNutt 1996). Our dataset includes the period in which each pack had (*i*) at least one individual fitted with a GPS collar recording hourly relocation data, and (*ii*) ground-based monitoring data on pack size and demography (i.e., 2012-2016; Table C4). Den locations and abandonment dates were determined from GPS data or by radio tracking collared individuals from a vehicle on the ground or from the air (182 Cessna fixed-wing aircraft with a radio tracking antenna). Den sites were repeatedly observed from a vehicle to estimate litter size (the maximum number of emergent pups that observers counted at the primary den; van der Meer et al. 2013; Davies et al. 2016, Alting et al. 2022) and pup survivorship to 3 months of age. GPS and radio collars were deployed following previously described procedures (Osofsky et al. 1996) and were in accordance with the guidelines established by the American Society of Mammologists (Sikes & The Animal Care and Use Committee of the American Society of Mammologists 2016). All field work was conducted by the Botswana Predator Conservation Trust under research permit EWT/8/36/4XXXVIII issued by the Ministry of Environment, Nature and Tourism (MENT).

Biophysical modeling

We used the program Niche Mapper to model spatiotemporally explicit costs of thermoregulation of wild dogs across our study area in northern Botswana (Porter and Gates 1969, Porter and Mitchell 2006, Kearney and Porter 2009, Natori and Porter 2007, Mathewson et al 2020, Rogers et al. 2021, Campbell-Staton et al. 2021, Verzuh et al. 2022). Based on fundamental principles of heat and mass exchange between an organism and its environment, Niche Mapper solves coupled energy balance equations using two sub-models that integrate site-specific characteristics of the environment (the 'microclimate' sub-model) and characteristics of the organism (the 'endotherm' sub-model). The model produces hourly and daily estimates of thermoregulatory costs (water loss and metabolic rate) to maintain homeothermy at a given location (Porter and Gates 1969, Porter 2016). The microclimate sub-model uses local climate data to calculate hourly or daily estimates of air temperature, wind speed, humidity, and solar radiation during the 'average' day within a user-supplied time interval (e.g., a day, week, or month depending on the desired output resolution). The accuracy of the microclimate sub-model has been validated across an

array of ecosystems (Porter et al. 1973, Natori et al. 2007, Kearney et al. 2014). The endotherm sub-model integrates user-supplied properties of the model organism that influence rates of heat transfer (e.g., allometry, metabolic rate, pelt characteristics) with vegetation characteristics and outputs from the microclimate model (Long et al. 2014, Fitzpatrick et al. 2015, Mathewson et al. 2015). In addition, the endotherm sub-model included both behavioral and physiological mechanisms for heat dissipation (e.g., angling the body away from the sun, seeking shade, or panting) (Natori et al. 2007). When Niche Mapper is unable to solve the energy balance equation in the climatic conditions specified by the user (i.e., the organism is either gaining or losing heat to the environment), the endotherm sub-model progresses sequentially through a suite of behavioral and physiological thermoregulatory responses from least costly to most costly, thereby producing conservative estimates of thermoregulatory costs that represent a 'best-case scenario' for an organism attempting to achieve heat and mass balance (Long et al. 2014).

Topographic, vegetative, and weather data from a larger study area can be used to extend the single-site Niche Mapper simulations and calculate variation in thermoregulatory costs across landscapes (Natori et al. 2007, Rogers et al. 2021). The landscape-level analysis performs microclimate simulations across the study area at a user-defined spatiotemporal resolution. The endotherm sub-model then uses the microclimate outputs, vegetation characteristics, and supplied organismal data to solve the energy and mass balance equation at each location (i.e., pixel) and time across the study area. Assembling model outputs across sites during a given time period allows the user to create a spatiotemporally explicit raster map of thermoregulatory costs within the study area (Porter et al. 2000, 2002).

We parameterized Niche Mapper's microclimate sub-model at the landscape-scale using publicly available data (Table C.1). Elevation data were obtained from a digital elevation map at 1-km resolution across our study area (Amatulli et al. 2018). Historic maximum and minimum daily temperatures were obtained for each year of our study (2012-2016) at 1-km resolution (Zhang et al. 2018). We averaged daily temperature at each pixel across our study area to obtain mean week-year maximum and minimum ambient temperatures. Percent cloud cover data were obtained from EarthEnv datasets, which use twice-daily MODIS satellite images integrated over 15 years (2000–2014) to generate monthly average cloud cover estimates (Wilson and Jetz 2016). Wind speed data were obtained from WoldClim 2 datasets, which interpolate climate data from > 10,000 weather stations integrated over 30 years (1970-2000) to generate monthly average wind speed estimates (Fick and Hijmans 2017). A microclimate model subroutine estimated relative humidity as a function of daily temperature range and assuming a constant mass of water in the air over the 24-hour interval (Geiger 1965, Porter and Mitchell 2006).

We parameterized Niche Mapper's endotherm sub-model separately for a non-reproductive female, a pregnant, and a lactating wild dog using published data on wild dog and related species' physiology

(Tables C.2-5). We used multipliers of basal metabolic rate (BMR) within the endotherm sub-model to account for heat produced by differing levels reproductive activity. For each modeled demographic, we parameterized the endotherm sub-model to simulate costs associated with resting in the shade throughout the full 24-hour day.

We used the package NicheMapR, the R implementation of the microclimate sub-model of Niche Mapper, in R version 4.2.2 to calculate environmental conditions in every pixel in our study area (Kearney and Porter 2016, R Core Team 2022). We wrote an R script to act as a data handler and call the endotherm sub-model to perform calculations of thermoregulatory costs for each modeled demographic (i.e., nonreproductive, pregnant and lactating) for each pixel in the study area. To help validate our Niche Mapper outputs, we conducted a metabolic chamber simulation that allowed us to compare the thermal neutral zone of our modeled animals to experimentally derived values (Figure C.1). Additionally, we used Latin hypercube sampling to evaluate the sensitivity of Niche Mapper outputs to variation in key physiological traits (Figure C2-4). Following previous authors who have conducted similar sensitivity analyses of Niche Mapper outputs for other species (e.g., Wang et al. 2018, Rogers et al. 2021, Campbell-Staton et al. 2021), we ran simulations for 1,000 random combinations of endotherm sub-model parameter values within specified ranges (Tables C.3). Both avenues of model validation provided strong support for the accuracy of our model predictions.

Statistical analyses

To assess the impact of thermoregulatory costs incurred during pregnancy on fecundity, we regressed litter size (i.e., maximum number of pups observed emerging from the den) against mean predicted rates of evaporative water loss at locations used during pregnancy using a generalized linear model with a Poisson error distribution. Ground-monitoring data enabled precise estimates of whelping dates for each litter included in our study (N = 25; Table C.4) and facilitated partitioning of GPS data among phases of the pup rearing cycle in each pack-year. Hourly movement data during pregnancy and lactation were available for 12 and 15 pack-years, respectively (Table C.4). Because African wild dogs are obligately social and rarely travel more than 1 km away from their pack mates while on the move (Hubel et al. 2016b), we assumed that any GPS-collared individual's use of the thermal landscape during the pregnancy phase of the pup rearing cycle represented the movement of the reproductive female within the pack. Accordingly, we included movement data from only one collared individual per pack-year to avoid pseudoreplication. In the two instances in which more than one individual was collared in the same pack-year, we used the reproductive female's GPS-collar data in analyses of space use during the pregnancy phase, and the nonreproductive individual's collar data in analyses of the lactation phase of the pup rearing cycle. To test that our results are not sensitive to the choice of which GPS-data we used for each

pack-year, we regressed litter size against mean predicted rates of evaporative water loss derived from each potential rarefication. Results from this analysis confirm that our results are robust to which collared individual in a given pack-year is included in the analysis.

To assess the impact of thermoregulatory costs incurred during lactation on recruitment of pups to weaning, we regressed the proportion of pups surviving to 3 months against mean predicted rates of evaporative water loss at den sites (N = 81) used by each reproductive female and her litter (N = 25) using a generalized liner mixed effects model with a beta error distribution and per-pack random intercepts. For instances in which all (n = 4) or none (n = 4) of the pups survived to 3 months of age, we specified pup survival as 0.999999 or 0.000001, respectively, to adhere to model assumptions.

To assess the influence of high-quality foraging habitats on wild dog reproductive success, we regressed use of high-quality foraging habitats against litter size, pup survivorship, and pack size. Recent research in our study area identified mixed woodland and dry grassland habitats as the preferred habitat of both impala (preferred wild dog prey) and lion (primary intraguild predation) and show that wild dog prefer to hunt in those high risk/reward habitats (Alting et al. 2021). We thus quantified use of high-quality foraging habitats as the proportion of GPS fixes during pregnancy or lactation that intersect pixels classified as *Acacia*- or *Combretum*-dominated dry woodlands or dry grassland habitats in a publicly available 30-m resolution raster of ecotypes in the Okavango Delta (McCarthy et al. 2007). We additionally verified that use of high-quality foraging habitats was not correlated with energetic costs (i.e., evaporative water loss) using a generalized linear model with a beta-error distribution and per-pack random intercepts.

We fit models using the *glmmTMB()* function in the *glmmTMB* package and inspected model residuals using the *simulateResiduals()* function in the *DHARMa* package in R (Brooks et al. 2017, Harting 2022). We found no evidence that model assumptions were violated.

Literature Cited

Abhrams, B., K. Rafiq, N.R. Jordan, and J.W. McNutt. 2022. Long-term, climate-driven phenological shift in a tropical large carnivore. *Proceedings of the National Academy of the Sciences, USA* 119:2121667119.

Alting, B.F., E. Bennitt, K.A. Golabek, B.J. Pitcher, J.W. McNutt, A.M. Wilson, H. Bates, and N.R. Jordan. 2021. The characteristics and consequences of African wild dog (*Lycaon pictus*) den site selection. *Behavioral Ecology and Sociobiology* 75:109.

Amatulli, G., S. Domisch, M.N. Tuanmu, B. Parmentier, A. Ranipeta, J. Malczyk, and W. Jetz. 2018. A suite of global, cross-scale topographic variables for environmental and biodiversity modeling. *Scientific Data* 5:180040.

Beever, E.A., L.E. Hall, J. Varner, A.E. Loosen, J.B. Dunham, M.K. Gahl, F.A. Smith, and J.J. Lawler. 2017. Behavioral flexibility as a mechanism for coping with climate change. *Frontiers in Ecology and the Environment* 15:299-308.

Boutin, S. 1990. Food supplementation experiments with terrestrial vertebrates: patterns, problems, and the future. *Canadian Journal of Zoology* 68:203– 220.

Bowers, S., S. Gandy, B. Anderson, P. Ryan, and S. Willard. 2009. Assessment of pregnancy in the late-getsation mare using digital infrared thermography. *Theriogenology* 72:373-377.

Brooks, M.E., K. Kristensen, K.J. van Benthem, A. Magnusson, C.W. Berg, H. J. Skaug, M. Machler, and B. M. Miller. 2017. *glmmTMB* balances sepped and flexibility among packages for zero-inflated generalized linear mixed modeling. *R Journal* 9:378-400.

Brown, J.H., and R.M. Sibly. 2006. Life-history evolution under a production constraint. *Proceedings of the National Academy of the Sciences USA* 103:17595-17599.

Cambell-Staton, S.C., R.H. Walker, S.A. Rogers, J. De León, H. Landecker, W. Porter, P.D. Mathewson, and R.A. Long. 2021. Physiological costs of undocumented human migration across the southern United States border. *Science* 374:1496-1500.

Carbone, C., J.T. du Toit, and I.J. Gordon. 1997. Feeding success in African wild dogs: does kleptoparasitism by spotted hyenas influence hunting group size? *Journal of Animal Ecology* 66:318-326.

Courchamp, F., and D.W. Macdonald. 2001. Crucial importance of pack size in the African wild dog, *Lycaon pictus*. *Animal conservation* 4:168-174.

Cozzi, G., F. Broekhuis, J.W. McNutt, L.A. Turnbull, D.W. Macdonald, and B. Schmid. 2012. Fear of the dark or dinner by moonlight? Reduced temporal partitioning among African's large carnivores. *Ecology* 93:2590-2599.

Creel, S., and N.M. Creel. 1995. Communal hunting and pack size in African wild dogs, *Lycaon pictus*. *Animal Behavior* 50:1325-1339.

Creel, S., and N.M. Creel. 1998. Six ecological factors that may limit African wild dogs, *Lycaon pictus*. *Animal Conservation* 1:1-9.

Creel, S., and N.M. Creel. 2015. Opposing effects of group size on reproduction and survival in African wild dogs. *Behavioral Ecology* 26:1414-1422.

Creel S., and N.M. Creel. 2002. *The African Wild Dog: Behaviour, Ecology, Conservation*. Princeton University Press: Princeton, New Jersey, USA

Creel, S. M.G.L. Mills, J.W. McNutt. 2004. Demography and population dynamics of African wild dogs in three critical populations. *In*: The Biology and Conservation of Wild Canids. Oxford University Press, London, UK.

Davies, A.B., D. Marneweck, D. Druce, and G. Asner. 2014. Den site selection, pack composition, and reproductive success in endangered African wild dogs. *Behavioral Ecology* 27:1869-187.

du Toit, J.T., and C.A. Yetman. 2005. Effects of body size on the diurnal activity budgets of African browsing ruminants. *Oecologia* 143:317-325.

Ellison, P.T. 2003. Energetics and reproductive effort. *American Journal of Human Biology* 15:342-351.

Fanshawe, J.H., and C.D. Fitzgibbon. 1993. Factors influencing the hunting success of an African wild dog pack. *Animal Behaviour* 45:479-490.

Fick, S.E., and R.J. Hijmans. 2017. WorldClim 2: new 1-km spatial resolution climate surfaces for global land areas. *International Journal of Climatology* 10.1002/joc.5086.

Forssman, K., C. Marneweck, M. O'Rjiain, H. Davies-Mostert, and M. Mills. 2018. Pup provisioning in the cooperatively breeding African wild dog, *Lycaon pictus*, is driven by pack size, social status, and age. *South African Journal of Wildlife Research* 48:013005.

Friebe, A., A.L. Evans, J.M. Arnewmo, S. Blanc, S. Brunberg, G. Feissner, J.E. Swenson, and A. Zedrosser. 2014. Factors affecting date of implantation, parturition, and den entry estimated from activity and body temperature in free-ranging brown bears. *PLoS ONE* 9:e101410.

Fretwell, S.D., and H. L. Lucas. 1969. On territorial behavior and other factors influencing habitat distribution in birds. *Acta Biotheoretica* 19:16-36.

Fretwell, S.D. 1972. *Populations in Seasonal Environments*. Princeton University Press, Princeton, NJ.

Fuller, A., D. Mitchell, S.K. Malyoney, and R. Hetem. 2016. Towards a mechanistic understanding of the responses of large terrestrial mammals to heat and aridity associated with climate change. *Climate Change Responses* 3:1-19.

Gaynor, K.M., C.E. Hojnowski, N.H. Carter, and J.S. Brashares. 2018. The influence of human disturbance on wildlife nocturnality. *Science* 360:1232-1235.

Gaillard, J.M., M. Festa-Bianchet, N.G. Yoccoz, A. Loison, and C. Toïgo. 2000. Temporal variation in fitness components and population dynamics of large herbivores. *Annual Review of Ecology and Systematics* 31:367-393.

Geiger, R. 1965. *The climate near the ground*. Harvard University Press: Massachusetts, USA.

Gorman, M.L., M.G. Mills, J.P. Raath, and J.R. Speakman. 1998. High hunting costs make African wild dogs vulnerable to kleptoparasitism by hyaenas. *Nature* 391:478-481.

Græsli, A.R., A. Thiel, B. Fuchs, F. Stenbacka, W. Neumann, J. Malmsten, N.J. Singh, G. Ericsson, J.M. Arnemo, and A.L. Evans. 2022. Body temperature patterns during pregnancy and parturition in moose. *Journal of Thermal Biology* 109:103334.

Hamilton, C.D., C. Lydersen, R.A. Ims, and K.M. Kovacs. 2016. Coastal habitat use by ringed seals (*Pusa hispida*) following a regional sea-ice collapse: importance of glacial refugia in a changing Arctic. *Marine Ecology Progress Series* 545:261-277.

Hammond, K.A. and J. Diamond. 1997. Maximal sustained energy budgets in humans and animals. *Nature* 386:457-462.

Hansen, P.J. 2009. Effects of heat stress on mammalian reproduction. *Philosophical Transactions of the Royal Society B* 364:3341-3350.

Hartig, F. 2022. *DHARMa:* Residual Diagnostics for Hierarchical (Multi-Level/Mixed) Regression Models, R package version 0.3.2.0.

Hitt, N.P., E.I. Snook, and D.L. Massie. 2017. Brook trout use of thermal refugia and foraging habitat influenced by brown trout. *Canadian Journal of Fish Aquatic Science* 74:406-418.

Huey, R.B., P.E., Hertz, and B. Sinervo. 2003. Behavioral drive versus behavioral inertia in evolution: A null model approach. *The American Naturalist* 161:357-366.

Hubel, T.Y., J.P. Myatt, N.R. Jordan, O.P. Dewhirst, J.W. McNutt, and A.M. Wilson. 2016a. Energy cost and return for hunting in African wild dogs and cheetahs. *Nature Communications* 7:11034.

Hubel, T.Y., J.P. Myatt, N.R. Jordan, O.P. Dewhirst, J.W. McNutt, and A.M. Wilson. 2016b. Additive opportunistic capture explains group hunting benefits in African wild dogs. *Nature communications* 7:11033.

Huxley, J. 1942. *Evolution: The Modern Synthesis.* Allen & Unwin, London, UK.

Jackson, C.R., R.J. Power, R.J. Groom, E.H. Masenga, E.E. Mjingo, R.D. Fyumagwa, E. Røskaft, and H. Davies-Mostert. 2014. Heading for the hills: Risk avoidance drives den site selection in African wild dogs. *PLoS One* 9:e99686.

Jackson, C.R., R.J. Groom, N.R. Jordan, and J.W. McNutt. 2017. The effect of relatedness and pack size on territory overlap in African wild dogs. *Movement Ecology* 5:10.

Johnson, M.S., and J.R. Speakman. 2001. Limits to sustained energy intake V. Effect of cold-exposure during lactation in *Mus musculus*. *Journal of Experimental Biology* 204:1967–77.

Jordan, N.J., K.A. Golabek, D.M. Behr, R.H. Walker, L. Plimpton, S. Lostrom, M. Claase, L.K. Van der Weyde, and J.W. McNutt. 2022. Priority of access to food and its influence on social dynamics of an endangered carnivore. *Behavioral Ecology and Sociobiology* 76:13.

Kearney, M.R. and W.P. Porter. 2009. Mechanistic niche modelling: combining physiological and spatial data to predict species' ranges. *Ecology Letters* 12:334-350.

Kearney M, Shine R, and Porter WP. 2009. The potential for behavioral thermoregulation to buffer "cold-blooded" animals against climate warming. *Proceedings of the National Academy of the Sciences, USA* 106: 3835–40.

Kearney, M. R., A. Shamakhy, R. Tingley, D. J. Karoly, A. A. Hoffmann, P. R. Briggs, and W. P. Porter. 2014. Microclimate modelling at macro scales: a test of a general microclimate model integrated with gridded continental-scale soil and weather data. *Methods Ecology and Evolution* 5:273-286.

Kearney, M.R. and W.P. Porter. 2016. NicheMapR—an R package for biophysical modeling: the microclimate model. *Ecography* 40:664-674.

Khaliq, I., C. Hof, R. Prizinger, K. Böhning-Gaese, and M. Pfenninger. 2014. Global variation in thermal tolerances and vulnerability of endotherms to climate change. *Proceedings of the Royal Society B* 281:20141097.

Khan, J.J., J.M.L. Richardson, and G.J. Tattersall. 2010. Thermoregulation and aggression in neonatal bearded dragons (*Pogona vitticeps*). *Physiology and Behavior* 100:180-186.

Kinahan, A.A., S.L. Pimm, and R.J. can Aarde. 2007. Ambient temperature as a determinant of landscape use in the savanna elephant, *Loxodonta africana*. *Journal of Thermal Biology* 32:47-58.

Kingdon, J. 1997. *The Kingdon Field Guide to African Mammals*. Bloomsbury Publishing: London, UK.

Krishnan, G., M. Bagath, P. Pragna, M. K. Vidya, J. Aleena, P. R. Archana, V. Sejian and R. Bhatta. 2017. Mitigation of the heat stress impact in livestock reproduction. In: *Theriogenology* InTechOpen: London, UK.

Król, E., M.S. Johnson, and J.R. Speakman. 2003. Limits to sustained energy intake VIII. Resting metabolic rate and organ morphology of laboratory mice lactating at thermoneutrality. *Journal of Experimental Biology* 206:4283– 4291.

Król, E. and J.R. Speakman. 2003a. Limits to sustained energy intake VI. Energetics of lactation in laboratory mice at thermoneutrality. Journal of Experimental Biology, 206, 4255– 4266.

Król, E., and J.R, Speakman. 2003b. Limits to sustained energy intake VII. Milk energy output in laboratory mice at thermoneutrality. *Journal of Experimental Biology* 206:4267–4281.

Król, E., M. Murphy, and J.R. Speakman. 2007. Limits to sustained energy intake. X. Effects of fur removal on reproductive performance in laboratory mice. *Journal of Experimental Biology* 210:4233-4243.

Legault, G., M.E. Bitters, A. Hastings, and B.A. Melbourne. 2020. Interspecific competition slows range expansion and shapes range boundaries. *Proceedings of the National Academy of the Sciences, USA* 117:26854-26860.

Lima, S.L., and L.M. Dill. 1990. Behavioral decision making under the risk of predation: a review and prospectus. *Canadian Journal of Zoology* 68:619-640.

Long, R.A., R.T. Bowyer, W.P. Porter, P. Mathewson, K.L. Monteith, and J.G. Kie. 2014. Behavior and nutritional condition buffer a large-bodied endotherm against direct and indirect effects of climate. *Ecological Monographs* 84:513-532.

Long, R.A., R.T. Bowyer, W.P. Porter, P. Mathewson, K.L. Monteith, S.L. Findholt, B.L. Dick, and J.G. Kie. 2016. Linking habitat selection to fitness-related traits in herbivores: the role of the energy landscape. *Oecologia* 181:709-720.

Malcolm, J.R., and K. Marten. 1982. Natural selection and the communal rearing of pups in African wild dogs (*Lycaon pictus*). *Behavioral Ecology and Sociobiology* 10:1-13.

Mathewson, P.D., L. Moyer-Horner, E.K. Beever, N.J. Briscoe, M. Kearney, J.M. Yahn, and W.P. Porter. 2017. Mechanistic variables can enhance predictive models of endotherm distributions: the American pika under current, past, and future climates. *Global Change Biology* 23:1048-1064.

Mathewson, P.D., W.P. Porter, L. Barrett, A. Fuller, S.P. Henzi, R.S. Hetem, C. Young, and R. McFarland. 2020. Field data confirm the ability of a biophysical model to predict wild primate body temperature. *Journal of Thermal Biology* 94:102754.

McCarthy, J., T. Bumbricht, and T.S. McCarthy. 2007. Ecoregion classification in the Okavango Delta, Botswana from multitemporal remote sensing. *International Journal of Remote Sensing* 26:4339-4357.

McNab, B.K. 2002. *The Physiological Ecology of Vertebrates: A View from Energetics*. Cornell University Press, Ithaca, New York, USA.

McNutt, J.W. 1996 Adoption in African wild dog, *Lycaon pictus*. *Journal of Zoology* 240:163-173.

McNutt, J.W., and J.B. Silk. 2008. Pup production, sex ratios, and survivorship in African wild dogs, *Lycaon pictus*. *Behavioral Ecology and Sociobiology* 62:1061-1067.

McNutt, J.W., R. Groom, and R. Woodroffe.2019. Ambient temperature provides an adaptive explanation for seasonal reproduction in a tropical mammal. *Journal of Zoology* 309:153-160.

Michelangeli, M., C.T. Goulet, H.S. Kang, B.B.M. Wong, and D.G. Chapple. 2018. Integrating thermal physiology within a syndrome: locomotion, personality, and habitat selection in an ectotherm. *Functional Ecology* 32:970-981.

Monfort, S.L., S.K. Wasser, K.L Mashburn, M. Burke, B. A. Brewer, and S.R. Creel. 1997. Steroid metabolism and validation of noninvasive endocrine monitoring in the African wild dog (*Lycaon pictus*). *Zoo Biology* 16:533-548.

Mosser, A., J.M. Fryxell, L. Eberly, and C. Packer. 2010. Serengeti real estate: density vs. fitness-based indicators of lion habitat quality. *Ecology Letters* 12:1050-1060.

Natori, Y. and W.P. Porter. 2007. Models of Japanese serow (*Capricornis crispus*) energetics predicts distribution on Honshu, Japan. *Ecological Applications* 17:1441-1459.

Owen-Smith, N., and V. Goodall. 2014. Coping with savanna seasonality: comparative daily activity patterns of African ungulates as revealed by GPS telemetry. *Journal of Zoology* 293:181-191.

Porter, W. P., J. W. Mitchell, W. A. Beckman, and C. B. DeWitt. 1973. Behavioral implications of mechanistic ecology: Thermal and behavioral modeling of desert ectotherms and their microenvironment. *Oecologia* 13:1-54.

Porter, W.P. and J.W. Mitchell. 2006. Method and system for calculating the spatial-temporal effects of climate and other environmental conditions on animals. US Patent:US7155377B2.

Porter, W. P. 2016. "Heat Balances in Ecological Contexts" in *A Biogeoscience Approach to Ecosystems*, E. Johnson, Y. Martin, Eds. Cambridge University Press: Cambridge, UK. 49-87.

R Core Team, R: A language and environment for statistical computing (R Foundation for Statistical Computing, Vienna, 2022); www.R-project.org/.

Rogers, S.A., C.T. Robbins, P.D. Mathewson, A.M. Carnahan, F.T. van Manan, M.A. Haroldson, W.P. Porter, T.R. Rogers, T. Soule, and R.A. Long. 2021. Thermal constraints on energy balance, behaviour, and spatial distribution of grizzly bears. *Functional Ecology* 35:398-410.

Sih A, Stamps J, Yang LH, et al. 2010. Behavior as a key component of integrative biology in a human-altered world. *Integrative and Comparative Biology* 50:934-944.

Sikes, R. and the Animal Care and Use Committee of the American Society of Mammologists. 2016. 2016 Guidelines of the American Society of Mammologists for the use of wild mammals in research and education. *Journal of Mammalogy* 97:663-688.

Sinha, R. S.A. Lone, A. Ranjan, A. Rahim, I. Devi, and S. Tiwari. 2017. The impact of climate change on livestock production and reproduction: ameliorative management. *International Journal of Livestock Research* 7:1-8.

Speakman, J.R., and J. McQueenie. 1996. Limits to sustained metabolic rate: The link between food intake, basal metabolic rate, and morphology in reproducing mice, *Mus musculus*. *Physiological Zoology* 68:746-769.

Speakman, J.R., and E. Król. 2010a. Maximal heat dissipation capacity and hyperthermia risk: Neglected key factors in the ecology of endotherms. *Journal of Animal Ecology* 79:726–746.

Speakman, J.R., and E. Król, 2010b. The heat dissipation limit theory and evolution of life histories in endotherms—Time to dispose of the disposable soma theory? *Integrative and Comparative Biology* 50:793–807.

Stearns, S.C. 1976. Life-history tactics: a review of the ideas. *The Quarterly Review of Biology* 51:3–47.

Taylor, C.R., K. Schmidt-Nielsen, R. Dmi'el, and M. Fedak. 1971. Effect of hyperthermia running during running in the African hunting dog. *American Journal of Physiology* 220:823-827.

Takahashi, M. 2012. Heat stress on reproductive function and fertility in mammals. *Reproductive Medicine and Biology* 11:37-47.

Therrien, J.F., S.D. Côté, N. Festa-Bianchet, and J.P. Ouellet. 2008. Maternal care in white-tailed deer: trade-off between maintenance and reproduction under food restriction. *Animal Behavior* 75:235-243.

Urison, N.T., and R. B. Buffenstein. 1995. Metabolic and body temperature changes during pregnancy and lactation in the naked mole rate (*Heterocephalus glaber*). *Physiological Zoology* 68:402-420.

van Beest, F., B. Van Moorter, and J.M. Milner. 2012. Temperature-mediated habitat use and selection by a heat-sensitive northern ungulate. *Animal Behavior* 84:723-735.

van Beest, F., and J.M. Milner. 2013. Behavioral responses to thermal conditions affect seasonal mass change in a heat-sensitive northern ungulate. *PLoS One* 11:e65972.

van Buskirk, J. 2012. Behavioural plasticity and environmental change. *In:* Behavioral responses to a changing world: mechanisms and consequences. Oxford University Press, New York, NY.

van der Meer, E., J. Mpofu, G. S. A. Rasmussen, and H. Fritz. 2013. Characteristics of African wild dog natal dens selected under different interspecific predation pressures. *Mammal Biology* 78:336–343

VanHorne, B. 1983. Density as a misleading indicator of habitat quality. *Journal of Wildlife Management* 47:893-901.

Veldhuis, M.P., E.S. Kihwele, J.P.G.M. Cromsigt, J.O. Ogutu, J.G.C. Hopcraft, N. Owen-Smith, and H. Olff. 2019. Large herbivore assemblages in a changing climate: incorporating water dependence and thermoregulation. *Ecology Letters* 22:1536-1546.

Veldhuis, M.P., T.R. Hofmeester, G. Balme, D.J. Druce, R.T. Pitman, and J.P.G.M. Cromsigt. 2020. Predation risk constrains herbivores adaptive capacity to warming. *Nature Ecology and Evolution* 4:1069-1074.

Verzuh, T., S.A. Rogers, P.D. Matewson, A. May, W.P. Porter, C. Class, L. Knox, T. Cufaude, L.E. Hall, R.A. Long, and K.L Monteith. 2022. Behavioral responses of a large, heat-sensitive mammal to climatic variation at multiple scales. *Journal of Animal Ecology* 92:619-634.

Wang, Y., W.P. Porter, P.D. Mathewson, P.A. Miller, R.W. Graham, J.W. Williams. 2018. Mechanistic modeling of environmental drivers of woolly mammoth carrying capacity declines on St. Paul Island. *Ecology* 99:2721-2730.

Wilson, A.M., and W. Jetz. 2016. Remotely sensed high-resolution global cloud dynamics for predicting ecosystem biodiversity distributions. *PLoS Biology* 14:e1002415.

Woodroffe, R., R. Groom, and J.W. McNutt. 2017. Hot dogs: high ambient temperatures impact reproductive success in a tropical carnivore. *Journal of Animal Ecology* 86:1329-1338.

Wells, K., R.B. O'Hara, B.D. Cooke, G.J. Mutze, T.A.A. Prowse, and D.A. Fordham. 2016. Environmental effects and individual body condition drive seasonal fecundity of rabbits: identifying acute and lagged processes. *Oecologia* 181:853-864.

Zhang, T., Y. Zhou, K. Zhao, Z. Zhu, G. Chen, J. Hu, and L. Wang. 2022. A global dataset of daily maximum and minimum near-surface air temperature at 1 km resolution over land (2000-2020). *Earth Systems Science Data* 14:5637-5649.

Appendix A: Supplemental materials for, "Chapter 1: Mechanisms of individual variation in large herbivore diets: roles of spatial heterogeneity and state-dependent foraging"

Supplemental Text

We used data from two prior vegetation surveys ('understory plots' in the floodplain and forage transects in the woodland) and two proxies for vegetation community composition within bushbuck home ranges (termite mound density and vegetation structure) to evaluate Tobler's (1970) first law of geography ("everything is related to everything else, but near things are more related than distant things") within our study area. Together, these four avenues of analysis affirm our assumption that geographic distance between home range centroids is a suitable proxy for dissimilarity in plant community composition.

Understory plots in floodplain plant communities

We used previously published data (Pansu et al. 2019) from recent vegetation surveys to quantify the relationship between plant community composition and geographic distance within the treeless interior of the floodplain habitat in Gorongosa. Tinley (1977) established 18 1-ha monitoring plots along three parallel transects extending outwards from Lake Urema (Fig. S1a). In June-August 2015, Pansu et al. (2019) resurveyed these plots by randomly placing 1215 1-m^2 quadrats and estimating the areal cover of each plant species and amount of bare ground in each quadrat using the Braun-Blanquet (1932) method; each species and bare ground estimate was binned according to its percent cover (1 = <5%; 2 = 6-25%; 3 = 26-50%; 4 = 51-75%; 5 = 76-95%; 6 = 96-100%). Bins were converted into relative-abundance estimates for each species using the median value of each bin (2.5, 15, 37.5, 62.5, 85, 98).

To test our prediction that plots farther away from one another differ more in plant community composition than closer plots, we used a Mantel test to evaluate the relationships between 1) the dissimilarity in the relative-abundance of plant species (Bray-Curtis dissimilarity) and average distance among quadrats within plots, and 2) the dissimilarity in the relative-abundance of plant species (Bray-Curtis distance) and the pairwise geographic distance between plots. We observed a significant, positive relationship between plant community dissimilarity and pairwise geographic distance within and among plots (Fig. S1b). This relationship demonstrates that differences in plant community composition increase with geographic distance in the floodplain habitat.

Forage transects quantify woodland plant communities

Because understory plot data only existed for the floodplain habitat, we also evaluated the relationship between plant communities and distance using data from forage transects (N = 100) sampled in May–June 2019 as part of a separate study, most of which fell within the woodland (Figure A.3a). The survey was designed to evaluate the distribution of key forages species (n = 32)—those that accounted for >95% of the diet of bushbuck and other spiral horned antelopes (*Tragelaphus* spp.)—previously quantified via DNA metabarcoding in Gorongosa (Pansu et al. 2019). Forage transect locations were randomly distributed throughout the main road network in our study area (Figure A.3a) and assigned a random orientation (0-360°). Along each 100-m transect, surveyors identified the plant rooted every 2.5-m interval (n = 40 points per transect) and recorded: (*i*) the plant taxon, if it was a forge species, (ii) 'other', if the taxon was not a forage species, or (*iii*) 'bare', if no plant was rooted at the point.

We quantified dissimilarity of plant community composition (presence/absence of each forage species along each transect) among transects using the Jaccard index. We used a Mantel test (Pansu et al. 2019) to evaluate the relationship between dissimilarity of plant community composition (Jaccard distance) along transects and the pairwise geographic distance between forage transect origins. We found a significant, positive relationship between plant community dissimilarity and geographic distance between forage transects (Figure A.3c). These results demonstrate that differences in plant community composition increase with geographic distance in the woodland habitat.

Vegetation structure

Plant species diversity is correlated with vegetation structure (Simonson et al. 2012, Davies and Asner 2014, Guo et al. 2017, George-Chacon et al. 2019). We thus used vegetation structure as a proxy for plant availability within bushbuck home ranges (95% minimum convex polygon, MCP). Methods for quantifying vegetation structure within bushbuck home ranges are outlined in the Main Text. We quantified the pairwise difference in vegetation structure between bushbuck home ranges using the Bray-Curtis index. We then evaluated whether differences in vegetation structure (Bray-Curtis distance) increased with pairwise geographic distance between bushbuck home range centroids (the arithmetic mean position of GPS fixes from each individual). Consistent with results from more direct measures of plant community composition, we found a significant, positive relationship between differences in vegetation structure and geographic distance between home range centroids (Figure A.3d). These results support our assumption that geographic distance between bushbuck home ranges is a suitable proxy for differences in plant community compositions.

Termite mound density as a proxy for plant communities

We used termite mound density as a proxy for plant community composition within bushbuck home ranges based on previous work in Gorongosa (Daskin et al. 2022) and elsewhere in southern Africa (Tinley 1977, Davies et al. 2015) documenting significant differences between mound-affiliated plant communities and plant communities in surrounding matrix habitats. Termite mounds are distributed throughout the Rift Valley floor in Gorongosa (Figure A.3b) and are pervasive in the woodland habitat (Figure A.1a) (Tinley 1977). Termite mounds are created by fungus farming termites (Macrotermitinae) that accumulate large mounds of earth and concentrate nutrients and moisture in the soils around their mounds, leading to distinctive plant communities associated with mounds that are more productive than plants in the surrounding matrix habitat (Grant and Scholes 2006). Thus, termite mounds are considered 'foraging hotspots' for large herbivores, which take advantage of the relatively high-quality plants associated with the nutrient and moisture-rich soils on and around the mound (Levick et al 2010).

We used digital terrain models derived from LiDAR data collected in 2019 to map the distribution of termite mounds across our study area and quantify the density of mounds within bushbuck home ranges. Using the hillshade tool in ArcGIS to visually transform the digital terrain model, we manually digitized the locations of termite mounds using changes in slope and shape to delineate mounds. Although we did not directly assess the accuracy of this approach, a previous study that used automated classification to map termite mounds in similar habitat from LiDAR data with coarser resolution (1.12 m) detected 78-90% of mounds >0.5-m tall (Davies et al. 2014), which are those most likely to be meaningful to antelopes. We used a Mantel test (Pansu et al. 2019) to evaluate the relationship between the pairwise difference in mound density within bushbuck home ranges (95% MCP) and the pairwise geographic distance between home range centroids. We found a significant, positive relationship between pairwise difference in mound density within bushbuck home ranges and geographic distance between home ranges (Fig. S1e). These results demonstrate that differences in the availability of mound-associated forage resources increase with geographic distance.

Supplemental Tables

Table A.1. Summary of principle component analysis of 12 nutritional condition metrics from adult female (*n* = 112) and male (*n* = 25) *Tragelaphus* antelopes in Gorongosa National Park, Mozambique 2014–2019. Each column (PC1-12) represents a principle component. >80% of the variance in these metrics was explained by the first two principle components (54.2% and 27.3% respectively).

	PC1	PC2	PC3	PC4	PC5	PC6	PC7	PC8	PC9	PC10	PC11	PC12
Standard deviation	2.550	1.808	0.805	0.649	0.580	0.538	0.480	0.357	0.310	0.207	0.175	0.086
Proportion of variance	0.542	0.273	0.054	0.035	0.028	0.024	0.019	0.011	0.008	0.004	0.003	0.001
Cumulative proportion of variance	0.542	0.814	0.868	0.903	0.931	0.955	0.975	0.985	0.993	0.997	0.999	1.000

Table A.2. **Principle component loadings for each of 12 nutritional condition metrics from adult female (*n* = 112) and male (*n* = 25) *Tragelaphus* antelopes in Gorongosa National Park, Mozambique 2014–2019.** Variables associated with body size loaded most strongly onto PC1, whereas variables associated with the amount of body fat loaded most strongly onto PC2.

	PC1	PC2	PC3	PC4	PC5	PC6	PC7	PC8	PC9	PC10	PC11	PC12
Max_fat	-0.23	-0.23	0.71	-0.43	0.43	-0.11	-0.08	0.05	-0.06	0.00	0.01	0.01
B_femoris	-0.31	0.18	0.25	0.15	-0.14	0.80	-0.22	0.04	0.26	0.06	0.03	0.03
L_dorsi	-0.35	0.17	-0.06	0.01	-0.02	0.10	-0.04	-0.52	-0.74	0.01	-0.13	0.04
SS_ligament	-0.19	-0.37	0.38	0.41	-0.43	-0.12	0.53	-0.15	0.06	-0.06	0.00	-0.01
Lumbar_vert	-0.24	-0.30	-0.12	0.68	0.45	-0.14	-0.37	0.12	-0.03	0.01	-0.04	-0.02
Sacrum	-0.22	-0.35	-0.42	-0.20	0.39	0.38	0.56	0.10	-0.01	0.00	0.00	-0.01
Base_tail	-0.24	-0.37	-0.14	-0.23	-0.48	-0.02	-0.27	0.52	-0.26	0.19	-0.24	0.02
Caudal_vert	-0.24	-0.38	-0.25	-0.27	-0.17	-0.10	-0.33	-0.53	0.38	-0.18	0.24	0.00
Chest_girth	-0.34	0.24	-0.07	0.01	-0.04	-0.18	0.08	0.28	-0.06	-0.23	0.53	0.60
Body_length	-0.33	0.26	-0.06	-0.05	0.04	-0.18	0.08	0.03	0.30	-0.39	-0.71	0.13
Hind_foot	-0.34	0.24	-0.07	-0.03	0.04	-0.26	0.12	-0.09	0.26	0.81	-0.01	-0.01
Net_weight	-0.34	0.25	-0.04	-0.02	-0.05	-0.13	0.05	0.20	-0.03	-0.25	0.28	-0.78

Table A.3. Fecal sampling intensity and other key variables for each bushbuck included in the study. 'Habitat' is a categorical indicator of which habitat type (floodplain or woodland) each bushbuck is affiliated with. 'Sex' indicates whether individuals are male ('M') or female ('F'). 'Lactation' is a categorical indicator of reproductive status, where 'Y' denotes lactating females, 'N' denotes non-lactating females, and 'N/A' denotes males.

ID	Sampling Start	Sampling End	Duration	Samples (*n*)	Habitat	Sex	Lactation
31471_18	18-Jun-18	11-Aug-18	54 days	11	woodland	F	N
31472_18	17-Jun-18	10-Aug-18	54 days	13	woodland	F	Y
31473_18	30-Jun-18	11-Aug-18	42 days	12	woodland	F	N
31483_18	15-Jun-18	3-Aug-18	49 days	6	floodplain	M	N/A
31765_18	30-Jun-18	11-Aug-18	42 days	6	floodplain	M	N/A
32006_18	27-Jun-18	11-Aug-18	45 days	12	floodplain	F	N
32009_18	15-Jun-18	10-Aug-18	56 days	14	woodland	F	N
32010_18	26-Jun-18	5-Aug-18	40 days	10	floodplain	M	N/A
32012_18	28-Jun-18	11-Aug-18	44 days	13	floodplain	M	N/A
31471_19	22-Jun-19	13-Aug-19	52 days	12	floodplain	F	Y
31472_19	23-Jun-19	5-Aug-19	43 days	12	floodplain	F	Y
31473_19	24-Jun-19	7-Aug-19	44 days	12	woodland	F	N
32005_19	18-Jun-19	8-Aug-19	51 days	12	woodland	F	N
32007_19	27-Jun-19	10-Aug-19	44 days	11	woodland	F	Y
32010_19	26-Jun-19	11-Aug-19	46 days	9	woodland	M	N/A

Table A.4. Pairwise contrasts in diet between each pair of bushbuck in the study population. Contrasts were calculated via permutational multivariate analysis of variance (n = 9,999 permutations) and the Holm-Bonferroni method to control for familywise error rate ('Adjusted *P'*). 'Pairwise comparison' identifies the individual diets represented in each contrast. 'Type' describes the habitat affiliation of each bushbuck in the contrast ('W' indicates a bushbuck affiliated with woodland habitat; 'FP' indicated affiliation with the floodplain). Contrasts that were not statistically significant ($P > 0.05$) after accounting for familywise error rate are noted with 'n.s.'

Pairwise comparison	Type	DF	pseudo-*F*	R^2	*P*	Adj. *P*	
32005_19 vs 31473_19	W v W	1,20	8.66	0.3	0.0001	0.011	
31473_18 vs 31473_19	W v W	1,19	16.98	0.47	0.0002	0.011	
32005_19 vs 32007_19	W v W	1,20	9.88	0.33	0.0001	0.011	
32005_19 vs 32009_18	W v W	1,24	7.17	0.23	0.0001	0.011	
32005_19 vs 32010_19	W v W	1,19	5.97	0.24	0.0002	0.011	
32005_19 vs 31471_18	W v W	1,20	11.87	0.37	0.0001	0.011	
32005_19 vs 31472_18	W v W	1,22	12.22	0.36	0.0001	0.011	
32005_19 vs 31473_18	W v W	1,21	10.81	0.34	0.0001	0.011	
32007_19 vs 32009_18	W v W	1,22	13.6	0.38	0.0001	0.011	
32007_19 vs 32010_19	W v W	1,17	12.8	0.43	0.0001	0.011	
32007_19 vs 31471_18	W v W	1,18	9.44	0.34	0.0001	0.011	
32007_19 vs 31472_18	W v W	1,20	13.06	0.39	0.0001	0.011	
32007_19 vs 31473_18	W v W	1,19	11.44	0.38	0.0001	0.011	
32007_19 vs 31473_19	W v W	1,18	7.72	0.3	0.0001	0.011	
32009_18 vs 32010_19	W v W	1,21	4.96	0.19	0.0004	0.011	
32009_18 vs 31471_18	W v W	1,22	11.64	0.35	0.0001	0.011	
32009_18 vs 31472_18	W v W	1,24	8.71	0.27	0.0001	0.011	
32009_18 vs 31473_18	W v W	1,23	9.01	0.28	0.0001	0.011	
32009_18 vs 31473_19	W v W	1,22	11.91	0.35	0.0001	0.011	
32010_19 vs 31471_18	W v W	1,17	11.16	0.4	0.0002	0.011	
32010_19 vs 31472_18	W v W	1,19	6.5	0.25	0.0011	0.011	
32010_19 vs 31473_18	W v W	1,18	6.15	0.25	0.001	0.011	
32010_19 vs 31473_19	W v W	1,17	12.44	0.42	0.0001	0.011	
31471_18 vs 31472_18	W v W	1,20	4.35	0.18	0.0011	0.011	
31471_18 vs 31473_18	W v W	1,19	6.39	0.25	0.0001	0.011	
31471_18 vs 31473_19	W v W	1,18	13.21	0.42	0.0001	0.011	
31472_18 vs 31473_18	W v W	1,21	2.43	0.1	0.0294	0.097	n.s.

31472_18 vs 31473_19	W v W	1,20	18.91	0.49	0.0001	0.011	
32006_18 vs 31765_18	FP v FP	1,16	12.73	0.44	0.0008	0.011	
32006_18 vs 32010_18	FP v FP	1,20	8.99	0.31	0.0002	0.011	
32006_18 vs 32012_18	FP v FP	1,23	8.76	0.28	0.0001	0.011	
32006_18 vs 31471_19	FP v FP	1,22	15.56	0.41	0.0001	0.011	
32006_18 vs 31472_19	FP v FP	1,22	15.48	0.41	0.0001	0.011	
32006_18 vs 31483_18	FP v FP	1,16	5.47	0.25	0.0036	0.022	
32010_18 vs 32012_18	FP v FP	1,21	8.09	0.28	0.0001	0.011	
32010_18 vs 31765_18	FP v FP	1,14	2.26	0.14	0.049	0.098	n.s.
32010_18 vs 31471_19	FP v FP	1,20	3.43	0.15	0.0038	0.022	
32010_18 vs 31472_19	FP v FP	1,20	4.15	0.17	0.0006	0.011	
32010_18 vs 31483_18	FP v FP	1,14	1.01	0.07	0.3944	0.394	n.s.
32012_18 vs 31765_18	FP v FP	1,17	16.32	0.49	0.0002	0.011	
32012_18 vs 31471_19	FP v FP	1,23	11.97	0.34	0.0001	0.011	
32012_18 vs 31472_19	FP v FP	1,23	14.71	0.39	0.0001	0.011	
32012_18 vs 31483_18	FP v FP	1,17	7.06	0.29	0.0002	0.011	
31765_18 vs 31471_19	FP v FP	1,16	6.6	0.29	0.0002	0.011	
31765_18 vs 31472_19	FP v FP	1,16	3.97	0.2	0.0015	0.011	
31765_18 vs 31483_18	FP v FP	1,11	2.51	0.2	0.0242	0.097	n.s.
31471_19 vs 31472_19	FP v FP	1,22	4.26	0.16	0.0001	0.011	
31471_19 vs 31483_18	FP v FP	1,16	4.93	0.24	0.0002	0.011	
31472_19 vs 31483_18	FP v FP	1,16	3.33	0.17	0.0005	0.011	
32005_19 vs 32012_18	W v FP	1,23	27.65	0.55	0.0001	0.011	
32005_19 vs 32006_18	W v FP	1,22	26.63	0.55	0.0001	0.011	
32005_19 vs 32010_18	W v FP	1,20	13.04	0.39	0.0001	0.011	
32005_19 vs 31765_18	W v FP	1,16	11.62	0.42	0.0004	0.011	
32005_19 vs 31471_19	W v FP	1,22	13.98	0.39	0.0001	0.011	
32005_19 vs 31472_19	W v FP	1,22	12.86	0.37	0.0001	0.011	
32005_19 vs 31483_18	W v FP	1,16	11.44	0.42	0.0001	0.011	
32007_19 vs 32010_18	W v FP	1,18	14.69	0.45	0.0001	0.011	
32007_19 vs 32012_18	W v FP	1,21	31.94	0.6	0.0001	0.011	
32007_19 vs 31765_18	W v FP	1,14	14.47	0.51	0.0001	0.011	
32007_19 vs 31471_19	W v FP	1,20	16.86	0.46	0.0001	0.011	

32007_19 vs 31472_19	W v FP	1,20	15.27	0.43	0.0001	0.011
32007_19 vs 31483_18	W v FP	1,14	13.63	0.49	0.0001	0.011
32009_18 vs 32010_18	W v FP	1,22	15.45	0.41	0.0001	0.011
32009_18 vs 32012_18	W v FP	1,25	35.68	0.59	0.0001	0.011
32009_18 vs 31765_18	W v FP	1,18	12.55	0.41	0.0001	0.011
32009_18 vs 31471_19	W v FP	1,24	16.89	0.41	0.0001	0.011
32009_18 vs 31472_19	W v FP	1,24	15.25	0.39	0.0001	0.011
32009_18 vs 31483_18	W v FP	1,18	13.38	0.43	0.0001	0.011
32010_19 vs 32012_18	W v FP	1,20	36.94	0.65	0.0001	0.011
32010_19 vs 31765_18	W v FP	1,13	17.1	0.57	0.0002	0.011
32010_19 vs 31471_19	W v FP	1,19	18.28	0.49	0.0001	0.011
32010_19 vs 31472_19	W v FP	1,19	17.03	0.47	0.0001	0.011
32010_19 vs 31483_18	W v FP	1,13	15.71	0.55	0.0004	0.011
31471_18 vs 31471_19	W v FP	1,21	19.56	0.49	0.0001	0.011
31471_18 vs 31472_19	W v FP	1,20	17.92	0.47	0.0001	0.011
31471_18 vs 31483_18	W v FP	1,14	16.15	0.54	0.0001	0.011
31472_18 vs 31472_19	W v FP	1,22	22.18	0.5	0.0001	0.011
31472_18 vs 31483_18	W v FP	1,16	20.75	0.56	0.0001	0.011
31473_18 vs 31483_18	W v FP	1,15	15.08	0.5	0.0002	0.011
31473_19 vs 31483_18	W v FP	1,14	15.43	0.52	0.0002	0.011
32006_18 vs 32007_19	FP v W	1,20	31.88	0.61	0.0001	0.011
32006_18 vs 32009_18	FP v W	1,24	32.14	0.57	0.0001	0.011
32006_18 vs 32010_19	FP v W	1,19	36.84	0.66	0.0001	0.011
32006_18 vs 31471_18	FP v W	1,20	37.57	0.65	0.0001	0.011
32006_18 vs 31472_18	FP v W	1,22	46.95	0.68	0.0001	0.011
32006_18 vs 31473_18	FP v W	1,21	35.58	0.63	0.0001	0.011
32006_18 vs 31473_19	FP v W	1,20	35.67	0.64	0.0001	0.011
32010_18 vs 32010_19	FP v W	1,17	15.63	0.48	0.0001	0.011
32010_18 vs 31471_18	FP v W	1,18	16.61	0.48	0.0001	0.011
32010_18 vs 31472_18	FP v W	1,20	21.19	0.51	0.0001	0.011
32010_18 vs 31473_18	FP v W	1,19	15.53	0.45	0.0001	0.011
32010_18 vs 31473_19	FP v W	1,18	16.09	0.47	0.0002	0.011
32012_18 vs 31471_18	FP v W	1,21	37.73	0.64	0.0001	0.011

32012_18 vs 31472_18	FP v W	1,23	47.8	0.68	0.0001	0.011
32012_18 vs 31473_18	FP v W	1,22	37.6	0.63	0.0001	0.011
32012_18 vs 31473_19	FP v W	1,21	36.01	0.63	0.0001	0.011
31765_18 vs 31471_18	FP v W	1,14	17.44	0.55	0.0002	0.011
31765_18 vs 31472_18	FP v W	1,16	21.28	0.57	0.0001	0.011
31765_18 vs 31473_18	FP v W	1,15	15.66	0.51	0.0003	0.011
31765_18 vs 31473_19	FP v W	1,14	16.54	0.54	0.0004	0.011
31471_19 vs 31472_18	FP v W	1,22	24.21	0.52	0.0001	0.011
31471_19 vs 31473_18	FP v W	1,21	15.25	0.42	0.0001	0.011
31471_19 vs 31473_19	FP v W	1,20	18.46	0.48	0.0001	0.011
31472_19 vs 31473_18	FP v W	1,21	15.67	0.43	0.0001	0.011
31472_19 vs 31473_19	FP v W	1,20	16.16	0.45	0.0001	0.011

Table A.5. Pairwise contrasts in diet based on occurrence (presence/absence) data each pair of bushbuck in the study population. Contrasts were calculated using permutational multivariate analysis of variance (n = 9,999 permutations) and the Holm-Bonferroni method to control for familywise error rate ('Adjusted *P'*). These results parallel those presented in Table A.4 using relative read abundance diet data. 'Pairwise comparison' identifies the individual diets represented in each contrast. 'Type' describes the habitat affiliation of each bushbuck in the contrast ('W' indicates a bushbuck affiliated with woodland habitat; 'FP' indicated affiliation with the floodplain). Contrasts that were not statistically significant ($P > 0.05$) after accounting for familywise error rate are noted with 'n.s.'

Pairwise comparison	Type	DF	pseudo-*F*	R^2	*P*	Adjusted *P*
32005_19 vs 31473_19	W v W	1,20	22.56	0.52	0.0001	0.011
31473_18 vs 31473_19	W v W	1,19	22.44	0.54	0.0001	0.011
32005_19 vs 32007_19	W v W	1,20	20.19	0.50	0.0001	0.011
32005_19 vs 32009_18	W v W	1,24	18.07	0.43	0.0001	0.011
32005_19 vs 32010_19	W v W	1,19	45.73	0.70	0.0001	0.011
32005_19 vs 31471_18	W v W	1,20	22.65	0.53	0.0001	0.011
32005_19 vs 31472_18	W v W	1,22	25.38	0.54	0.0001	0.011
32005_19 vs 31473_18	W v W	1,21	22.56	0.52	0.0001	0.011
32007_19 vs 32009_18	W v W	1,22	24.85	0.53	0.0001	0.011
32007_19 vs 32010_19	W v W	1,17	9.73	0.36	0.0001	0.011
32007_19 vs 31471_18	W v W	1,18	13.48	0.43	0.0001	0.011
32007_19 vs 31472_18	W v W	1,20	19.41	0.49	0.0001	0.011
32007_19 vs 31473_18	W v W	1,19	18.32	0.49	0.0001	0.011
32007_19 vs 31473_19	W v W	1,18	10.97	0.38	0.0002	0.011
32009_18 vs 32010_19	W v W	1,21	7.90	0.27	0.0001	0.011
32009_18 vs 31471_18	W v W	1,22	19.95	0.48	0.0001	0.011
32009_18 vs 31472_18	W v W	1,24	11.32	0.32	0.0001	0.011
32009_18 vs 31473_18	W v W	1,23	10.16	0.31	0.0001	0.011
32009_18 vs 31473_19	W v W	1,22	25.56	0.54	0.0001	0.011
32010_19 vs 31471_18	W v W	1,17	8.08	0.32	0.0001	0.011
32010_19 vs 31472_18	W v W	1,19	6.67	0.26	0.0001	0.011
32010_19 vs 31473_18	W v W	1,18	8.60	0.32	0.0001	0.011
32010_19 vs 31473_19	W v W	1,17	11.35	0.40	0.0001	0.011
31471_18 vs 31472_18	W v W	1,20	5.89	0.23	0.0002	0.011
31471_18 vs 31473_18	W v W	1,19	5.45	0.22	0.0003	0.011

31471_18 vs 31473_19	W v W	1,18	16.21	0.47	0.0002	0.011	
31472_18 vs 31473_18	W v W	1,21	2.86	0.12	0.0187	0.056	n.s.
31472_18 vs 31473_19	W v W	1,20	26.10	0.57	0.0001	0.011	
32006_18 vs 31765_18	FP v FP	1,16	7.40	0.32	0.0011	0.011	
32006_18 vs 32010_18	FP v FP	1,20	4.09	0.17	0.0033	0.013	
32006_18 vs 32012_18	FP v FP	1,23	14.03	0.38	0.0001	0.011	
32006_18 vs 31471_19	FP v FP	1,22	8.42	0.28	0.0001	0.011	
32006_18 vs 31472_19	FP v FP	1,22	14.45	0.40	0.0001	0.011	
32006_18 vs 31483_18	FP v FP	1,16	2.24	0.12	0.0577	0.115	n.s.
32010_18 vs 32012_18	FP v FP	1,21	7.64	0.27	0.0001	0.011	
32010_18 vs 31765_18	FP v FP	1,14	6.22	0.31	0.0004	0.011	
32010_18 vs 31471_19	FP v FP	1,20	6.62	0.25	0.0001	0.011	
32010_18 vs 31472_19	FP v FP	1,20	9.98	0.33	0.0001	0.011	
32010_18 vs 31483_18	FP v FP	1,14	1.57	0.10	0.1587	0.159	n.s.
32012_18 vs 31765_18	FP v FP	1,17	14.07	0.45	0.0003	0.011	
32012_18 vs 31471_19	FP v FP	1,23	8.43	0.27	0.0001	0.011	
32012_18 vs 31472_19	FP v FP	1,23	18.00	0.44	0.0001	0.011	
32012_18 vs 31483_18	FP v FP	1,17	10.47	0.38	0.0002	0.011	
31765_18 vs 31471_19	FP v FP	1,16	7.58	0.32	0.0001	0.011	
31765_18 vs 31472_19	FP v FP	1,16	8.27	0.34	0.0002	0.011	
31765_18 vs 31483_18	FP v FP	1,11	4.38	0.30	0.0024	0.012	
31471_19 vs 31472_19	FP v FP	1,22	4.22	0.16	0.0005	0.011	
31471_19 vs 31483_18	FP v FP	1,16	33.33	0.61	0.0001	0.011	
31472_19 vs 31483_18	FP v FP	1,16	7.47	0.32	0.0004	0.011	
32005_19 vs 32012_18	W v FP	1,23	57.10	0.71	0.0001	0.011	
32005_19 vs 32006_18	W v FP	1,22	48.29	0.69	0.0001	0.011	
32005_19 vs 32010_18	W v FP	1,20	45.73	0.70	0.0001	0.011	
32005_19 vs 31765_18	W v FP	1,16	26.28	0.62	0.0002	0.011	
32005_19 vs 31471_19	W v FP	1,22	21.53	0.49	0.0001	0.011	
32005_19 vs 31472_19	W v FP	1,22	27.46	0.56	0.0001	0.011	
32005_19 vs 31483_18	W v FP	1,16	31.99	0.67	0.0002	0.011	

32007_19 vs 32010_18	W v FP	1,18	64.52	0.78	0.0001	0.011
32007_19 vs 32012_18	W v FP	1,21	68.56	0.77	0.0001	0.011
32007_19 vs 31765_18	W v FP	1,14	42.96	0.75	0.0004	0.011
32007_19 vs 31471_19	W v FP	1,20	30.91	0.61	0.0001	0.011
32007_19 vs 31472_19	W v FP	1,20	40.75	0.67	0.0001	0.011
32007_19 vs 31483_18	W v FP	1,14	46.50	0.77	0.0005	0.011
32009_18 vs 32010_18	W v FP	1,22	56.12	0.72	0.0001	0.011
32009_18 vs 32012_18	W v FP	1,25	71.78	0.74	0.0001	0.011
32009_18 vs 31765_18	W v FP	1,18	28.19	0.61	0.0001	0.011
32009_18 vs 31471_19	W v FP	1,24	25.52	0.52	0.0001	0.011
32009_18 vs 31472_19	W v FP	1,24	32.81	0.58	0.0001	0.011
32009_18 vs 31483_18	W v FP	1,18	38.08	0.68	0.0001	0.011
32010_19 vs 32012_18	W v FP	1,20	44.65	0.69	0.0001	0.011
32010_19 vs 31765_18	W v FP	1,13	25.76	0.66	0.0004	0.011
32010_19 vs 31471_19	W v FP	1,19	20.62	0.52	0.0001	0.011
32010_19 vs 31472_19	W v FP	1,19	27.16	0.59	0.0001	0.011
32010_19 vs 31483_18	W v FP	1,13	26.07	0.67	0.0004	0.011
31471_18 vs 31471_19	W v FP	1,21	31.28	0.61	0.0001	0.011
31471_18 vs 31472_19	W v FP	1,20	44.20	0.69	0.0001	0.011
31471_18 vs 31483_18	W v FP	1,14	48.09	0.77	0.0005	0.011
31472_18 vs 31472_19	W v FP	1,22	46.49	0.68	0.0001	0.011
31472_18 vs 31483_18	W v FP	1,16	56.18	0.78	0.0004	0.011
31473_18 vs 31483_18	W v FP	1,15	39.75	0.73	0.0002	0.011
31473_19 vs 31483_18	W v FP	1,14	42.95	0.75	0.0002	0.011
32006_18 vs 32007_19	FP v W	1,20	63.14	0.76	0.0001	0.011
32006_18 vs 32009_18	FP v W	1,24	52.47	0.69	0.0001	0.011
32006_18 vs 32010_19	FP v W	1,19	40.44	0.68	0.0001	0.011
32006_18 vs 31471_18	FP v W	1,20	62.18	0.76	0.0001	0.011
32006_18 vs 31472_18	FP v W	1,22	71.07	0.76	0.0001	0.011
32006_18 vs 31473_18	FP v W	1,21	53.59	0.72	0.0001	0.011
32006_18 vs 31473_19	FP v W	1,20	58.25	0.74	0.0001	0.011

32010_18 vs 32010_19	FP v W	1,17	39.37	0.70	0.0001	0.011
32010_18 vs 31471_18	FP v W	1,18	64.72	0.78	0.0001	0.011
32010_18 vs 31472_18	FP v W	1,20	76.95	0.79	0.0001	0.011
32010_18 vs 31473_18	FP v W	1,19	54.77	0.74	0.0001	0.011
32010_18 vs 31473_19	FP v W	1,18	59.53	0.77	0.0001	0.011
32012_18 vs 31471_18	FP v W	1,21	71.01	0.77	0.0001	0.011
32012_18 vs 31472_18	FP v W	1,23	85.25	0.79	0.0001	0.011
32012_18 vs 31473_18	FP v W	1,22	66.21	0.75	0.0001	0.011
32012_18 vs 31473_19	FP v W	1,21	65.16	0.76	0.0001	0.011
31765_18 vs 31471_18	FP v W	1,14	45.90	0.77	0.0002	0.011
31765_18 vs 31472_18	FP v W	1,16	47.13	0.75	0.0001	0.011
31765_18 vs 31473_18	FP v W	1,15	34.26	0.70	0.0001	0.011
31765_18 vs 31473_19	FP v W	1,14	39.49	0.74	0.0001	0.011
31471_19 vs 31472_18	FP v W	1,22	33.86	0.61	0.0001	0.011
31471_19 vs 31473_18	FP v W	1,21	24.37	0.54	0.0001	0.011
31471_19 vs 31473_19	FP v W	1,20	29.01	0.59	0.0001	0.011
31472_19 vs 31473_18	FP v W	1,21	33.33	0.61	0.0001	0.011
31472_19 vs 31473_19	FP v W	1,20	37.71	0.65	0.0001	0.011

Supplemental Figures

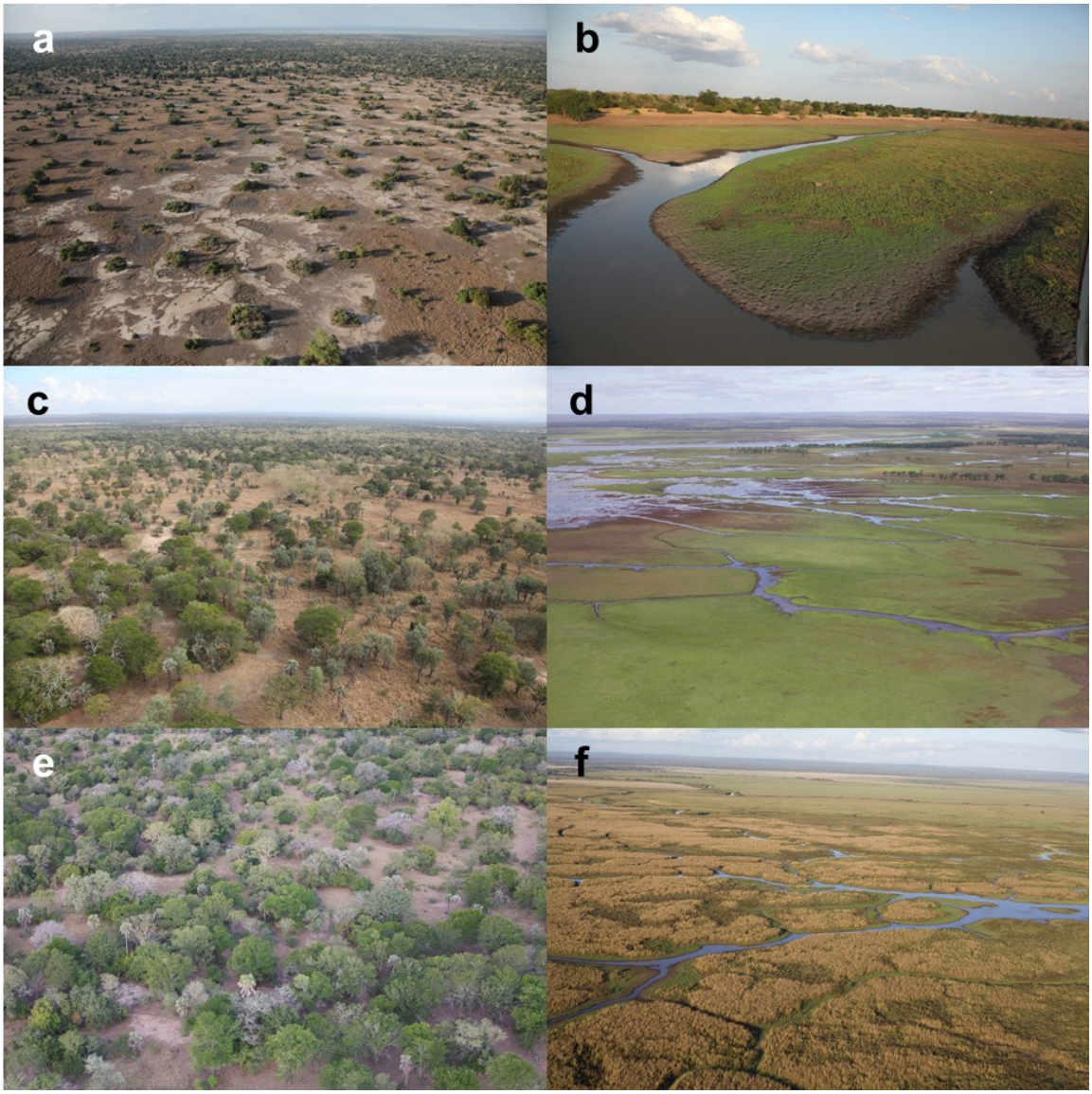

Figure A.1. Representative aerial photographs of woodland (A,C,E) and floodplain (B,D,F) habitats in Gorongosa. Woodland habitats include a mix of *Acacia*, *Combretum*, and palm savanna, are commonly dominated by termitaria thickets (A, clusters of trees and shrubs that grow on termite mounds), and span a range of canopy covers from relatively open forest and salt pans (C) to denser, closed-canopy forest (E). The floodplain grassland habitat is a productive (B), seasonally flooded (D) landscape dominated by grasses, forbs, and subshrubs (F) bordered by sparsely wooded savanna (visible in B, D).

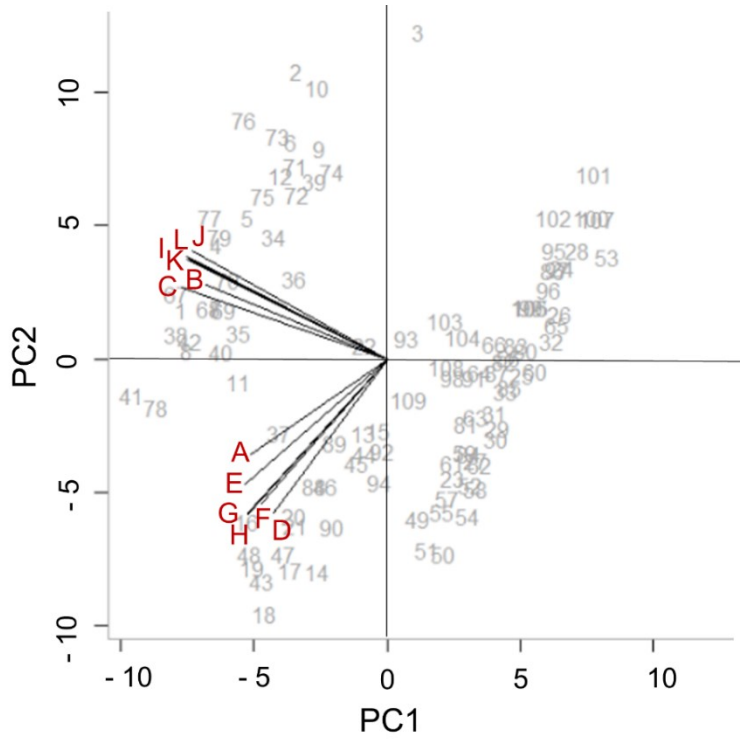

Figure A.2. Principle component analysis of 12 nutritional condition metrics collected from adult female (*n* = 112) and male (*n* = 25) *Tragelaphus* antelopes (bushbuck, nyala, and kudu) in Gorongosa National Park, Mozambique 2014–2019. Nutritional condition metrics were collected at the time of capture and included: (A) maximum rump fat depth, (B) thickness of the *biceps femoris* muscle, (C) thickness of the *longissimus dorsi* muscle, (D) palpation score at the sacrosciatic ligament, (E) palpation score at the lumbar vertebrae, (F) palpation score at the sacrum, (G) palpation score at the base of tail, (H) palpation score at the caudal vertebrae, (I) chest girth, (J) body length, (K) hind foot length, and (L) body weight. Together, Principle Component 1 (PC1) and Principle Component 2 (PC2) explained > 80% of the variance in these data. Black arrows show the projections of the original variables, and each grey number represents an individual antelope. Nutritional condition metrics associated with body size (e.g., muscle thicknesses, body weight) loaded most strongly onto PC1 and those associated with body fat (e.g., palpation scores, max fat) loaded most strongly onto PC2. In ungulates, body fat represents energy stores available for maintenance and reproduction and is commonly used as a measure of individuals' overall nutritional condition. Thus, we used the inverse of PC2 as an intuitive index of nutritional condition of bushbuck so that larger scores reflect individuals in better nutritional condition.

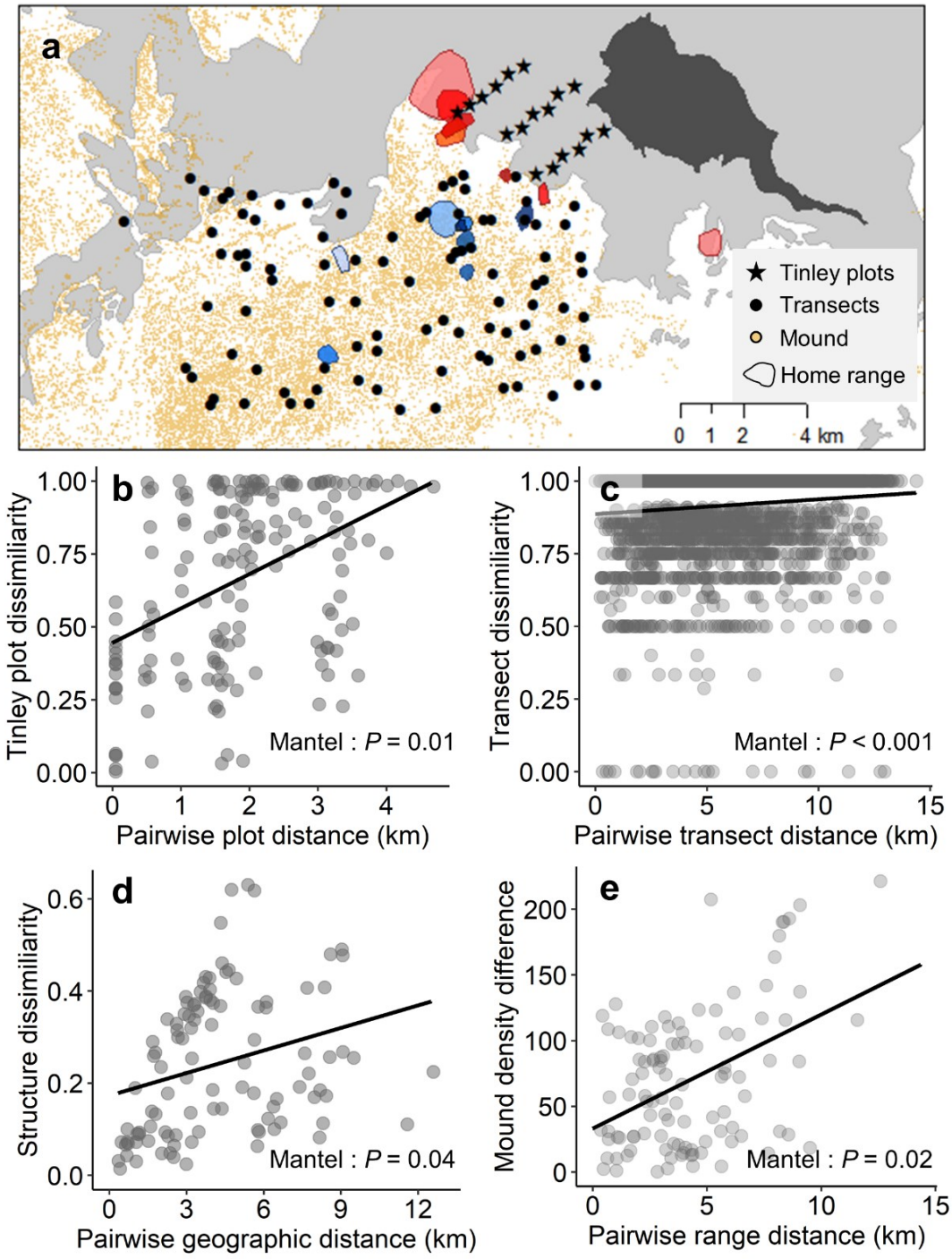

Figure A.3. Plant community dissimilarity increases with geographic distance in Gorongosa National Park, Mozambique. (A) Map of study area illustrating the locations of previous vegetation surveys (Tinley plots, stars; transects, circles), termite mounds (tan dots), and bushbuck home-range locations relative to floodplain (light grey) and woodland (white) habitats surrounding Lake Urema (dark grey). Bushbuck home ranges (95% minimum convex polygons) affiliated with the floodplain are noted in shades of red and those associated with the woodland are noted in shades of blue. P-values in each panel are from Mantel's permutation tests for similarity between two matrices.

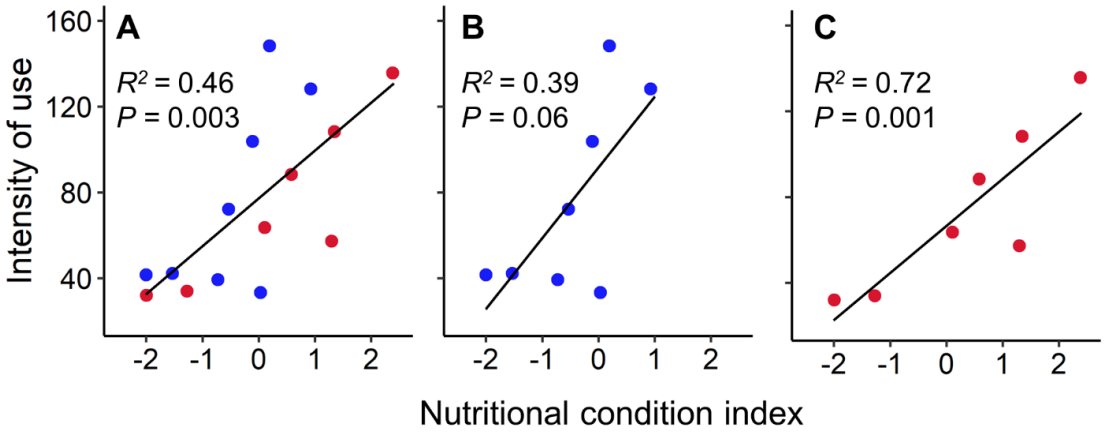

Figure A.4. Relationship between nutritional condition and intensity of use index calculated using all available hourly GPS data collected during bushbuck sampling periods (June – August) in Gorongosa National Park, Mozambique. Blue points represent woodland-associated bushbuck; red points represent floodplain-associated bushbuck. Consistent with our findings from data rarified to the first 21 days after capture (the period for which hourly data were available for all sampled individuals), we found a strong, positive relationship between nutritional condition and intensity of home-range use for the population as a whole (A) and for bushbuck associated with the floodplain habitat (C), and a marginally significant relationship for woodland-associated bushbuck (B). Although results are consistent between the two methods of calculating the index, intensity of use is sensitive to sample size (Almeida et al. 2019), and thus we present only results using the rarified dataset in the Main Text (Fig. 4d,e,f).

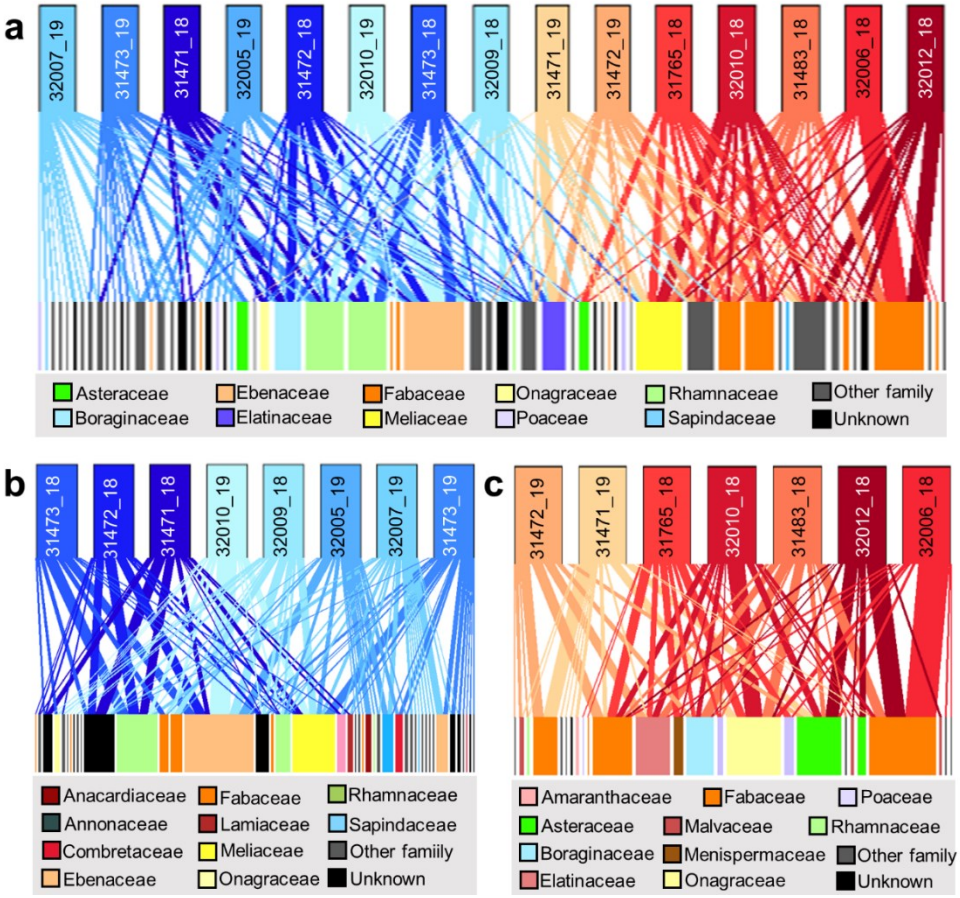

Figure A.5. **Bipartite plant-herbivore interaction network for individual bushbuck.** Results for all bushbuck in the study are shown in A and results partitioned by habitat association are shown in B (woodland) and C (floodplain). Lines connect individuals (top) to dietary plant mOTUs (bottom, colored by plant taxonomic family). Width of lines represents the relative read abundance of the plant mOTU in the individual's diet, while the width of the bottom rectangles represents the relative abundance of each plant mOTU in the database. Only mOTUs that represent >1% of each individual's diet are displayed.

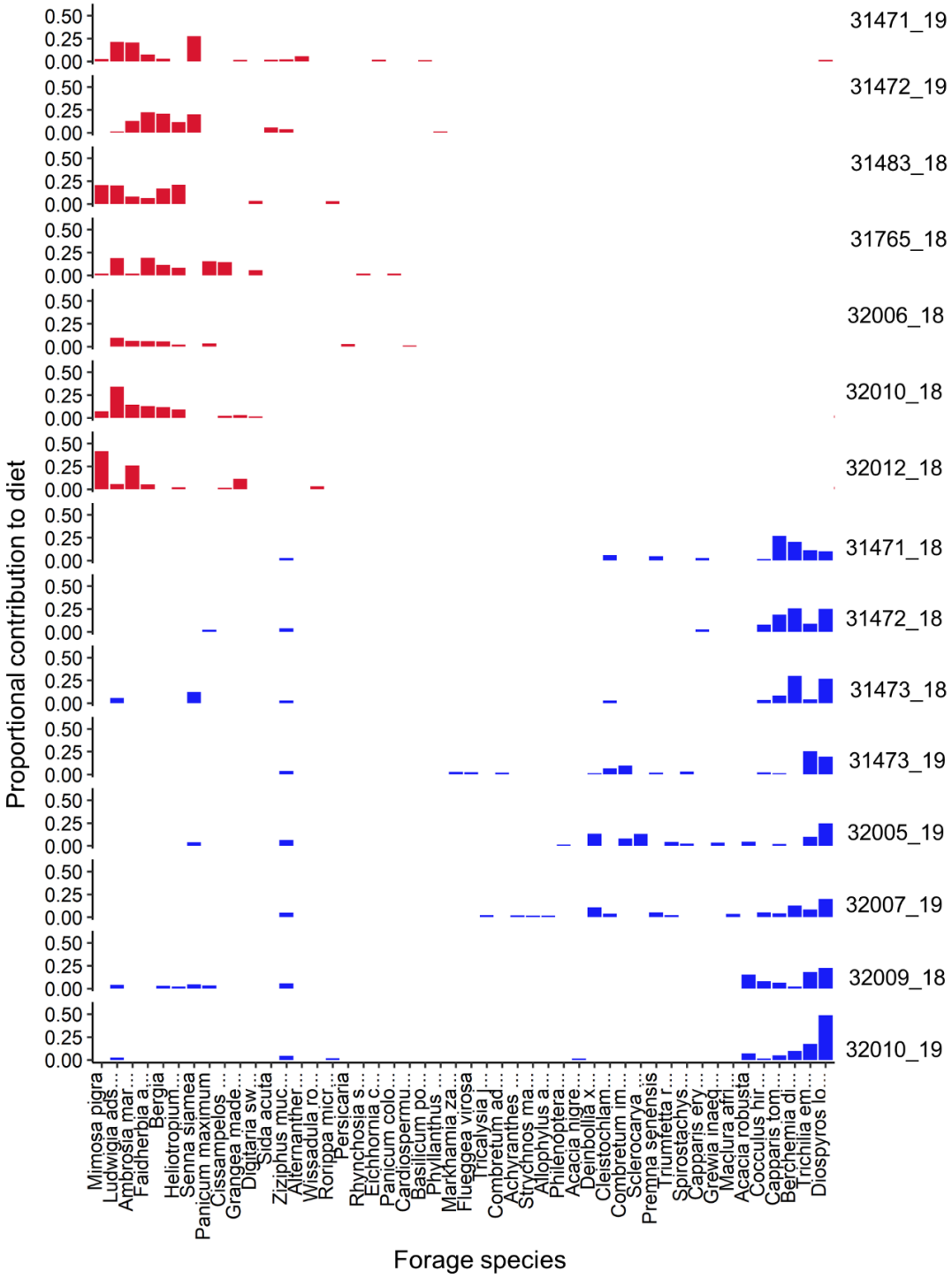

Figure A.6. **Individual diet histograms for bushbuck in Gorongosa illustrating variation in diet composition among individuals.** Each panel represents an individual, labeled to the right of graph; red bars, floodplain bushbuck; blue bars, woodland bushbuck. Y-axes show the relative read abundance of each plant taxon in each individual's diet. All mOTUs that represent > 1% of at least one individual's diet and could be mapped to plant taxa with known nutritional quality are displayed.

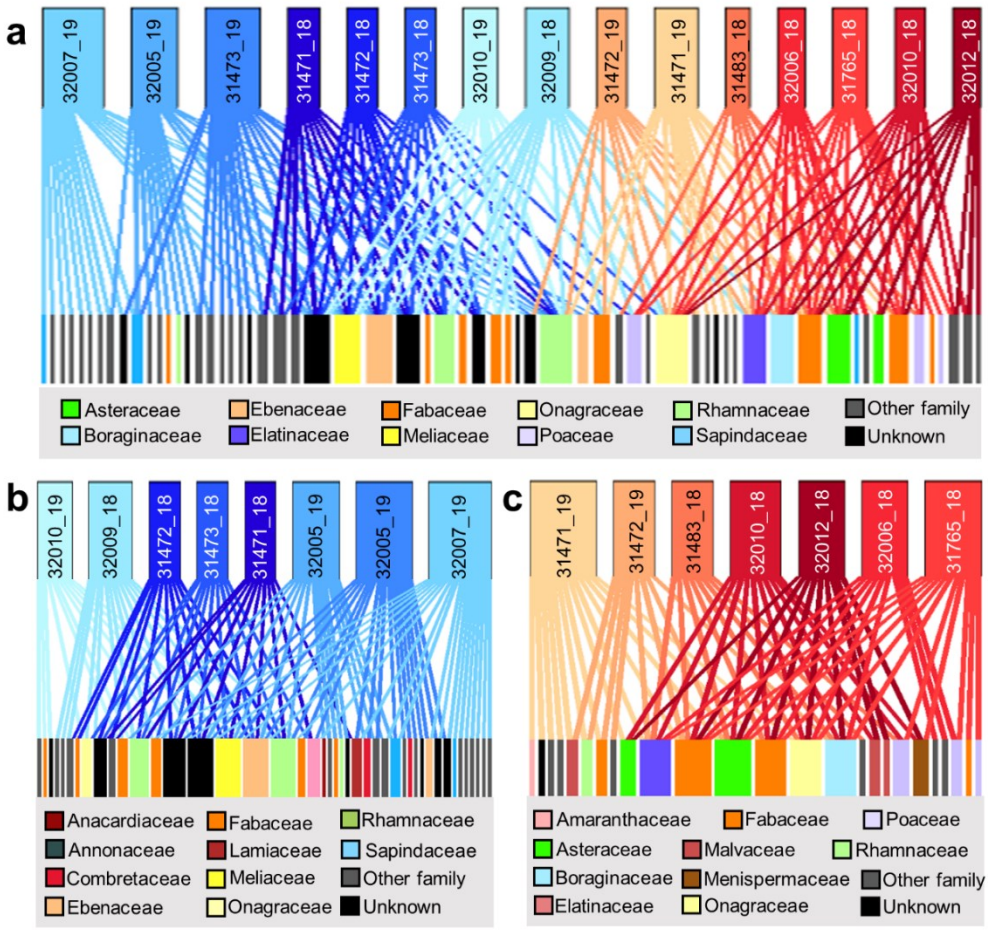

Figure A.7. Bipartite plant-herbivore interaction network for individual bushbuck calculated from presence/absence data. This occurrence-based analysis of all diet plant taxa accounting for > 1% of reads in fecal DNA metabarcoding analysis parallels the relative read abundance-based results presented in Figure A.5. Results for all bushbuck in the population are shown in A and results partitioned by habitat association are shown in B (woodland) and C (floodplain). Lines connect individuals (top) to dietary plant mOTUs (bottom, colored by plant family). Width of the top rectangles represent the relative breadth of individual diets; width of the bottom rectangles represent the relative abundance of each plant mOTU in the database.

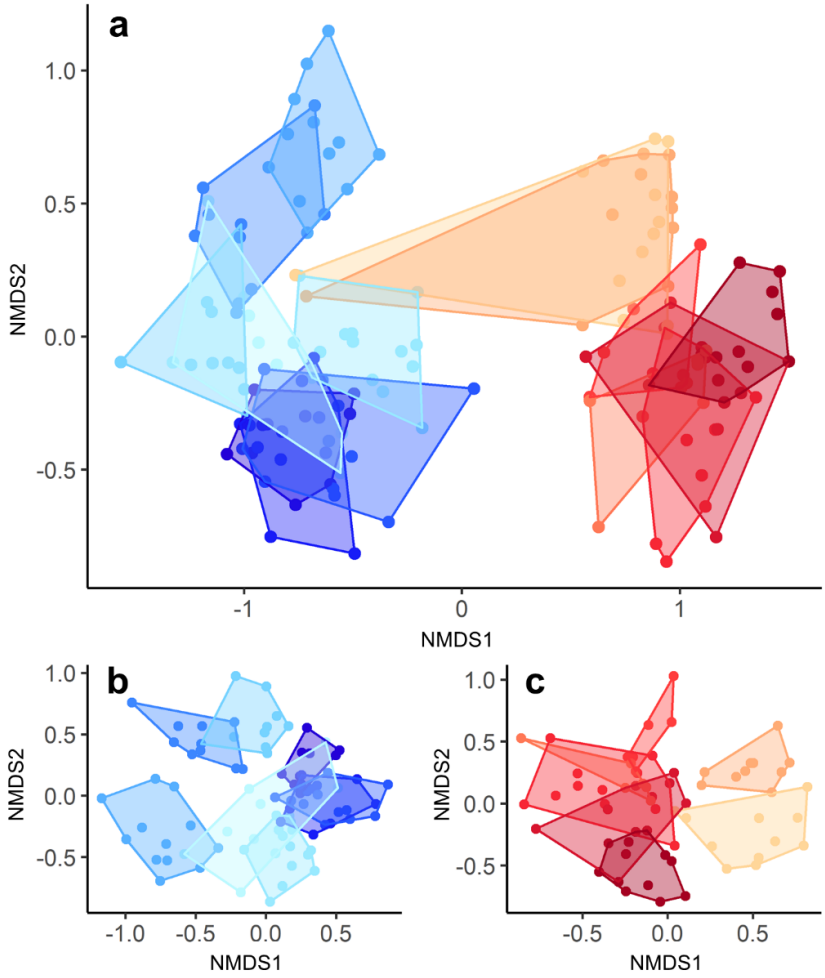

Figure A.8. Non-metric multidimensional scaling (NMDS) ordinations showing relative dissimilarity (Jaccard index) in the taxonomic composition (presence/absence) of individual fecal samples (points; *n* = 160) and dry-season diets (polygons; *n* = 15) of bushbuck in Gorongosa National Park, Mozambique. This occurrence-based analysis of all diet plant taxa accounting for > 1% of reads in fecal DNA metabarcoding analysis parallels the analysis of relative read abundance presented in Figure 2. Results for the full population are shown in A, and results partitioned by habitat association are shown in B (woodland, blue) and C (floodplain, red). Points in closer proximity to one another indicate more similar diets; polygons are convex hulls around all samples from each individual. Two individuals captured in woodland moved into floodplain shortly after collaring (outlying red points in A are those collected at capture); we excluded these initial woodland samples from the analysis of floodplain diet (C). We observed significant differences in individual diets, both across all individuals (perMANOVA: pseudo-$F_{14,144} = 28.74$, , $P \leq 0.001$, $R^2 = 0.74$) and within habitat types (woodland: pseudo-$F_{7,80} = 15.15$, $P \leq 0.001$, $R^2 = 0.57$; floodplain: psudeo-$F_{6,62} = 11.27$, $P \leq 0.001$, $R^2 = 0.52$).

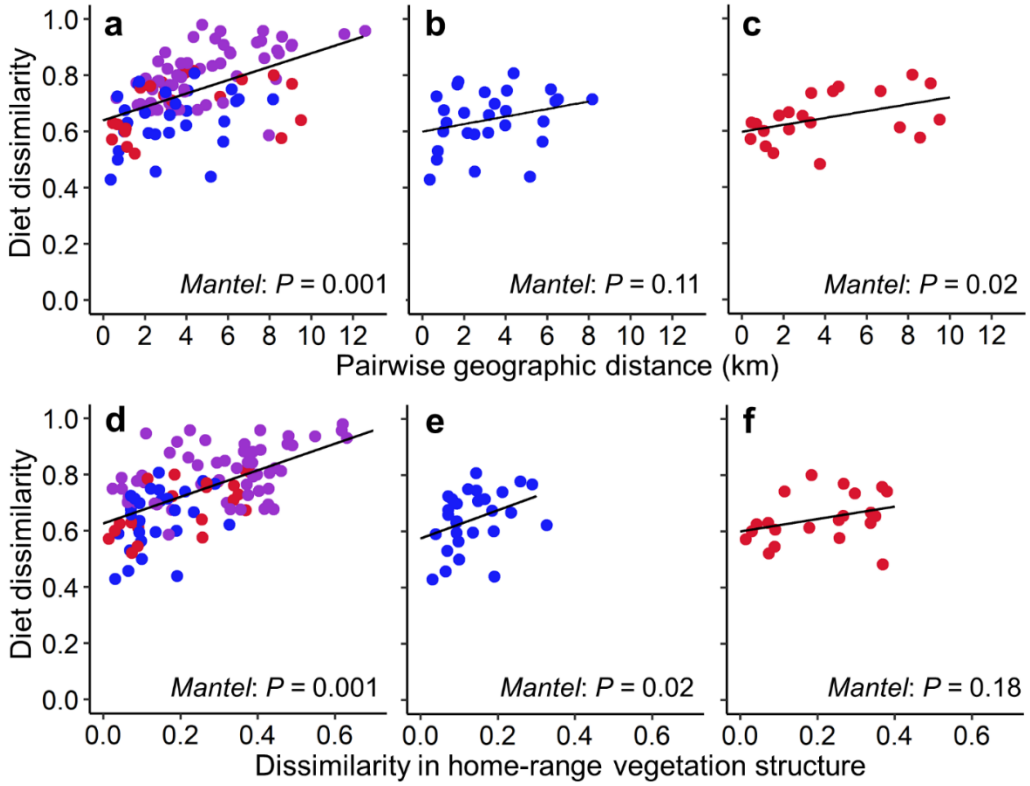

Figure A.9. Relationship between bushbuck diet composition (presence/absence) and spatial variation in the distribution of resources in Gorongosa. This occurrence-based analysis of all diet plant taxa accounting for > 1% of reads in fecal DNA metabarcoding analysis parallels the analysis of relative read abundance presented in Figure 3. We evaluated the relationship between pairwise diet dissimilarity (Jaccard index) and distance between home-range centroids (km) for all pairs of GPS-collared bushbuck (A), woodland-associated bushbuck (B), and floodplain-associated bushbuck (C). Additionally, we evaluated the relationship between pairwise diet dissimilarity and dissimilarity in home-range vegetation structure (Bray-Curtis index) between all pairs of GPS-collared bushbuck (D), woodland-associated bushbuck (E), and floodplain-associated bushbuck (F). Blue points illustrate pairwise comparison between two woodland-affiliated individuals, red points between two floodplain-affiliated individuals, purple points between a woodland and a floodplain affiliated individual. We quantified vegetation structure by calculating the proportion of LiDAR points classified as ground-level, low, medium, and high vegetation and using the Bray-Curtis index to quantify pairwise compositional dissimilarity between home ranges based on those proportions. P-values in each panel are from Mantel's permutation tests for similarity between two matrices.

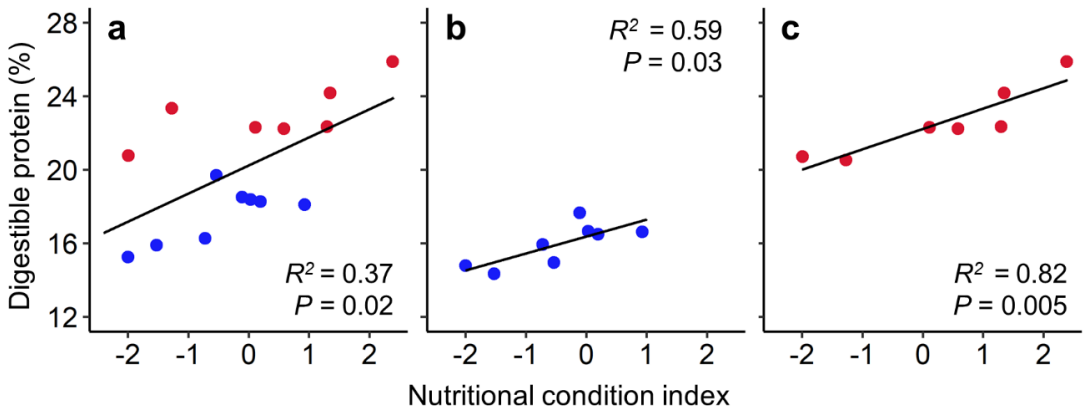

Figure A.10. Relationships between a multivariate index of nutritional condition (see Methods) and bushbuck diet quality quantified with occurrence (presence/absence) data in Gorongosa. We estimated the quality of individual bushbuck diets by calculating weighted average of DP in the standardized diet of each bushbuck assuming equal contribution of each present mOTU to the bushbuck diet as the weighting factor. This occurrence-based analysis of all diet plant taxa accounting for > 1% of reads in fecal DNA metabarcoding analysis parallels the analysis of relative read abundance presented in Figure 4d,e,f. Blue points represent bushbuck with home ranges affiliated with woodland habitat; red points represent bushbuck with home ranges affiliated with floodplain habitat. R^2 and P-values are from ordinary least-squares linear regression models.

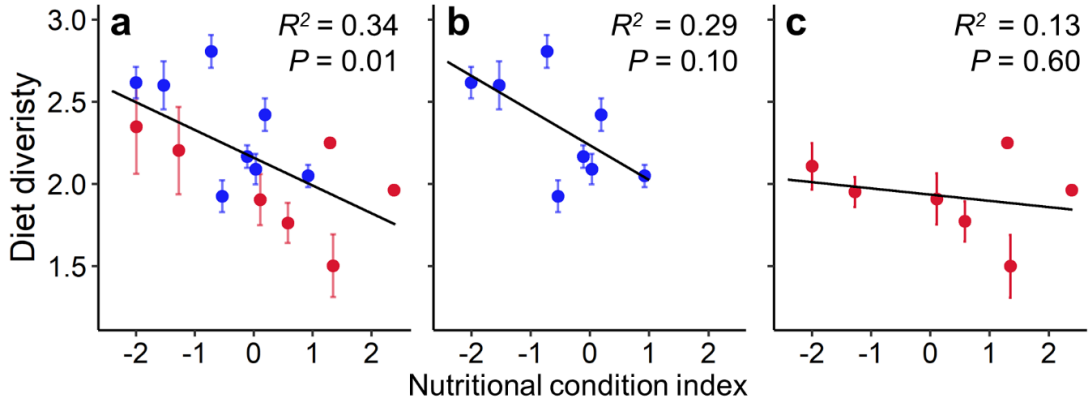

Figure A.11. Relationship between bushbuck nutritional condition (multivariate index of condition; see Methods) and diet diversity (Shannon Weaver index) in Gorongosa National Park, Mozambique. Blue points represent woodland-associated bushbuck; red points represent floodplain-associated bushbuck. Bushbuck in good nutritional condition had less diverse diets than their counterparts in poorer condition (A; mean ± SD unique mOTUs across 1,000 iterations of randomly drawing 6 samples for each individual, see Methods). This relationship persisted for bushbuck associated with woodland habitat (B) but not for bushbuck associated with floodplain habitat (C). R^2 and P-values are reported from ordinary least-squares linear regression models.

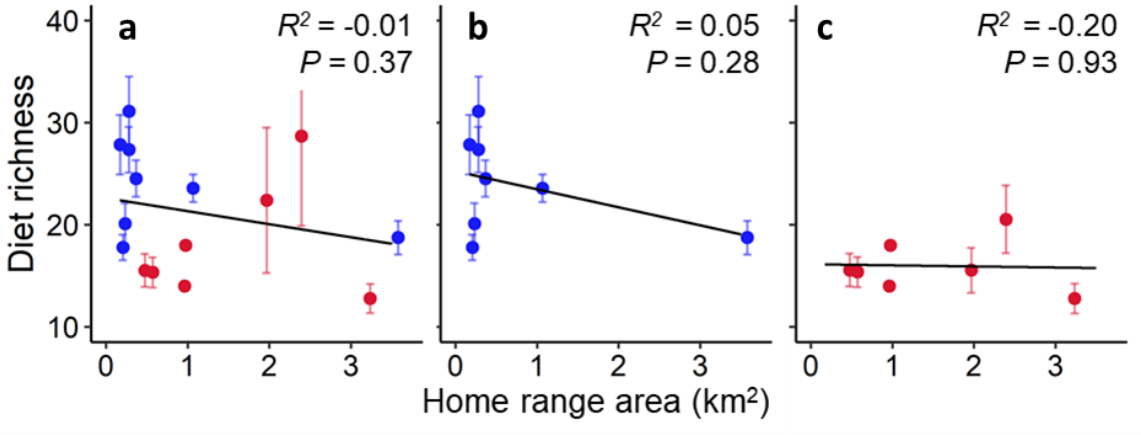

Figure A.12. Relationship between bushbuck diet richness and home range area (km^2) in Gorongosa National Park, Mozambique. Blue points represent woodland-associated bushbuck; red points represent floodplain-associated bushbuck. We used 95% minimum convex polygons (MCP) derived from hourly GPS-location data to estimate individual bushbuck home ranges during our sampling period in each year. We observed no relationship between diet richness (mean ± *SD* mOTUs among 1,000 iterations of randomly drawing 6 samples for each individual) and home-range size across (A) or within (B,C) habitat types. R^2 and *P*-values are reported from ordinary least-squares linear regression models.

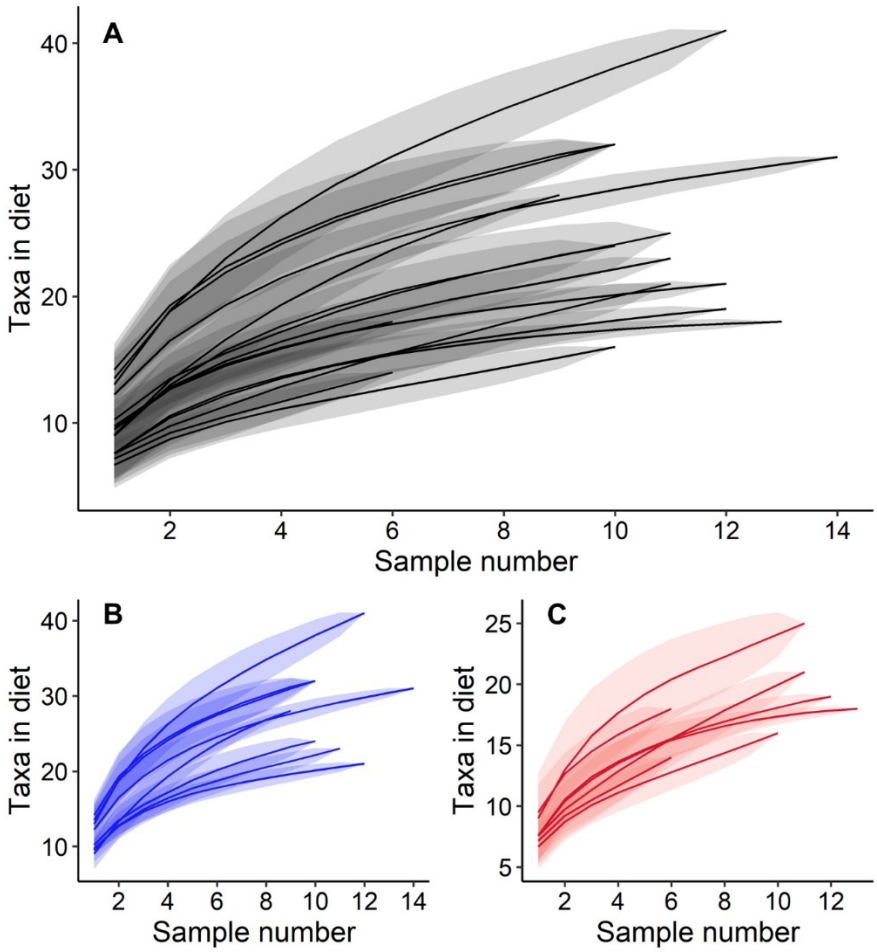

Figure A.13. **Mean species accumulation curves (lines) ± 1 SD (shading) for individual bushbuck diets in Gorongosa.** We evaluated the relationship between sampling intensity and the number of plant taxa present in bushbuck diets for (A) the full sample population (n = 15), (B) woodland-associated individuals (n = 8, blue), and (C) floodplain-associated individuals (n = 7, red). We find that a standardized sample size of 6 is not universally sufficient for individual dietary richness to approach an asymptote, despite being sixfold greater than the sampling depth in several recent analyses of individual specialization in ungulates (Bison et al. 2015, Pansu et al. 2019, Jesmer et al. 2020). However, relationships of relative diet richness among individuals appear largely conserved across sampling intensities (i.e., only 2/15 lines cross the curves of other individuals as richness as sample size increases).

Appendix B: Supplemental materials for, "Chapter 2: Trait-based sensitivity of large mammals to a catastrophic tropical cyclone"

Materials and Methods

Study system

Gorongosa National Park is located at the southern end of the Great Rift Valley (-18.96°, 34.36°) approximately 100 km from the Mozambique Channel (Figure 2.1a). The Rift Valley runs through the center of the park and encompasses Lake Urema, a large (dry season extent ≈ 18 km^2), shallow (dry season depth ≈ 1.5 m) body of water fed by multiple rivers within the 9300 km^2 Urema catchment (Böhme et al. 2006). Most annual rainfall (mean ≈ 850 mm, IQR 650–1080 mm between 1957 and 2018) occurs during a single wet season from November–April; in that period, Lake Urema expands and floods a large portion of the Rift Valley floor (up to 780 km^2) (Tinley 1977, Guyton et al. 2020). When floodwaters recede as the dry season progresses (May–October), water becomes increasingly scarce and Lake Urema persists as a critical perennial water source. Our study area encompassed the region south and west of Lake Urema, an area that is largely accessible by dirt roads and supports dense concentrations of wildlife. Within this area, vegetation structure and hydrology distinguish three habitat types: (1) floodplain-grassland (≈ 8–20 m above sea level), a seasonally flooded, highly productive lawn of grasses and forbs that supports a large portion of Gorongosa's ungulate biomass, (2) floodplain-savanna transition (≈ 20–25 m above sea level), characterized by intermittent, short-duration flooding and stands of water-tolerant trees (e.g., fever trees, *Vachellia xanthophoea*; white acacia, *Faidherbia albida*; and palms, *Hyphaene* spp.), and (3) savanna woodland (> 25 m above sea level), an infrequently flooded region with a diverse community of tree species and a full continuum of canopy cover (Figure B.2; Atkins et al. 2019, Becker et al. 2021, Guyton et al. 2020, Tinley 1977, Stalmans & Beilfuss 2008).

Gorongosa historically supported vast herds of large-bodied grazers (hippopotamus, *Hippopotamus amphibius*; Cape buffalo, *Syncerus caffer*; blue wildebeest, *Connochaetes taurinus*; and zebra, *Equus quagga*; size range 198–1,466 kg) along with substantial populations of large carnivores (lion, *Panthera leo*; leopard, *P. pardus*; African wild dog, *Lycaon pictus*) (Tinley 1977). During and after the Mozambican Civil War (1977–1992), much of which occurred in Gorongosa, all large-mammal populations declined by >90% (Stalmans et al. 2019) and leopard and wild dog were extirpated. By 2018, restoration efforts had helped to recover total large-herbivore biomass to 95% of pre-war estimates, including all of the ungulate species present in 1972; lion abundance rebounded to at least 50% of the estimated historical population size by 2016 and has continued to increase, although the exact population

size in 2019 is unknown (Guyton et al. 2020, Pringle 2017, Stalmans et al. 2019*,* Bouley et al. 2018). A founding pack of African wild dogs was reintroduced to the park in 2018 (Bouley et al. 2021); leopard and hyena were not reintroduced until 2020 and 2022, respectively, after our study was complete. Gorongosa's megafauna was thus largely intact in terms of species composition at the time of our study, but community structure was shifted relative to the pre-war baseline in favor of mesoherbivores (size range 17–204 kg): waterbuck (*Kobus ellipsiprymnus*), southern reedbuck (*Redunca arundinum*), warthog (*Phacochoerus africanus*), impala (*Aepyceros melampus*), and oribi (*Ourebia ourebi*) collectively accounted for 67% of biomass density in 2018, whereas the formerly dominant large-bodied grazers remained comparatively rare (Stalmans et al. 2019).

Tropical cyclones are relatively common in Mozambique: between 1980 and 2007, an average of 1.18 cyclones per year made landfall on the Mozambican coast (Cabral et al. 2017). However, Idai (a category 4 intense tropical cyclone), which made landfall over the port city of Beira on 15 March 2019, was by some measures the most severe cyclone on record in the Southern hemisphere (Warren 2019*,* Cabral 2017). Idai caused widespread infrastructural damage throughout Mozambique, Zimbabwe, and Malawi, incurring more than US $32 billion in damages, and resulting in >1,600 injuries and >600 deaths (Charrua et al. 2021). When Cyclone Idai passed over Gorongosa, >200 mm of rain fell (nearly a quarter of the long-term annual mean), and maximum sustained wind speeds exceeded 93 km hr^{-1} (remotely sensed data: Global Disaster Alert and Coordinate System 2019).

We integrated data from multiple, concurrent research projects in Gorongosa to capture individual and population-level responses of the two extant large carnivores (lion and wild dog) and the 13 most abundant ($n > 500$ in 2018) and widespread large-herbivore species (Stalmans et al. 2019) to Cyclone Idai: savanna elephant (*Loxodonta africana*), buffalo, sable antelope (*Hippotragus niger*), wildebeest, waterbuck, greater kudu (*Tragelaphus strepsiceros*), hartebeest (*Alcelaphus buselaphus*), nyala (*Tragelaphus angasii*), warthog, reedbuck, impala, bushbuck (*Tragelaphus sylvaticus*), and oribi. These species span two orders of magnitude in body mass and encompass a wide range of habitat associations, including a range of 12–82% distributional overlap with floodplain habitat (see *Aerial wildlife surveys*) (Figure B.1; Kingdon 1977). Densities of all species consistently increased between 2000 and 2018 (Stalmans et al. 2019). Six large-herbivore species were not included in this study because they were insufficiently abundant and/or restricted to a narrow range of inaccessible habitats; species with $n < 200$ counted in 2018 included eland (*Tragelaphus oryx*), zebra, bushpig (*Potamochoerus larvatus*), common duiker (*Sylvicapra grimmia*), and red duiker (*Cephalophus natalensis*), while hippopotamus numbered > 500 in 2018 but were largely confined to interior wetland in and around Lake Urema. Data were not

available for all study species in every analysis. Movement data were available for African wild dog, lion, elephant, sable, kudu, nyala, and bushbuck that were equipped with GPS collars when Idai made landfall; camera traps produced sufficient sample sizes only for waterbuck, warthog, nyala, impala, and bushbuck; and nutritional condition data were only available for bushbuck, nyala, and kudu. Diet and abundance data were available for all study species.

Quantifying flood depth and extent

We tracked flood depths throughout the main road network in Gorongosa before and after Cyclone Idai using loggers deployed in 2018. Between 18 August and 16 November 2018, we installed 46 automated water-level loggers (HOBO U20L-01; Onset Corp., Bourne, MA, USA) around the southern floodplain of Lake Urema and in adjoining savanna (Figure B.3b). These loggers were deployed in a regular grid with 1.8-km spacing between locations, covering a 120-km^2 minimum convex polygon. An additional logger was deployed indoors in the park's research headquarters to record atmospheric pressure, which we later used to correct raw pressure readings from the other sensors (i.e., to obtain pressure of water, independent of air pressure). The area of study for the flood-sensor network broadly aligned with that of most ecological research conducted in Gorongosa since 2012.

All sensors were set to record water levels every 4 h and were deployed inside slotted PVC pipes set vertically into the ground and capped with PVC to reduce disturbance by wildlife; pipes were lashed with stainless steel zip ties to rebar stakes driven 60–100 cm into the ground. We measured the depth from ground level to the bottom of each hole in which a sensor was deployed for later corrections of measured water depths above ground.

Between June and September 2019, as floodwaters receded and deployment sites became accessible, we retrieved logger data. Of the 46 loggers deployed, one was crushed by a fallen tree, one was damaged by animals, and seven were missing from their housings. Data were transferred from the remaining 37 sensors to a hard drive using the HOBO Waterproof Data Shuttle (#U-DTW-1) and HOBOWare software (Onset Corp.; Bourne, MA, USA). Upon inspection, we found corrupted data in the records of three sensors (one for the full length of deployment, one from 1 April 2019 onwards, and one from 1 January 2019 onwards). We removed these data from our analyses. We truncated sensor data from 16 November 2018 at 04:00 to 21 June 2019 at 08:00. For each sensor, we subtracted atmospheric pressure from the raw recorded pressure to yield water pressure. This enabled us to calculate water depths at each location using HOBOWare and its Barometric Compensation Assistant tool. We further corrected each water depth by

subtracting the appropriate hole depth from each sensor's data, which yielded estimated water depths above ground level (i.e., excluding any water that filled the holes in which sensors were placed).

We used an inverse distance weighting function to interpolate water depths (30-m resolution) from the corrected measurements at each logger location across the minimum convex polygon encompassing the locations of all 46 original loggers, plus a 1-km buffer. We interpolated water depths in program R using the function 'idw' in package gstat (Pebesma 2004, R Core Team 2020). In the absence of extensive validation data (e.g., manually measured depth records), we considered it best to use a relatively simple interpolation method as opposed to, for example, kriging. We used a high power ($p = 7$) to strongly weight interpolated water levels toward values at the nearest measured water depth, because all else equal, closer locations should have more similar water depths. When we tested the interpolation using lower powers (i.e., $p = 3$ and $p = 5$), the additional influence of distant sensors led to unrealistic spotting patterns.

Because the flood-sensor network did not fully overlap with the extent of GPS-collar data (see: Movement analyses), we used publicly available geospatial data on flooding in Mozambique after Cyclone Idai from the UN Operational Satellite Applications Programme (UNOSAT) to assess herbivores' behavioral adjustments to the flood edge (Figure B.21). The dataset included satellite-detected surface waters (10-m resolution) in the central provinces of Mozambique, as observed from Sentinel-1 imagery acquired from 13–26 March 2019 (UNOSAT 2019).

NDVI analysis

To evaluate how the increased extent and duration of flooding after Cyclone Idai impacted vegetation productivity, and hence the availability of green forage for herbivores, we compared the mean monthly normalized difference vegetation index (NDVI) curves from 2019 with those from 20 bracketing years (2000-2018, 2020). NDVI is a measure of greenness, with low values (close to 0) indicating low aboveground primary productivity and high values (close to 1) indicating high productivity (Western et al. 2015). We analyzed how NDVI in 2019 differed from normal years within (i) the remotely sensed area of Idai-induced flooding within the Gorongosa Rift Valley, (ii) the area within our flood-sensor array that was newly flooded (>1.0 m) after Idai, and (iii) a 748-km2 polygon defined by the movements of GPS-collared antelopes in 2014–2019 (Daskin et al. 2022) that encompassed the floodplain margin and adjacent higher-elevation savanna-woodland habitats. We used the map of flooding generated on 26 March 2019 from UN satellite data (UNOSAT 2019) to delineate the flooded area. The original spatial product contained 647 individual spatial polygons that we merged into a single bounding polygon [i.e.,

alpha-shape based on α = 1600, to prevent holes in the polygon, implemented with R package alphahull (Pateiro-Lopez & Rodriquez-Casal 2016)].

We calculated NDVI from MODIS data downloaded using the MODIStsp package (50) in R and extracted monthly 1-km vegetation index products (MOD13A and MYD13A3) with NDVI, quality, usefulness, and land/water bands from February 2000 to December 2020 (MYD13A3 products are available only from July 2002 onwards). We restricted spatial extent to the three focal areas described above. We retained only pixels with quality labels 0 or 1 (indicating unobscured pixels), usefulness labels <3 (highest quality estimates), and land labels of 1 (indicating pixel values did not represent water); other pixels were assigned 'NA'. To generate one estimate of NDVI per pixel per month, we averaged the pixel-level NDVI values between the two products (MOD13A and MYD13A3). For each focal area, we then calculated the mean monthly NDVI value across the extracted pixels. We compared NDVI in each month of 2019 to the inter-annual mean and standard deviation (SD) from 2000–2018 and 2020 (Fig. 3a, fig. S11) by computing the NDVI anomaly (Z-score) for each month, where $Z > 2$ or < -2 indicates that NDVI in 2019 was more than two standard deviations from the long-term monthly mean (51).

Animal movement analysis

To evaluate fine-scale responses of mammals to Cyclone Idai, we used movement data from GPS-collared bushbuck (2019: $n = 8$; 2020: $n = 8$; 2015: $n = 4$), nyala (2019: $n = 4$; 2020: $n = 5$; 2015: $n = 9$), kudu (2019: $n = 12$; 2020: $n = 10$; 2015: $n = 8$), sable (2019: $n = 3$), elephant (2019: $n = 13$), wild dog (2019: $n = 1$ pack), and lion (2019: $n = 8$) collected as part of ongoing, long-term studies in Gorongosa (Arumoogum 2022, Branco et al. 2019, Bouley et al. 2019, 2021, Daskin et al. 2022, Mamugy 2016). A single pack of 14 African wild dogs was reintroduced in June 2018, and the dominant female of that pack had an active GPS collar during our study (Bouley et al. 2021); because African wild dogs are an obligately social species that live and hunt communally and there were no other packs in the park during our study, we considered the movement data from this female to be representative of the entire wild dog population in Gorongosa (Bouley et al. 2021). We rarified herbivore and lion GPS data to include only individuals in separate herds or prides, to ensure movement behaviors were independently sampled. We measured body weights of bushbuck and female nyala by weighing individuals while they were immobilized for collaring. Male nyala, kudu, and sable are too large to be weighed in the field; instead, we used chest-girth measurements for these individuals to predict body mass based on regressions that developed for antelopes in this study system (Daskin et al. 2022). Chest girth measurements were not available for elephants; we thus assumed individual weights to be equal to the average sex-specific adult

body mass reported in (Kingdon 1997). All animal handling procedures were in accordance with guidelines established by the American Society of Mammalogists (Sikes and the Animal Care and Use Committee of the American Society of Mammalogists 2016). Bushbuck, nyala, and kudu handling procedures were approved by the Animal Care and Use Committees at the University of Idaho (protocol # IACUC-2019-32) and Princeton University (protocol #2075F-16). Sable handling procedures were approved by the animal ethics committee at the University of Witwatersrand (animal ethics number #2013/47/2A). Elephant handling procedures were approved by the Animal Care and Use Committee at the University of Idaho (protocol #2015-39) and by the Gorongosa Conservation Department. Lion and African wild dog handling procedures were approved by the Gorongosa Conservation Department.

We first evaluated how distance to flood waters, elevation, and proximity to termite mounds influenced the movement decisions of GPS-collared animals during the first two weeks after the onset of flooding (i.e., 04:00 15 March 2019, the hour at which >10% of water loggers in the network detected an increase in flood depth) using step-selection functions (SSFs; Avgar et al. 2016, Muff et al. 2019). Termite mounds created by fungus-farming *Macrotermes* spp.—substantial hillocks that can grow to >5 m tall and >20 m diameter—are ubiquitous throughout the wooded portions of our study area (Tarnita et al. 2017) and are selected by browsing antelopes owing to their dense and nutrient-rich woody plant assemblages (Muff et al. 2019). We predicted that mammals would avoid the edge of the flood and select for high ground at each of two spatial grains (higher-elevation areas and termite mounds within those areas) in the wake of the cyclone. We fit separate SSFs for each species for the two-week intervals before (04:00 March 1 – 04:00 March 15, 2019) and after (04:00 March 15 – 04:00 March 29, 2019) Idai. We paired each observed time step (i.e., segments linking consecutive GPS relocations, which occurred at 1-hr intervals for bushbuck, nyala, kudu, elephant; 3-hr intervals for lion and wild dog; 8-hr intervals for sable) with 10 random steps drawn from the distribution of step lengths and turning angles observed for each individual. For each 'used' (actual) and 'available' (random) step, we extracted (*i*) distance to flood waters (m), estimated from satellite-derived flood-extent shapefiles (UNOSAT 2019), (*ii*) elevation (m above sea level), extracted from a LiDAR-based digital terrain model (0.5 m horizontal, 0.1 m vertical resolution) (WGS Geospatial Solutions Aerial Surveys, Ltd.; see UNOSAT 2019 for details), and (*iii*) presence or absence of a termite mound (mounds were manually digitized in a hillshade rendering of the LiDAR-derived digital terrain model and buffered by 10 m to account for potential error in GPS collar fixes; see *27* for details). We limited all observed and random steps to the extent of the LiDAR-derived products from which we extracted environmental covariates; one kudu was thus excluded from SSF analysis because its home range did not overlap with the extent of environmental covariates. Only two of eight GPS collars on lions in the weeks before and after Idai collected data at regular intervals and were

appropriate for SSF analysis. To facilitate direct comparison of model results among species, we standardized all predictor variables by subtracting the mean from each observation and dividing by the standard deviation. We compared standardized environmental covariate values between used and available steps in each time interval using conditional logistic regression in the *survival* package in R (Fortin et al. 2005, Therneau 2020). We considered a difference in selection between the 'before' and 'after' cyclone windows to be statistically significant when the 95% confidence intervals around their respective coefficients did not overlap (Figure 2.2a, Figure B.5c, Figure B.19a).

Three collared bushbuck died within a week of Idai's landfall, whereas the remaining five survived until their collars dropped off in May 2019. To assess whether these groups exhibited different patterns of selection for flood edge, elevation, and termite mounds, we filtered GPS location data to include only the week before (04:00 8 March – 04:00 15 March 2019) and the week after Idai made landfall (04:00 15 March – 04:00 22 March 2019) and fit separate SSFs to the data from each period for the group that survived and the group that died (Figure B.5c). SSF fitting procedure and statistical inference were as described above.

We also evaluated whether, when, and to what extent collared individuals were displaced from their home ranges after the onset of flooding from Cyclone Idai. We partitioned each individual's GPS locations into temporal bins that spanned (*i*) the month before the cyclone (04:00 15 Feb. – 04:00 15 March), and (*ii*) 6 weekly bins after the onset of flooding. We then calculated (a) distance between the centroid of movement (i.e., geographic mean of GPS fixes) in the month before Idai and the centroids of movement of each weekly interval thereafter, and (b) proportional overlap between the individual's home range before Idai [derived from 95% fixed-kernel utilization distributions (UD)] and each weekly home range in the six weeks after landfall. To compare displacement observed after Idai to normal patterns of movement, we used GPS data from representative non-cyclone time periods, which varied among species depending on data availability. For bushbuck, nyala, and kudu, we used GPS data collected during the same intervals around 15 March in 2015 and 2020 (years for which data in those periods were available) and calculated the distance between centroids of movement and UD overlap between the month before March 15th (date of Idai's landfall in 2019) and each weekly interval thereafter (Figure 2.2b, Figure B.6). Data were not available prior to 2019 for sable, elephant, wild dog, and lion, so we partitioned GPS data for those species into a 'before' home range (1 Jan.– 1 Feb. 2019) and 6 subsequent weekly 'after' intervals for comparison (Figure 2.2b, Figure B.6, Figure B.19b). We used Welch's two-sample *t*-tests to compare displacement metrics for each species in each interval between before- and after-cyclone periods.

We evaluated the roles of body size (*log*-transformed to fit model assumptions) and association with floodplain habitat (Figure B.1) in predicting displacement of herbivores in the aftermath of Idai using generalized linear mixed-effects models (GLMM) with a beta-error distribution (our proportional response variable was bounded by 0 and 1) and per-species random intercepts (Figure B.7). We fit the model using the *glmmTMB()* function in the *glmmTMB* package and inspected model residuals using the *simulateResiduals()* function in the *DHARMa* package in R (Brooks et al. 2017, Hartig 2022). We found no evidence that model assumptions were violated.

Camera trap analysis

To evaluate cyclone effects on the spatial distribution of large mammals, we used data from a systematic long-term camera trap grid established in 2016. Cameras (Bushnell TrophyCam; 2016–2018, $n = 60$; 2018–2019, $n = 48$) were deployed over a 300-km^2 area south of Lake Urema in the center of 5-km^2 hexagonal cells, such that each camera was ~2.4 km from six nearest neighbors (Gaynor et al. 2021). Cameras, with infrared sensors triggered by heat and motion, were oriented toward game trails or open areas showing signs of animal activity to maximize detections (Gaynor et al. 2021). Of the 48 cameras deployed at the time of the cyclone, 30 survived the flooding. We rarified data across years to the 30 surviving cameras for subsequent analysis, identified the species and number of animals in each photograph, and generated a corresponding record of detections. We subset the database to evaluate mammal activity in 2019 and in two non-cyclone years (2017, 2018) for subsequent analyses. We thinned camera data to remove repeated sightings of the same individuals (>15 minutes apart; Gaynor et al. 2021). We then summed the remaining detections into month-long bins from 15 March to 15 October in each year. Five herbivore species—waterbuck, warthog, nyala, impala, and bushbuck—had sufficient data for inclusion in statistical analyses (i.e., >10 sightings in each monthly bin after March 15th in 2017, 2018, and 2019).

We evaluated whether the distributions of herbivores in the months after Idai were significantly different than in non-cyclone years, and whether that effect varied with distance to Lake Urema (a proxy for flood intensity; Figure 2.1c, Figure B.3b). For each species, we used a GLMM with a negative binomial distribution to model the number of detections in each month at each camera, offset by the log-transformed number of days each camera was active within each month (to account for search effort) and by the total number of detections across the camera trap grid in each month (to account for the potential impact of variable abundance among years). This analysis tested for (*i*) monthly differences in herbivore distribution after landfall in 2019 compared to the same months in non-cyclone-affected years (2017,

2018), and (*ii*) whether observed differences were modulated by distance from the lake (indicated by the three-way interaction among the categorical variable for cyclone occurrence, distance from lake, and month after landfall) (Brooks et al. 2017). A significant, negative interaction term indicated that herbivores were more concentrated farther from the lake after Idai than in normal years, and that that effect varied with month after cyclone landfall (Figure B.10). We included site and year as random intercepts to account for unmeasured variation among camera locations and between non-cyclone years. We conducted all analyses using the *glmmTMB* package (Brooks et al. 2017) and inspected model residuals with the *simulateResiduals()* function in the *DHARMa* package in R (Hartig 2022).

Carnivore diet composition

Carnivore diets were quantified using two methods. First, we used previously published observations of lion and wild dog kills in Gorongosa from 2017–2020 (Bouley et al. 2021). We partitioned these data into three periods—before cyclone, 1–3 mo. after landfall, and 4–9 mo. after landfall—to explore how prey selection changed after Cyclone Idai. For lions, these periods comprised $n = 61$, 10, and 22 observed kills, respectively. For wild dogs, they comprised $n = 43$, 5, and 23 kills, respectively.

Kill data suggested that wild-dog (but not lion) diets shifted dramatically in the immediate post-cyclone period (April–June 2019). Therefore, we also used DNA metabarcoding of wild dog scats to explore cyclone-induced dietary turnover. Following the reintroduction of wild dogs, the Gorongosa Carnivore Conservation Unit collected wild-dog scat opportunistically between June 2018 and December 2019. In total, 102 scats were collected for DNA metabarcoding from free-ranging wild dogs. Samples were collected with unused nitrile gloves and placed in an unused Ziploc bag. Sampling date and location were recorded on the bag, which was then placed on ice for transport to the field laboratory. At the field laboratory, samples were frozen at -20^{o} C until processing. Once every three months, all samples collected in the intervening period were thawed and processed for DNA extraction. Sample processing involved homogenizing each thawed sample by massaging the zip-lock bag between thumb and forefinger. A pea-sized subsample was then transferred from the zip-lock bag to a plastic tube containing silica beads and 750uL DNA lysis/conservation buffer (Xpedition Lysis/Stabilization Solution; Zymo Research, CA, USA). We then capped the tube and vortexed it for 30 s to break apart the subsample, exposing it to the buffer. Samples were heat-treated at 72^{o} C for 30 min before being frozen at -20^{o} C for transport to Princeton University, USA.

In our Biosafety Level 2 facility at Princeton University dedicated to fecal DNA analysis, we extracted DNA from the samples using Zymo Quick-DNA Soil/Fecal Microbe MiniPrep kits (Zymo Research, CA,

USA) following manufacturer instructions. DNA extractions comprised batches of 29 samples (wild-dog samples were extracted as part of a broader extraction session involving other species) and one negative extraction control (750uL DNA lysis buffer). Extracted DNA from wild-dog scats was then compiled onto two 96-well plates for DNA amplification. We amplified DNA in the samples, targeting the mitochondrial 16S gene to amplify mammal DNA using an established primer pair (MamP007F, 5'-CGAGAAGACCCTATGGAGCT-3'; MamP007R, 5'-CCGAGGTCRCCCCAACC-3'; *63*). To multiplex PCR products, we tagged the forward and reverse primers with 8-nt tags that each differed by at least 4 nucleotides to enable samples to be distinguished after sequencing. To limit amplification of wild-dog DNA, we included a wild-dog specific blocking primer (5'-GGAGCTTTAATTAACTAACCCAAGCTTACGG-3') with a C3-spacer added to the 3' end and a six-base overlap with MamP007F (first six bases of primer sequence, underlined). PCRs contained 2µL of extracted DNA, 0.5U of AmpliTaq Gold (Applied Biosystems, MA), 0.2µg BSA (New England Biolabs, MA), 0.2µM of each primer, 0.2mM of each dNTP (New England Biolabs, MA), 2mM MgCl2 (Applied Biosystems, MA), 1X GeneAmp PCR Buffer II (Applied Biosystems, MA), and 2µM of the blocking primer for a final volume of 20µL. Thermocycling conditions were: initial denaturing (95° C, 10 min), 45 cycles of denaturing (95° C, 30 s), annealing (52° C, 30 s), elongation (72° C, 30 s), and a final extension (72° C, 7 min). All PCRs were performed in triplicate and included negative extraction controls, negative PCR controls, and positive PCR controls (where DNA template was provided as a sequence designed *in silico* to comprise: 5'-10 random bases, MamP007F, a 75-base random barcode, MamP007R, 10 random bases-3'). We pooled PCR products by plate and purified them with a MinElute PCR Purification kit (Qiagen, MD). Purified PCR products from each DNA plate were then submitted for sequencing as equimolar libraries to the Lewis-Sigler Institute for Integrative Genomics at Princeton University where Illumina tags were appended with a low-cycle PCR approach and libraries were sequenced in paired-end (2 x 150bp) on a NovaSeq SP 300-nt platform.

Sequences were curated and filtered using the OBITools bioinformatic pipeline (Boyer et al. 2016). Forward and reverse reads were paired using *illuminapairedend* (minimum score = 40). Sequences were then assigned to the samples they came from (*ngsfilter*; two errors allowed) while sequences that were unaligned, contained ambiguous bases, or were outside the expected barcode length ($40 < x < 140$bp) were removed. Identical sequences were aggregated (*obiuniq*) and any sequences with only one read in the dataset (i.e., singletons) were removed (*obigrep -p 'count>1'*). Taxonomic identifiers were assigned to each sequence using the *ecotag* command and a reference database for 16S created using *in silico* PCR and the EMBL taxonomic library (release 143). Only sequences belonging to Mammalia (taxonomic ID: 40674) were retained in the dataset. Putative chimeras and PCR errors were identified and removed using

the *obiclean* command (parameters: -d 1; -r 0.25). Sequences whose abundance was highest in controls were considered contaminants and removed. PCR replicates were removed if their read depth fell below a critical threshold (1000 reads), or if they were above the 95% quantile for contaminant read abundance. The consistency among PCR replicates was confirmed by comparing their composition. If replicate-replicate dissimilarity was > 95% quantile of inter-replicate dissimilarity, or if an inter-replicate comparison fell within the inter-sample distribution of dissimilarity, it was removed from the dataset. When two or more PCR replicates remained in the dataset, their composition was averaged to give the mean scat-level sequence composition. Finally, we limited the data to sequences that had a perfect match to the reference dataset, and we removed sequences accounting for < 1% of each sample's relative read abundance (RRA) to reduce the likelihood of false positives (Pansu et al. 2022).

The bioinformatically filtered dataset comprised 87 wild-dog scat samples and 17 prey sequences. To make these samples comparable, we rarefied their composition to 1000 reads, repeated this procedure 1000 times, and used the average RRA of prey sequences across this ensemble to represent each sample's composition. To avoid pseudoreplication, we combined samples collected on the same date because wild dogs hunt, kill, and eat together, and more than one scat was often collected from the same den/kill on the same day. We therefore averaged the composition of these samples, yielding a final sample count of n = 42. To investigate the effect of Cyclone Idai on wild-dog diet, we split the final dataset into three periods: before the cyclone (n = 23, sampled between June 24 and December 5, 2018); 1–3 months after landfall (n = 5, sampled between April 7 and June 9, 2019); and 4–9 months after landfall (n = 14, sampled between July 16 and December 14, 2019). With these temporal slices of wild-dog diet, we tested whether diets immediately following the cyclone were significantly different from pre-cyclone or later post-cyclone diets. We evaluated whether there was an overall compositional difference among the three dietary periods and then tested each pair of periods separately using the *adonis2* function in the R package *vegan* (Oksanen et al. 2020). We visualized these results with non-metric multidimensional scaling (using the Bray-Curtis dissimilarity index and the *metaMDS* function in vegan; Oksanen et al. 2020), averaging across scats from the same dietary period. One outlier sample (for which 96% of RRA came from the African civet, *Civetticis civetta*) was excluded from this analysis because this sample may have been civet feces misidentified as a wild-dog scat. Adjusting the post-cyclone dietary periods to balance sample sizes (i.e., April 7–July 30, 2019, n = 9; and August 3–December 14, 2019, n = 10) did not qualitatively alter results; therefore, we present the data using a June/July split because it focuses the first post-cyclone period on the proximate flooding effects and represents a natural break in sampling (June 9–July 16 compared with July 30–August 3).

Herbivore diet composition

As for wild dog diets, we used DNA metabarcoding to quantify the composition of herbivore diets in Gorongosa. Samples were collected before (2016, 2018) and after (2019) the cyclone in three seasons: the late wet season (April–May), early dry season (June–July, 2016 only), and late dry season (October–November). These data were generated as part of a long-term study of the Gorongosa food web, and we followed previously published protocols for studying herbivore diets in Gorongosa (Atkins et al. 2019, Becker et al. 2021, Branco et al. 2019, Daskin et al. 2022, Guyton et al. 2020, Pansu et al. 2019, 2022, Potter et al. 2022, Walker et al. 2022). Raw data for samples collected from 2016–2018 are publicly available on Dryad in association with previous publications (https://doi.org/10.5061/dryad.63tj806 and https://doi.org/10.5061/dryad.sxksn02zc), and raw data for 2019 samples are deposited in a Dryad archive associated with this study.

Fecal samples were collected by driving Gorongosa's road network and opportunistically collecting samples from defecating ungulates. Occasionally, samples were collected from animals immobilized for GPS-collaring (Atkins et al. 2019, Branco et al. 2019, Daskin et al. 2022, Walker et al. 2022). For each sample, we recorded the GPS coordinates of the defecation site and a classification of the surrounding habitat type. We collected samples with unused nitrile gloves and deposited them in labeled, unused zip-lock bags, which we immediately placed on ice in a cooler until we returned to Gorongosa's field laboratory for processing later the same day. There, we homogenized samples within the collection bag, transferred pea-sized subsamples into labeled tubes containing beads and buffer, vortexed the tubes, and stored them at -20°C pending transport to Princeton University, as described above for wild dogs. Each sample was subjected to an antiviral treatment (72°C for 30 minutes) before import into the United States, as mandated by US Department of Agriculture permit #130123 to RMP.

On arrival at Princeton University, we extracted DNA from each sample as described above for wild dogs, including one negative extraction control per batch of 29 samples. In triplicate for each sample, we amplified the P6 loop of the chloroplast *trn*L(UAA) intron, a widely used barcode for degraded plant DNA, using primers with a unique 8-nt tag at the 5' end that enabled pooling of uniquely identifiable PCR products for sequencing in a single high-throughput run (Taberlet et al. 2007). Sequencing libraries were prepared with a PCR-free approach (2016) or low-cycle PCR (2018-19), and sequencing was performed on Illumina MiSeq and HiSeq 2500 platforms. We processed sequenced data using the *OBITools* package (Boyer et al. 2016). These procedures were the same as described above for wild dogs, except that sequences with fewer than 10 reads were discarded (rather than singletons only) to optimize

filtering efficiency, and that taxonomy was assigned with a local plant DNA reference library based on vouchered specimens collected in Gorongosa (Pansu et al. 2019). Only when the local library assignment score was <98%, we assigned taxonomy by secondary comparison to a global database compiled from the European Molecular Biology Laboratory (release 143) and local databases of plants from Serengeti National Park, Tanzania, and Laikipia, Kenya (Gill et al. 2019). PCR replicates were retained if they were within the 95% quantile of overall inter-replicate dissimilarity and did not fall within the distribution of inter-sample dissimilarities. We averaged the number of reads across all retained PCR replicates for each sample and removed molecular operational taxonomic units (mOTUs) accounting for <1% of reads per sample (Guyton et al. 2020). Finally, we rarified sample read depth to 1,250 reads to facilitate comparisons among samples and converted the mOTU-by-sample matrices into proportional abundance (i.e., relative read abundance, RRA) of each plant mOTU per sample. As in our previous dietary studies from Gorongosa, we use RRA data for inference given evidence that RRA of the *trn*L-P6 marker (*i*) provides a reasonable first-order approximation of proportional consumption (Craine et al. 2015, Kartzinel et al. 2015, Willersley et al. 2014), (*ii*) has yielded inferences in our previous studies that qualitatively match those based on presence-absence data (Guyton et al. 2020, Kartzinel et al. 2015, Pansu et al. 2019), and (*iii*) generally provides a fuller and more accurate characterization of population-level diets than presence-absence data alone (Deagle et al. 2019, Littleford-Colquhoun et al. 2022). The final dataset comprised 13 herbivore species, 1470 fecal samples, and 332 mOTUs (Table B.3).

We evaluated the cyclone's impact on herbivores' diet composition in two complementary ways. First, for each herbivore species and seasonal period, we visualized dietary Bray-Curtis dissimilarity between each pair of fecal samples using non-metric multidimensional scaling [NMDS; *metaMDS()* function in *vegan* (Oksanen et al. 2020)] of samples collected in 2018 (no cyclone) and 2019 (cyclone) and tested for significant differences as a function of year using permutational multivariate analysis of variance (perMANOVA; Figure B.12).

Second, to test whether dietary turnover from before to after Cyclone Idai were greater than usual, we computed the population-level diet of each species (the mean RRA of each mOTU across samples) and compared Bray-Curtis dissimilarity [*vegdist()* function in *vegan* (Oksanen et al. 2020)] for each species between the late-dry season 2018 and the late-wet season 2019 (the sampling periods immediately before and after Idai) with that observed between all other cross-seasonal pairs of sampling periods available for each species (late-wet, early-dry, late-dry seasons of 2016, 2018, and 2019, excluding the cyclone-affected late-wet season of 2019), both consecutive and nonconsecutive. Bushbuck and hartebeest were excluded from this analysis owing to low sample sizes in the 2019 late-wet season. To ensure that sample-

size imbalance among seasons and species (mean = 17.4, min = 8, max = 40) did not otherwise bias our results, we randomly rarefied a species' samples from a given collection period (season and year) to $n = 8$, the minimum sample size among species sampled in every season and calculated average population-level diets and turnover based on this subset. We repeated this process 1000 times and used the mean turnover value for each comparison in our analyses. We tested whether turnover across the cyclone-affected period was greater than usual using a GLMM with a beta error distribution, a fixed effect of cyclone occurrence, and random intercepts for herbivore species. Note that the inclusion of nonconsecutive seasons/years in the baseline for this comparison makes for an liberal definition of a 'normal' seasonal turnover, and thus a conservative test of the dietary anomaly induced by Cyclone Idai, because the baseline includes turnover between disparate seasons/years (e.g., the dry season of 2016 with the wet season of 2018).

Herbivore dietary attributes

To test whether herbivore dietary diversity changed with cyclone-induced vegetation shifts, we quantified diet breadth as the number of plant families present per fecal sample (per sample data avoid confounding effects of sample size on richness estimates) in each season of 2016, 2018, and 2019 (data were available for all seasons in the latter two years, and for the early dry season in 2016). For each season, we used a Poisson GLMM with a fixed categorical effect for year and per-species random intercepts to test if family-level richness was significantly different in the cyclone year, 2019.

We tested whether proportional consumption of grasses—the primary axis of dietary differentiation in large herbivores (Pansu et al. 2022)—shifted in response to cyclone-induced flooding and accompanying shifts in understory productivity (Figure B.3a) using beta GLMMs for each season with a fixed categorical effect of year and per-species random intercepts. Here, we modeled mean grass RRA per species rather than per sample to avoid an inordinately large number of zeroes and also used zero-inflation terms for the dry-season models to satisfy model assumptions.

We analyzed forage traits using the locally collected plant-trait database and protocols of Potter et al. (2022). We focused a priori on a subset of 6 plant traits associated with forage quality and/or susceptibility to flooding: mean field-measured height of the plant species (taller plants such as trees and shrubs should be less depleted by inundation), digestible protein content (a chief and often limiting macronutrient), dry-matter digestibility (another key component of diet quality), lignin (an indigestible structural component of cell walls that is most abundant in woody plants), phosphorus (a major mineral nutrient), and sodium (another micronutrient that is often limiting for herbivores). Following Potter et al. (2022) dietary sequences that did not match plants in the traits dataset were discarded and the RRA for

each sample recomputed; samples with < 60% of original reads matched were removed (n = 1360 of 1470 samples retained; median reads preserved = 98.1%). We then multiplied the RRA of each mOTU by the trait value of the matched plant taxon to obtain a weighted estimate of each trait in each sample. We tested for differences in these attributes (per sample) using linear mixed-effects models for each season with fixed categorical effects of year and per-species random intercepts; the plant-height response was log transformed and the other metrics (expressed as proportions) were logit transformed.

We used the *adonis2()* function in the *vegan* package in R to conduct perMANOVA tests of niche differentiation between each pair of species in each season and year (Oksanen et al. 2020). We used the R^2 statistic from each perMANOVA as an index of the strength of niche partitioning (Pansu et al. 2022): greater R^2 values indicate that herbivore species' identity explains a greater proportion of variance in dietary dissimilarity and are thus indicative of stronger interspecific differentiation. Because the results of *adonis2()* can be influenced by sample size and sample sizes differed among sampling periods, we randomly rarefied species' samples to reduce inter-annual differences between sample sizes. Species represented by $n > 8$ samples in a sampling period were randomly rarefied to $n = 8$ samples, this procedure was repeated 1000 times, and the mean R^2 value across iterations was used in analyses. To evaluate whether the strength of niche differentiation differed between 2019 and non-cyclone years (2016, 2018), we analyzed these R^2 values using per-season GLMMs with a beta-error distribution, a fixed categorical effect of year, and per-species random intercepts.

Nutritional condition

We compared mean nutritional condition of bushbuck, nyala, and kudu after Cyclone Idai (June–July 2019) with mean condition of these species in years prior to the cyclone (June–July 2014, 2015, 2016, and 2018). Nutritional condition reflects endogenous energy reserves available for maintenance, growth, and reproduction and is a key correlate of fitness in ungulates, influencing survivorship, pregnancy rates, vulnerability to predation, and neonatal birth mass (Parker et al. 2009). Data on nutritional condition were collected during capture and collaring for an ongoing study of spiral-horned antelopes in Gorongosa (details in Atkins et al. 2019, Daskin et al. 2022*,* Walker et al. 2022).

While antelope were immobilized, we measured body dimensions (body and hind-foot length, chest girth), collected ultrasonography data (maximum rump-fat depth, thickness of biceps femoris and longissimus dorsi muscles), and conducted standardized palpation scoring of the sacrosciatic ligament, lumbar vertebrae, sacrum, base of the tail, and caudal vertebrae [based on protocols developed for North American ungulate (Cook et al. 2010)]. Because equations for converting these measurements into

estimates of ingesta-free body fat have not been validated for African ungulates, we followed an approach that we have previously used for Gorongosa antelopes (Atkins et al. 2019, Becker et al. 2021*,* Walker et al. 2022) to develop an index of relative nutritional condition using principal component analysis. Together, principal component 1 (PC1) and principal component 2 (PC2) explained 80% of the variance in these data (Table A.1). Nutritional condition metrics associated with body size (e.g., muscle thicknesses, body length) loaded most strongly onto PC1, whereas those associated with body fat (e.g., palpation scores, max fat) loaded most strongly onto PC2 (Table A.2; Figure A.2). Thus, we used PC2 as an index of nutritional condition (i.e., endogenous fat reserves) and report the inverse of PC2 such that larger values equate to more available fat, consistent with methods and results in (Atkins et al. 2019, Becker et al. 2021*,* Walker et al. 2022). We used Welch's two-sample *t*-tests (Figure 2.4a) in R to test for differences in mean nutritional condition among individuals of each species before (2014–2016, 2018) and after Idai (2019).

Aerial wildlife surveys

Gorongosa conducts biennial aerial wildlife counts (Stalmans et al. 2019, Stalmans & Peel 2020*)*. We used data from surveys conducted in 2014, 2016, 2018, and 2020 (the four years in which a total count was conducted within a standardized 193,500-ha block at the core of the park) to evaluate population trends before versus after Idai. Detailed methods are in (Stalmans et al. 2019). Briefly, counts were conducted by trained park personnel from a Bell JetRanger helicopter with all four doors removed to enhance visibility. Surveys were conducted at a constant height of 50-55 m above the ground at 96 km hr^{-1} along a series of parallel, 500-m wide transects. All animals within 250 m on either side of the center line were individually counted and their location recorded using a GPS; when a large herd was observed, the pilot circled to enable an accurate count, and when necessary, photographs were used to count all individuals. M.E.S. participated in all aerial surveys, and all surveys were flown by the same pilot (M. Pingo, Sunrise Aviation).

We used count data from 2014–2018 to establish study species' association with floodplain habitat under normal (non-cyclone) conditions. Following Atkins et al. (2019), we quantified association with floodplain as the mean relative abundance of each species in floodplain habitat across survey years [i.e., the proportion of individuals counted within the treeless interior area around Lake Urema, as delineated by a pre-existing habitat classification (Stalmans & Beilfuss 2008)].

We evaluated whether the proportional change in herbivores' abundance between two pairs of consecutive 'normal' survey years (2014–2016, 2016–2018) differed significantly from the proportional

change in abundance between surveys before vs. after Idai (2018–2020) to establish whether the cyclone impacted herbivore trajectories. We calculated proportional change in abundance of each herbivore population as the difference in total number of individuals counted between surveys divided by the number of individuals counted in the earlier survey [e.g., (count in 2016 - count in 2014)/count in 2014]. We fit a linear mixed-effects model with a Gaussian-error distribution, proportional change in abundance as the response variable, a categorical indicator of cyclone incidence ('cyclone', 'no cyclone') as the main predictor, and a per-species random intercept. We fit model using the *glmmTMB()* function in the *glmmTMB* package and inspected model residuals using the *simulateResiduals()* function in the *DHARMa* package in R (Brooks et al. 2017, Hartig 2022), yielding no evidence that model assumptions were violated. Next, we evaluated whether herbivore species' body mass, affiliation with exposed habitat, or proportion of diet normally made up of grasses (mean grass RRA in the early dry seasons of 2016 and 2018) explained the patterns of population growth/decline before or after Idai using linear regression. We used Akaike information criterion corrected for small sample size (AICc) for model selection among the set of 16 candidate models including main effects and interactions of herbivore mass, habitat affiliation, and diet composition (Table B.2).

Supplemental Tables

Table B.1. Parameter estimates from species-specific models of monthly herbivore distribution (proportion of detections at each camera site) after March 15th in the cyclone year (2019) versus two representative 'normal' years (2017, 2018). Columns are GLMM parameter estimates (β), associated standard errors (SE) and *P*-values. Predictors are distance (m) from Lake Urema, log_{10}-transformed to adhere to model assumptions ('lake'); time after cyclone landfall on 15 March 2019 ('month', continuous variable of month since landfall); and whether or not a cyclone occurred in the given year ('cyclone', coded as binary variable '1', non-cyclone years as '0'). Models pertain to results presented in Figures B.9-10. Boldface denotes significant effects ($P \leq 0.05$). The three-way cyclone:lake:month interaction reflects evidence that the cyclone changed herbivore's distribution relative to Lake Urema compared to typical years and that the effect changed over the months since landfall (see: Figure B.10).

Waterbuck (*Kobus ellipsiprymnus*)	β	SE	*P*-value
Intercept	**11.83**	**2.86**	**< 0.001**
cyclone	**-17.40**	**4.46**	**< 0.001**
lake	**-2.06**	**0.32**	**< 0.001**
month	-0.70	0.50	0.16
cyclone:lake	**1.99**	**0.50**	**< 0.001**
cyclone:month	**2.33**	**0.86**	**0.007**
lake:month	0.07	0.06	0.22
cyclone:lake:month	**-0.26**	**0.10**	**0.006**
Warthog (*Phacochoerus africanus*)	β	SE	*P*-value
Intercept	**10.67**	**2.80**	**< 0.001**
cyclone	**-22.68**	**4.08**	**< 0.001**
lake	**-1.97**	**0.31**	**< 0.001**
month	**-1.46**	**0.39**	**< 0.001**
cyclone:lake	**2.53**	**0.45**	**< 0.001**
cyclone:month	**3.83**	**0.83**	**< 0.001**
lake:month	**0.17**	**0.04**	**< 0.001**
cyclone:lake:month	**-0.42**	**0.09**	**< 0.001**
Nyala (*Tragelaphus angasii*)	β	SE	*P*-value
Intercept	**-19.40**	**6.21**	**0.002**
cyclone	-9.86	6.89	0.15
lake	**1.35**	**0.68**	**0.05**
month	-0.04	0.96	0.96
cyclone:lake	1.02	0.75	0.17

cyclone:month	**4.04**	**1.42**	**0.004**
lake:month	0.002	0.11	0.97
cyclone:lake:month	**-0.43**	**0.16**	**0.005**
Impala (*Aepyceros melampus*)	*β*	SE	*P*-value
Intercept	**12.66**	**4.60**	**0.006**
cyclone	**-15.22**	**5.23**	**0.004**
lake	**-2.27**	**0.51**	**< 0.001**
month	**-2.76**	**0.55**	**< 0.001**
cyclone:lake	**1.77**	**0.57**	**0.002**
cyclone:month	**2.85**	**1.05**	**0.007**
lake:month	**0.32**	**0.06**	**< 0.001**
cyclone:lake:month	**-0.32**	**0.12**	**0.005**
Bushbuck (*Tragelaphus sylvaticus*)	*β*	SE	*P*-value
Intercept	3.70	2.92	0.20
cyclone	-2.11	4.27	0.62
lake	**-1.14**	**0.32**	**< 0.001**
month	-0.22	0.45	0.46
cyclone:lake	0.21	0.47	0.66
cyclone:month	0.45	0.88	0.61
lake:month	0.03	0.05	0.55
cyclone:lake:month	-0.04	0.10	0.67

Table B.2. Candidate models for predicting proportional changes in herbivore abundance between 2018 (before Cyclone Idai) and 2020 (after the cyclone). Each model is an ordinary least squares regression, and candidate predictors included *log*-transformed herbivore body mass ('Mass'), proportion of diet normally composed of grass ('Grass'), and affiliation with floodplain habitat ('Floodplain').

Model	Adj. R^2	AICc	ΔAICc	AICŵ
Mass	0.28	7.04	0	0.31
Floodplain	0.22	8.00	0.96	0.19
Mass + Floodplain	0.36	8.54	1.50	0.15
Mass + Grass	0.34	8.86	1.82	0.13
Intercept only	*NA*	8.90	1.86	0.12
Grass	-0.005	11.29	4.25	0.04
Grass + Floodplain	0.20	11.43	4.39	0.03
Mass + Grass + Floodplain	0.40	11.95	4.91	0.03
Mass + Grass + Floodplain + Mass:Grass	0.42	17.24	10.20	0.00
Mass + Grass + Floodplain + Mass:Floodplain	0.41	17.67	10.63	0.00
Mass + Grass + Floodplain + Grass:Floodplain	0.32	19.34	12.30	0.00
Mass + Grass + Floodplain + Mass:Floodplain + Mass:Grass	0.38	26.79	19.75	0.00
Mass + Grass + Floodplain + Mass:Grass + Grass:Floodplain	0.37	27.12	20.08	0.00
Mass + Grass + Floodplain + Mass:Floodplain + Grass:Floodplain	0.35	27.47	20.43	0.00
Mass + Grass + Floodplain + Mass:Floodplain + Mass:Grass + Grass:Floodplain	0.28	42.37	35.33	0.00
Mass + Grass + Floodplain + Mass:Floodplain + Mass:Grass + Grass:Floodplain + Mass:Grass:Floodplain	0.20	67.44	60.40	0.00

Table B.3. Summary of large-herbivore fecal samples used for analyses of diet composition, in descending order of total sample size. LWS = late-wet season, EDS = early-dry season, and LDS = late-dry season. The final row reports the mean number of samples per species in each collection period. Late-wet season sample sizes for bushbuck and hartebeest were insufficient for analysis.

		Collection periods						
Common name	Latin name	2016 EDS	2018 LWS	2018 EDS	2018 LDS	2019 LWS	2019 EDS	2019 LDS
Waterbuck	*Kobus ellipsiprymnus*	40	18	33	16	20	30	17
Warthog	*Phacochoerus africanus*	19	20	30	12	14	28	14
Impala	*Aepyceros melampus*	23	25	30	19	22	29	18
Oribi	*Ourebia ourebi*	16	13	28	16	9	30	16
Reedbuck	*Redunca arundinum*	12	12	28	15	11	30	15
Elephant	*Loxodonta africana*	21	15	22	19	15	15	15
Sable	*Hippotragus niger*	17	6	18	15	22	18	14
Wildebeest	*Connochaetes taurinus*	29	13	16	15	12	7	11
Kudu	*Tragelaphus strepsiceros*	13	13	20	14	13	14	15
Nyala	*Tragelaphus angasii*	10	13	15	10	17	14	13
Buffalo	*Syncerus caffer*	17	11	12	12	11	9	8
Bushbuck	*Tragelaphus sylvaticus*	18	*0*	16	13	*0*	15	11
Hartebeest	*Alcelaphus buselaphus*	12	*0*	14	14	*0*	8	12
Mean		19	14.5	21.7	14.6	15.1	19	13.8

Supplemental Figures

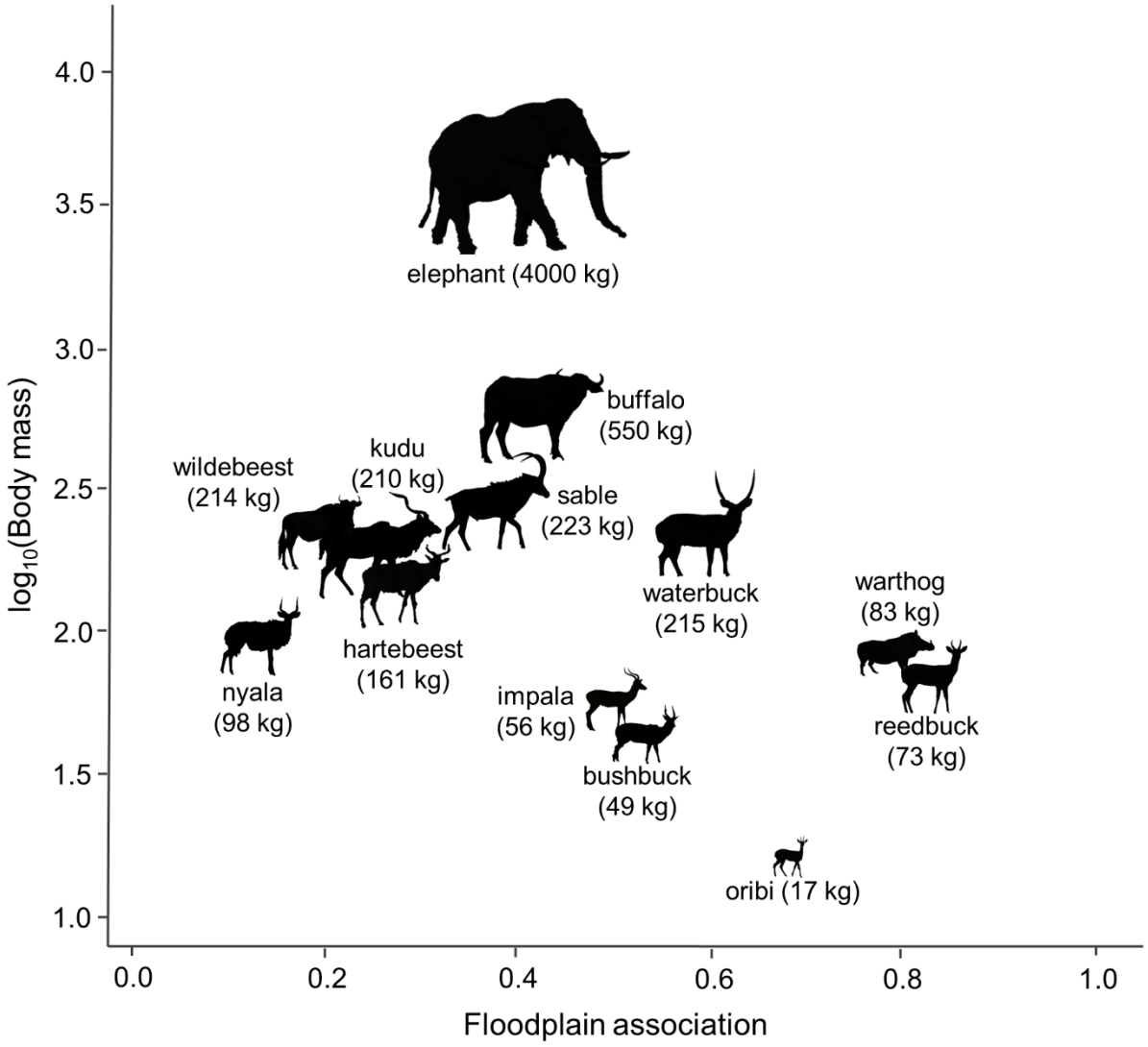

Figure B.1. The 13 ungulate species in this study spanned a broad spectrum of body size and affiliation with low-elevation floodplain habitat. Body size is reported as the mean mass for each species given by Kingdon (1977) and *log*-transformed to facilitate plotting. Body mass of study species spanned two orders of magnitude and a broad range of association with floodplain habitat (nyala, 12%, to reedbuck, 81%). Body size and floodplain association were not correlated (Pearson's correlation test: $r = 0.04$, $df = 38$, $P = 0.80$).

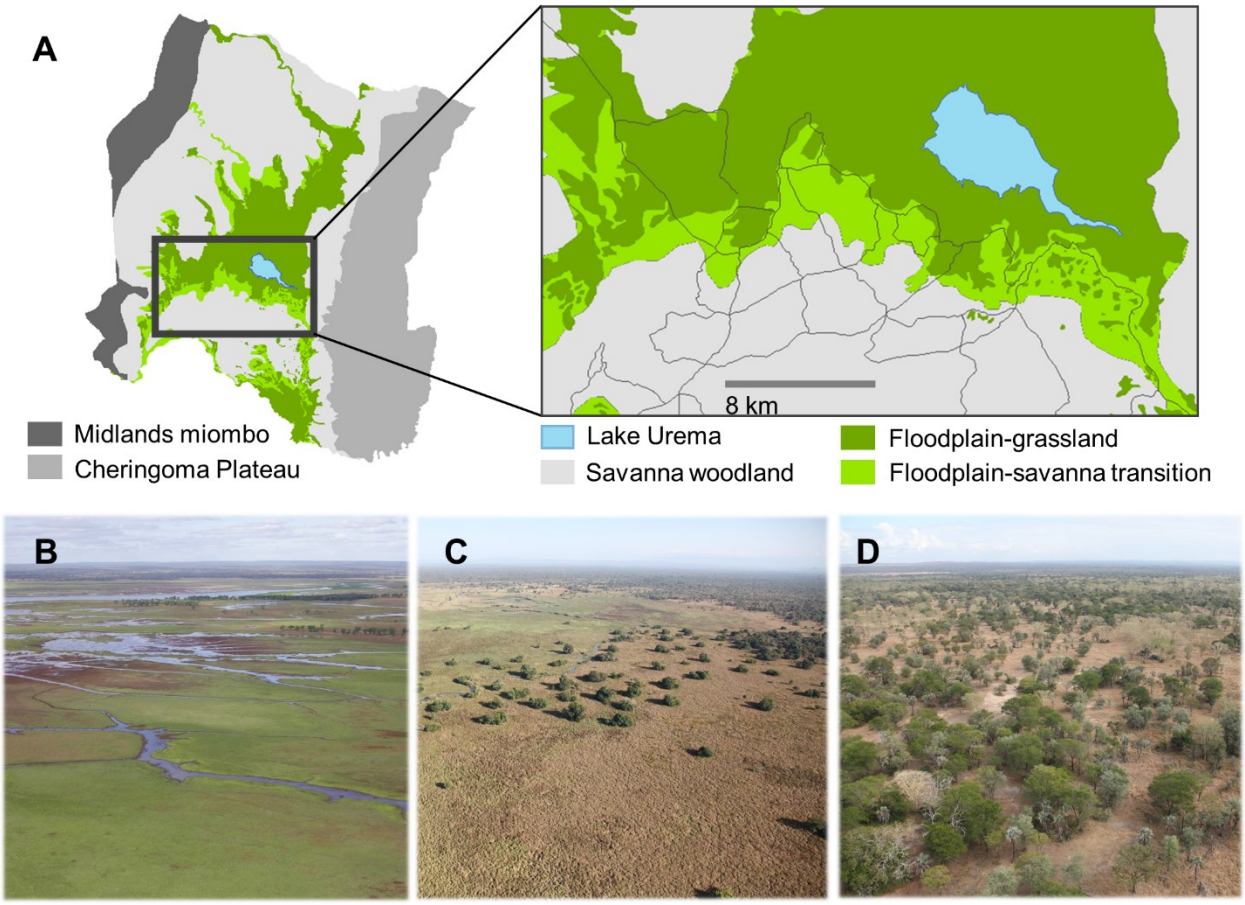

Figure B.2. Three primary habitats typify our study area within Gorongosa. (**A**) Our study area lies south of Lake Urema in the Rift Valley between the higher-elevation Rift escarpments. (**B**) A representative photo of the interior floodplain, a low elevation (8-20 m above sea level), seasonally flooded lawn of grasses and forbs. (**C**) A representative photo of floodplain-savanna transition (20-25 m above sea level), a sparsely wooded habitat characterized by intermittent flooding and stands of flood-tolerant trees. (**D**) A representative photo of savanna woodland (> 25 m above sea level), a habitat that supports a diverse community of tree species and a full continuum of canopy cover.

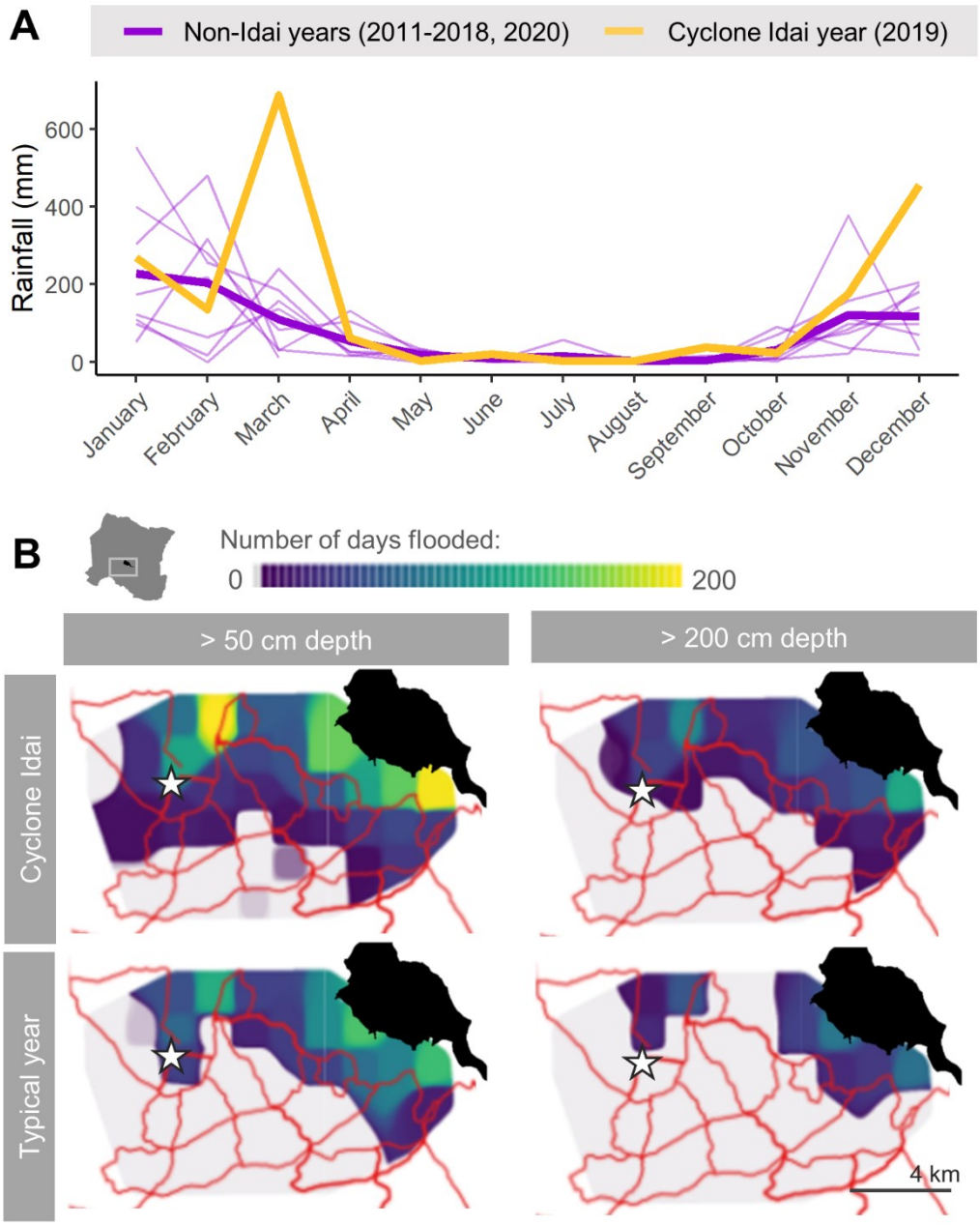

Figure B.3. Heavy cyclone rains caused flood waters to rise rapidly and to persist for longer and at greater depths than in a typical year. (**A**) Thin purple lines show monthly rainfall during each non-cyclone years (2011-2018, 2020); thick purple line shows mean monthly rainfall across all non-cyclone years; thick yellow line shows monthly rainfall in the year of Idai. Cyclone Idai (March 2019) more than tripled the typical amount of rainfall. (**B**) Flood waters extended farther into the road network (red lines) and persisted longer (blue-yellow color scale) in the year Cyclone Idai made landfall (2019, top maps) than in the subsequent year (2020, bottom maps). White stars mark Lion House's location within the study area, to contextualize the photographs in Figure B.4.

Figure B.4. Time-lapse photographs taken from Lion House, a structure at the floodplain-grassland interface, showing the flood progression. (**A**) Lion House (>5 km from Lake Urema, see Figure B.3) before Idai (early March 2019) when the seasonal flood waters had largely receded in the surrounding floodplain. This picture was taken via drone by the Gorongosa Restoration Project. (**B**) Lion House was submerged by flood waters following Idai to the extent that only the roof remained above the water line (photo date: March 22, 2019). This picture was taken from a helicopter during post-Idai humanitarian aid efforts by the Gorongosa Restoration Project. Over the course of two days (15-17 March 2019; **C**-**F**), flooding prompted by Cyclone Idai rose by >3-m adjacent to Lion House and persisted for ~2 months (**G,H**). Photos courtesy of Dr. Piotr Naskrecki.

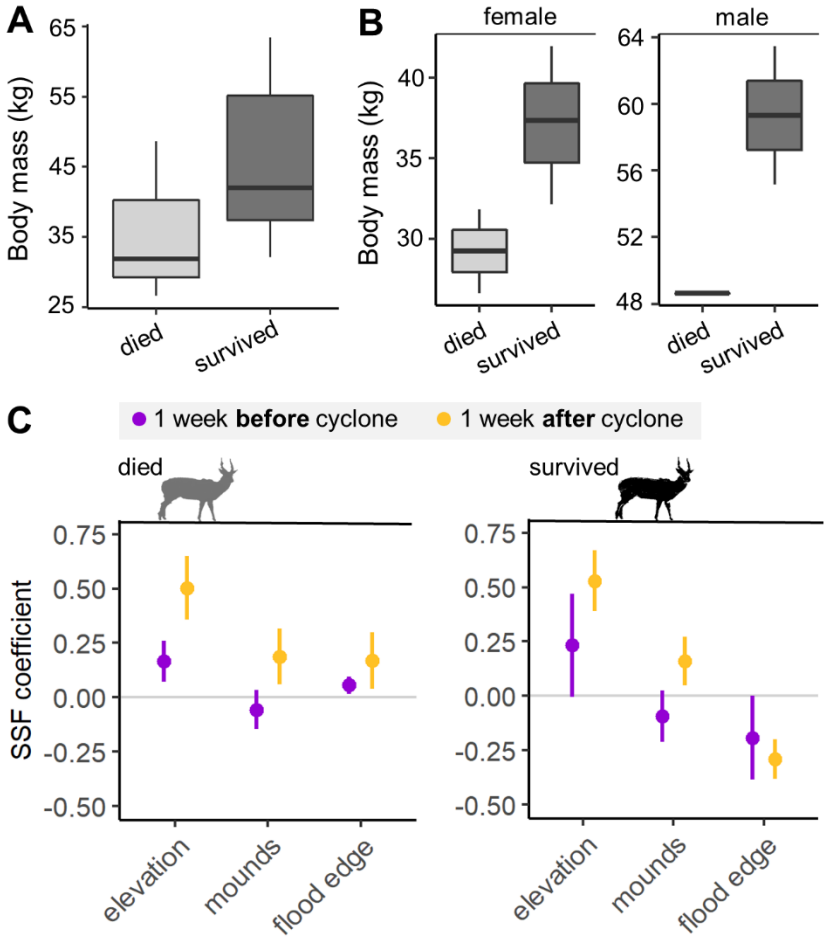

Figure B.5. Body size and movement behaviors of bushbuck that died (n = 3) versus those that survived (n = 5) after Cyclone Idai made landfall. Bushbuck that died in the flood were smaller than those that survived (**A**) and included the two smallest (of five) females and the single smallest (of three) male (**B**). Boxplots show the median and interquartile range; whiskers show the minimum and maximum weights of each group. (**C**) Coefficients and 95% confidence intervals (CIs) from step-selection functions (SSFs) that quantified selection for elevation, termite mounds, and distance to flood waters in the week before (purple) and after (yellow) Idai passed over the park. Positive coefficients are indicative of selection and negative coefficients of avoidance; CIs not overlapping zero indicate significant selection or avoidance; CIs not overlapping each other indicate significant differences in movement behavior before vs. after cyclone landfall. Although bushbuck that perished in the aftermath of Cyclone Idai significantly increased their selection for higher elevations and termite mounds (indicated by non-overlapping CIs for all coefficients estimated before and after Cyclone landfall), they were not able to avoid the flood edge (indicated by positive coefficients) and ultimately died.

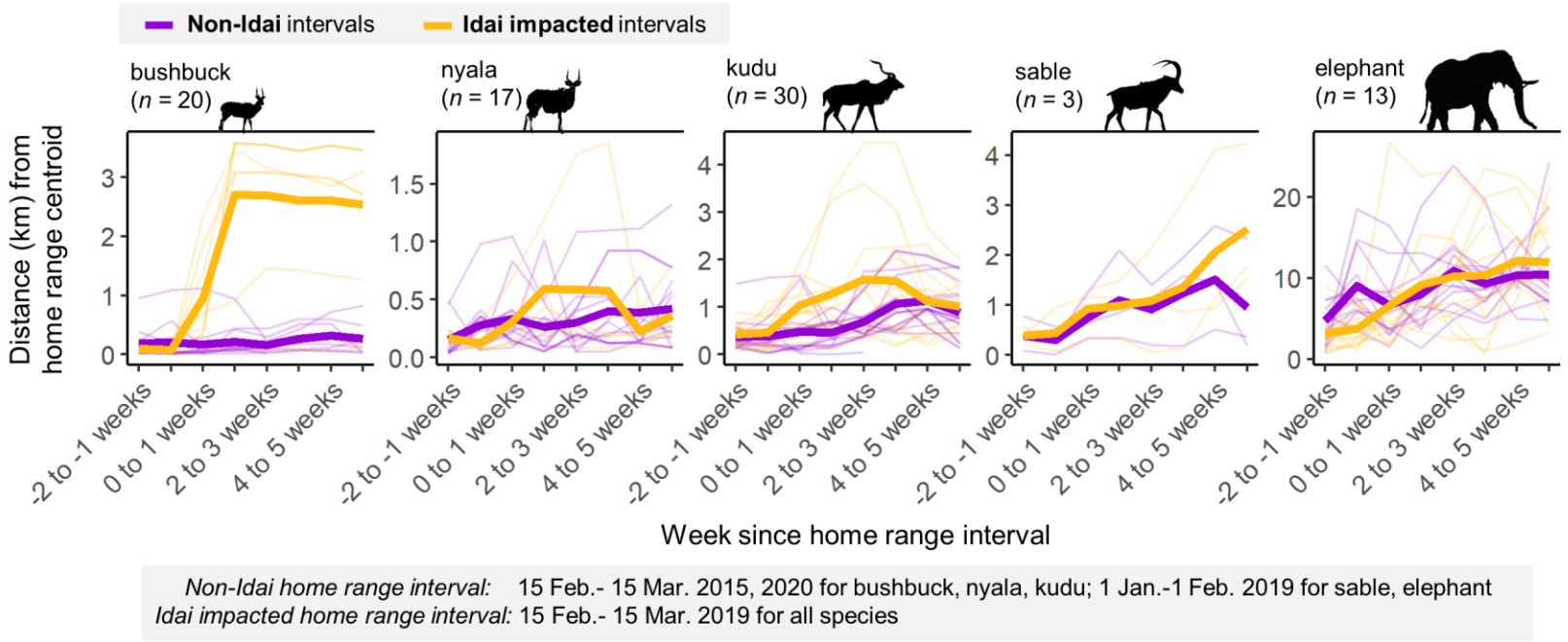

Figure B.6. Many GPS-collared herbivores moved away from their home-range centroids to a greater extent after (yellow) than before (purple) Cyclone Idai. Thin lines show individual movements; thick lines show the mean across individuals. Within the first week after Idai's landfall, bushbuck (2019: $n = 8$) had moved significantly farther from their home ranges centroids than normal (Welch's two sample t-test: $\overline{X}_{cyclone} = 0.95$, $\overline{X}_{no\ cyclone} = 0.18$, $t = 2.59$, $P = 0.03$), an effect that intensified over the next week ($\overline{X}_{cyclone} = 2.70$, $\overline{X}_{no\ cyclone} = 0.22$, $t = 5.26$, $P < 0.001$) and persisted over the next month. Kudu (2019: $n = 12$) had also moved significantly farther away from their home-range centroids in the week after landfall ($\overline{X}_{cyclone} = 1.04$, $\overline{X}_{no\ cyclone} = 0.48$, $t = 3.23$, $P = 0.004$), but returned to normal patterns of movement within a month. Some individual nyala, sable, and elephant exhibited similarly anomalous displacement from their home range centroids after the cyclone, but these trends were not pronounced at the population level [nyala (2019: $n = 4$), 0-1 week: $\overline{X}_{cyclone} = 0.31$, $\overline{X}_{no\ cyclone} = 0.33$, $t = -0.17$, $P = 0.87$; sable ($n = 3$), 0-1 week: $\overline{X}_{cyclone} = 0.93$, $\overline{X}_{no\ cyclone} = 0.74$, $t = 0.46$, $P = 0.67$; elephant ($n = 13$), 0-1 week: $\overline{X}_{cyclone} = 6.63$, $\overline{X}_{no\ cyclone} = 6.65$, $t = -0.01$, $P = 0.99$].

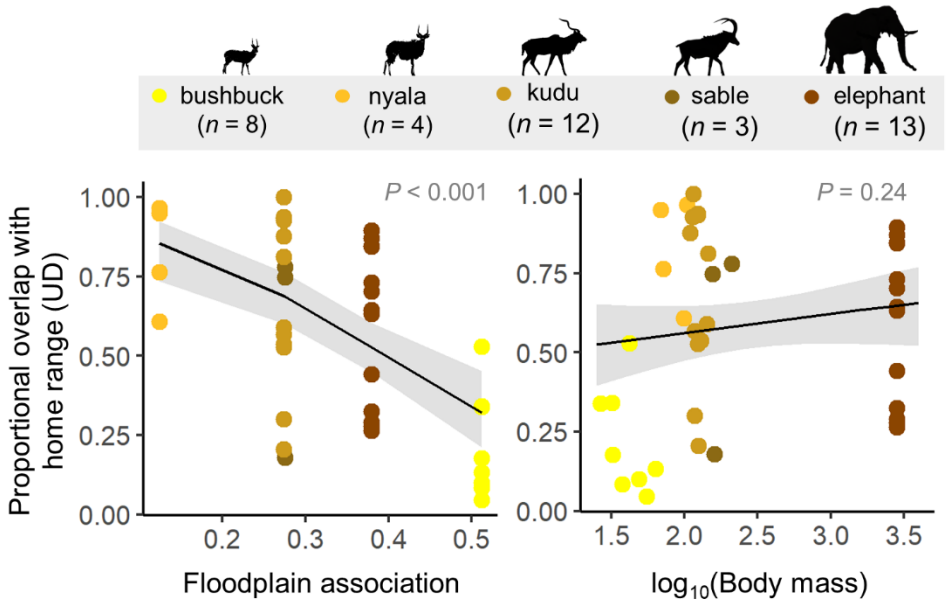

Figure B.7. Herbivore species' affiliation with low-elevation habitat predicted individual-level displacement after Idai. Floodplain association significantly predicted the magnitude of GPS-collared individuals' displacement [overlap with home ranges estimated by utilization distributions (UD) via 95% kernel density estimation] in the first week after Idai, whereas body mass did not have a significant effect after accounting for habitat affiliation (mixed-effects model with a beta-error distribution and per-species random intercepts: $\beta_{floodplain} = -6.49$, SE = 1.51, $P < 0.001$; $\beta_{log(mass)} = 0.25$, SE = 0.21, $P = 0.24$). Model-predicted effects (black line with shaded 95% confidence intervals) illustrate the strength and direction of each relationship.

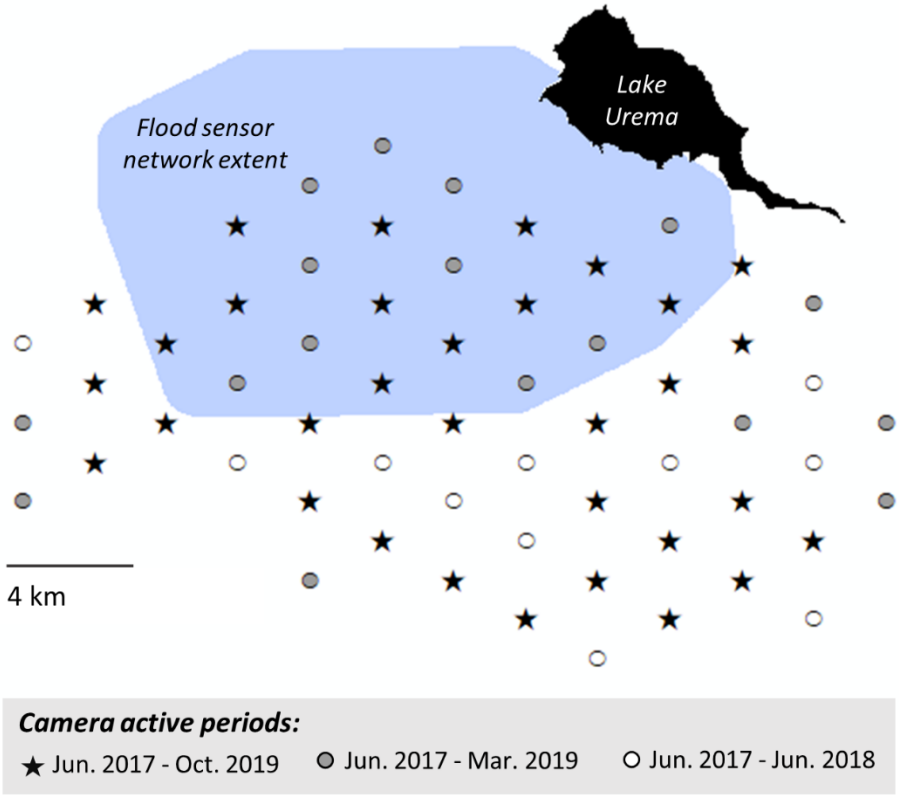

Figure B.8. Spatial extent of camera trap grid and flood sensor network relative to Lake Urema. 30 of 48 camera traps deployed in the park in 2019 produced usable data (stars, surviving cameras; grey dots, failed cameras after Idai; white dots, camera locations that were vacant for maintenance at the time of Cyclone Idai).

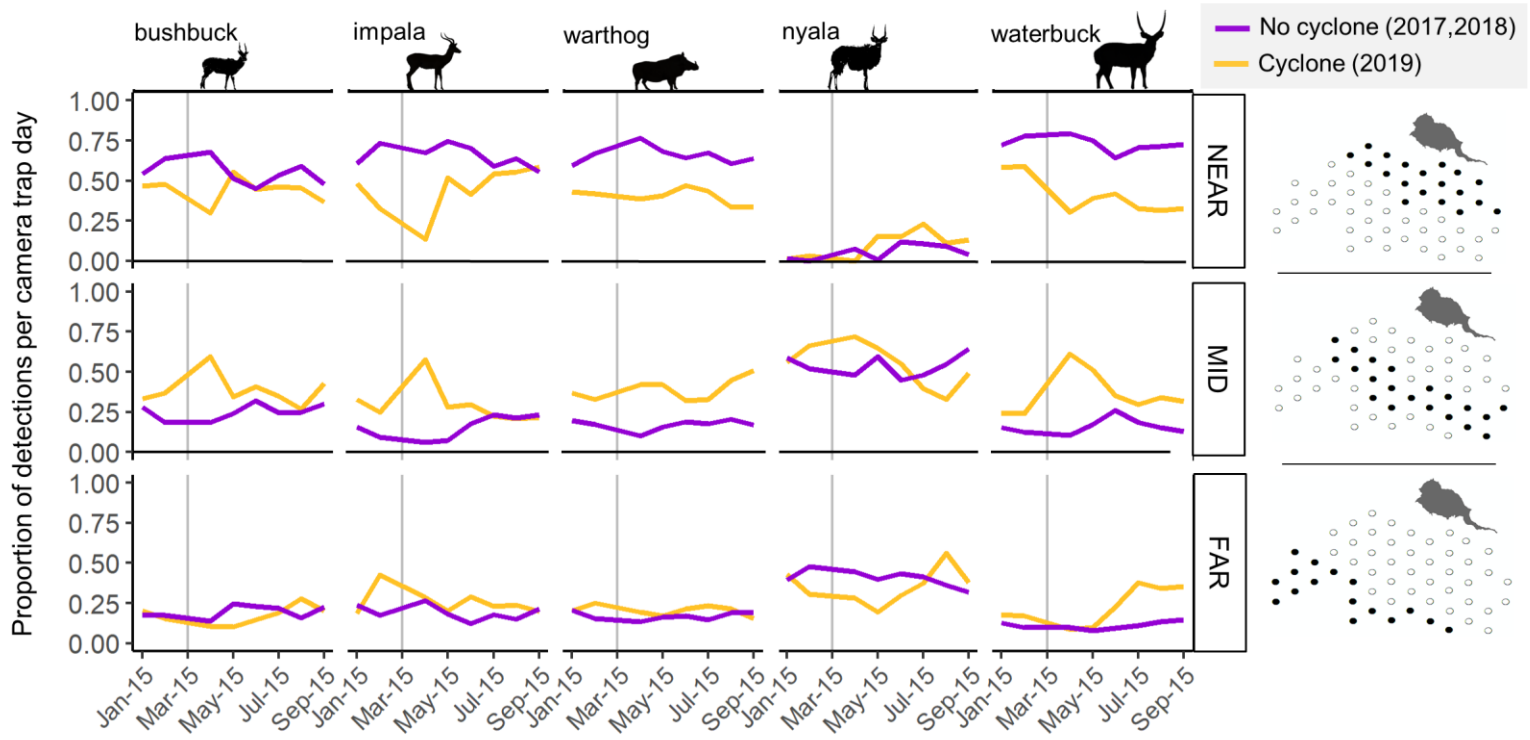

Figure B.9. The distribution of several common herbivore species shifted away from the floodplain and into higher-elevation areas after Idai. Distribution (proportion of total detections per camera trap day) of five well-sampled herbivore species relative to camera distance from Lake Urema (binned to facilitate visualization as 'near', 'mid', and 'far') in the year Cyclone Idai made landfall (2019; yellow line) and in two representative non-cyclone years (purple line, average across 2017 and 2018). Camera-grid locations in each bin (here including cameras that were both active and inactive during the cyclone for ease of visualization; see Figure B.8), are denoted with black dots at right). Vertical lines on each figure panel show the date Idai made landfall in 2019. In general, herbivores were distributed in higher-elevation areas farther from Lake Urema after Cyclone Idai than in normal years, and this effect persisted for varying durations across species (Table B.1, Figure B.10).

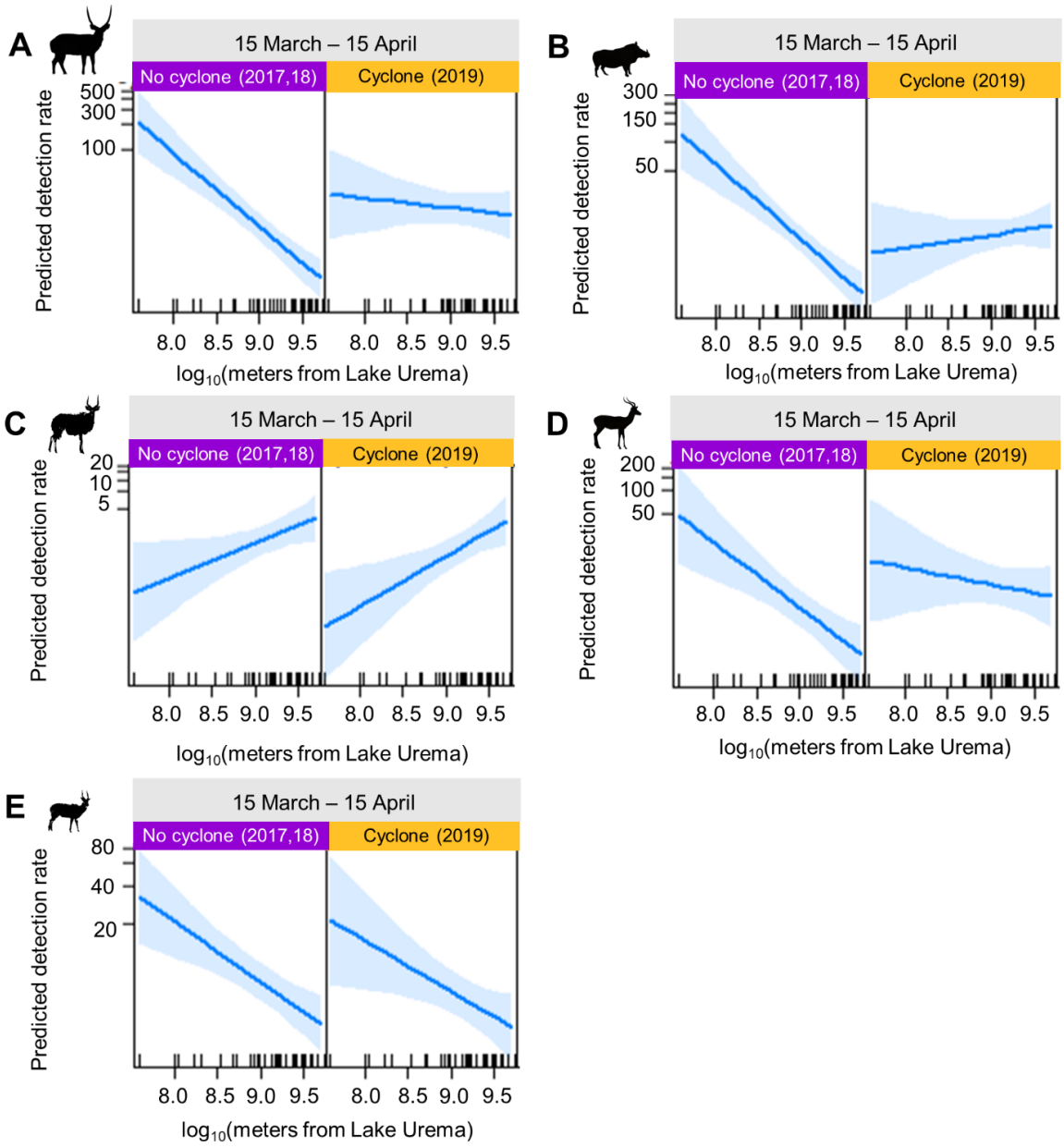

Figure B.10. Predicted camera-trap detection rate as a function of distance from Lake Urema in the first month after Idai (15 March – 15 April) vs. the same period in non-cyclone years (2017-2018). We fit a GLMM with a negative binomial distribution to the data for each species (**A-E**) to test for differences in distribution in each month after landfall in 2019 and the same month in non-cyclone-affected years and to evaluate whether distance from the lake modulated those relationships (site and year included as random intercepts, offset terms included to account for search effort and total detections; see Materials and Methods). Three-way interactions between cyclone incidence, month, and distance from the lake were significant for waterbuck (A), warthog (B), and impala (D), as illustrated by differences in slope between 'cyclone' and 'no cyclone' periods (table S1). The three-way interaction was also significant for nyala (C), though the effect was driven by shifts in nyala distribution after the first month post-cyclone, as illustrated by similar slopes in the 15 March – 15 April 'cyclone' and 'no cyclone' period.

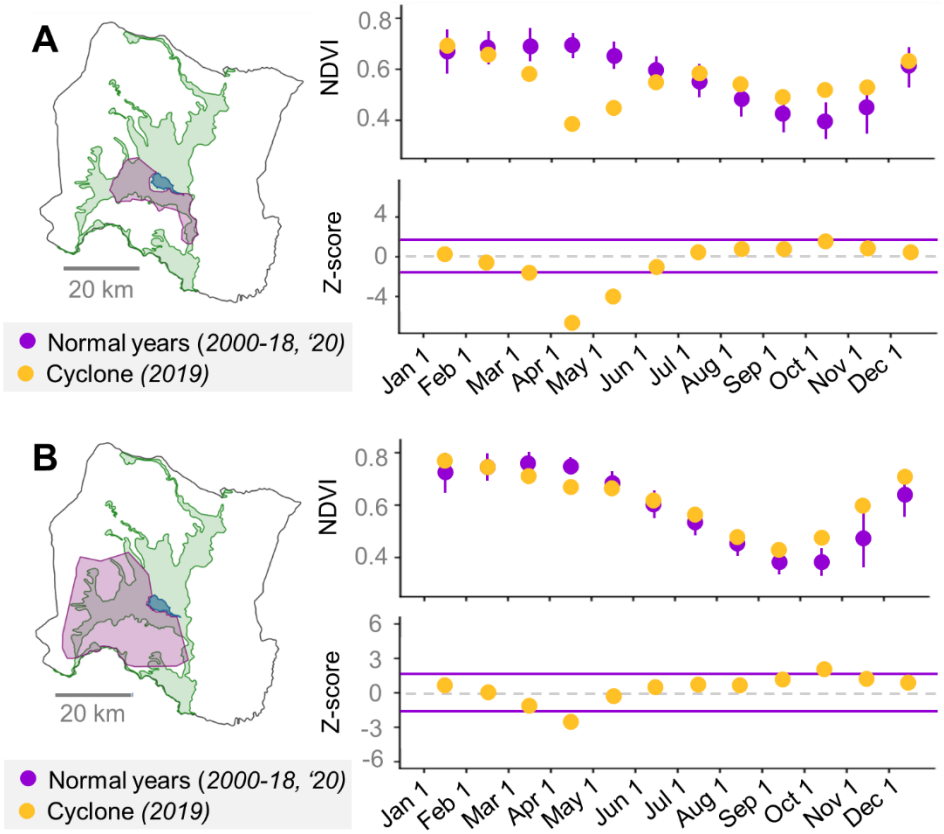

Figure B.11. Understory plant phenology during the year of Cyclone (2019; yellow) relative to bracketing years (2000-2018, 2020; purple) at two different spatial scales (red polygons). Top graphs in each panel show mean (± SE) NDVI values; bottom graphs show *Z*-scores indicating significant differences ($|Z| > 2$) between 2019 and non-cyclone years (**A**) In the area of Idai-induced flooding, we observed significant differences in NDVI in March–May and October of 2019 compared to normal years. (**B**) These effects were muted when the focal area was expanded to include higher-elevation habitat outside the flood zone [here, the 95% minimum convex polygon of location data from GPS-collared spiral-horned antelopes in the years 2014-2019 (Daskin et al. 2022)].

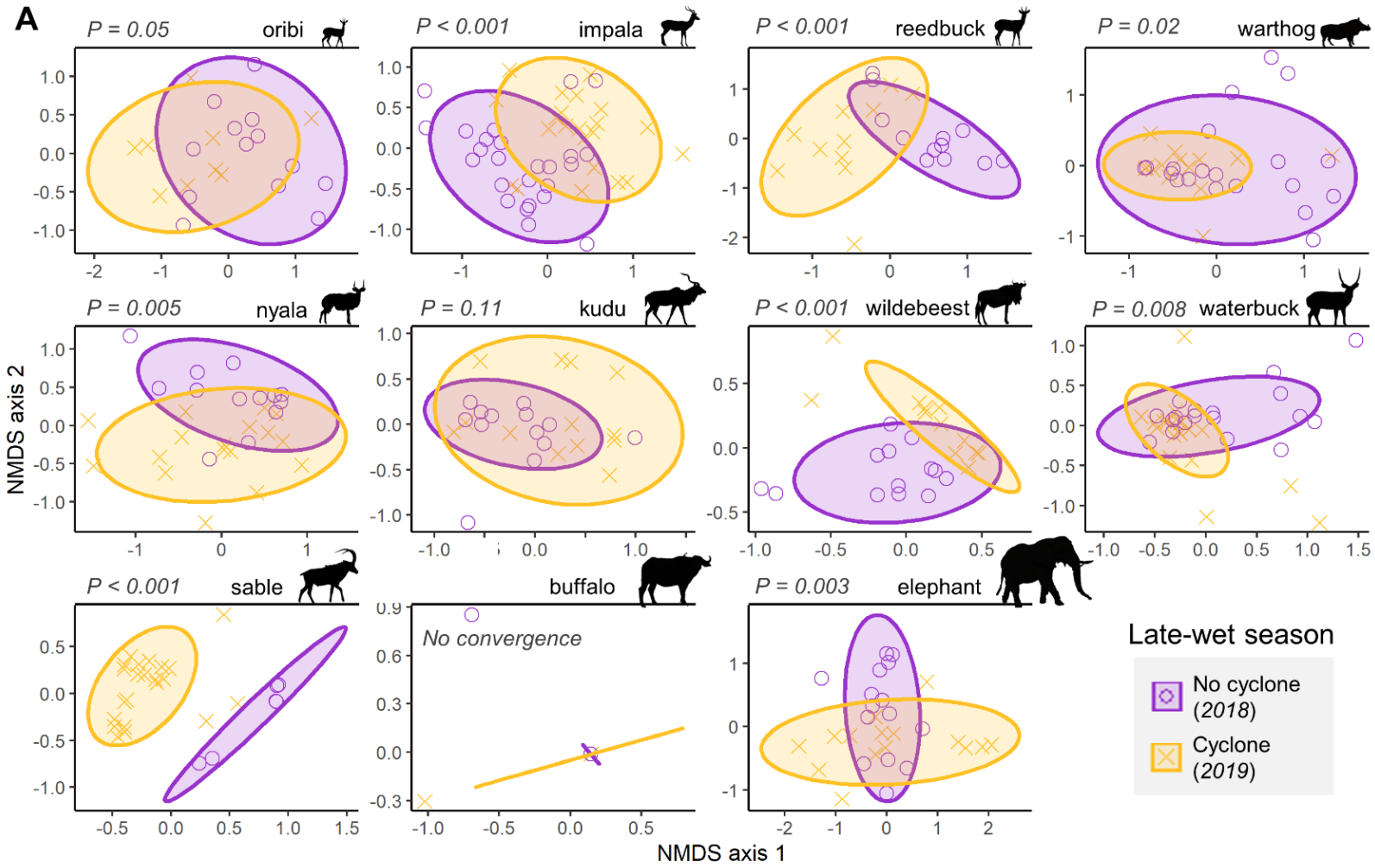
A
P = 0.05
oribi
P < 0.001
impala
P < 0.001
reedbuck
P = 0.02
warthog
P = 0.005
nyala
P = 0.11
kudu
P < 0.001
wildebeest
P = 0.008
waterbuck
P < 0.001
sable
buffalo
No convergence
P = 0.003
elephant
NMDS axis 2
NMDS axis 1
Late-wet season
No cyclone (2018)
Cyclone (2019)

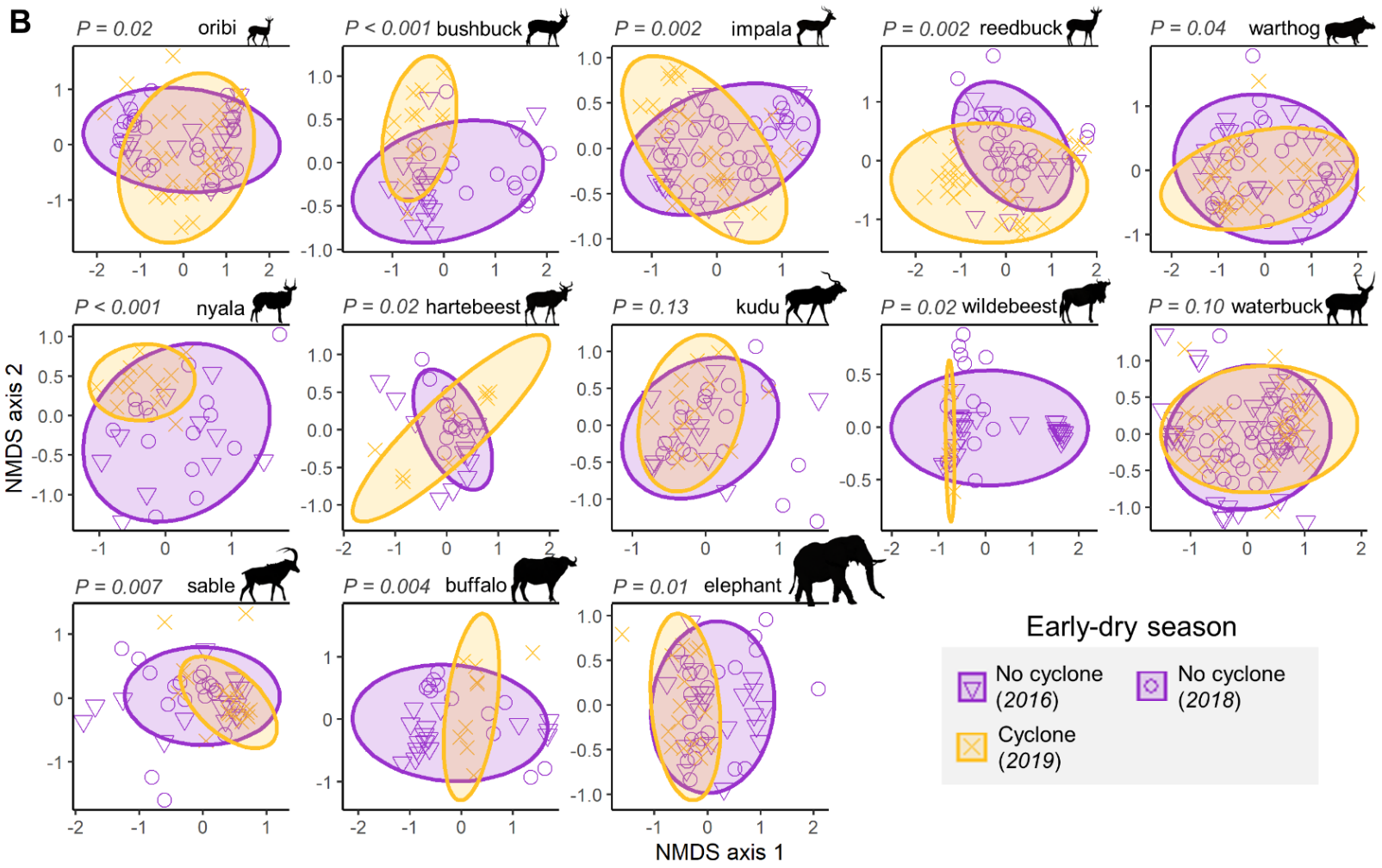
B
P = 0.02 oribi
P < 0.001 bushbuck
P = 0.002 impala
P = 0.002 reedbuck
P = 0.04 warthog
P < 0.001 nyala
P = 0.02 hartebeest
P = 0.13 kudu
P = 0.02 wildebeest
P = 0.10 waterbuck
P = 0.007 sable
P = 0.004 buffalo
P = 0.01 elephant
NMDS axis 2
NMDS axis 1
Early-dry season
No cyclone (2016)
No cyclone (2018)
Cyclone (2019)

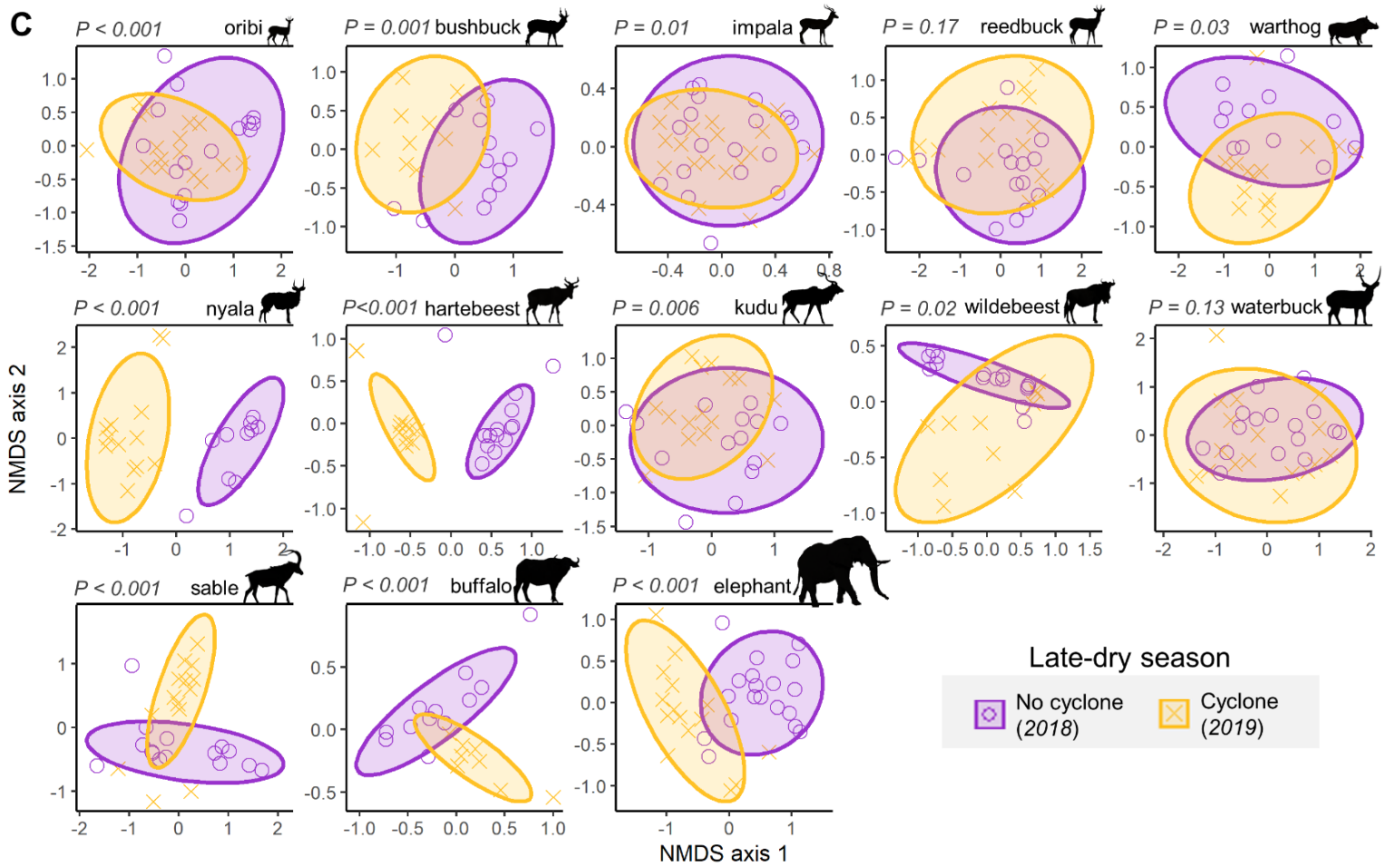

Figure B.12. Nonmetric multidimensional scaling ordinations of Bray-Curtis dietary dissimilarity after Cyclone Idai (2019; yellow) relative to non-cyclone years (2018, 2016; purple). Each point represents one fecal sample, with distance between points reflecting degree of dissimilarity; ellipses show 95% confidence level derived from the multivariate *t*-distribution and represent diet breadth for each species in the (**A**) late-wet season, (**B**) early-dry season, and (**C**) late-dry season with a. Sample sizes are in table S3. 2016 data were available only for the early-dry season (B), and bushbuck and hartebeest are omitted from the late-wet season (A) owing to insufficient sample size. P-values are from pairwise perMANOVA tests between cyclone and non-cyclone years for each species within each season; all but 5 of 36 tests (kudu in the late-wet and early-dry seasons, waterbuck in the early- and late-dry seasons, reedbuck in the late-dry season) indicated statistically significant dietary differentiation between cyclone and non-cyclone years, although the magnitudes of these differences varied.

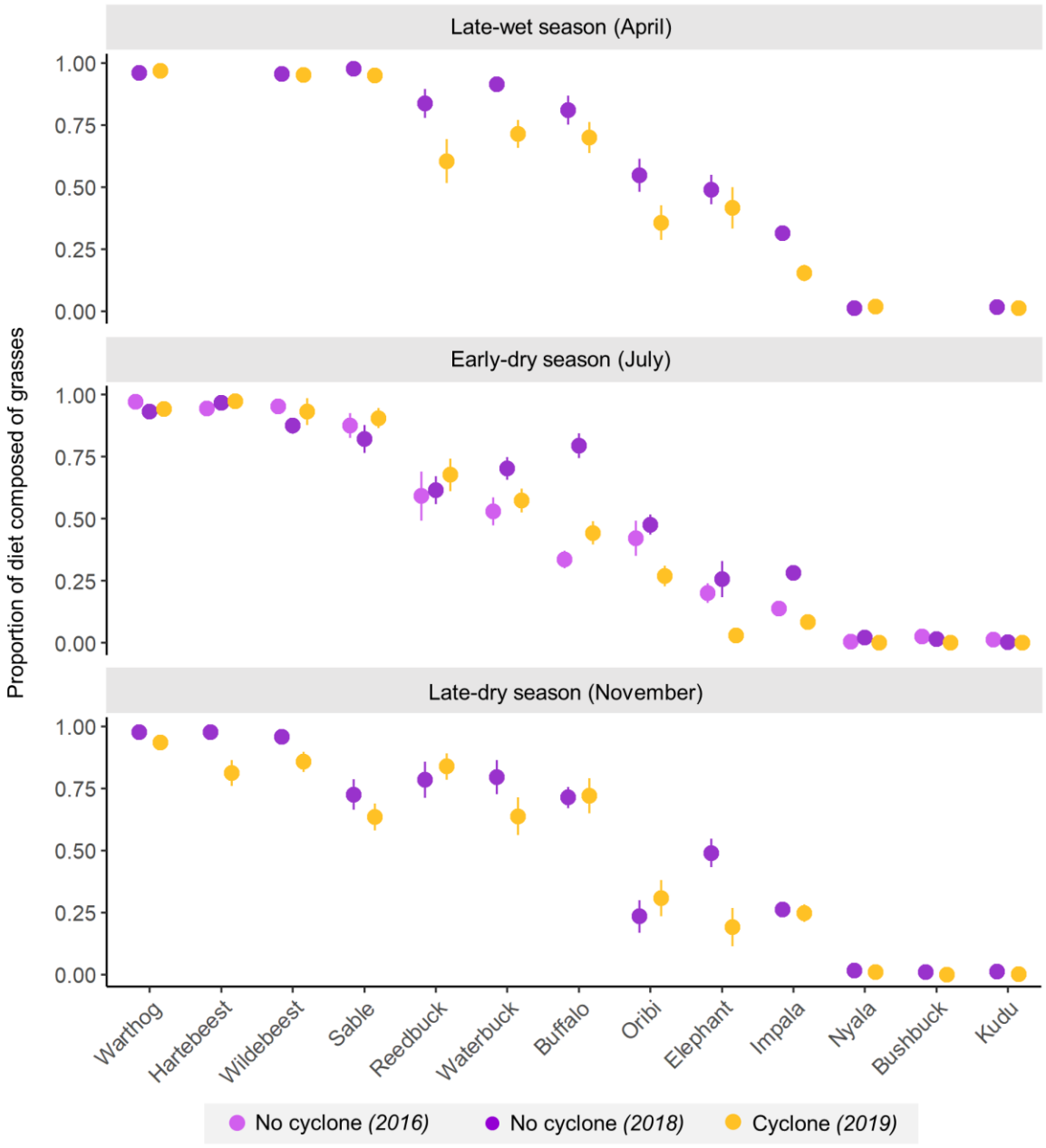

Figure B.13. Proportional consumption of grasses after Idai (2019; yellow) relative to non-cyclone years (2016, 2018; purple). Y-axes show relative read abundance (RRA) of all dietary sequences corresponding to plants in the family Poaceae; points and error bars show mean ± SE. Species are ordered from left to right in decreasing order of proportional grass consumption. Sample sizes are in Table B.3. As in other herbivore diet analyses, 2016 data were available only for the early-dry season, and bushbuck and hartebeest were omitted from wet season contrasts owing to insufficient sample size. Overall, proportional grass consumption was significantly lower in all seasons after Idai than in 2018, albeit not relative to the 2016 early-dry season (GLMM, beta-error distribution, fixed effect of year, per-species random intercepts; late wet: $\beta_{2018} = 0.73$, $SE = 0.12$, $P < 0.001$; early-dry: $\beta_{2016} = 0.12$, $SE = 0.21$, $P = 0.56$; $\beta_{2018} = 0.57$, $SE = 0.23$, $P = 0.01$; late-dry, $\beta_{2018} = 0.46$, $SE = 0.19$, $P = 0.02$).

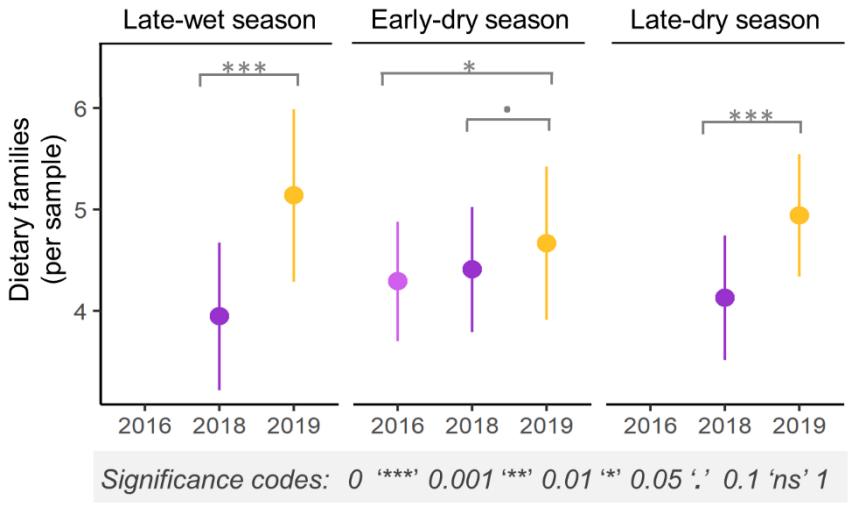

Figure B.14. Herbivore dietary richness was greater after Cyclone Idai (2019, yellow) than in non-cyclone years (2016, 2018; purple). Points and error bars show mean ± SE plant families detected per herbivore fecal sample. Sample sizes are in Table B.3. For each season, we tested whether per-sample dietary richness differed between years using a mixed-effects model with a Poisson error distribution, fixed effect of year, and per-species random intercepts. Dietary richness was greater in all seasons after Idai than in previous years, although statistical support was marginal for the early-dry season comparison with 2018 (late-wet: β_{2018} = -0.29, SE = 0.04, $P < 0.001$; early-dry: β_{2016} = -0.09, SE = 0.04, P = 0.02; β_{2018} = -0.06, SE = 0.04, P = 0.09; late-dry β_{2018} = -0.17, SE = 0.04, $P < 0.001$).

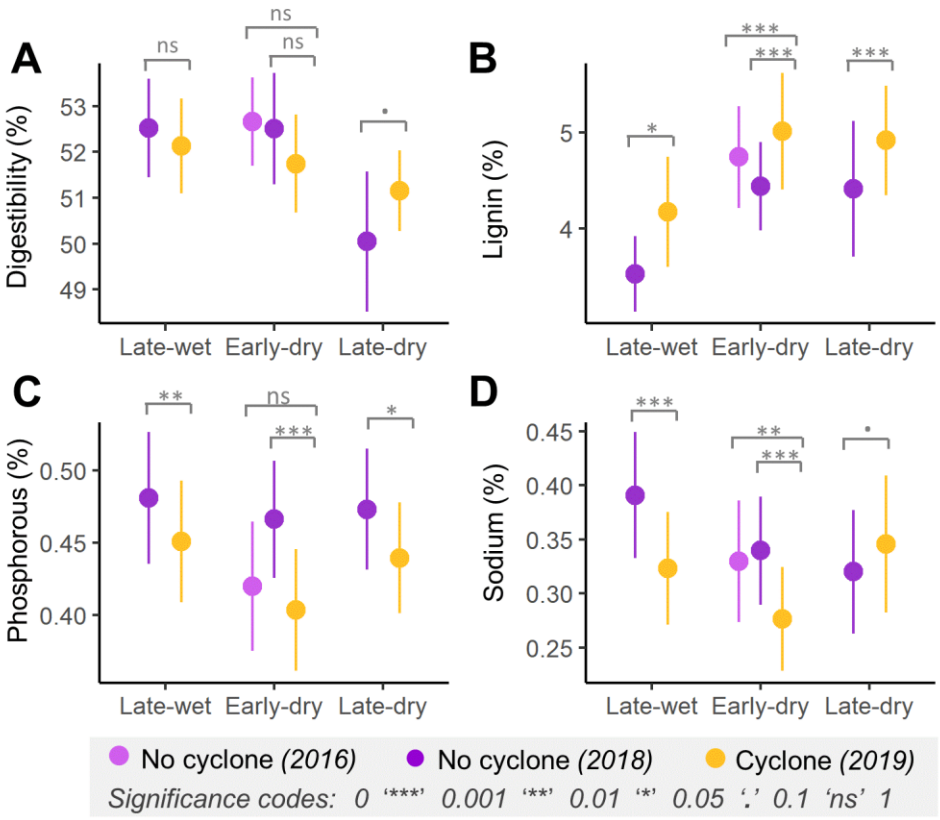

Figure B.15. Nutritional quality metrics of herbivore diets after Cyclone Idai (2019, yellow) relative to non-cyclone years (2016, 2018; purple). Points and error bars show mean ± SE. We fit separate linear mixed-effects models with per-species random intercepts to evaluate the effect of Idai on percent dry-matter digestibility (A), lignin (B), phosphorus (C), and sodium (D) in each season. A Gaussian distribution was used because it produced smaller deviations in model residuals from theoretical quantiles than the beta distribution. (**A**) Digestibility was non-significantly lower after Idai in the late-wet (β_{2018} = 0.01, *SE* = 0.02, *P* = 0.49) and early-dry seasons (β_{2016} = 0.03, *SE* = 0.02, *P* = 0.14; β_{2018} = 0.03, *SE* = 0.02, *P* = 0.15) but higher than normal in the late-dry season (β_{2018} = -0.05, *SE* = 0.02, *P* = 0.05), corresponding with the unseasonal flush of understory plant productivity (Fig. 3a, fig. S11). (**B**) Lignin content, which disproportionally reduces digestibility and is associated with consumption of woody plants (*Potter et al. 2022*), was significantly higher than normal throughout the year after Idai (late-wet: β_{2018} = -0.10, *SE* = 0.04, *P* = 0.01; early-dry, β_{2016} = -0.05, *SE* = 0.03, *P* = 0.15; β_{2018} = -0.12, *SE* = 0.03, *P* < 0.001; late-dry: β_{2018} = -0.14, *SE* = 0.04, *P* < 0.001). (**C**) Phosphorus content was lower than normal after Idai in all seasons (late-wet: β_{2018} = 0.07, *SE* = 0.03, *P* = 0.005; early-dry: β_{2016} = 0.04, *SE* = 0.03, *P* = 0.12; β_{2018} = 0.16, *SE* = 0.03, *P* < 0.001; late-dry: β_{2018} = 0.07, *SE* = 0.03, *P* = 0.02). (**D**) Sodium content was significantly lower than normal in the late-wet (β_{2018} = 0.25, *SE* = 0.06, *P* < 0.001) and early-dry (β_{2016} = 0.21, *SE* = 0.06, *P* = 0.001; β_{2018} = 0.34, *SE* = 0.06, *P* < 0.001) seasons after Idai, but rebounded by the late-dry season (β_{2018} = -0.11, *SE* = 0.07, *P* = 0.10).

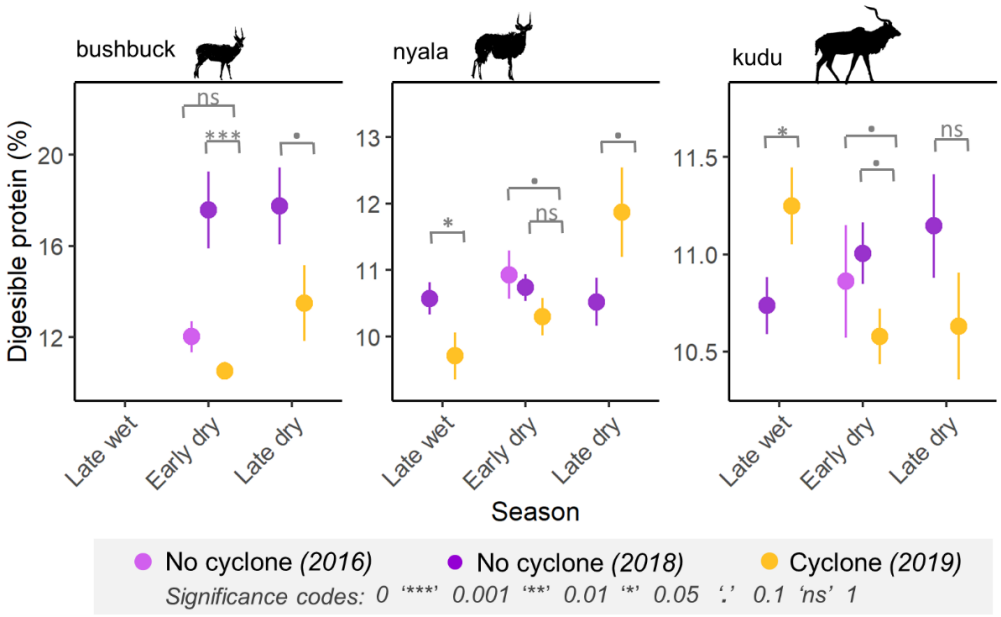

Figure B.16. Diet quality (digestible protein content) for bushbuck, nyala, and kudu after Cyclone Idai (2019; yellow) relative to non-cyclone years (2016, 2018; purple). Points and error bars show mean ± SE. We show data for these three species individually (cf. Figure 2.3c) to support the link between post-cyclone shifts in diet quality and the observed shifts in nutritional condition (Fig. 4a); in general agreement with those trends, Cyclone Idai depressed diet quality for smaller-bodied species (bushbuck and nyala) in the intervals leading up to and encompassing the body-condition measurements (conducted in the early-dry season), whereas kudu diets were significantly more protein rich in the late-wet season after Idai and only marginally poorer in the early-dry season Bushbuck diets were lower in digestible protein after Cyclone Idai in both seasons for which data are available, although this difference was non-significant for the early-dry season comparison with 2016. Bushbuck: early-dry: $\beta_{2016} = 0.13$, $SE = 0.13$, $P = 0.32$; $\beta_{2018} = 0.51$, $SE = 0.13$, $P < 0.001$; late-dry: $\beta_{2018} = 0.30$, $SE = 0.18$, $P = 0.09$). Nyala: late-wet: $\beta_{2018} = 0.10$, $SE = 0.05$, $P = 0.05$; early-dry: $\beta_{2016} = 0.07$, $SE = 0.04$, $P = 0.10$; $\beta_{2018} = 0.05$, $SE = 0.04$, $P = 0.19$; late-dry: $\beta_{2018} = -0.12$, $SE = 0.07$, $P = 0.09$. Kudu: late-wet: $\beta_{2018} = -0.05$, $SE = 0.02$, $P = 0.03$; early-dry: $\beta_{2016} = 0.04$, $SE = 0.03$, $P = 0.10$; $\beta_{2018} = 0.04$, $SE = 0.03$, $P = 0.10$; late-dry: $\beta_{2018} = 0.05$, $SE = 0.04$, $P = 0.16$.

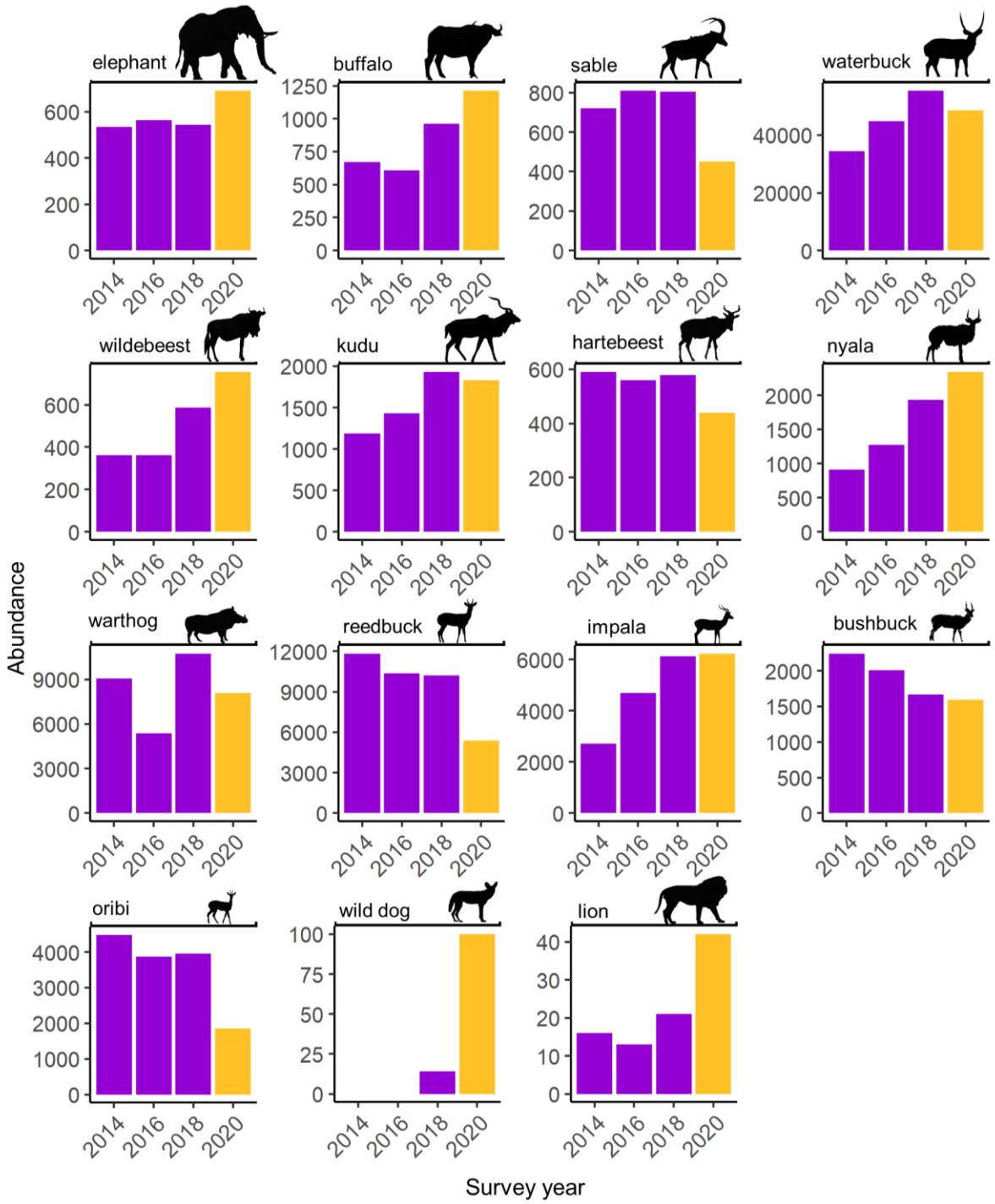

Figure B.17. Abundance of large mammals in the years before (purple) and after (yellow) Cyclone Idai. Data are from Gorongosa's biennial helicopter-based wildlife counts, except for wild dog for which we used monitoring data from Gorongosa's Conservation Program. Data are from total counts conducted over a standardized 193,500 ha area in the core of the park; lions are difficult to count from the air and these data underestimate total abundance, but we consider them a reliable index of relative abundance across years.

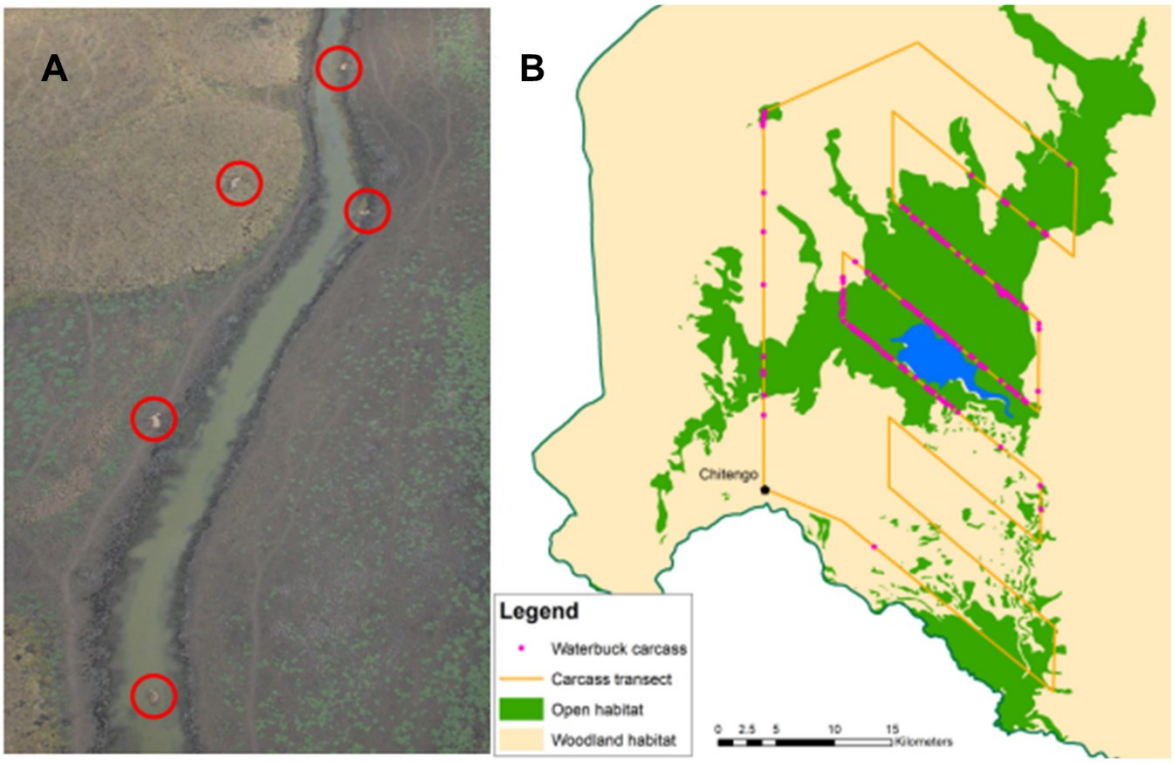

Figure B.18. Carcasses were counted as part of the October 2020 aerial wildlife survey in Gorongosa. Carcasses were not counted in wildlife surveys prior to 2020 but were systematically counted in that year (7 months after Cyclone Idai) when observers spotted an unusually high number of dead animals. (**A**) Five waterbuck carcasses around a channel in the floodplain. (**B**) Distribution of waterbuck carcasses (pink dots) observed along a dedicated 250 km x 500 m wide transect (orange outline). Observers counted an average of 2.93 dead waterbuck per km^2 along the transect, and densities were more than 30-fold higher in the floodplain (7.44 per km^2) than in savanna-woodland (0.24 per km^2). By comparison, waterbuck densities were only 5-fold higher in the floodplain than the savanna in 2018, suggesting that prolonged inundation and food scarcity in the floodplain after Cyclone Idai (Becker et al. 2021).

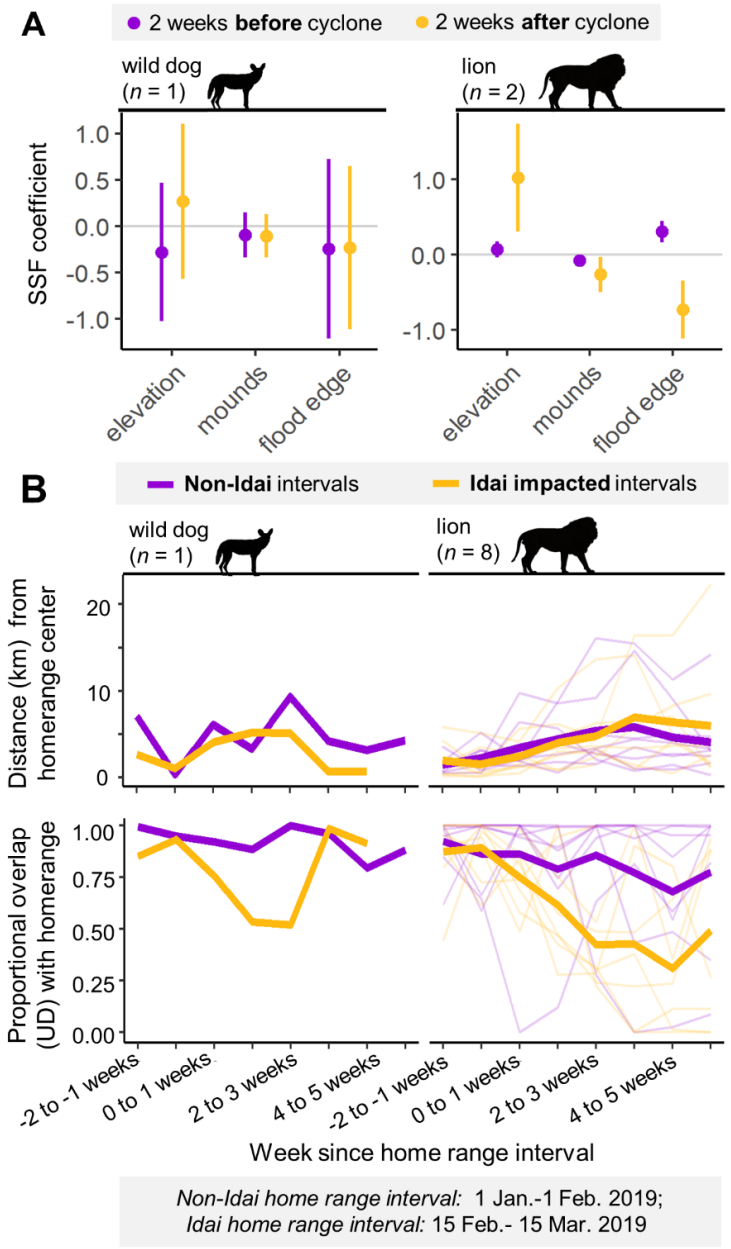

Figure B.19. Carnivore movement behavior after Cyclone Idai. (**A**) Coefficients and 95% confidence intervals from step-selection functions (SSFs) from GPS telemetry data for Gorongosa's two apex carnivore species, showing selection for elevation, termite mounds, and distance to flood waters in the two weeks before (purple) and two weeks after (yellow) Idai passed over the park (analogous to herbivore data in Figure 2.2). African wild dogs and lion increased their selection for higher elevations and their avoidance of flood waters after Idai, lions significantly so (evidenced by non-overlapping confidence intervals). Only two of eight GPS collars on lions in the weeks before and after Idai collected data at regular intervals and were appropriate for SSF analysis. (**B**) Some carnivores moved away from their home-range centroids (top, bold yellow line) and spent less time in their original home ranges (bottom, bold yellow line) in the weeks after Idai made landfall than in periods unaffected by a cyclone (purple line; comparing movement 1 Jan. – 1 Feb. to movement in weekly bins thereafter), though not significantly so.

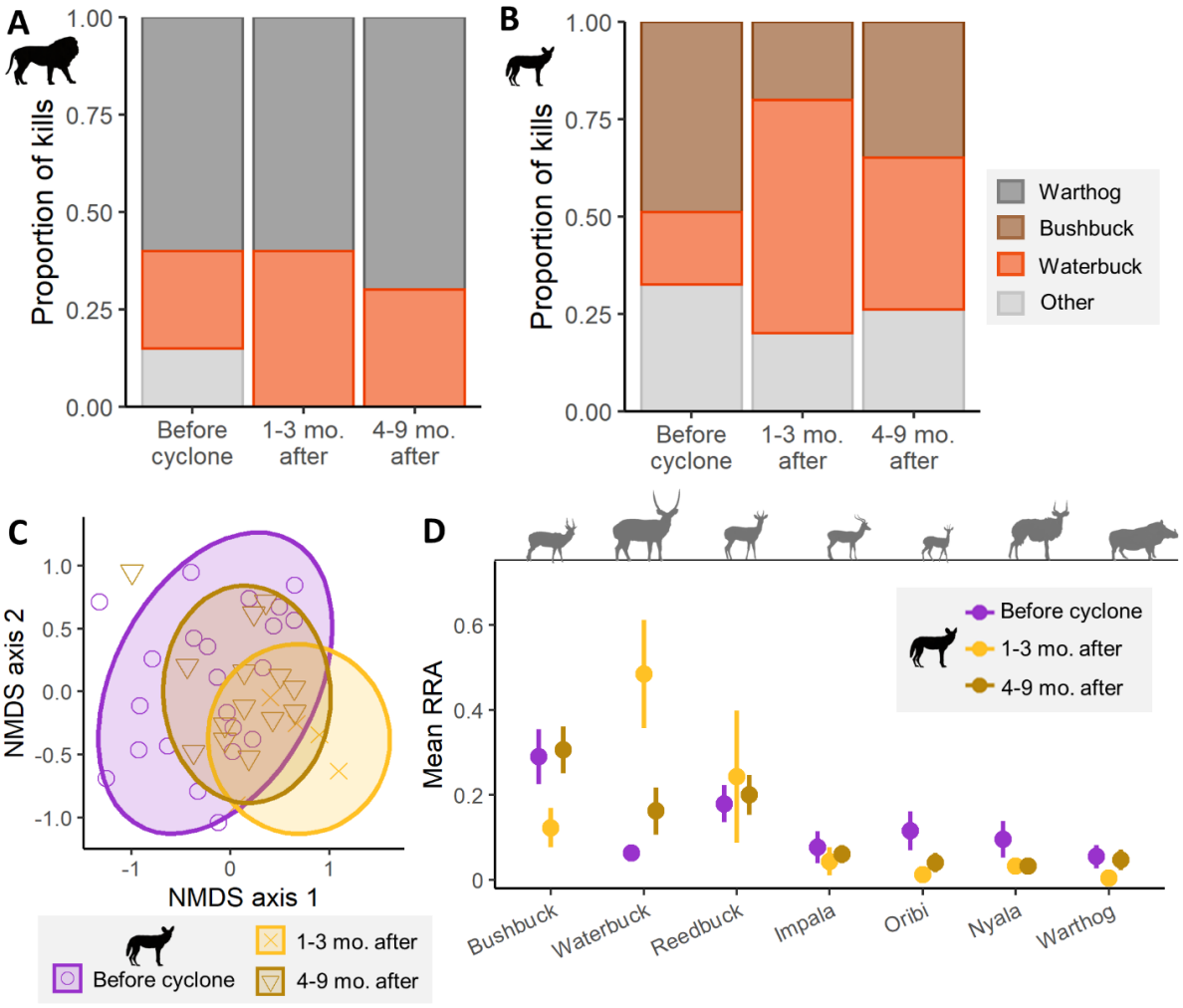

Figure B.20. Diets of lion and African wild dog before and after Cyclone Idai. (**A**) The proportion of prey species in documented lion kills did not shift substantially after the cyclone. (**B**) Waterbuck temporarily replaced bushbuck as the predominant prey species in documented wild dog kills in the three months after the cyclone. This shift was associated with significant overall differences in wild dog diets before versus immediately after the cyclone, as quantified via DNA-metabarcoding and illustrated by (**C**) NMDS ordination of Bray Curtis compositional dissimilarity among diet samples collected before and after the cyclone, and (**D**) relative read abundances (RRA) of prey species in wild dog diets.

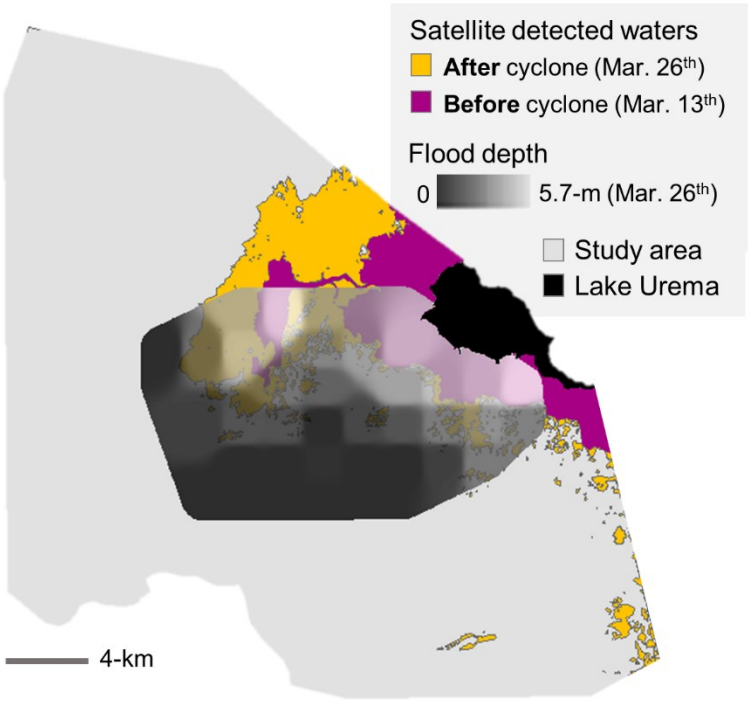

Figure B.21. Flood depths measured a field-deployed sensor array overlaid on a satellite-derived map of water extent before (purple) and after (yellow) Cyclone Idai made landfall on 15 March 2019. Flood sensors were more sensitive to shallow water than remotely sensed data but covered only a fraction of the study area. Therefore, we used satellite-derived maps of the flood waters, which were available at the same extent as the full study area, to quantify the extent of the flood before (purple) and after (yellow) Idai made landfall and to assess avoidance of the flood edge by GPS-collared mammals.

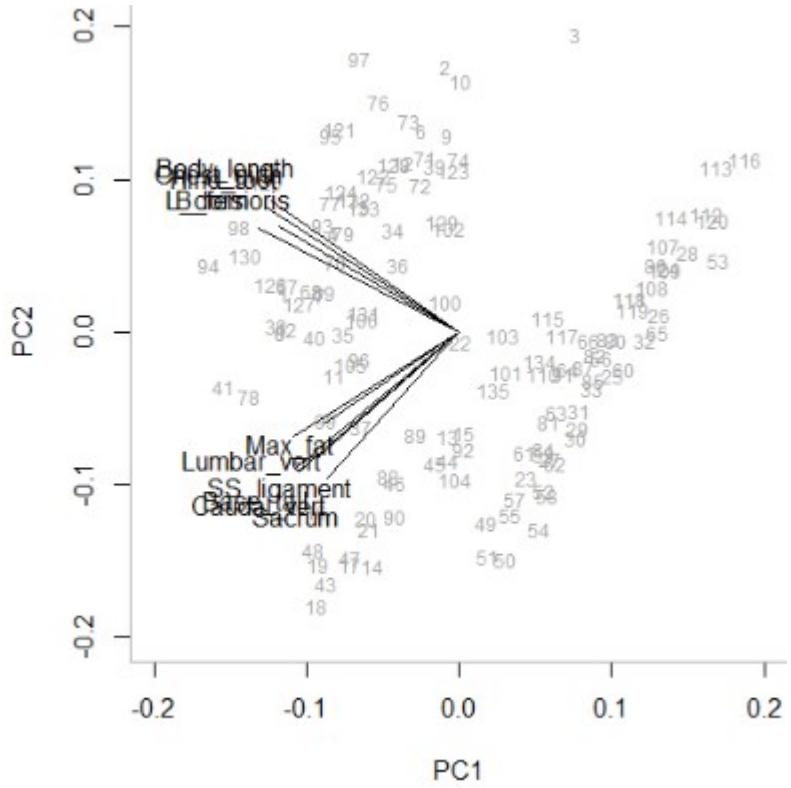

Figure B.22. Principal component analysis of 11 nutritional condition metrics collected from adult *Tragelaphus* spp. antelopes (*n* = 136) from 2014-2019 in Gorongosa. Nutritional condition metrics were collected at the time of capture. Together, Principal Component 1 (PC1) and Principal Component 2 (PC2) explained 80% of the variance in these data. Black arrows show projections of the original variables, and each grey number represents an individual antelope, the position of which reflects the individual's score based on the first two principal components. Nutritional condition metrics associated with body size (i.e., body length, 'Body_length'; hind foot length, 'Hind_foot'; chest girth, 'Chest_girth'; the thickness of biceps femoris, 'B_femoris', and longissimus dorsi, 'L_dorsi', muscles) loaded most strongly onto PC1, whereas metrics associated with body fat (i.e., maximum rump fat depth, 'Max_fat'; and palpation scores at the sacrosciatic ligament, 'SS_ligament'; lumbar vertebrae, 'Lumbar_vert'; sacrum, 'Sacrum'; base of tail, 'Base_tail'; and caudal vertebrae, 'Caudal_vert') loaded most strongly onto to PC2. Accordingly, we used the inverse of PC2 as an index of nutritional condition of antelope in this study.

Literature Cited

Arumoogum, N. 2022. Spatiotemporal niche dynamics of a reassembling herbivore ensemble in southern Africa. PhD thesis, University of the Witwatersrand, Johannesburg, South Africa.

Atkins, J. L., R. A. Long, J. Pansu, J. H. Daskin, A. B. Potter, M. Stalmans, C. E. Tarnita, and R. M. Pringle. 2019. Cascading impacts of large-carnivore extirpation in an African ecosystem. *Science* 364:173-177.

Avgar, T., J. R. Potts, M. A. Lewis, and M. S. Boyce. 2016. Integrated step selection analysis: bridging the gap between resource selection and animal movement. *Methods in Ecology and Evolution* 7:619-630.

Böhme, B., F. Steinbruch, R. Gloaguen, H. Heilmeier, and B. Merkel. 2006. Geomorphology, hydrology, and ecology of Lake Urema, central Mozambique, with a focus on lake extent changes. *Physics and Chemistry of the Earth* 31:745-752.

Bouley, P., M. Poulos, R. Branco, and N. H. Carter. 2018. Post-war recovery of the African lion in response to large-scale ecosystem restoration. *Biological Conservation* 227:233-242.

Bouley, P., A. Paulo, M. Angela, C. Du Plessis, and D. G. Marneweck. 2021. The successful reintroduction of African wild dogs (Lycaon pictus) to Gorongosa National Park, Mozambique. *PLoS ONE* 16:e0249860.

Boyer, F., C. Mercier, A. Bonin, Y. Le Bras, P. Taberlet, and E. Coissac. 2016. OBITOOLS: a UNIX-inspired software package for DNA metabarcoding. *Molecular Ecology Resources* 16:176-182.

Branco, P. S., J. A. Merkle, R. M. Pringle, J. Pansu, A. B. Potter, A. Reynolds, M. Stalmans, and R. A. Long. 2019. Determinants of elephant foraging behavior in a coupled human-natural system: is brown the new green? *Journal of Animal Ecology* 88:780-792.

Brooks, M. E., K. Kristensen, K. J. van Benthem, A. Magnusson, C. W. Berg, H. J. Skaug, M. Machler, and B. M. Miller. 2017. glmmTMB balances speed and flexibility among packages for zero-inflated generalized linear mixed modeling. *R Journal* 9, 378-400.

Busetto, L., and L. Ranghetti, 2016. MODIStsp: An R package for automatic preprocessing of MODIS Land Products time series. *Computers and Geosciences*. 97:40-48.

Cabral, P., G. Augusto, A. Akande, A. Costa, N. Amade, S. Niquisse, A. Atumane, A. Cuna, K. Kazemi, R. Mlucasse, and R. Santha. 2017. Assessing Mozambique's exposure to coastal climate hazards and erosion. *International Journal of Disaster Risk Reduction* 23:45-52.

Cook., R. C., J. G. Cook, T. R. Stephenson, W. L. Myers, S. M. Mccorquodale, D. J. Vales, L. L. Irwin, P. B. Hall, R. D. Spencer, S. L. Murphie, K. A. Schoenecker, and P. J. Miller. 2010. Revisions of rump fat and body scoring indices for deer, elk, and moose. *Journal of Wildlife Management* 74:880-896.

Craine, J. M., E.G. Towne, M. Miller, and N. Fierer. 2015. Climatic warming and the future of bison as grazers. *Scientific Reports* 5:16738.

Deagle, B. E., A. C. Thomas, J. C. McInnes, L. J. Clarke, E. J. Vesterinen, E. L. Clare, T. R. Kartzinel, and J. P. Eveson. 2019. Counting with DNA in metabarcoding studies: How should we convert sequence reads to dietary data? *Molecular Ecology* 28:391-406.

Fortin, D., H. L. Beyer, M. S. Boyce, D. W. Smith, T. Duchesne, and J. S. Mao. 2005. Wolves influence elk movements: behavior shapes a trophic cascade in Yellowstone National Park. *Ecology* 86:1320-1330.

Giguet-Covex, C., J. Pansu, R. Arnaud, *et al*. 2014. Long livestock farming history and human landscape shaping revealed by lake sediment DNA, *Nature Communications* 5:3211.

Gill, B. A., P. M. Musili, S. Kurukura, A. A. Hassan, J. R. Goheen, W. J. Kress, M. Kuzmina, R. M. Pringle, and T. R. Kartzinel. 2019. Plant DNA-barcode library and community phylogeny for a semi-arid Eastern African savanna. *Molecular Ecology Resources* 19:838-846.

Guyton, J. A., J. Pansu, M. C. Hutchinson, T. R. Kartzinel, A. B. Potter, T. C. Coverdale, J. H. Daskin, A. G. da Conceição, M. J. S. Peel, M. E. Stalmans, and R. M. Pringle. 2020. Trophic rewilding revives biotic resistance to shrub invasion. *Nature Ecology and Evolution* 4:712-724.

Hartig, F. 2022. DHARMa: Residual Diagnostics for Hierarchical (Multi-Level/Mixed) Regression Models, R package version 0.3.2.0.

Kartzinel, T. R., P. A. Chen, T. C. Coverdale, D. L. Erickson, W. J. Kress, M. L. Kuzmina, D. I. Rubenstein, W. Wang, and R. M. Pringle. 2015. DNA metabarcoding illuminates dietary

niche partitioning by African large herbivores. *Proceedings of the National Academy of the Sciences USA* 112:8019-8024.

Kilsch, A., and C. Atzberger. 2016. Operational drought monitoring in Kenya using MODIS NDVI time series. *Remote Sensing* 8:1-22.

Kolstad, K. W. 2021. Predictions and precursors of Idai and 38 other tropical cyclones and storms in the Mozambique Channel. *Quarterly Journal of the Royal Meteorological Society* 147:45-57.

Littleford-Colquhoun, B. L., P. T. Freeman, V. I. Sackett, C. V. Tulloss, L. M. McGarvey, C. Geremia, and T. R. Kartzinel. 2022. The precautionary principle and dietary DNA metabarcoding: Commonly used abundance thresholds change ecological interpretation. *Molecular Ecology* 31:1615-1626.

Mamugy F. 2016. Does predation or competition shape the home range and resources selection by sable antelope (*Hippotragus niger*) in the Gorongosa National Park, Mozambique? MSc thesis, University of the Witwatersrand, Johannesburg, South Africa.

Muff, S., J. Signer, and J. Fieberg. 2019. Accounting for individual-specific variation in habitat-selection studies: efficient estimation of mixed-effects models using Bayesian or frequentist computation. *Journal of Animal Ecology* 89:80-92.

Oksanen, J., F. Guillaume Blanchett, M. Friendly, R. Kindt, P. Legendre, D McGlinn, P.R. Minchin, R.B. O'Hara, G.L. Simpson, P. Soymos, M.H.H. Stevens, E. Szoecas, and H. Wagner. 2020. vegan: Community Ecology Package. R package version 2.5-6.

Pansu, J., J. A. Guyton, A. B. Potter, J. L. Atkins, J. H. Daskin, B. Wursten, T. R. Kartzinel, and R. M. Pringle. 2019. Trophic ecology of large herbivores in a reassembling African ecosystem, *Journal of Ecology* 109:1355-1376.

Parker, K. L., P. S. Barboza, and M. P. Gillingham. 2009. Nutrition integrates environmental responses of ungulates. *Functional Ecology* 23:57-69.

Pateiro-Lopez, and B. A. Rodriquez-Casal. 2022. Generalization of the convex hull of a sample of points in a plane, CRAN v.2.5.

Pebesma, E. 2004. Multivariable geostatistics in S: the gstat package. *Computers and Geosciences* 30:683–91.

Pringle, R. M. 2017. Upgrading protected areas to conserve wild biodiversity. *Nature* 54:91-99.

R Core Team. 2020. R: A Language and Environment for Statistical Computing, Vienna, Austria. Available at: https://www.R-project.org/

Sikes, R. 2016. Animal Care and Use Committee of the American Society of Mammalogists. 2016 Guidelines of the American Society of Mammalogists for the use of wild animals in research and education. *Journal of Mammology* 97:633-688.

Stalmans, M., and R. Beilfuss. 2008. Landscapes of the Gorongosa National Park. Gorongosa National Park.

Stalmans, M. E., and M. Peel. 2020. Aerial wildlife count of the Gorongosa National Park, Mozambique, November 2020.

Taberlet, P., E. Coissac, F. Pompanon, *et al*. 2007. Power and limitation of the chloroplast trnL (UAA) intron for plant DNA barcoding. *Nucleic Acids Research* 35:e14.

Tarnita, C., J. A. Bonachela, E. Sheffer, J. A. Guyton, T. C. Coverdale, R. A. Long, and R. M. Pringle. 2017. A theoretical foundation for multi-scale regular vegetation patterns. *Nature* 541:398-401.

Therneau, T. 2020. A package for survival analysis in R. CRAN.

Tinley, K.L. 1977. PhD thesis, University of Pretoria, Pretoria, South Africa.

UNOSAT. 2019. Cumulative satellite detected waters extent overview between 13 & 26 March 2019 over Sofala province, Mozambique.

Walker, R. H., M. C. Hutchinson, A. B. Potter, J. A. Becker, R. A. Long, and R. M. Pringle. 2022. Mechanisms of individual variation in large herbivore diets: roles of spatial heterogeneity and state-dependent foraging. *Ecology* e3921.

Western, D., V. N. Mose, J. Worden, and D. Maltumo. 2015. Predicting extreme droughts in savannah Africa: A comparison of proxy and direct measures in detecting biomass fluctuations, trends, and their causes. *PLoS ONE* 10:e0136516.

Willersley, E., J. Davison, J. Moora, *et al*. 2014. Fifty thousand years of Arctic vegetation and megafaunal diet. *Nature* 506:47-15.

Appendix C: Supplemental materials for, "Chapter 3: Competition mediates fitness costs of heat sensitivity in a tropical carnivore"

Supplemental Tables

Table C.1. Values and sources for key environmental parameters included in the microclimate sub-model of Niche Mapper.

Parameter	Source	Value
Configuration factors	Warren Porter, personal communications	Between animal and sky = 0.5; between animal and ground = 0.3
Soil thermal conductivity	Abu-hamdeh & Reeder (2000)	0.35 W/m^{o}C
Substrate reflectivity	Markvart and Castañer (2003)	16%
Substrate density	Sharma (1997*)*	2650 kg/m^3
Substrate specific heat	Ren et al. (2003)	837 J/ kgK
Substrate longwave infrared emissions	Sellers (1965)	90%
Percent shade		100%
Cloud cover	Wilson & Jetz 2016	3.4 – 85.7%
Air Temperature	Zhang et al. 2022	-4.9 – 42.5^{o}C
Elevation	Amatulli et al. 2018	922-960 m
Wind speed	Fick & Hijmans 2017	0 – 3.5 ms^{-1}

Table C.2. Values and sources for key physiological and morphological parameters included in the endothermic sub-model of Niche Mapper for African wild dogs.

Parameter	Source	Value
Body mass – nonreproductive, lactating	Mid-range weight of African wild dogs (Estes 1990, Gorman et al 1998)	25 kg
Body mass – pregnant	Midpoint of measured 15-25% increase in body weight in the last month of pregnancy for domestic dogs (Fontaine 2012)	30 kg
Height	Height at shoulder reported for 28-kg African wild dog by Smithers (1983)	75 cm
Percent body fat	Mean fat mass of free ranging grey wolves across individuals and seasons in Nelchina Basin, Alaska (Hilderbrand & Golden 2013)	8.5 %
Target core body temperature	Resting steady state value reported for African wild dogs in Taylor et al (1971)	38°C
Maximum core body temperature	Two degree increase in core temperature reported after exercise in African wild dogs by Taylor et al (1971)	40°C
Basal metabolic rate (BMR)	Resting metabolic rate from allometric equation for 25 kg domestic dog (Gorman et al 1998, Walters et al. 1993). Same equation produces rate within 3% of single empirical value for 9.5 kg African wild dog (Taylor et al 1971, Gorman et al 1998).	60.4 W
BMR multiplier for activity	Measured from doubly labeled water trials for African wild dogs (Gorman 1998)	5.2
BMR multiplier for reproduction – pregnancy	Midpoint of measured 1.25-1.5-fold increase in maintenance energy requirements after 40^{th} day of gestation in domestic dogs (Fontaine 2012)	0.375
BMR multiplier for reproduction – lactation	Midpoint of measured 2.5-3-fold increase in maintenance energy requirements during the third and fourth weeks post-partum in domestic dogs (Fontaine 2012)	1.75
Hair diameter	Measured value for African wild dog (Wiley 2012)	70 μm
Hair reflectivity (350–2,500 nm)	Measured value (integrated across wavelengths) on sandy-colored hair by Warren Porter in 2021.	0.17
Hair density	Measured from adult female African wild dog in study area population in July 2021.	100 cm^{-2}
Torso fur length (dorsal, ventral)	Measured from adult female African wild dog in study area population in July 2021.	24.0, 10.0 mm

Torso fur depth (dorsal, ventral)	Measured from adult female African wild dog in study area population in July 2021.	16.4, 2.0 mm
Head/Neck fur length (dorsal, ventral)	Measured from adult female African wild dog in study area population in July 2021.	22.5, 50.0 mm
Head/Neck fur depth (dorsal, ventral)	Measured from adult female African wild dog in study area population in July 2021.	11.1, 39.9 mm
Legs fur length (dorsal, ventral)	Measured from adult female African wild dog in study area population in July 2021.	10.0, 11.0 mm
Legs fur depth (dorsal, ventral)	Measured from adult female African wild dog in study area population in July 2021.	1.0, 1.5 mm
Tail fur length (dorsal, ventral)	Measured from adult female African wild dog in study area population in July 2021.	30.0, 30.0 mm
Tail fur depth (dorsal, ventral)	Measured from adult female African wild dog in study area population in July 2021.	8.6, 8.6 mm
Temperature difference between inspired and expired air	Mean across six mongrel dogs in a warm, dry climate (Baile et al. 1987).	10°C
Minimum temperature difference from core to periphery	Measured difference between central body and extremity skin temperature in domestic dog at start of challenge trial (Peterson & Seagrave 1983)	1°C
Oxygen extraction efficiency maximum	Measured in mongrel dogs at atmospheric oxygen levels (Cain & Chapler 1979)	30%
Thermal conductivity of flesh	Mean of measured values for canine kidney, liver, and heart muscle (Valvano et al. 1985, 1987)	0.498

Table C.3. Range of parameter values and associated sources used in a sensitivity analysis of evaporative water loss predictions from Niche Mapper for African wild dogs at a representative location (23.78253, -19.17917) in our study area.

	Minimum	Maximum	Reference
Torso fur depth (mm) dorsal, ventral	13.9, 1.7	18.9, 2.3	± 15% of measured value from adult female in study population
Torso fur length (mm) dorsal, ventral	20.4, 8.5	27.6, 11.5	± 15% of measured value from adult female in study population
Torso hair diameter (μm)	59.5	80.5	± 15% of value reported in Wiley (2022)
Torso hair density (cm^{-2})	85	115	± 15% of measured value from adult female in study population
Temperature difference, inspired and expired air (°C)	7.3	12.7	Range of values for mongrel dogs in a warm, dry climate (Bailey et al. 1987)
Temperature difference, core to skin (°C)	0.5	3.0	Range of values in domestic dogs (Peterson & Seagrave 1983)
Maximum core body temperature (°C)	38.5	42.5	Range of values from no heat storage to dangerous hyperthermic temperature (Olfosky et al. 1996)
Body mass (kg)	20	30	Range of weights in African wild dog species description (Estes 1990)
Body fat (%)	3.3	15.9	Range of fat mass in free-ranging wolves (Hilderbrand & Golden 2013)

Table C.4. Pack characteristics, GPS collar data availability, and number of dens used for each litter. We included a total of 25 litters from 16 packs in our analyses. Due to differences in sampling regimes during the study (2012-2016), not all litters had a pack member equipped with a GPS collar in all phases of the pup rearing cycle. Litter is a unique identifier for each litter, ordered alphanumerically by pack code and year; Pack code is a unique identifier for a wild dog pack; Year is the year in which the litter was born; Pack size denotes the number of wild dogs > 1 year of age in each pack-year, which can change significantly among years for the same pack due to yearling recruitment and/or dispersal events; Pregnancy movement is a binary variable indicating whether (yes, Y) or not (no, N) GPS data were available during the pregnancy phase of the pup rearing cycle for the given pack-year; Lactation movement is a binary variable indicating whether (yes, Y) or not (no, N) GPS data were available during the lactation phase of the pup rearing cycle for the given pack-year; Dens used denotes the number of dens used to rear pups during the lactation phase in each pack-year.

Litter	Pack code	Year	Pack size (N)	Pregnancy movement?	Lactation movement?	Dens used (N)
1	AP	2014	12	Y	Y	4
2	AP	2015	8	Y	Y	2
3	AP	2016	8	N	N	4
4	DB	2014	12	N	Y	2
5	DB	2015	6	Y	Y	3
6	FV	2014	9	N	Y	4
7	HT	2014	10	Y	Y	5
8	HT	2015	11	Y	Y	6
9	HT	2016	4	Y	Y	3
10	HW	2012	7	Y	Y	3
11	HU	2015	9	N	Y	2
12	KB	2012	6	Y	Y	3
13	KW	2014	8	N	Y	4
14	MB	2014	11	N	Y	7
15	MB	2015	14	Y	Y	6
16	MB	2016	6	N	N	2
17	MK	2012	4	Y	Y	3
18	MT	2012	11	N	N	4
19	MU	2016	9	N	N	3
20	PA	2016	6	N	N	2
21	RV	2015	3	N	N	1
22	SA	2012	2	Y	Y	2
23	ZU	2014	10	Y	Y	3
24	ZU	2015	4	N	N	1
25	ZU	2016	10	N	N	2

Supplemental Figures

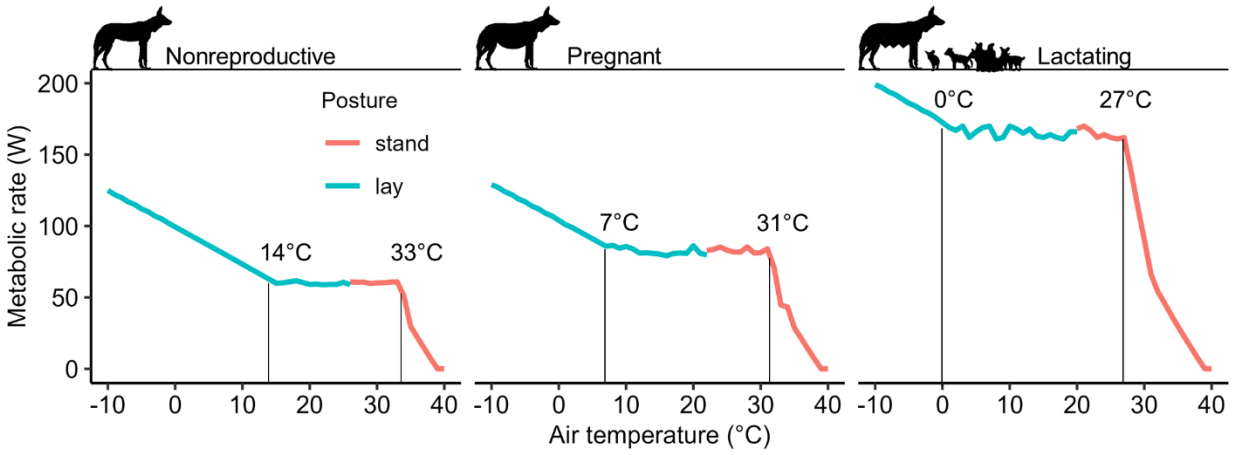

Figure C.1. Predicted metabolic rates (Watts) from Niche Mapper for nonreproductive (25 kg), pregnant (30 kg), and lactating (25 kg) African wild dogs (*Lycaon pictus*) as a function of air temperature and thermal radiation. Metabolic rates were estimated by running the endotherm sub-model for each demographic in a 'metabolic chamber' simulation. The simulation assumed no heat input from solar radiation and that all microclimatic variables remained constant (relative humidity = 5%, wind speed = 0.1 m/s) except air and radiant temperature, which were simultaneously increased from -40 to 40°C in 1°C increments. The thermal neutral zone is the range of temperatures within which the predicted metabolic rate remains within 5% of the target metabolic rate while the individual is standing to facilitate heat loss (red lines) or laying in a flat or curled posture to facilitate heat retention (blue lines). Air temperatures at which the predicted metabolic rate no longer remains within 5% of the basal rate represent the upper and lower critical temperatures under those conditions (noted on each plot with annotated vertical lines). The simulated upper critical temperature (UTC) for the nonreproductive individual aligns well with the lone empirical estimate from metabolic chamber experiments on a non-reproductive, 8.5-kg African wild dog (between 30-35°C; Fig. 2 in Taylor et al. 1971), and the lower critical temperature (LCT) aligns with measurements on cold-acclimated dingos (10°C; Sheild 1972; LCT not available in the literature for wild dogs).

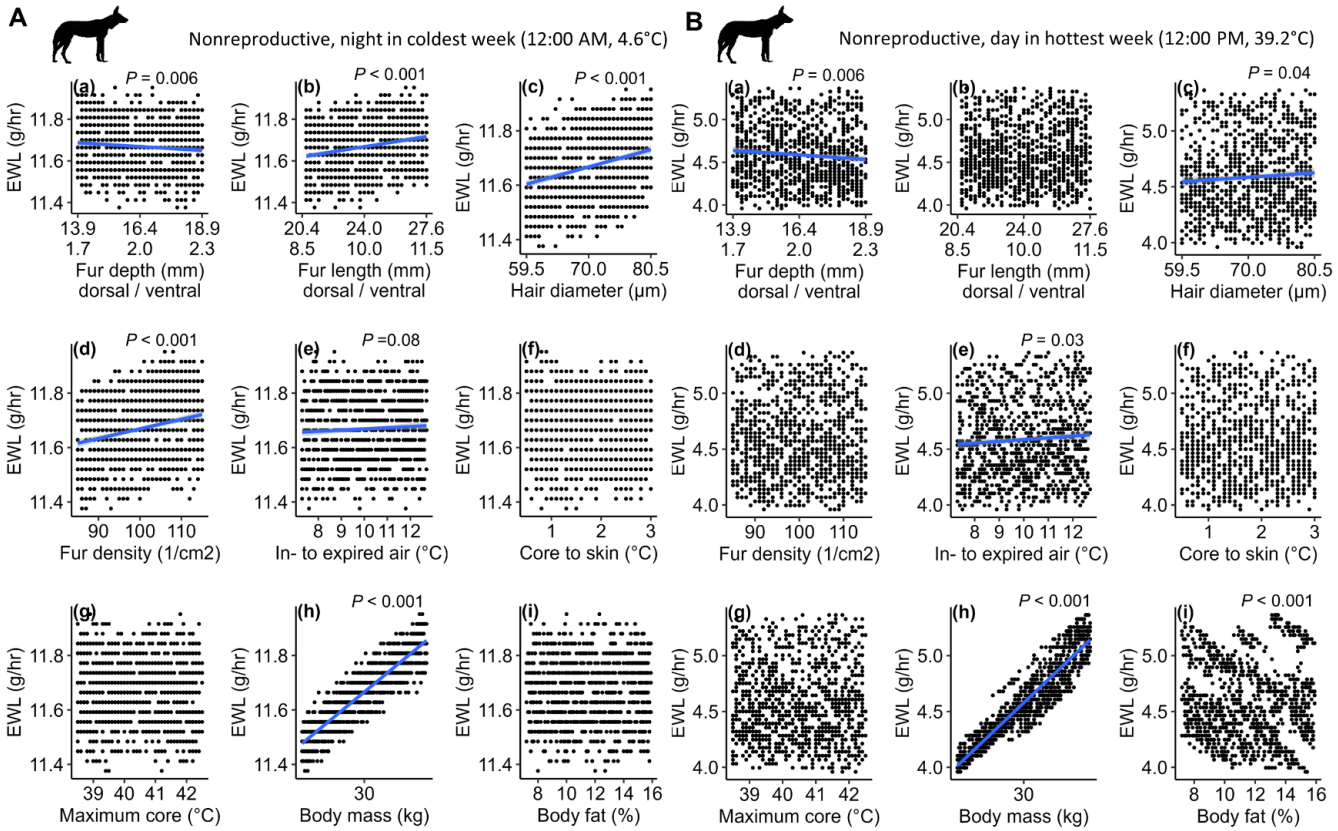

Figure C.2. Relationships between variation in key parameters included in Niche Mapper and predicted evaporative water loss (EWL; g hr^{-1}) for a nonreproductive African wild dog resting in the shade. The microclimate sub-model for this sensitivity analysis was parameterized with values from a randomly selected location (23.78253, -19.17917) in our study area, and results represent EWL predicted (**A**) at midnight during the coldest week (July 18-24) and (**B**) at midday during the hottest week (January 1-7) of a typical year (Fick et al. 2017). Each point represents one random sample (n = 1,000) from a Latin hypercube design (Wang et al. 2018); trend lines (blue) and p-values are from simple linear regression models ($\alpha = 0.10$). Model parameters evaluated were (a) torso fur depth (mm), (b) torso fur length (mm), (c) torso hair diameter (µm), (d) torso fur density (hairs per cm^2), (e) temperature difference between inspired and expired air (°C), (f) temperature difference between core and skin (°C), (g) maximum core body temperature (°C), (h) body mass (kg), (i) body fat (%); see Table C.3. (A) At cold temperatures, EWL results from Niche Mapper are most sensitive to variation in fur parameters, difference between inspired and expired air, and mass. (B) At hot temperatures, EWL results from Niche Mapper are most sensitive to variation in fur depth and diameter, difference between inspired and expired air, and mass.

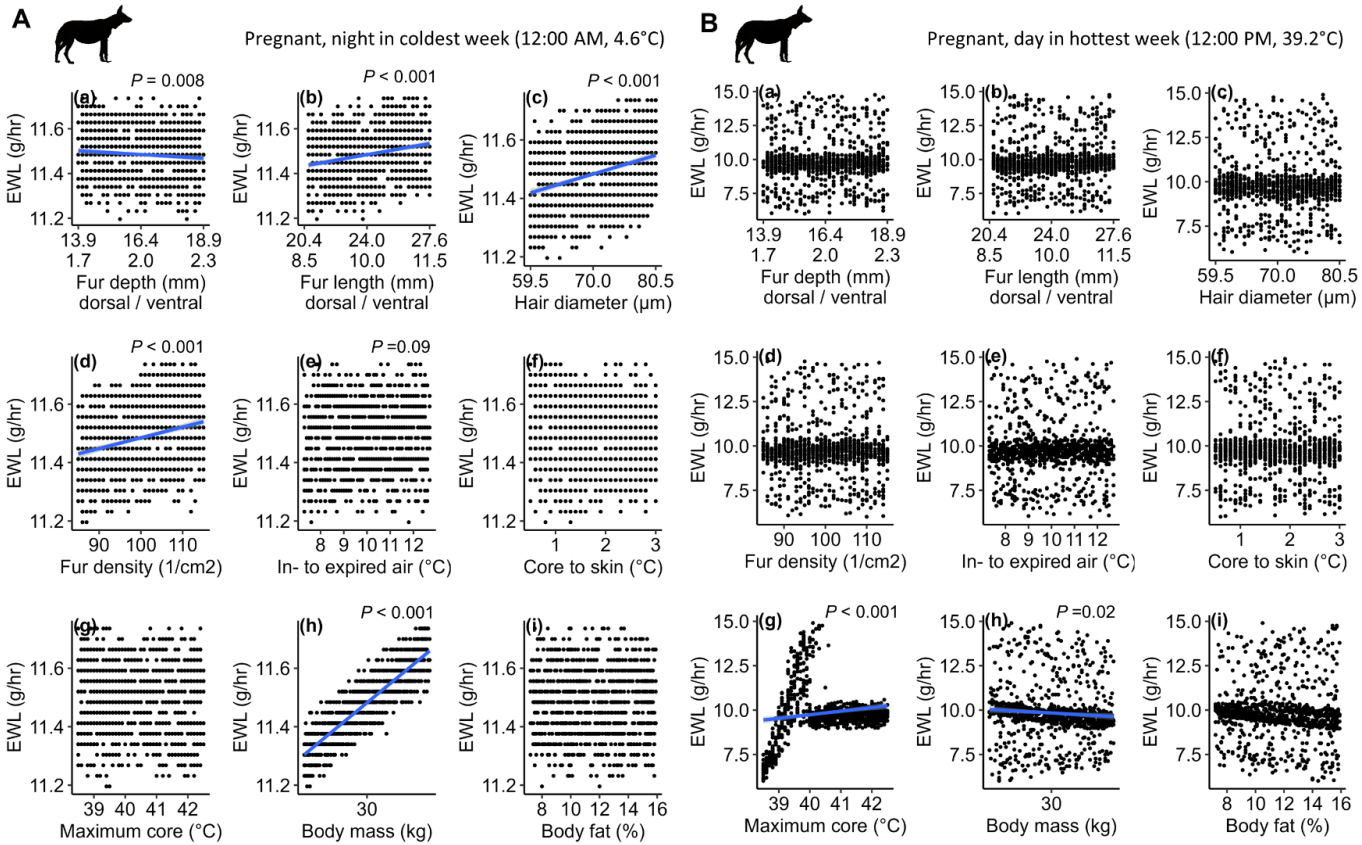

Figure C.3. Relationships between variation in key parameters included in Niche Mapper and predicted evaporative water loss (EWL; g hr^{-1}) for a pregnant African wild dog resting in the shade. The microclimate sub-model for this sensitivity analysis was parameterized with values from a randomly selected location (23.78253, -19.17917) in our study area, and results represent EWL predicted (**A**) at midnight during the coldest week (July 18-24) and (**B**) at midday during the hottest week (January 1-7) of a typical year (Fick et al. 2017). Each point represents one random sample (n = 1,000) from a Latin hypercube design (Wang et al. 2018); trend lines (blue) and p-values are from simple linear regression models ($\alpha = 0.10$). Model parameters evaluated were (a) torso fur depth (mm), (b) torso fur length (mm), (c) torso hair diameter (µm), (d) torso fur density (hairs per cm^2), (e) temperature difference between inspired and expired air (°C), (f) temperature difference between core and skin (°C), (g) maximum core body temperature (°C), (h) body mass (kg), (i) body fat (%); see Table C.3. (A) At cold temperatures, EWL results from Niche Mapper are most sensitive to variation in fur parameters and mass. (B) At hot temperatures, EWL results from Niche Mapper are most sensitive to the maximum core temperature and mass.

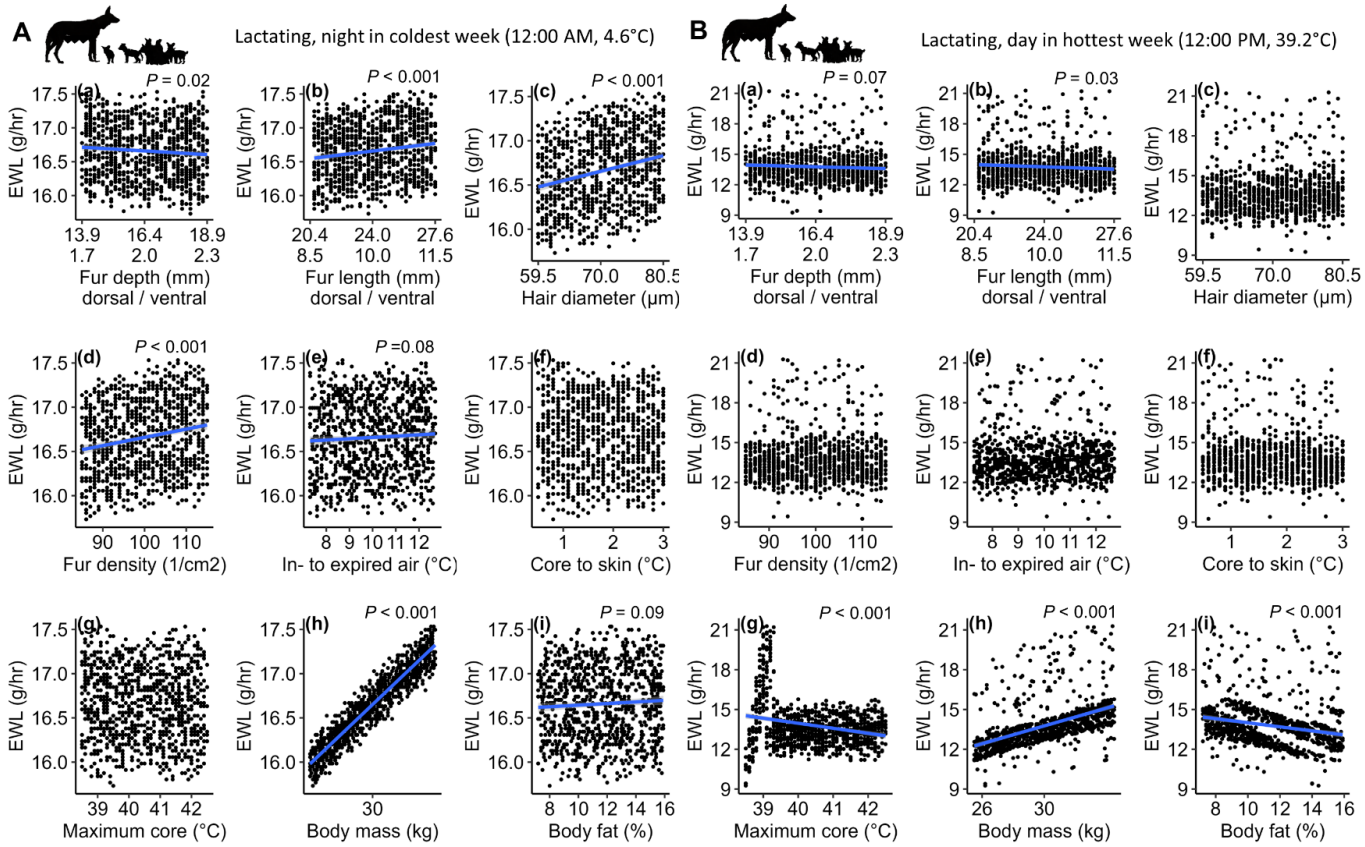

Figure C.4. Relationships between variation in key parameters included in Niche Mapper and predicted evaporative water loss (EWL; g hr^{-1}) for a lactating African wild dog resting in the shade. The microclimate sub-model for this analysis was parameterized with values from a randomly selected location (23.78253, -19.17917) in our study area, and results represent EWL predicted (**A**) at midnight during the coldest week (July 18-24) and (**B**) at midday during the hottest week (January 1-7) of a typical year (Fick et al. 2017). Each point represents one random sample (n = 1,000) from a Latin hypercube design (Wang et al. 2018); trend lines (blue) and p-values are from simple linear regression models ($\alpha = 0.10$). Model parameters evaluated were (a) torso fur depth (mm), (b) torso fur length (mm), (c) torso hair diameter (µm), (d) torso fur density (hairs per cm^2), (e) temperature difference between inspired and expired air (°C), (f) temperature difference between core and skin (°C), (g) maximum core body temperature (°C), (h) body mass (kg), (i) body fat (%); see Table C.3. (A) At cold temperatures, EWL results from Niche Mapper are most sensitive to variation in fur parameters, mass, and body fat. (B) At hot temperatures, EWL results from Niche Mapper are most sensitive to fur length and depth, maximum core temperature, mass, and fat.

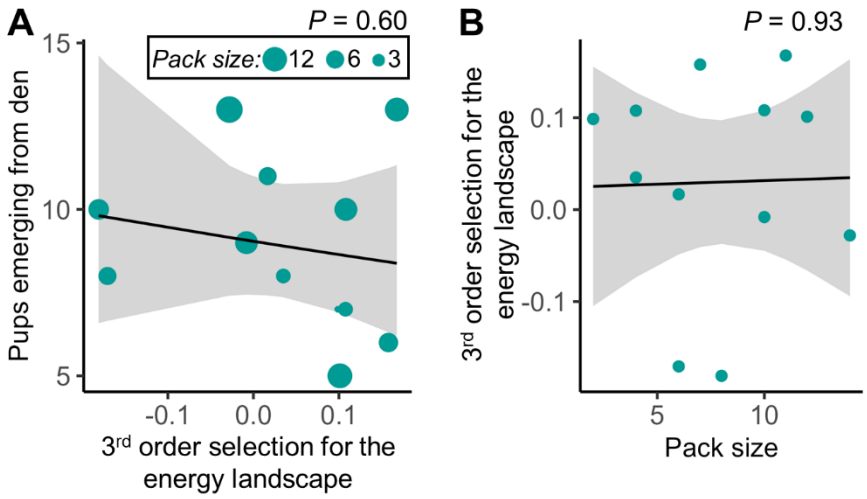

Figure C.5. Relationships among litter size, pack size, and strength of selection for the energy landscape (evaporative water loss, EWL, L/D) within home ranges during the pregnancy phase of the pup rearing cycle. We estimated within-home-range (3rd order, Johnson 1980) resource selection functions for each pack-year (N = 12) that negative coefficients indicate selection for lower-cost areas and positive coefficients indicate the opposite. Home ranges were estimated via 99% kernel density isopleths of hourly GPS data collected for each pack-year during the pregnancy phase of the pup rearing cycle using the *amt* package in R (Signer et al. 2019).We quantified within-home-range availability by extracting attribute data to random points [10x observed, generated with the *spsample*() function in the *sp* package in R (Pebsma and Bivand 2005)] distributed throughout each pack-year home range. We evaluated wild dogs' selection for the energy landscape by fitting separate generalized linear mixed models with a binomial error distribution and logit link function. We included a random intercept for each week so that use and availability were compared at the appropriate time scale and marginal coefficients represented each pack-year's relative selection for low-cost areas within their home range averaged across weeks. (**A**) We evaluated the impact of 3rd-order selection for the energy landscape on litter size by fitting a mixed-effects model that included marginal coefficients from the resource selection function as the predictor variable and the number of pups emerging from the den as the response, with a Poisson-error distribution and per-pack random intercepts ($\beta_{\text{Selection}} = -0.45$, SE = 0.86, $P = 0.60$). (**B**) To evaluate whether larger packs were more selective for lower-cost habitats within their home ranges, we used pack size as the predictor and selection for the energy landscape (coefficients from the RSF) as the response in a mixed effects model with a Gaussian-error distribution and per-pack random intercepts ($\beta_{\text{Pack size}} = 0.0008$, SE = 0.009, $P = 0.93$).

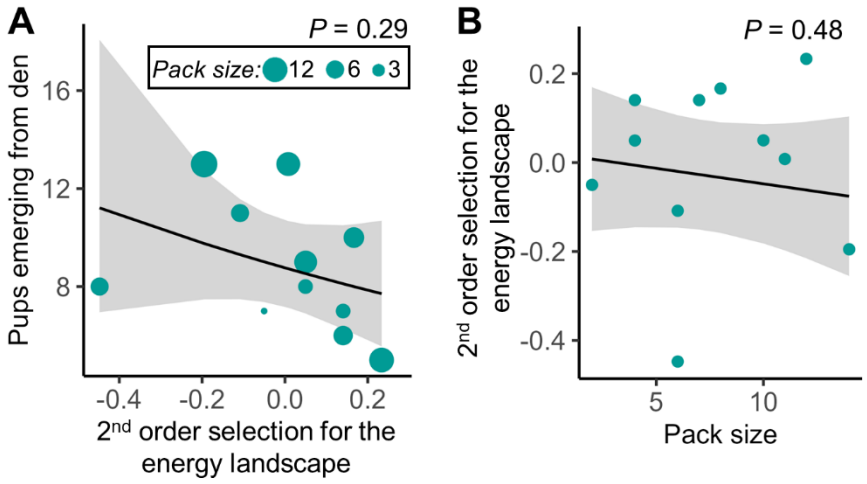

Figure C.6. Relationships among litter size, pack size, and strength of selection for the energy landscape (evaporative water loss, L/D) across the study area during the pregnancy phase of the pup rearing cycle. We estimated landscape-scale (2nd order, Johnson 1980) resource selection functions for each pack-year (N = 12) that negative coefficients indicate selection for lower-cost areas across our study area and positive coefficients indicate the opposite. Our study areas was bounded by the 99% kernel density isopleths of hourly GPS data collected across all pack-years during the pregnancy phase of the pup rearing cycle using the *amt* package in R (Signer et al. 2019). We quantified availability by extracting attribute data to random points [10x observed, generated with the *spsample*() function in the *sp* package in R (Pebsma and Bivand 2005)] distributed throughout within our study area. We evaluated wild dogs' selection for the energy landscape by fitting generalized linear mixed models with a binomial error distribution and logit link function to the scaled attribute data from used (GPS locations from African wild dogs) and random locations. Our interest was in the conditional, or pack-year-level, parameter estimates generated by including a random intercept and uncorrelated random slope for energy costs (grouped by pack-year nested within week so that use and availability were compared at the appropriate time scale) (*sensu* Long et al. 2016). The conditional slopes represented each pack-year's strength of selection for low-cost habitats (indicated by negative values; selection for high-cost areas indicated by positive values) relative to the population mean. (**A**) We used conditional slopes from the fitted RSF as the predictor variable to evaluate the influence of selection for the energy landscape during pregnancy on litter size (mixed effects model with Poisson-error distribution and per-pack random intercepts: $\beta_{\text{Selection}} = -0.55$, SE = 0.52, $P = 0.29$). (**B**) To evaluate whether larger packs were more selective for the energy landscape, we used the conditional slopes as the response and pack size as the predictor in a mixed effects model with a Gaussian error distribution and per-pack random intercepts ($\beta_{\text{Pack size}} = -0.007$, SE = 0.01, $P = 0.48$).

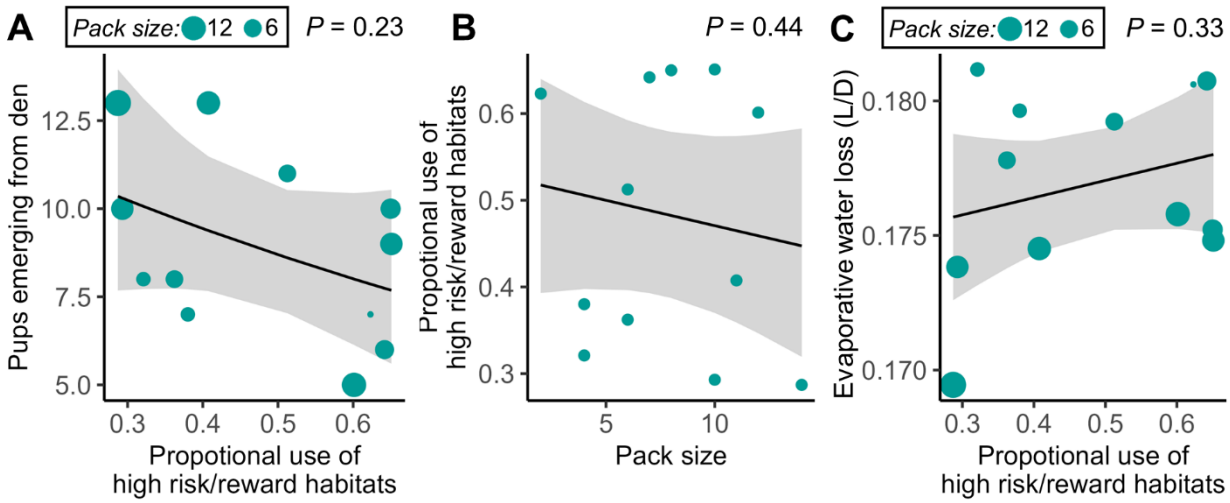

Figure C.7. Use of high risk/reward habitats by pregnant African wild dogs (N = 12) did not impact fecundity, scale with pack size, or predict mean energetic costs imposed by the environment. Recent work in our study area identified mixed woodland and dry grassland habitats as the preferred habitat of both impala (preferred wild dog prey) and lion (primary intraguild predator) and showed that wild dogs prefer to hunt in those high risk/reward habitats (Alting et al. 2021). (**A**) Contrary to the prediction that use of habitats preferred by prey should increase nutritional resources available to support reproduction, and should thus improve reproductive success, proportional use of high risk/reward habitats did not significantly impact litter size (mixed effects model with Poisson-error distribution and per-pack random slopes: $\beta_{\text{Habitat use}} = -0.82$, SE = 0.68, $P = 0.23$). (**B**) We also find that more dominant, larger packs did not use high risk/reward habitats more than smaller packs (mixed effects model with beta-error distribution and per-pack random slopes: $\beta_{\text{Pack size}} = -0.02$, SE = 0.03, $P = 0.44$). (**C**) There was no correlation between use of high risk/reward habitats and predicted costs of thermoregulation (i.e., evaporative water loss, L/D) incurred by pregnant wild dogs (mixed effects model with Gaussian-error distribution and per-pack random slopes: $\beta_{\text{Habitat use}} = 0.006$, SE = 0.007, $P = 0.33$).

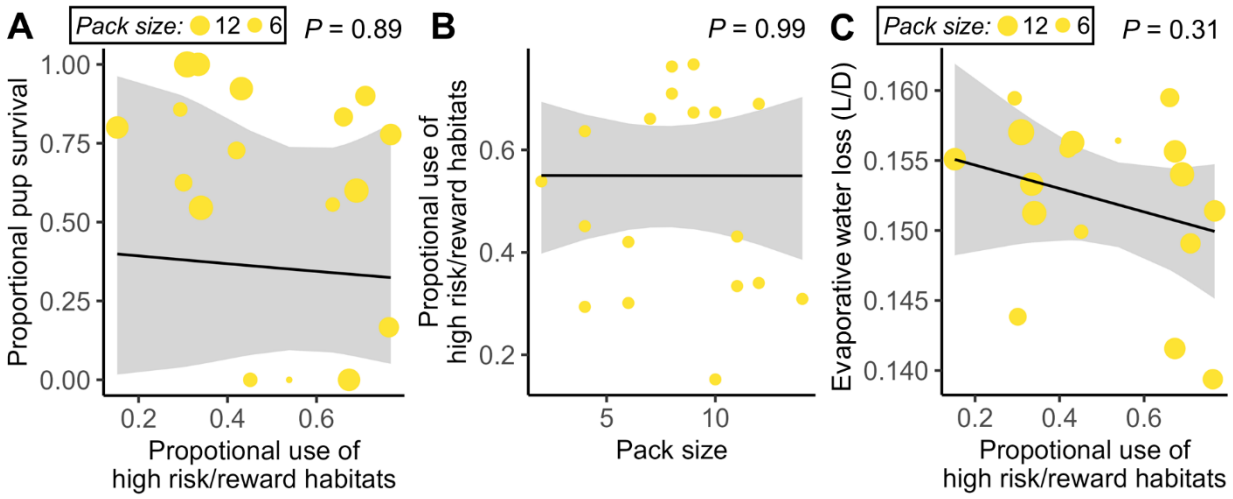

Figure C.8. Use of high risk/reward habitats by nonreproductive African wild dogs (N = 17) during the lactation phase of the pup rearing cycle did not impact survivorship, scale with pack size, or predict mean energetic costs imposed by the environment. Recent work in our study area identified mixed woodland and dry grassland habitats as the preferred habitat of both impala (preferred wild dog prey) and lion (primary intraguild predation) and show that wild dog prefer to hunt in those high risk/reward habitats (Alting et al. 2021). During the lactation/denning phase of the pup rearing cycle, non-reproductive dogs hunt and provision the lactating female, who typically remains at the den site with the pups. (**A**) Contrary to the prediction that packs that use prey preferred habitats increase nutritional resources available to support reproduction, and should thus improve reproductive success, proportional use of these high risk/reward habitats did not significantly impact pup survivorship to weaning (mixed effects model with beta-error distribution and per-pack random slopes: $\beta_{\text{Habitat use}} = -0.53$, SE = 3.9, $P = 0.89$). (**B**) We additionally find that dominant, larger packs did not use high risk/reward habitats more than smaller packs (mixed effects model with beta-error distribution and per-pack random slopes: $\beta_{\text{Pack size}} = -0.0003$, SE = 0.04, $P = 0.99$). (**C**) There was no correlation between these habitats and modeled energetic costs of thermoregulation (i.e., evaporative water loss, L/D) for non-reproductive wild dogs (mixed effects model with Gaussian-error distribution and per-pack random slopes: $\beta_{\text{Habitat use}} = -0.008$, SE = 0.008, $P = 0.31$).

Literature Cited

Abu-hamdeh, N. H., and R. C. Reeder. 2000. Soil thermal conductivity: Effects of density, moisture, salt concentration, and organic matter. *Soil Science Society of Am*erica 64:1285-1290.

Amatulli, G., S. Domisch, M.N. Tuanmu, B. Parmentier, A. Ranipeta, J. Malczyk, and W. Jetz. 2018. A suite of global, cross-scale topographic variables for environmental and biodiversity modeling. *Scientific Data* 5:180040.

Baile, E.M., R.W. Dahlby, B.R. Wiggs, G.P. Parsons, and P.D. Pare. 1987. Effect of cold and warm dry air hyperventilation on canine airway blood flow. *Journal of Applied Physiology* 62:526-532.

Cain, S. and C. Chapler. 1979. Oxygen extraction by canine hindlimb during hypoxic hypoxia. *Journal of Applied Physiology* 46:1023-1028.

Fick, S.E., and R.J. Hijmans. 2017. WorldClim 2: new 1-km spatial resolution climate surfaces for global land areas. *International Journal of Climatology* 10.1002/joc.5086.

Fontaine, E. 2012. Food intake and nutrition during pregnancy, lactation and weaning in the dam and offspring. *Reproduction in Domestic Animals* 47:326-330.

Gorman, M.L., M.G. Mills, J.P. Raath, and J.R. Speakman. 1998. High hunting costs make African wild dogs vulnerable to kleptoparasitism by hyaenas. *Nature* 391:478-481.

Hilderbrand, G.V., and H.N. Golden. 2013. Body composition of free-ranging wolves (*Canis lupis*). *Canadian Journal of Zoology* 91:1-6.

Hubel, T.Y., J.P. Myatt, N.R. Jordan, O.P. Dewhirst, J.W. McNutt, and A.M. Wilson. 2016. Energy cost and return for hunting in African wild dogs and cheetahs. *Nature Communications* 7:11034.

Johnson, D.H. 1980. The comparison of usage and availability measurements for evaluating resource preference. *Ecology* 61:65-71.

Long, R.A., R.T. Bowyer, W.P. Porter, P. Mathewson, K.L. Monteith, S.L. Findholt, B.L. Dick, and J.G. Kie. 2016. Linking habitat selection to fitness-related traits in herbivores: the role of the energy landscape. *Oecologia* 181:709-720.

Markvart, T., and L. Castañer. 2003. *Practical Handbook of Photovoltaics: Fundamentals and Applications*. Elsevier Press: Amsterdam, Netherlands.

Pebesma E.J., and R.S. Bivand. 2005. Classes and methods for spatial data in R. *R News* 5:9–13.

Peterson, J.N. and R.C. Seagrave. 1983. Experimental and theoretical study of temperature regulation in the immersed dog. *IEEE Transactions on Biomedical Engineering* 30:590-600.

Ren, T., T.E. Ochsner, R. Horton, and Z. Ju. 2003. Heat-pulse method for soil water content measurement: influence of the specific heat of the soil solids. *Soil Science Society of Am*erica 67:1631-1634.

Sellers, W. D. 1965. *Physical climatology*. University of Chicago Press: Chicago, USA.

Sharma, V. 1997. *Environmental and Engineering Geophysics*. Cambridge University Press: Cambridge, UK.

Sheild, J. 1972. Acclimation and energy metabolism of the dingo, *Canis dingo*, and the coyote, *Canis latrans*. *Journal of Zoology* 168:483-501.

Taylor, C.R. and N.H. Heglund. 1982. Energetics and mechanics of terrestrial locomotion. *Annual Review of Physiology* 44:97-107.

Taylor, C.R., K. Schmidt-Nielsen, R. Dmi'el, and M. Fedak 1971. Effect of hyperthermia running during running in the African hunting dog. *American Journal of Physiology* 220:823-827.

Valvano, J.W., J.R. Cochran, and K.R. Diller. 1985. Thermal conductivity and diffusivity of biomaterials measured with self-heated thermistors. *International. Journal of Thermophysiological* 6:301-311.

Valvano, J.W. and B. Chitsabesan. 1987. Thermal conductivity and diffusivity of arterial wall and atherosclerotic plaque. *Lasers Life Science* 1:219-229.

Walters, L.M., G.K. Ogilvie, M.D. Salman, L. Joy, M.J. Fettman, M.S. Hand, and S.L. Wheeler. 1993. Repeatability of energy expenditure measurements in clinically normal dogs by use of indirect calorimetry. *American Journal of Veterinarian Research* 54:1881–1885.

Wang, Y., W.P. Porter, P.D. Mathewson, P.A. Miller, R.W. Graham, and J.W. Williams. 2018. Mechanistic modeling of environmental drivers of woolly mammoth carrying capacity declines on St. Paul Island. *Ecology* 99: 2721-2730.

Wiley, K.D. 'African wild dog (Lycaon pictus)'. A microscopical study of exotic animal hairs: Part 2. Materials Analysis: The McCrone Group. URL: https://www.mccrone.com/mm/a-microscopical-study-of-exotic-animal-hairs-part-2/

Wilson, A.M., and W. Jetz. 2016. Remotely sensed high-resolution global cloud dynamics for predicting ecosystem biodiversity distributions. *PLoS Biology* 14:e1002415.

Winstanley, R.K., W.A. Buttemer, and G. Saunders. 1999. Fat deposition and seasonal variation in body composition of red foxes (*Vulpes vulpes*) in Australia. *Canadian Journal of Zoology* 77:406-412.

Zhang, T., Y. Zhou, K. Zhao, Z. Zhu, G. Chen, J. Hu, and L. Wang. 2022. A global dataset of daily maximum and minimum near-surface air temperature at 1 km resolution over land (2000-2020). *Earth Systems Science Data* 14:5637-5649.